Investigating sterically-stabilised pH-responsive Pickering emulsifiers as microcapsule membranes

Mohamed Soyeb Abdul Razak Manga

Submitted in accordance with the requirements for the degree of
Doctor of Philosophy

The University of Leeds
Institute of Particle Science and Engineering
School of Process, Environmental and Materials Engineering

October, 2013

The candidate confirms that the work submitted is his own, except where work which has formed part of jointly-authored publications has been included. The contribution of the candidate and the other authors to this work has been explicitly indicated below. The candidate confirms that appropriate credit has been given within the thesis where reference has been made to the work of others.

Refereed Journal Articles

1. Q. Yuan, O. J. Cayre, **M. Manga**, R. A. Williams and S. Biggs, Preparation of particle-stabilized emulsions using membrane emulsification, *Soft Matter*, 2010, **6**, 1580-1588.
2. O. J. Cayre, J. Hitchcock, **M. S. Manga**, S. Fincham, A. Simoes, R. A. Williams and S. Biggs, pH-responsive colloidosomes and their use for controlling release, *Soft Matter*, 2012, **8**, 4717-4724.
3. **M. S. Manga**, O. J. Cayre, R. A. Williams, S. Biggs and D. W. York, Production of solid-stabilised emulsions through rotational membrane emulsification: influence of particle adsorption kinetics, *Soft Matter*, 2012, **8**, 1532-1538.

Acknowledgements

I would like to begin by firstly thanking my supervisors Prof. Simon Biggs and Prof. Richard Williams for giving me the opportunity to work on this fascinating project and for their insightful discussions and encouragement. They have allowed me to develop my own research interests and the opportunity to travel and cement my position within the research community. I hope I have repaid the faith you have shown in me.

To Dr. Olivier Cayre, you have not only mentored me throughout this project but have also been a great friend. A special thank you for helping me get to grips with the more difficult concepts of this thesis.

I would like to say a special thank you to Prof. Lyn Walker, Prof. Shelly Anna and Dr. Matt Reichert of Carnegie Mellon University, U.S.A., for allowing me the opportunity to visit and work in their labs and trusting me with your in-house built Microtensiometer device!

I am also grateful to Dr. Gaelle Bacquey, Dr. Maggy Manguian, Dr. N. Chagneux for their help with the synthesis and characterisation of the pH-responsive polymer used in this study. I would like to thank Dr. Alexandre Richez for his help on determining the grafting density of the polymers using ^{1}H NMR. I would also like to acknowledge Mr. James Hitchcock for his contribution towards the preparation and characterization of the colloidosome microcapsule work presented in Chapter 6. The contribution made by James and myself has been fully and explicitly indicated in the thesis.

A big thank you goes out to Dr. Timothy Hunter, Dr. Huai (Grace) Yow and Dr. Betime Nuhiji and the rest of the CPEG crew both past and present for making my journey through this PhD very enjoyable. I would like to acknowledge my industrial supervisor Prof. Dave York for his input into my work. P&G (Newcastle) are thanked for awarding me a case award and providing financial support for my project.

To my parents, Abdul Razak and Khurshida, I thank you for providing me with the opportunity to attain the best education possible. I have really appreciated your patience, support and backing over so many years, without you none of this would

have been possible. To my brothers, Faisal and Zubair, thank you for all your support, well wishes and for all the fun times we have had together. To my wife, Asiyah for all her help and encouragement.

Abstract

In this study, polystyrene latex particles sterically stabilised using a diblock copolymer; poly(methyl methacrylate – block - poly(2-dimethylaminoethyl methacrylate) (pMMA-b-pDMAEMA) are investigated for use as emulsifiers, their adsorption to an oil-water interface, their effect on droplet size control via rotary membrane emulsification and fabrication of smart colloidosome microcapsules. The particles are synthesized using emulsion polymerisation and the particle size can be controlled by changing the polymer block length and reaction temperature.

Emulsion studies using these latex particles show that both the pH and electrolyte concentrations affect emulsion stability to oil coalescence. At high pH's, stable emulsions are formed due to the affinity of the particles to the interface. At low pH, protonation of the amine groups reduces the affinity and thus coalescence is observed. Increasing the electrolyte concentration improves emulsion stability but causes an increase in droplet size due to adsorption of flocculated/aggregated particles.

The solid-stabilised emulsions are used as a template to produce colloidosome microcapsules. The pDMAEMA chains on the particle surface are cross-linked producing a robust capsule shell. The oil core is removed and it is demonstrated that the membrane shell, expands and contracts in response to changes in environmental pH. Furthermore it is shown that the microcapsules can be used for the retention and release of 'model' dextran molecules.

Rotational membrane emulsification was employed to produce emulsion droplets with controlled sizes, stabilised by silica and pH-responsive latex particles. It was found that changes in the droplet size due to variations in the processing parameters could be related back to the kinetics involved in particle adsorption. Tensiometry experiments were performed to probe adsorption kinetics by measuring changes in dynamic interfacial tension. It was found that that bare particles do not change the tension, whereas with core-shell particles the change is pH dependent.

Table of Contents

List of Tables

List of Figures

CHAPTER 1: INTRODUCTION

The role of particles in the stabilization of fluid-fluid interfaces has been recognized as being very important in industrial processing. Industrial applications that utilize emulsions such as the food, cosmetic, pharmaceutical and agrochemical industries have driven the increased interest in studying particle stabilised emulsions.

Although Ramsden[1] reported the stabilisation of emulsions using particles, it was Pickering[2] who conducted the first systematic study. It was the contribution made by his work in this area that earned the name 'Pickering emulsions' for particle stabilised emulsions. The physical advantage of using particulates over surfactant emulsifiers, is that particulates achieve high attachment energies to the liquid-liquid interface and once attached they effectively remain irreversibly adsorbed.[3] In contrast, surfactant molecules rapidly adsorb and desorb from the interface exchanging from the bulk.[4] It should be mentioned that in the case of particle stabilised emulsions, both the particle size and wettability characterised by its contact angle will influence the amount of energy that will be required to detach the particles from the interface. This required detachment energy is proportional to the square of the particle radius and the particles are most strongly adsorbed at the interface when an interfacial contact angle of 90° is achieved. It has been demonstrated that particle stabilised emulsions can be used for the fabrication of new of class materials such as 'colloidosome' microcapsules.[5-7]

Conventional methods to produce emulsions are based on rotor-stator dispersing machines (e.g. stirred vessels and tooth disc dispersing machines), high-pressured homogenizers[8] and ultrasonic systems. These conventional systems use turbulent eddies and cavity formations to disrupt the two immiscible liquids to produce dispersions of fine droplets of one liquid into the other. These methods face numerous problems during large scale manufacturing. In large vessels eddies cannot be generated and controlled consistently over a large period of time, this limits the control achieved on the size distribution and sizes required. Another problem encountered is the fact that these systems cannot be consistently reproduced from batch to batch due to their inability to produce monodispersed systems, specifically

because of in-homogeneity in the process. Furthermore, these processes are energetically costly, which leads to high manufacturing costs.

The production of emulsions using a drop by drop production technique allows greater control of features such as droplet size and polydispersity, under the correct operating conditions.[9] Several examples of drop by drop technologies include microfluidics, cross-flow,[10] vibrating[11] and rotating membrane emulsification.[12, 13] The advantage of membrane emulsification over the conventional counterparts is that it results in highly monodisperse droplets created with low levels of energy input[14] that can easily be scaled up for large scale manufacturing with the addition of more membranes to the setup. Another advantage is that the droplet sizes are dependent on the choice of membrane and not on the turbulence, i.e. inhomogeneous eddies.

Aims of thesis

The aim of this work is to investigate pH-responsive sterically stabilised latex particles as Pickering emulsifiers, in particular their adsorption to an oil/water interface, exerting control over droplet size using Rotational Membrane Emulsification and for the fabrication of smart colloidosome microcapsules. The latex particles are sterically stabilised using poly(methyl methacrylate – block - poly(2-dimethylaminoethyl methacrylate) (pMMA-b-pDMAEMA). Initially the influence of the pDMAEMA chain length and the polymerisation temperature on the particle size will be investigated. It is important that these latex particles are well characterised in order to understand their roles as particulate emulsifiers. The role of these latex particles to adsorb onto liquid-liquid interfaces and stabilise the emulsions from coalescence will be systematically investigated as a function of environmental pH and ionic concentration. The potential of using particle stabilised emulsions as templates for the manufacture of novel colloidosome microcapsules will be investigated. In this study the use pH stimuli will be used to control the porosity of the microcapsule membrane to demonstrate successful retention and release of model molecules.

Finally the possibility of producing particle-stabilised emulsions using a rotary membrane emulsification device will be investigated by firstly using model silica colloids. This will scope the potential of using the sterically stabilised latex particles to control droplet production. In this study the effect of various chemical and mechanical parameters will be investigated.

Structure of thesis

Chapter 2

Chapter 2 is written to provide the reader with an overview on the theory of emulsion and emulsion stability and techniques used for their production. This chapter introduces the concept of emulsions, emulsion stability and the role of emulsifiers. In particular, the differences between surfactant and particulate emulsifiers will be introduced. This chapter concludes by outlining various techniques employed to produce emulsions comparing conventional methods with drop by drop techniques.

Chapter 3

The third chapter is written to provide a literature review regarding the fundamental theory behind membrane emulsification. In particular, details are given regarding the membrane and processing parameters that dictate the droplet size and size distribution obtained using these devices.

Chapter 4

Chapter 4 details the materials and methodology employed within this work introducing a number of techniques that will be used to gain characteristic information about the particulate systems used in this study and how this affects their adsorption to liquid-liquid interfaces.

Chapter 5

The fifth chapter investigates the synthesis and characterisation of sterically stabilised latex particles. In particular looking at the effect of polymer chain length and polymerisation temperature on the particle size. Also presented in this chapter is the characterisation of the pH-responsive polymer used in this work.

Chapter 6

Chapter 6 looks at the use of the sterically stabilised latex particles to a stabilise emulsions. In particular the role of pH and ionic strength is evaluated. The stability of the emulsions prepared using latex particles with two different polymer chain lengths is presented. Also presented in this chapter is the fabrication of pH-

responsive colloidosome microcapsules using the particle stabilised emulsions as templates.

Chapter 7

Chapter 7 presents a systematic study regarding the production of controlled emulsion droplets using model silica colloids and the sterically stabilised latex particles. The influence of various chemical and mechanical parameters on the droplet size and droplet size distribution is presented.

Chapter 8

Chapter 8 investigates the use of tensiometry of probing particle adsorption kinetics. In this study, experimentation using two devices; a) pendant drop tensiometry and b) microtensiometry are presented. The role and effect of numerous particulate systems on the dynamic interfacial tension is presented.

Chapter 9

Chapter 9 contributes as an additional assessment of the importance of this work in the context of broader scientific and industrial development.

References

1. W. Ramsden, Separation of solids in the surface-layers of solutions and 'suspensions' (observations on surface-membranes, bubbles, emulsions, and mechanical coagulation)., Preliminary Account, *Proc. R. Soc. London*, 1903, **72**, 156-164.
2. S. U. Pickering, Emulsions, *J. Chem. Soc., Trans.*, 1907, **91**, 2001-2021.
3. B. P. Binks and T. S. Horozov eds., *Colloidal Particles at Liquid Interfaces*, Cambridge University Press, Cambridge, 2006.
4. B. P. Binks, Particles as surfactants-similarities and differences, *Curr. Opin. Colloid Interface Sci.*, 2002, **7**, 21-41.
5. O. D. Velev and K. Nagayama, Assembly of latex particles by using emulsion droplets. 3. Reverse (water in oil) system, *Langmuir*, 1997, **13**, 1856-1859.
6. A. D. Dinsmore, M. F. Hsu, M. G. Nikolaides, M. Marquez, A. R. Bausch and D. A. Weitz, Colloidosomes: Selectively permeable capsules composed of colloidal particles, *Science*, 2002, **298**, 1006-1009.
7. Q. Yuan, O. J. Cayre, S. Fujii, S. P. Armes, R. A. Williams and S. Biggs, Responsive core-shell latex particles as colloidosome microcapsule membranes, *Langmuir*, 2010, **26**, 18408-18414.
8. H. Karbstein and H. Schubert, Developments in the continuous mechanical production of oil-in-water macro-emulsions, *Chem. Eng. Process.*, 1995, **34**, 205-211.
9. A. J. Gijsbertsen-Abrahamse, A. van der Padt and R. M. Boom, Status of cross-flow membrane emulsification and outlook for industrial application, *J. Membrane Sci.*, 2004, **230**, 149-159.
10. S. J. Peng and R. A. Williams, Controlled production of emulsions using a crossflow membrane: Part I: Droplet formation from a single pore, *Chem. Eng. Res. Des.*, 1998, **76**, 894-901.
11. R. G. Holdich, M. M. Dragosavac, G. T. Vladisavljević and S. R. Kosvintsev, Membrane emulsification with oscillating and stationary membranes, *Ind. Eng. Chem. Res.*, 2010, **49**, 3810-3817.
12. G. T. Vladisavljević and R. A. Williams, Manufacture of large uniform droplets using rotating membrane emulsification, *J. Colloid Interface Sci.*, 2006, **299**, 396-402.

13. N. Aryanti, R. A. Williams, R. Hou and G. T. Vladisavljević, Performance of rotating membrane emulsification for o/w production, *Desalination*, 2006, **200**, 572-574.

14. C. Charcosset, I. Limayem and H. Fessi, The membrane emulsification process - a review, *J. Chem. Technol. Biotechnol.*, 2004, **79**, 209-218.

CHAPTER 2: THEORY AND PRINCIPLES OF EMULSIFICATION

NOMENCLATURE

A	Hamaker constant
D	Diffusion coefficient
d	Particle separation distance
ε	Electron charge
G	Gibbs free energy
g	Gravitational constant
dH	Enthalpy
k	Boltzmann constant
M	Molar mass
P	Pressure
R	Ideal gas constant
r	Radius of particle
S	Solubility
dS	Entropy
T	Absolute temperature
t	Time
V_A	Potential energy of attractive forces
V_M	Molar volume
V_R	Potential energy of repulsive forces
V_T	Total energy of interaction
κ	Function of ionic composition
ρ	Density
π	Solvent permeability
η	Viscosity
ζ	Zeta potential
θ	Contact angle

ABBREVIATIONS

CV	Coefficient of Variation
DLVO	Derjaguin, Landau, Verwey, Overbeek
HLB	Hydrophilic Lipophilic Balance
MC	Microchannel
O/W	oil-in-water emulsion
PDMS	poly(dimethyl siloxane)
PMMA	poly(methyl methacrylate)
W/O	water-in-oil emulsion
W/O/W	water-in-oil-in-water emulsion

2.1. Introduction

An emulsion can be described as a colloidal dispersion where one immiscible liquid is dispersed as fine droplets in another. Emulsions are a biphasic system containing a continuous phase (e.g. water) and a dispersed phase (e.g. oil). For a system composed of oil and water, there are two types of emulsions that can be created; oil in water (O/W) and water in oil (W/O) emulsions as illustrated in Figure 2.1. Emulsions can also be created with other types of liquids such as ionic liquid.[1] Emulsions play pivotal roles in the formulations of many products within the cosmetics (hand creams, body milk and sun-block,[2] pharmaceuticals (creams, ointments, drug carriers)[3] and chemicals industries (paints and coatings).[4]

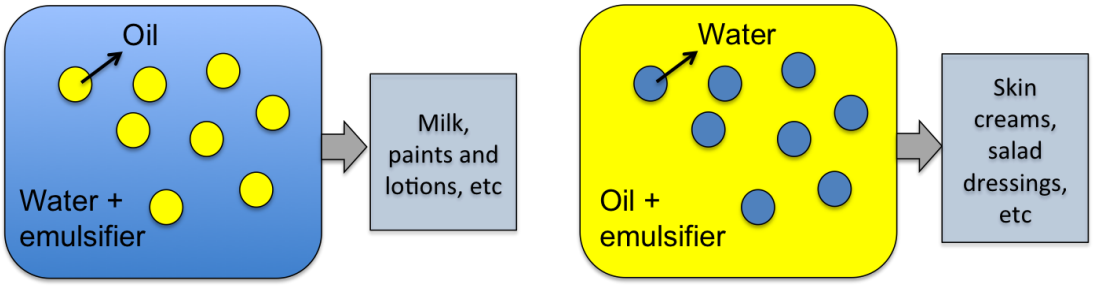

Figure 2.1. Illustration of O/W and W/O emulsions and a few examples of their uses in applications.

A third type of emulsion that can be created is known as a multiple emulsion (Figure 2.2). Multiple emulsions are complex systems and consist of smaller droplets inside the dispersed phase such as water in oil in water (W/O/W) or vice versa. They are widely used to encapsulate active ingredients in myriad applications.[5]

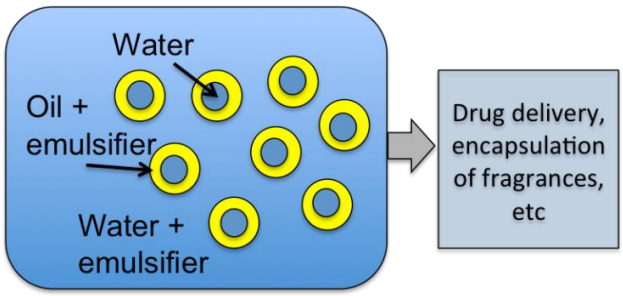

Figure 2.2. Illustration of an multiple emulsion (W/O/W) and a few examples of their uses in applications.

2.2. Emulsion stability

The stability of emulsions is an important parameter as it dictates the shelf life and application of a product. For example in the food industry different degrees of stability are needed to achieve a variety of products. Some emulsions are required to remain stable for long periods of time (days, months or years) e.g. mayonnaise to achieve a longer shelf life. On the other hand there are instances where having unstable emulsions can also be advantageous. This is evident in the manufacture of ice cream mix and margarine premix where the emulsion is required to be stable for very short periods of time (seconds, minutes or hours). This is because the emulsion is merely an intermediate process step towards the manufacture of the final product. In oil recovery, the heavy oils contain asphaltenes that act as surfactants and stabilise both O/W and W/O emulsions. These emulsions need to be broken to successfully recover the oil.[6]

Emulsions are inherently thermodynamically unstable systems.[7] This is because the surface of each droplet is an interface between immiscible phases and contact between them is energetically unfavourable and needs to be minimised.[8] Their breakdown which occurs through different phenomena (creaming, flocculation, coalescence, phase inversion and Ostwald ripening which are illustrated in Figure 2.3)[9] can be kinetically slowed down by the addition of stabilisers (see Section 2.3). These processes are mentioned in more detail in the following subsections.

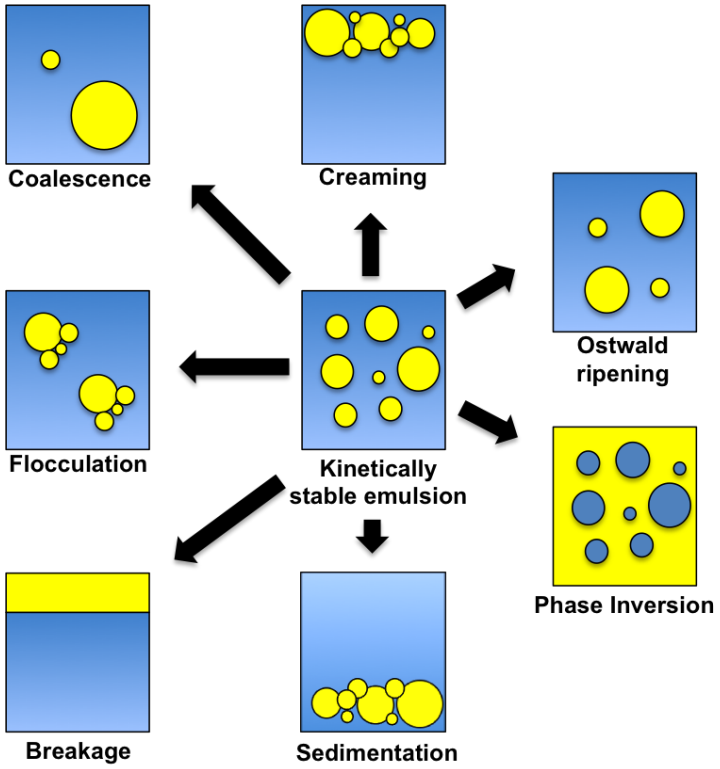

Figure 2.3. Illustration of processes that cause instabilities in emulsions. *Redrawn from Ref [9]*.

2.2.1. Creaming and sedimentation

Creaming and sedimentation are processes that result from external forces usually gravitational, due to the density difference of the emulsion droplets in comparison to the continuous liquid that surrounds them.[10] When the gravitational force exceeds the thermal motion acting on the droplet (Brownian motion), the emulsion droplets will either cream (if their density is lower than the surrounding liquid) or sediment (if their density is higher than the surrounding liquid). Generally most oils have a lower density than water so O/W emulsions cream, whereas W/O emulsions sediment.

Creaming and sedimentation can be limited if the liquids used are of matching density, by the addition of a weighting agent (usually a higher density oil) to the oil phase causing an overall increase in density of the oil phase, or by increasing the viscosity of the dispersed phase or by an overall reduction in the average droplet size (increase in Brownian motion).

The relationship between creaming or sedimentation rate with the average particle size, viscosity of continuous phase and the density of both phases can be defined by Stokes law (for dilute systems) as illustrated by Equation 2.1.[11]

$$U_{stokes} = -\frac{2gr^2(\rho_2 - \rho_1)}{9\eta_1} \qquad \text{(Equation 2.1)}$$

where U_{stokes} is the creaming or sedimentation velocity (if the value is positive then creaming occurs and if negative then sedimentation prevails), g is gravitational acceleration (9.81 ms^{-2}), ρ is density with subscripts *1* and *2* denoting continuous and dispersed phases and η is the viscosity of the continuous phase.

In concentrated emulsions the Stokes law serves only as an approximation due to hindered settling/creaming. Hindered settling/creaming prevents the droplets from sedimenting/creaming independently, they are influenced by the motion of the surrounding droplets. The hindered behaviour can be described by applying a correction factor to the Stokes law.[12]

2.2.2. Flocculation and Coalescence

Droplet flocculation and coalescence are the resulting phenomena when collisions between emulsion droplets occur. Emulsions are in constant motion due to external mechanical forces, Brownian motion (thermal energy), gravitational separation. This causes the droplets to collide with each other, resulting in the droplets to either move away or remain together aggregated on the resultant attractive and repulsive forces acting on them. Flocculation occurs when the droplets collide and the van der Waals attractive forces exceed the repulsive forces causing the droplets to form aggregates, whilst retaining their individual structural integrity[9] (see DLVO theory in Section 2.3.1).

Coalescence is a process resultant of two droplets colliding with each other and then merging to form a single large droplet. When two droplets collide with each other, the contact zone deforms and flattens. The thin interstitial film (with uneven thickness) that exists between the two interfaces interact via van der Waals forces

that cause the film to drain and become unstable due to thermal fluctuations at the interface.[13, 14] At a critical film thickness, the film ruptures and the droplets join together. The influence of the interaction force acting over the contact area is known as the disjoining pressure.[15] A positive disjoining pressure leads to a stable film whilst a negative value will lead to film rupture, causing the droplets to merge. This occurs as it is thermodynamically favourable to decrease the contact area between the oil and water phases.

In particle stabilised emulsions, between the extremes of total stabilisation and total coalescence is an intermediate process known as arrested coalescence.[16] When the two droplets begin to coalesce, the progress can be halted by opposing forces, resulting in an arrested structure that resembles a stable-doublet. This process is also termed as partial coalescence[17]. For arrested coalescence to occur a resistance is needed before complete coalescence occurs that stabilises the arrested structure against further shape relaxation. If coalescence does persist it will eventually lead to the complete breakdown of the emulsion to form two separate layers of the immiscible liquids.

2.2.3. Ostwald ripening

Ostwald ripening is a thermodynamically driven process that is a result of the solubility (chemical potential) difference between small and large droplets. In this process larger droplets grow at the expense of the smaller ones through mass transportation of the dispersed phase from one drop to another through the continuous phase as illustrated by Figure 2.4.[18]

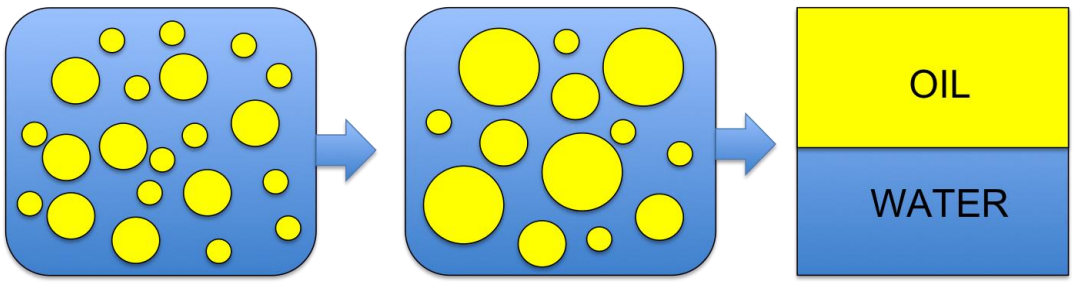

Figure 2.4. Illustrating the process of Ostwald ripening leading to complete emulsion breakage.

The ripening process is driven by differences in Laplace pressure, ΔP, between droplets of different radii;

$$\Delta P = P_{in} - P_{out} = \frac{2\gamma}{r} \qquad \text{(Equation 2.2)}$$

where P_{in} is the pressure inside the droplet, P_{out} is the pressure outside the droplet, γ is the interfacial tension and r is the droplet radius.

The pressure difference is higher in small droplets forcing the oil phase out to deposit onto the larger ones. This effect is also increased with increasing radius of curvature of the droplet.[19] Ostwald ripening can be limited by; a) controlling the droplet size and size distribution, b) reducing the interfacial tension and c) controlling the composition of the droplet to limit large differences in solubility[9] and is described by Equation 2.3.

$$\frac{d(r)^3}{dt} = \frac{8\gamma V_M SD}{9RT} \qquad \text{(Equation 2.3)}$$

where r is the droplet radius, t is time, γ the interfacial tension, V_M the molar volume of the dispersed phase, S the solubility of the dispersed phase, D the diffusion coefficient of the dispersed phase, R the ideal gas constant and T is the absolute temperature.

2.3. Emulsifiers

Emulsifiers are surface active agents used to kinetically stabilise emulsions, by adsorbing onto freshly formed oil-water interface and forming a protective membrane that prevents droplet aggregation and coalescence.[9] There are a range of emulsifiers used within emulsion production including surfactants, particles (Pickering emulsions) and proteins (food emulsions). However in this thesis only the use of surfactants and in particular particulates as emulsifiers will be described in the subsequent sub sections.

2.3.1. Surfactants

Surfactants are amphiphilic molecules that have both hydrophilic and hydrophobic properties. The structure of these amphiphilic molecules comprise of a hydrophilic head and a hydrophobic tail (Figure 2.5). The hydrophilic head interact with polar solvents whereas the hydrophobic tails are preferably solubilised by non-polar solvents such as oil. Surfactants diffuse to the interface and rapidly adsorb and desorb onto/from the interface. They stabilise emulsions by lowering the interfacial tension at the oil-water interface and also form an electrical or mechanical barrier preventing droplet coalescence.[20]

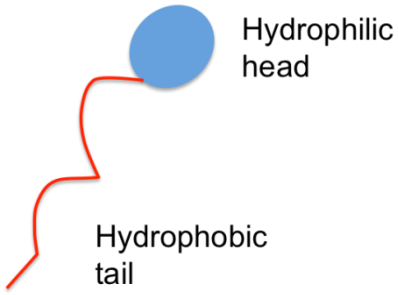

Figure 2.5. Illustration of a surfactant molecule consisting of a hydrophilic head and a hydrophobic tail.

Excess surfactant in polar solution results in the aggregation of these molecules to form micelles. In micelles the hydrophobic tails arrange themselves so that are situated inside away from the polar solvent, whilst the hydrophilic head group arrange themselves to interact with the polar solvent. The structure of these micelles in polar solvents is shown schematically in Figure 2.6.

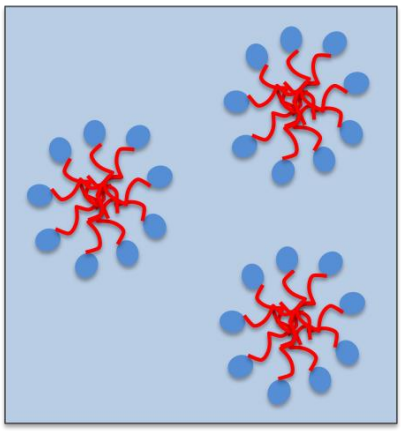

Figure 2.6. Structure of micelles formed from aggregated surfactant molecules in polar solvents e.g. water. *Adapted from Ref. [15]*.

In addition, surfactants stabilise oil-water interfaces using the Gibbs-Marangoni effect as illustrated by Figure 2.7.[7] The effect is caused by rapid surface mobility of the molecules responding to convective motions due to local differences in interfacial tension.

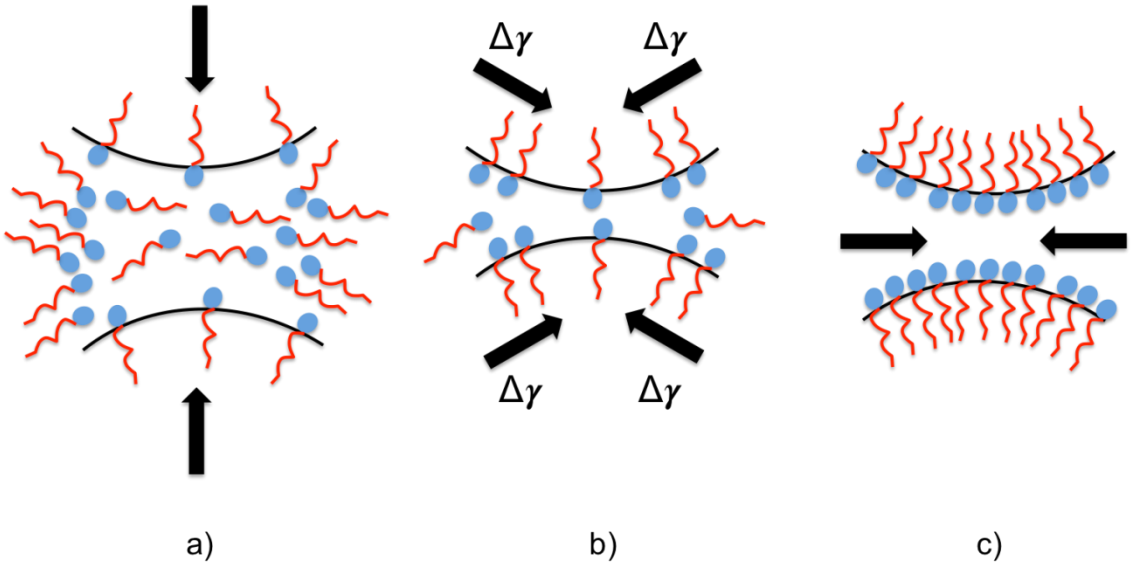

Figure 2.7. Gibbs-Marangoni effect on two droplets approaching each other during emulsification. *Adapted from Ref. [7]*.

When two droplets insufficiently covered with surfactant molecules move towards each other, the droplets acquire more surfactant molecules at its surface during the approach (Figure 2.7a). However, at the point where the film between the droplets is

thinnest, the concentration of surfactant molecules available for adsorption will be the lowest, causing a local increase in the interfacial tension, γ. This local increase in the interfacial tension causes the surfactant molecules to move towards the site of the highest interfacial tension (Figure 2.7b). This gradient in the interfacial tension causes streaming of the liquid along the surface (the Marangoni effect) causing the two droplets to move away from each other (Figure 2.7c).[7]

In industrial formulations, surfactants are characterized by HLB (Hydrophilic Lipophilic Balance) numbers that determine how hydrophilic or lipophilic the surfactant is. The concept was developed by Griffin in 1949 and later improved by Davies in 1957. Griffin[21] proposed that the HLB number was calculated by:

$$HLB = 20 \times \frac{M_h}{M} \qquad \text{(Equation 2.4)}$$

where M_h is the molecular mass of the hydrophilic group and M is the molecular mass of the whole molecule.

Surfactants that have a HLB number of 0 will be completely hydrophobic and those that have a number close to 20 will be hydrophilic. However, Davies[22] modified this to take into account the strength of the hydrophilic head groups and proposed:

$$HLB = 7 + ((m \times M_h) - (n - M_l)) \qquad \text{(Equation 2.5)}$$

where m and M_h are the number and molecular mass of the hydrophilic groups and n and M_l are the number and molecular mass of the lipophilic groups.

HLB numbers are used to distinguish the types of surfactants to be used as emulsifiers according to the Bancroft rule,[23] that states; 'The phase in which an emulsifiers is more soluble constitutes as the continuous phase.' This was later revised to 'the phase containing the surfactant aggregates becomes the continuous phase of an emulsion'.[24] Therefore surfactants whose HLB values are below 7 produce W/O emulsions (i.e. more soluble in oil) and those greater than 13 produce

O/W emulsions (more soluble in water).[15] A major drawback of using the HLB system to select surfactant as emulsifiers is that it makes no allowance for changes in the HLB values with changing emulsification conditions such as the temperature, nature of the oil, presence of co-surfactants and other additives.[25] In addition the HLB theory ignores the importance of the electric double layer, the placement of the emulsifier, the percentage of emulsifier that should be used and how the different components interact. Therefore the theory should be used as a starting point when selecting surfactants as emulsifiers.

Surfactants can be classified according to the polar head group that usually contains heteroatoms such as oxygen, nitrogen and sulphur. These functionalities on the head group makes the emulsifier anionic, cationic, amphoteric or non-ionic. Anionic surfactants carry a negative charge with a small positive counter-ion (alkylbenzene sulfonates and lauryl sulfate etc.). Cationic surfactants are positively charged and have a small negative counter-ion (quaternary ammoniums). Amphoteric surfactants carry both positive and negative charges on the same molecule (amino acids and phospholipids), whilst a non-ionic surfactant carries no formal charge (where the hydrophilic group is based on an alcohol, phenol etc. and the hydrophobic group consists of alkyls or alkylbenezenes.[26] Some examples of these surfactants are given in Figure 2.8. [27]

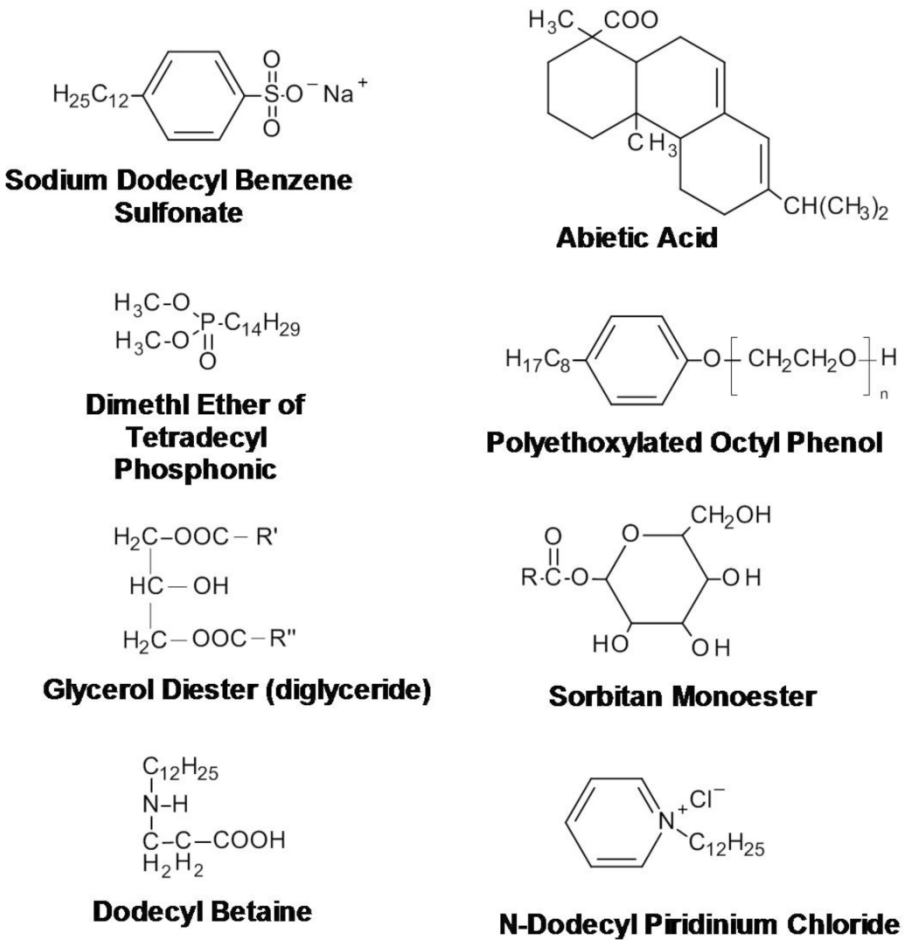

Figure 2.8. Examples of a few commonly used surfactants as emulsifiers. *Redrawn from Ref. [27]*.

The charges present on the surfactant molecules help to stabilise emulsion droplets by forming an electrical barrier preventing droplet coalescence. The polar head of the surfactant will align on the droplet surface and this electric charge will cause repulsion between the droplets.

An explanation of the stability of colloids in aqueous media determined from the potential energy of interaction between two approaching surfaces (e.g. particles, droplets) was proposed and explained in the 1940's by two independent research groups. The proposed theory and explanation is commonly referred to as the DLVO theory (Derjaguin and Landau,[28] and Verwey and Overbeek).[29] The theory aims to calculate the total interaction energy (V_T) between surfaces at close proximity, using the electrostatic attractive van der Waals forces (V_A) and the repulsive interactions (V_R).

$$V_T = V_R + V_A \qquad \text{(Equation 2.6)}$$

The attractive van der Waals energy are weak forces that dominate at very close distances as expressed by Equation 2.7, which was derived by Hamaker.[30]

$$V_A = \frac{-A}{\left(12\pi d^2\right)} \qquad \text{(Equation 2.7)}$$

where A is the Hamaker constant, π the solvent permeability and d the surface separation distance.

The repulsive energy arises from the electric surface charge, which is influenced by the electric double layer (Chapter 4).

$$V_R = 2\pi\varepsilon r\zeta^2 \exp(-\kappa d) \qquad \text{(Equation 2.8)}$$

where ε is the dielectric constant of the solvent, r is the particle radius, ζ the zeta potential, κ is the Debye-Hückel screening parameter based on ionic concentration (κ^{-1} is the characteristic length of the electric double layer).

The theory predicts the summation of the electric double layer interaction and the van der Waals interaction (Figure 2.9).[31] The double-layer repulsion energy is approximately an exponential function of the distance between the surfaces with a range of the order of the thickness of the double layer. The van der Waals attraction potential decreases as an inverse power of the distance between the surfaces. As a result the van der Waals attraction energies dominate at small and at a large separation distance. At intermediate distances the electric double layer repulsion may predominate. If the potential energy of interaction is greater than the thermal energy of the surfaces, then the system will be stable. The maximum height of this barrier depends on the magnitude of the zeta potential (Chapter 4) and the range of the repulsive forces. Another feature of the potential energy curves is the presence of a secondary minima at large separation distances. This results in loose and easily

reversible flocculation. As the repulsive forces are exceeded, the surfaces are held by strong van der Waals attraction forces in the primary minimum, forming larger clusters which require a significant amount of energy to break up the aggregates.[15]

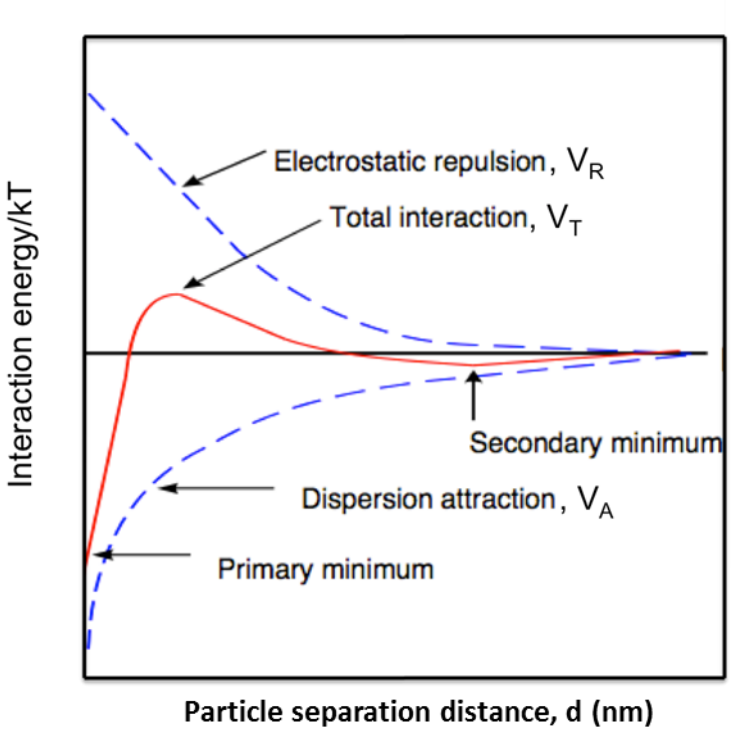

Figure 2.9. Illustration of how the energy of interaction is affected by change in the separation distance between the surfaces of two particles. Where V_R is the double layer interaction energy, V_T is the total energy of interaction and V_A is the London-van der Waals attractive energy. *Adapted from Ref. [31]*.

A number of assumptions are made in the DLVO theory, these are;[15]

- Infinite flat surface,
- Uniform surface charge density,
- No redistribution of the surface charge i.e., the surface electric potential remains constant
- The electric potential remains unchanged i.e. no change in the concentration profile of the surface charge determining ions and counter-ions, and
- The solvent exerts influence via a dielectric constant only.

Some of the assumptions mentioned above are far from real particle dispersion systems. The particle surface is not indefinitely flat and the surface charge density and distribution of the surface change may change when two charged particles meet together. In spite of these assumptions the theory works well in explaining the interactions as long as the following conditions are met:[15]

- The dispersion is very dilute i.e., charge density and distribution not interfered by other particles,
- No other forces apart from van der Waals and the electrostatic potential are present i.e., gravity is negligible or the particles are small,
- The geometry of the particles are simple i.e., the surface properties of the particle as well as the electric potential in the surrounding medium are the same,
- Diffusive double layer i.e., distribution of the counter-ions and surface charge determining ions are determined by the electrostatic force, entropy of the dispersion and Brownian motion.

2.3.3. Colloidal particles

Colloidal particles used as emulsifiers typically range from a few nanometers to a few microns. These particles behave similarly to surfactants as they can also accumulate and adsorb onto an liquid-liquid interface. A key parameter of particles at liquid-liquid interfaces is the three phase contact angle, θ. This is the angle measured between the tangents to the solid particle surface and the liquid-liquid interfaces as illustrated by Figure 2.10.[32] The angle is measured through one of the liquids, conventionally through the more polar liquid. The angle is dependent on the surface free energies i.e. the interfacial tensions at the particle-oil, γ_{po}, particle-water, γ_{pw}, and oil-water, γ_{ow}, interface as described by Young's equation;[32]

$$\cos\theta = \frac{\gamma_{po} - \gamma_{pw}}{\gamma_{ow}} \qquad \text{(Equation 2.9)}$$

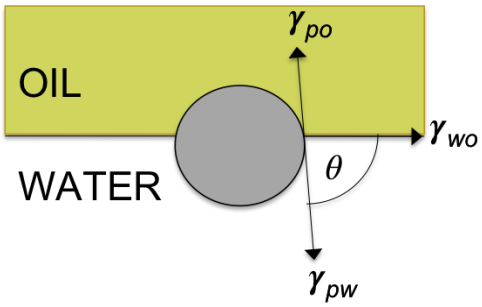

Figure 2.10. Definition of the three phase contact angle, θ, for a colloidal particle at a liquid-liquid interface.

If the particle is preferentially wetted by water (i.e. hydrophilic, $\gamma_{po} > \gamma_{pw}$) the contact angle will be $0° \leq \theta \leq 90°$, whilst if preferentially wetted by the oil (i.e. hydrophobic, $\gamma_{po} < \gamma_{pw}$) the contact angle will be $90° \leq \theta \leq 180°$,[32] this is represented diagrammatically in Figure 2.11.

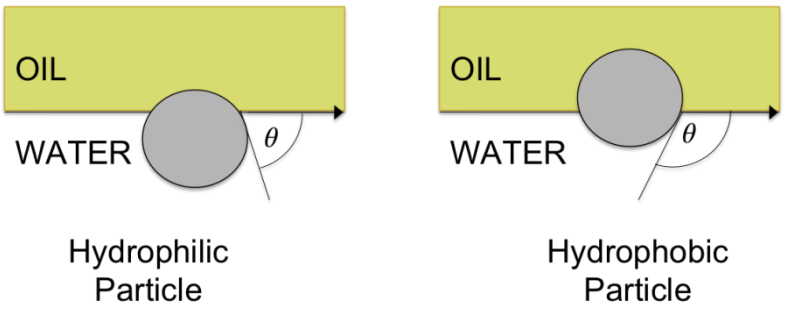

Figure 2.11. Illustration of the position made by a particle at a planar oil-water interface for a contact angle, θ, measured through the water phase to distinguish nature of particle.

The position of the particles at the interface of an particle stabilised emulsion is illustrated in Figure 2.12.[10]

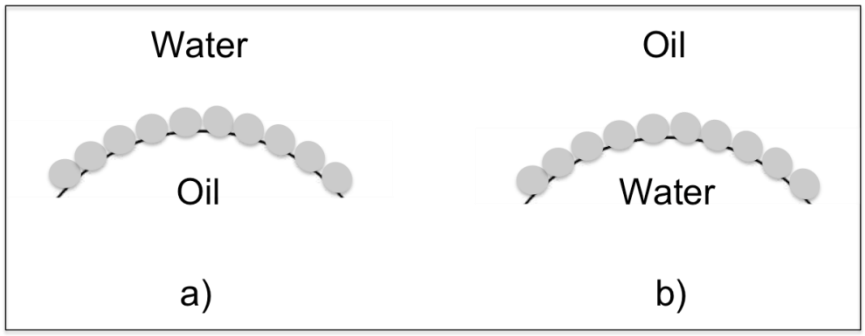

Figure 2.12. Illustration of particle stabilised emulsion droplet; a) O/W emulsion and b) W/O emulsion. *Redrawn from Ref. [10]*.

In particle stabilised emulsions there are at least two mechanisms of stabilisation.[33] In the first mechanism, the particles are required to adsorb to the liquid-liquid interface and remain there forming a dense film around the droplet, to impede coalescence by acting as a mechanical barrier. The second mechanism is the development of a 3-dimensional network of particles in the continuous phase which surrounds the droplet and adds additional stability to the emulsion droplet. It has been shown that with particle stabilised emulsions, even millimetre sized droplets can be stable to coalescence.[34]

A third mechanism by which colloidal stability can be achieved is via steric stabilisation. This arises from the presence of large molecules (polymers) adsorbed or grafted onto the particle surface.[35] When two particles meet the adsorbed layer of polymer on the particles are compressed that reduces the entropy (i.e. $\Delta S < 0$, assuming that the change in enthalpy, ΔH is negligible) causing an increase in the overall Gibbs free energy, ΔG. When the distance between the colloids is less than the thickness of the polymer layer, the reduction in thickness produces a repulsive force, increasing the overall Gibbs free energy (Equation 2.10).[36]

$$dG = dH - TdS > 0 \qquad \text{(Equation 2.10)}$$

2.4. Colloidal particles vs. surfactants as emulsifiers

One of the main advantages in using particles over surfactants as emulsifiers, is that the particles achieve high attachment energies to the interface and once adsorbed they are effectively irreversibly adsorbed.[37] Surfactants on the other hand continually and rapidly adsorb to and desorb from the interface. It should be noted that both the particle size and contact angle will influence the energy of attachment achieved, as very small particles do not attach as strongly as larger ones. This is highlighted by equation 2.11 that shows the influence of both particle size and contact angle on the energy needed to remove particles from the interface.

$$\Delta G_d = \pi r^2 \gamma_{ow} (1 \pm \cos\theta)^2 \qquad \text{(Equation 2.11)}$$

where ΔG_d is the free energy of detachment, r the particle radius, γ is the interfacial tension between phases and *cos* θ is the contact angle made with the interface. The sign for the *cos* θ in the brackets is taken as negative for removal of particles into water and positive for removal into oil.[38]

The effect of particle radius on the energies required for particle detachment, from a planar liquid-liquid interface (with an interfacial tension of 24.9 mN m^{-1}) is illustrated in Figure 2.13.[38] It shows clearly that particle sizes of less than 0.5 nm in radius can be easily detached with energies of a few *kT* (where *k* is the Boltzmann constant, that relates the absolute temperature, *T*, and the kinetic energy contained in each molecule of an ideal gas). This is comparable to surfactant systems and may not be very effective stabilisers. For a particle radius of 10 nm it is clear from the figure that the energy required for detachment is large around 10,000 *kT*. It also highlights that at large particle radii the contact angle is less critical for effective adsorption and the energies required for detachment are very high and hence the particles are effectively irreversibly adsorbed.[38]

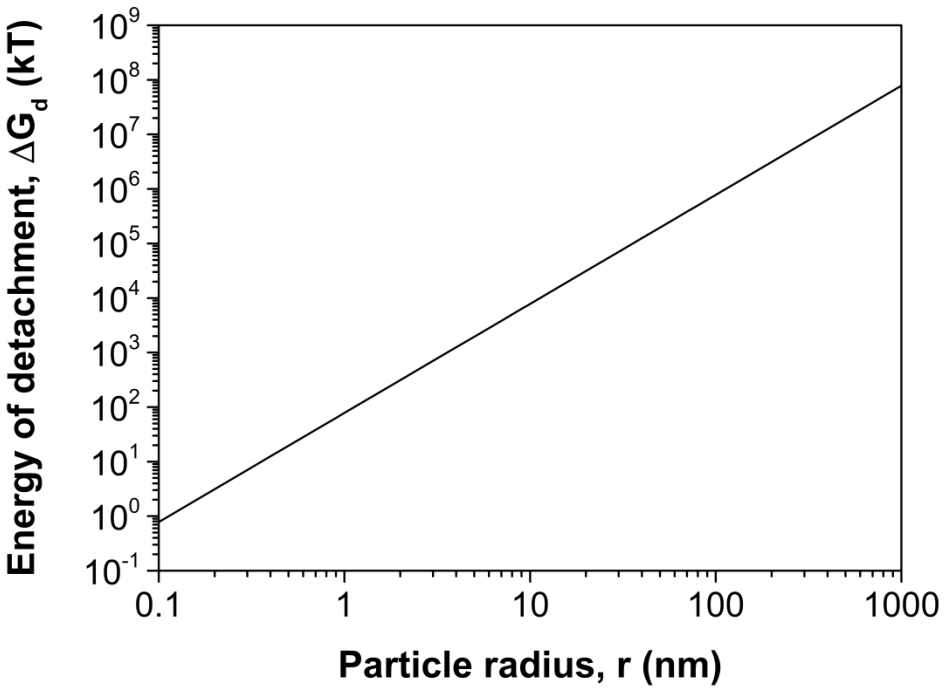

Figure 2.13. Illustrating the variations in energies required to detach a particle exhibiting a contact angle of 90°, from a planar oil-water interface. The interfacial tension value is taken as 24.9 mN m^{-1}. *Redrawn and adapted from Ref. [38]*.

The effect of particle contact angle on the free energy of particle detachment from an oil-water interface is illustrated in Figure 2.14.[39] The plot shows that the energies of detachment into water is much smaller than into the oil for an particle preferentially dispersed in water, whilst the values are higher for water than oil when the particle is preferentially dispersed in oil. The line drawn on the plot shows that free energy of detachment is highest at 90°, corresponding to the state where the particle is wetted by both the oil and water phases. Either side of 90°, the energies of detachment decrease towards 0 *kT*. These data are on the basis of a particle radius of 800 nm at an interface which has a tension of 24.9 mN m^{-1} (similar to the silica particles at the tricaprylin/water interface reported in Chapter 7).

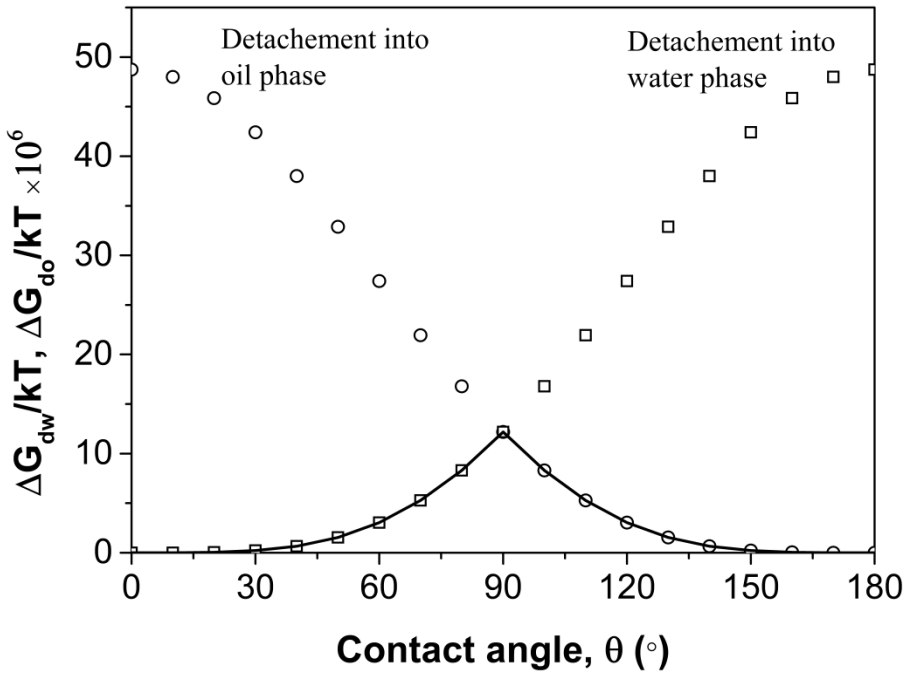

Figure 2.14. Illustrating the free energy of particle detachment of 800 nm particles into the water phase, ΔG_{dw} (squares) and oil phase, ΔG_{do} (circles), with an interfacial tension of 24.9 mN m^{-1}. The line is drawn to denote ΔG_d as per Equation 2.7. *Redrawn and adapted from Ref. [39]*.

A further advantage of using particulates as emulsifiers is that they can be further manipulated by adding a degree of functionality to their surface. For example, particles can be sterically stabilised with a polymer on the surface that is responsive to external stimuli such as pH, temperature and/or light. Such 'smart' emulsifiers can then be used as building blocks to prepare novel materials such as colloidosome microcapsules[40] and liquid marbles etc.[41]

2.5. Production of Emulsions

The production of emulsions can be classified as a) conventional (where high shear and high-energy input is required) b) membrane based processing (membrane emulsification, which will be discussed in greater detail in Chapter 3), c) microchannel and microfluidic emulsification. These processes will be discussed in detail in the following sub-sections.

2.5.1. Conventional production processes

Conventional productions of emulsions in industry are based on a large input of energy via mechanical processes, breaking down one of the liquid phases into small droplets within the other phase. These emulsions are produced using rotor stator machines, high pressured homogenizers and ultrasonic devices and are illustrated in Figure 2.15.[42, 43]

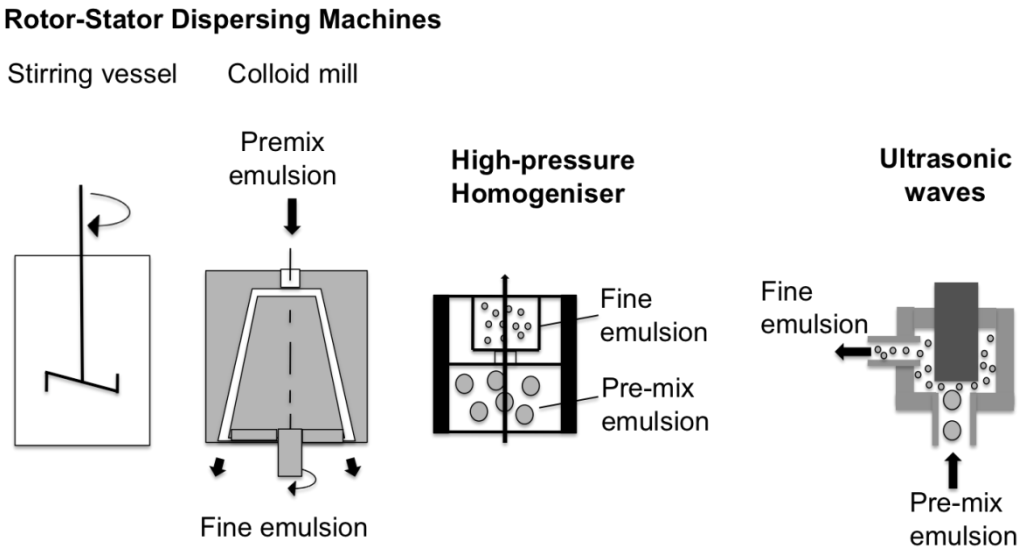

Figure 2.15. Illustration of conventional processes to produce emulsions. *Redrawn from Refs. [42 and 43]*.

Rotor-stator dispersing machines comprise of both a rotating as well as a fixed part. Stirred vessels are the simplest examples of rotor-stator machines and are used to

produce emulsions usually in batches or semi-continuously. The formation of the dispersed droplets is caused by fluid disruption due to turbulent eddies generated between the rotor and stator.[7] Although it is commonly used in the food industry it has a number of drawbacks. The efficiency is poor and this leads to long emulsification times and broad droplet size distributions. These drawbacks are addressed and improved in colloid mills and tooth disc dispersing machines.[43]

In colloid mills the emulsion is disrupted in a conical gap by the rotor and stator which can be either smooth, toothed or grooved. The disruption is controlled by adjusting the rotational speed, gap width and the flow rates.[42] In toothed disc dispersing machines the rotor and stator have one or multiple discs that have teeth of various designs. They have low maintenance cost and are easy to handle.[43]

High pressure homogenizers as well as pistons can be used to pump premix emulsions through a narrow orifice under very high pressure. The pump generates energy which enables the nozzle to disintegrate the droplets and can handle throughputs of 1 to 1000 L hr^{-1}.[42, 43] The design of the nozzle influences the flow patterns of the emulsion entering and this helps to disintegrate the droplets.[44] The disruption of the droplets is due to inertial forces acting in the turbulent flow and shear forces in the laminar flow.

In ultrasonic methods, waves (frequency > 18 kHz) disrupt the droplets by cavitations in a high turbulence zone. This method is used to prepare low viscous emulsions batch-wise and produces fine emulsion droplets. To produce droplets continuously, necessary modifications resulting in the addition of a flow chamber of a special design is needed into which the ultrasonic waves propagate. This method has drawbacks as the power induced is limited and suffers from technical limits for very high throughputs.[43]

2.5.2. Microchannel emulsification

Microchannel (MC) emulsification was developed in the 1990's and utilizes devices fabricated by lithography. The devices are primarily existent in two forms, 1) MC array device (consisting of comb like channel arrays, which are micron sized, on a silicon chip), 2) straight through MC device (consisting of tens of thousands of pores with oblong cross sections).[45]

The MC array device also consists of a terrace and a well (Figure 2.16)[46, 47] which is sealed using a glass plate when being used. The disperse phase is pushed through the arrays and forms individual flattened barrels in the terrace area.[46] When the flattened barrels develop near the edge of the terrace, they inflate into the well forming monodisperse droplets. The sizes and size distribution attained are governed by the channel size, shape, width, height of terrace and the interfacial tension of the emulsion system.

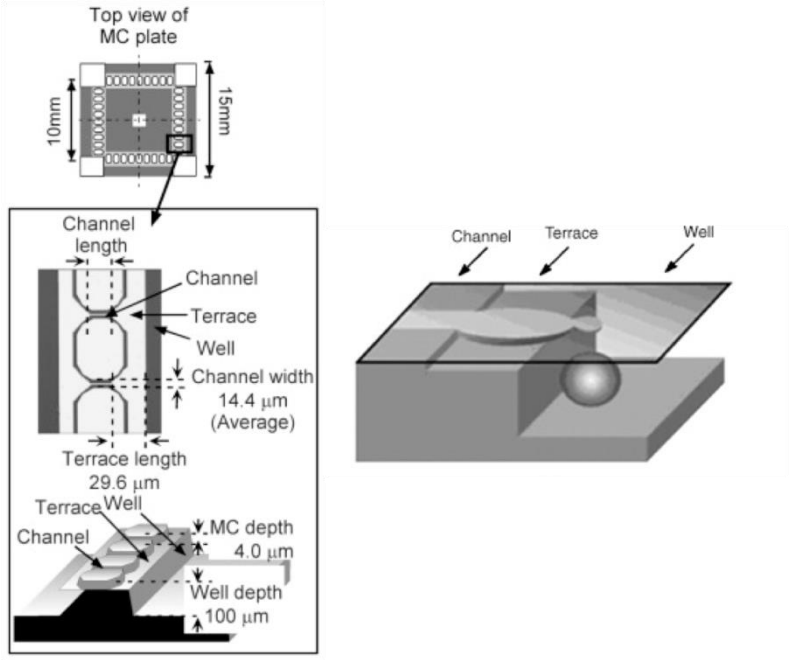

Figure 2.16. Illustration of a microchannel plate composing of a channel, terrace and well. *Taken from Refs. [46 and 47].*

The surface hydrophilicity of the channel is very important.[48] MC plates that are hydrophobic will produce W/O emulsions, whereas hydrophilic ones will produce O/W emulsions. Therefore the right materials need to be chosen for the specific emulsion system required. MC plates so far have been made of different materials including silicon, quartz glass and stainless steel.[49] The device can produce emulsions in the range of 4-190 μm with a coefficient of variation (CV) (ratio of the standard deviation and the mean) values of less than 5%.

In straight through MC emulsification devices the MC plate consists of thousands of uniformly sized channels and terrace lines fabricated usually onto silicon. The

emulsification process does not require any mechanical stress to make the droplets.[50] Rather the process is based on spontaneous transformation of the dispersed phased through the channel due to effects of interfacial tension.[51] A typical straight through MC emulsification device is shown in Figure 2.17.[50]

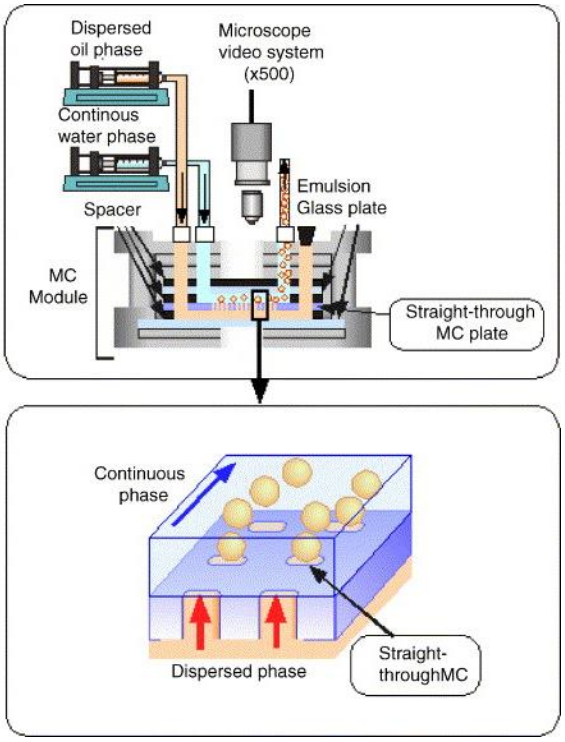

Figure 2.17. Typical straight through MC emulsification device. *Taken from Ref. [50]*.

Although microchannel emulsification can produce emulsion droplets with good control over their droplet size and size distributions. They are regarded to be highly sophisticated and expensive technologies because of the high precision needed in fabricating such devices. Furthermore, these emulsification techniques produce very low flux of the dispersed phase and therefore question marks remain over their scalability.

2.5.3. Microfluidic emulsification

Microfluidic devices allow the production of monodispersed emulsion droplets in a drop by drop manner allowing careful and precise manufacturing.[52] This method of

emulsification is so far an academic exercise and that despite its large advantages, it is limited to the production of small volumes which restricts its application. These devices can be defined as a microfluidic where one or more of the channels have at least one dimension less than a millimeter.[53] Such devices can be manufactured as 2D or 3D systems. 2D systems have been intensively studied where the channel is confined to uniform depths, e.g. t-junctions,[54-57] cross-junctions,[58-60] flow focusing channels,[51-64] and co flow channels.[55, 65-67] Monodisperse emulsion droplets are achieved by flowing the dispersed and continuous phases under low Reynolds (measure of the ratio of inertial forces to viscous forces) and capillary (relative effect of the viscous forces versus interfacial tension at an interface) numbers with coefficients of variation (CV) values of 1 - 3%. The production of these droplets using a microfluidic device with t-junctions is shown in Figure 2.18.[45]

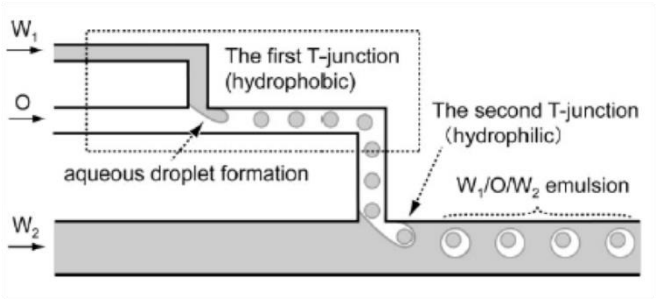

Figure 2.18. Illustrating the production of monodisperse emulsion droplets (Water/Oil/Water, W/O/W) from microfluidic devices containing two t-junctions. *Taken from Ref. [45]*.

Common types of microfluidic devices used are; 1) soft microfluidic devices fabricated by soft lithography in elastomeric materials such as poly(dimethyl siloxane) (PDMS),[68] 2) microfluidic glass devices manufactured by etching or micromachining in quartz glass or glassy polymers such as poly(methyl methacrylate) (PMMA),[65] 3) microchannel (MC) array devices fabricated in single crystal silicon by photolithography and wet-etching or deep-reactive ion etching processing.[69]

Emulsions can also be created using microfluidics capillaries[52] where the device consists of coaxial assemblies of glass capillaries on glass slides. The advantage of using capillaries is that their wettability can be controlled by modifying the surface using reagents to change hydrophobic glass into hydrophilic and vice versa. To set

up a simple microfluidic capillary device, a circular glass capillary is slid into a square capillary. Then two liquids are introduced within the circular capillary and the square capillary, respectively, as shown in Figure 2.19.[52] Since the direction of both fluids is the same, this is known as a co-flow microfluidic capillary device.

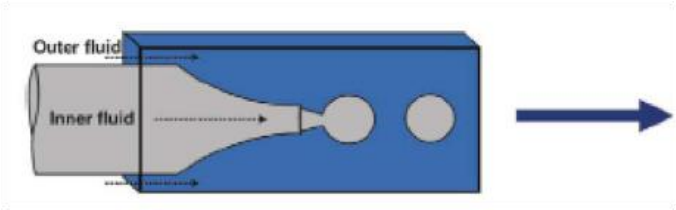

Figure 2.19. Schematic illustration of a co-flow microfluidic capillary device. *Taken from Ref. [52]*.

When the flow rates of both fluids are low, monodisperse droplets form periodically from the tip of the orifice.[70] Once the flow rate is increased above a critical value the flow at the tip becomes a jet and produces droplets later downstream as shown in Figure 2.20.[52]

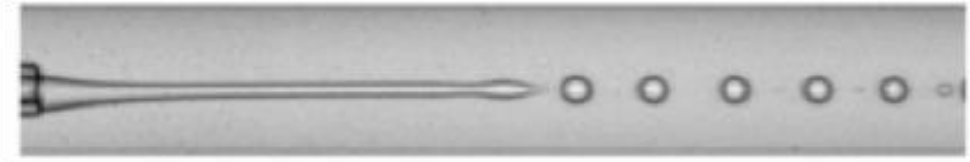

Figure 2.20. Illustration of a jet stream formed by increasing the flow rate of the continuous phase above a critical value, whilst keeping the dispersed phase at a constant rate in a microfluidic capillary. *Taken from Ref. [52]*.

An alternative arrangement is to use a flow focusing microfluidic capillary device[70, 71] as shown in Figure 2.21.[52] Both the fluids are introduced from opposite ends within the square capillary. The inner fluid becomes flow focused by the outer fluid into the narrow orifice of the circular capillary. An advantage of using this setup is that the droplets formed can be smaller than the orifice typically 1-5 μm.[52]

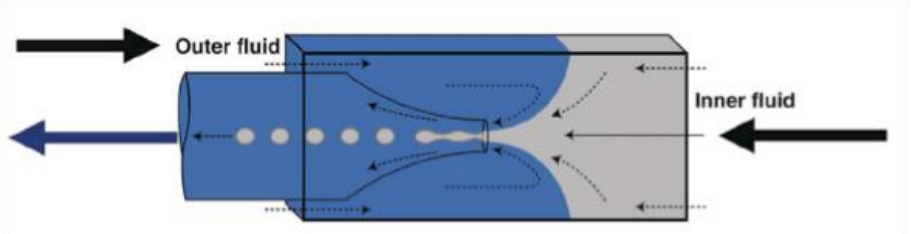

Figure 2.21. Schematic illustration of a flow focused microfluidic capillary device. *Taken from Ref. [52]*.

In addition to producing emulsion droplets, microfluidic devices have also been used for fabrication of polymeric particles such as solid liquid microspheres,[72] Janus particles,[66] and core shell particles.[73]

2.5.4. Membrane emulsification

In membrane emulsification a force in the form of low pressure pushes the disperse phase through a membrane into the continuous phase. Although advances have been made in emulsification using membrane devices, the full exploitation of their benefits are limited due to the irregularities in the microstructure and surface properties of current membranes.[74] Membrane emulsification techniques utilise a low dispersed phase flux through the membrane. In addition membrane fouling from particulates and the adsorption of species can lead to blocked membrane pores and changes in the wetting properties of the membrane. However, it is superior in comparison to the conventional counterparts as it results in highly monodisperse droplets created with low levels of energy input, which can easily be scaled up for large scale manufacturing with the addition of more membranes to the setup.

References

1. B. P. Binks, A. K. F. Dyab and P. D. I. Fletcher, Novel emulsions of ionic liquids stabilised solely by silica nanoparticles, *Chem. Commun.*, 2003, 2540-2541.
2. R. Brummer, ed., *Rheology Essentials of Cosmetic and Food Emulsions*, Springer, Berlin, 2006.
3. F. Nielloud and G. Marti-Mestres, *Pharmaceutical Emulsions and Suspensions*, Marcel Dekker, New York, 2000.
4. C. Charcosset, I. Limayem and H. Fessi, The membrane emulsification process - a review, *J. Chem. Technol. Biotechnol.*, 2004, **79**, 209-218.
5. L.-Y. Chu, A. S. Utada, R. K. Shah, J.-W. Kim and D. A. Weitz, Controllable monodisperse multiple emulsions, *Angew. Chem., Int. Ed.*, 2007, **46**, 8970-8974.
6. H. J. Neumann and B. Paczyńska-Lahme, Petroleum emulsions, micro-emulsions, and micellar solutions, In: *Dispersed Systems*, eds. K. Hummel and J. Schurz, Springer, Berlin, 1988, vol. 77, 123-126.
7. P. Walstra, Principles of emulsion formation, *Chem. Eng. Sci.*, 1993, **48**, 333-349.
8. J. N. Israelachvili, ed., *Intermolecular and Surface Forces*, Academic Press, New York, 1992.
9. D. J. McClements, ed., *Food emulsions: Principles, Practice, and Techniques*, CRC Press, Florida, 1999.
10. E. Dickinson, ed., *An Introduction to Food Colloids*, Oxford University Press, Oxford, 1992.
11. R. Chanamai and D. J. McClements, Dependence of creaming and rheology of monodisperse oil-in-water emulsions on droplet size and concentration, *Colloids Surf. A: Physicochem. Eng. Asp.*, 2000, **172**, 79-86.
12. P. Ghosh, ed., Colloid and Interface Science, Phi Learning, New Delhi, 2009.
13. E. Dickinson and R. Miller, eds. *Food Colloids: Fundamentals of Formulation*. Vol. 258. Royal Society of Chemistry, Cambridge, 2001.
14. N. Bremond, A. R. Thiam and J. Bibette, Decompressing Emulsion Droplets Favors Coalescence, *Phys. Rev. Lett.*, 2008, **100**, 24501-24505.
15. D. J. Shaw, ed., *Introduction to Colloid and Surface Chemistry*, Butterworth-Heinemann, London, 1992.

16. A. B. Pawar, M. Caggioni, R. Ergun, R. W. Hartel and P. T. Spicer, Arrested coalescence in Pickering emulsions, *Soft Matter*, 2011, **7**, 7710-7716.
17. K. Boode, P. Walstra and A. E. A. de Groot-Mostert, Partial coalescence in oil-in-water emulsions, 2. Influence of the properties of the fat, *Colloids Surf. A: Physicochem. Eng. Asp.*, 1993, **81**, 139-151.
18. A. S. Kabalnov and E. D. Shchukin, Ostwald ripening theory: applications to fluorocarbon emulsion stability, *Adv. Colloid Interface Sci.*, 1992, **38**, 69-97.
19. I. Capek, Degradation of kinetically-stable o/w emulsions, *Adv. Colloid Interface Sci.*, 2004, **107**, 125-155.
20. D. Lu and D. G. Rhodes, Mixed composition films of spans and tween 80 at the air-water interface, *Langmuir*, 2000, **16**, 8107-8112.
21. W. C. Griffin, Calculation of HLB values of non-ionic surfactants, *J. Soc. Cosmet. Chem.*, 1954, **5**, 249-256.
22. J. T. Davies, A quantitative kinetic theory of emulsion type, I. Physical chemistry of the emulsifying agent, *Proc. Int. Cong. Surface Activ.*, 1957, 426-438.
23. W. D. Bancroft, Theory of emulsification, *J. Phys. Chem.*, 1913, **17**, 501-519.
24. B. P. Binks, Emulsions, *Annual Reports Progr. Chem., Sect. C*, 1995, **92**, 97-134.
25. T. J. Lin, Surfactant location and required HLB, *J. Soc. Cosmet. Chem.*, 1970, **21**, 365-375.
26. G. L. Hasenhuettl and R. W. Hartel, eds., *Food Emulsifiers and Their Applications*, Chapman & Hall, New York, 1997.
27. J. L. Salager, ed., Surfactants: types and uses. Version 2, Universidad De Los Andes, Merida-Venezuela, 2002
28. B. Derjaguin and L. Landau, The theory of stability of highly charged lyophobic sols and coalescence of highly charged particles in electrolyte solutions, *Acta Physicochim. URSS*, 1941, **14**, 633-652.
29. E. Verwey and J. T. G. Overbeek, *Theory of the stability of lyophobic colloids*, Elsevier, Amsterdam, 1948.
30. H. Hamaker, The London-van der Waals attraction between spherical particles, *Physica*, 1937, **4**, 1058-1072.

31. M. Elimelech, J. Gregory, X. Jia and R. A. Williams, eds., *Particle Deposition and Aggregation: Measurement, Modelling, and Simulation*, Butterworth-Heinemann, Oxford, 1998.
32. B. P. Binks and T. S. Horozov, eds., *Colloidal Particles at Liquid Interfaces*, Cambridge University Press, Cambridge, 2006.
33. R. Aveyard, B. P. Binks and J. H. Clint, Emulsions stabilised solely by colloidal particles, *Adv. Colloid Interface Sci.*, 2003, **100-102**, 503-546.
34. X. Zhai and S. Efrima, Chemical and Physical Aspects of Macroemulsions Stabilized by Interfacial Colloids, *J. Phys. Chem.*, 1996, **100**, 11019-11028.
35. D. H. Napper, ed., *Polymeric Stabilization of Colloidal Dispersions*, Academic Press, London, 1983.
36. C. D. Anderson and E. S. Daniels, eds., *Emulsion Polymerisation and Latex Applications*, Vol. 14, Smithers Rapra Technology, 2003.
37. B. P. Binks and C. P. Whitby, Silica particle-stabilized emulsions of silicone oil and water: aspects of emulsification, *Langmuir*, 2004, **20**, 1130-1137.
38. B. P. Binks, Particles as surfactants-similarities and differences, *Curr. Opin. Colloid Interface Sci.*, 2002, **7**, 21-41.
39. B. P. Binks and T. S. Horozov, Particles at Liquid Interfaces: An Introduction, In: *Colloidal Particles at Liquid Interfaces,* eds. B. P. Binks and T. S. Horozov, Cambridge University Press, Cambridge, 2006.
40. Q. Yuan, O. J. Cayre, S. Fujii, S. P. Armes, R. A. Williams and S. Biggs, Responsive core-shell latex particles as colloidosome microcapsule membranes, *Langmuir*, 2010, **26**, 18408-18414.
41. G. McHale and M. I. Newton, Liquid marbles: Principles and applications, *Soft Matter*, 2011, **7**, 5473-5481.
42. H. Karbstein and H. Schubert, Developments in the continuous mechanical production of oil-in-water macro-emulsions, *Chem. Eng. Process.*, 1995, **34**, 205-211.
43. H. P. Schuchmann and H. Schubert, Product design in food industry using the example of emulsification, *Eng. Life Sci.*, 2003, **3**, 67-76.
44. M. Stang, H. Schuchmann and H. Schubert, Emulsification in high-pressure homogenizers, *Eng. Life Sci.*, 2001, **1**, 151-157.
45. T. Nisisako, Microstructured devices for preparing controlled multiple emulsions, *Chem. Eng. Technol.*, 2008, **31**, 1091-1098.

46. Q. Yuan and R. A. Williams, Large scale manufacture of magnetic polymer particles using membranes and microfluidic devices, *Particuology*, 2007, **5**, 26-42.

47. S. Sugiura, M. Nakajima, T. Oda, M. Satake and M. Seki, Effect of interfacial tension on the dynamic behaviour of droplet formation during microchannel emulsification, *J. Colloid Interface Sci.*, 2004, **269**, 178-185.

48. T. Kawakatsu, G. Trägårdh and C. Trägårdh, Production of W/O/W emulsions and S/O/W pectin microcapsules by microchannel emulsification, *Colloids Surf. A: Physicochem. Eng. Asp.*, 2001, **189**, 257-264.

49. G. T. Vladisavljević and R. A. Williams, Recent developments in manufacturing particulate products from double emulsion templates using membrane and microfluidic devices, In: *Multiple Emulsions: Technology and applications*, ed. A. Aserin, Wiley, New Jersey, 2007, 121-164.

50. I. Kobayashi, M. Nakajima and S. Mukataka, Preparation characteristics of oil-in-water emulsions using differently charged surfactants in straight-through microchannel emulsification, *Colloids Surf. A: Physicochem. Eng. Asp.*, 2003, **229**, 33-41.

51. S. Sugiura, M. Nakajima, S. Iwamoto and M. Seki, Interfacial tension driven monodispersed droplet formation from microfabricated channel array, *Langmuir*, 2001, **17**, 5562-5566.

52. R. K. Shah, H. C. Shum, A. C. Rowat, D. Lee, J. J. Agresti, A. S. Utada, L.-Y. Chu, J.-W. Kim, A. Fernandez-Nieves, C. J. Martinez and D. A. Weitz, Designer emulsions using microfluidics, *Mater. Today*, 2008, **11**, 18-27.

53. G. T. Vladisavljević, I. Kobayashi and M. Nakajima, Generation of highly uniform droplets using asymmetric microchannels fabricated on a single crystal silicon plate: Effect of emulsifier and oil types, *Powder Technol.*, 2008, **183**, 37-45.

54. T. Thorsen, R. W. Roberts, F. H. Arnold and S. R. Quake, Dynamic pattern formation in a vesicle-generating microfluidic device, *Phys. Rev. Lett.*, 2001, **86**, 4163-4166.

55. T. Nisisako, T. Torii and T. Higuchi, Droplet formation in a microchannel network, *Lab Chip*, 2002, **2**, 24-26.

56. D. R. Link, S. L. Anna, D. A. Weitz and H. A. Stone, Geometrically mediated breakup of drops in microfluidic devices, *Phys. Rev. Lett.*, 2004, **92**, 054503.

57. J. H. Xu, G. S. Luo, S. W. Li and G. G. Chen, Shear force induced monodisperse droplet formation in a microfluidic device by controlling wetting properties, *Lab Chip*, 2006, **6**, 131-136.

58. R. Dreyfus, P. Tabeling and H. Willaime, Ordered and disordered patterns in two-phase flows in microchannels, *Phys. Rev. Lett.*, 2003, **90**, 144505.

59. B. Zheng, J. D. Tice and R. F. Ismagilov, Formation of droplets of alternating composition in microfluidic channels and applications to indexing of concentrations in droplet-based assays, *Anal. Chem.*, 2004, **76**, 4977-4982.

60. L.-H. Hung, K. M. Choi, W.-Y. Tseng, Y.-C. Tan, K. J. Shea and A. P. Lee, Alternating droplet generation and controlled dynamic droplet fusion in microfluidic device for CdS nanoparticle synthesis, *Lab Chip*, 2006, **6**, 174-178.

61. S. L. Anna, N. Bontoux and H. A. Stone, Formation of dispersions using "flow focusing" in microchannels, *Appl. Phys. Lett.*, 2003, **82**, 364-366.

62. Q. Xu and M. Nakajima, The generation of highly monodisperse droplets through the breakup of hydrodynamically focused microthread in a microfluidic device, *Appl. Phys. Lett.*, 2004, **85**, 3726-3728.

63. P. C. Lewis, R. R. Graham, Z. Nie, S. Xu, M. Seo and E. Kumacheva, Continuous Synthesis of Copolymer Particles in Microfluidic Reactors, *Macromolecules*, 2005, **38**, 4536-4538.

64. H. Zhang, E. Tumarkin, R. Peerani, Z. Nie, R. M. A. Sullan, G. C. Walker and E. Kumacheva, Microfluidic production of biopolymer microcapsules with controlled morphology, *J. Am. Chem. Soc.*, 2006, **128**, 12205-12210.

65. S. Okushima, T. Nisisako, T. Torii and T. Higuchi, Controlled production of monodisperse double emulsions by two-step droplet breakup in microfluidic devices, *Langmuir*, 2004, **20**, 9905-9908.

66. T. Nisisako, T. Torii, T. Takahashi and Y. Takizawa, Synthesis of monodisperse bicolored Janus particles with electrical anisotropy using a microfluidic co-flow system, *Adv. Mater.*, 2006, **18**, 1152-1156.

67. T. Nisisako and T. Torii, Formation of biphasic Janus droplets in a microfabricated channel for the synthesis of shape-controlled polymer microparticles, *Adv. Mater.*, 2007, **19**, 1489-1493.

68. Y. Xia and G. M. Whitesides, Soft Lithography, *Annu. Rev. Mater. Sci.*, 1998, **28**, 153-184.

69. T. Kawakatsu, Y. Kikuchi and M. Nakajima, Regular-sized cell creation in microchannel emulsification by visual microprocessing method, *J. Am. Oil Chem. Soc.*, 1997, **74**, 317-321.

70. A. S. Utada, L. Y. Chu, A. Fernandez-Nieves, D. R. Link, C. Holtze and D. A. Weitz, Dripping, jetting, drops, and wetting: The magic of microfluidics, *MRS Bull.*, 2007, **32**, 702-708.

71. A. M. Gañán-Calvo and J. M. Gordillo, Perfectly monodisperse microbubbling by capillary flow focusing, *Phys. Rev. Lett.*, 2001, **87**, 274501.

72. S. Sugiura, M. Nakajima, J. Tong, H. Nabetani and M. Seki, Preparation of monodispersed solid lipid microspheres using a microchannel emulsification technique, *J. Colloid Interface Sci.*, 2000, **227**, 95-103.

73. S. Peng, M. Zhang, X. Niu, W. Wen, P. Sheng, Z. Liu and J. Shi, Magnetically responsive elastic microspheres, *Appl. Phys. Lett.*, 2008, **92**, 012108.

74. H. S. Ribeiro, J. J. M. Janssen, I. Kobayashi and M. Nakajima, Membrane Emulsification in Food Applications, In: *Membrane Technology: Volume 3: Membranes for Food Applications*, eds. K.-V. Peinemann, S. P. Nunes, L. Giorno, Wiley-VCH, Weinheim, 2011.

CHAPTER 3: PRINCIPLES OF MEMBRANE EMULSIFICATION

NOMENCLATURE

d_p	Pore diameter
F	Force
J_d	Disperse phase flux
K	Permeability
P_c	Critical permeation pressure
$P_{c,\,in}$	Mean pressure of continuous phase at membrane pore inlet
$P_{c,\,out}$	Mean pressure of continuous phase at membrane pore outlet
P_d	Mean pressure of dispersed phase
P_{tm}	Transmembrane pressure
γ	Interfacial tension
μ	Dynamic viscosity
θ	Contact angle

ABBREVIATIONS

ME	Membrane Emulsification
PECVD	Plasma Enhanced Chemical Vapour Deposition
PGPR	Poly(glycerol polyricinoleate)
PTFE	Poly(tetrafluorothylene)
RME	Rotary Membrane Emulsification
SDS	Sodium Dodecyl Sulphate
SPG	Shirasu Porous Glass
XME	Cross-flow Membrane Emulsification

3.1. Introduction

Conventional processes for the manufacturing of emulsions are based on the use of turbulent eddies and cavity formations to disrupt the two immiscible liquids to produce dispersions of fine droplets of one liquid into the other.[1] These methods face numerous problems during large scale manufacturing. In large vessels, eddies cannot be generated and controlled consistently over a large period of time, which limits the control achieved on the produced emulsion mean droplet size and size distribution.[2] Additionally, emulsions produced using this technique are unlikely to be consistently reproduced from batch to batch due to the in-homogeneity in the process. Furthermore, these processes are energetically costly, which therefore leads to high manufacturing costs.

In order to overcome some of these limitations, an alternative technique called 'membrane emulsification' (ME) was developed in the late 1980's. This technique made use of either Shirasu Porous Glass membranes (SPG, made from Shirasu a type of volcanic ash, lime and boric acid), developed by Nakashima and Shimizu,[3] or ceramic tubular membranes, developed by Williams *et al*.[4] Highly droplet size uniform O/W and W/O emulsions can be produced using this method, where the dispersed phase is expressed from the membranes into the continuous phase. In this technique a membrane with an extensive array of pores is required for the simultaneous production of a large number of droplets to ensure a meaningful emulsification rate.[5] The dispersed phase is usually permeated through the membrane under an applied pressure and is expressed in a drop-by-drop manner from the pores of the membrane into the continuous phase as illustrated by Figure 3.1. In addition, the continuous phase is sheared across the membrane surface to facilitate droplet detachment.

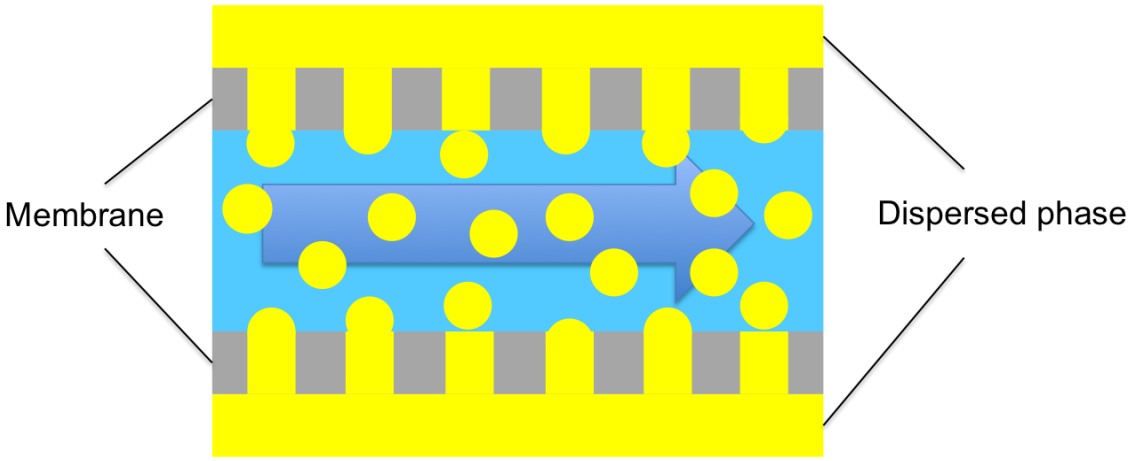

Figure 3.1. Schematic illustration of the membrane emulsification process. The arrow illustrates the direction in which the continuous phase flows across the membrane surface (cross flow). *Redrawn from Ref. [4]*.

By careful selection of the porous membrane and optimisation of the flux rate of dispersed phase and cross-flow velocity of the continuous phase, the mean droplet size and size distribution can be carefully controlled.[2] Under certain conditions, this approach allows for the production of emulsions with very narrow droplet size distributions[6, 7] and potentially near monodisperse emulsions.[8] In addition the ME process requires a low energy input (typically 10^4 – 10^6 Jm^{-3} compared with 10^6 – 10^9 Jm^{-3} for conventional production processes) and the apparent shear stress is far lower in comparison to its conventional counterparts.[6-8] Here, droplets are formed individually by a drop-by-drop permeation of the dispersed phase through the membrane and not by attrition of larger droplets under high shear.

In the literature, the ME methods reported so far are of two types; direct ME and premix ME as depicted by Figure 3.2.[9]

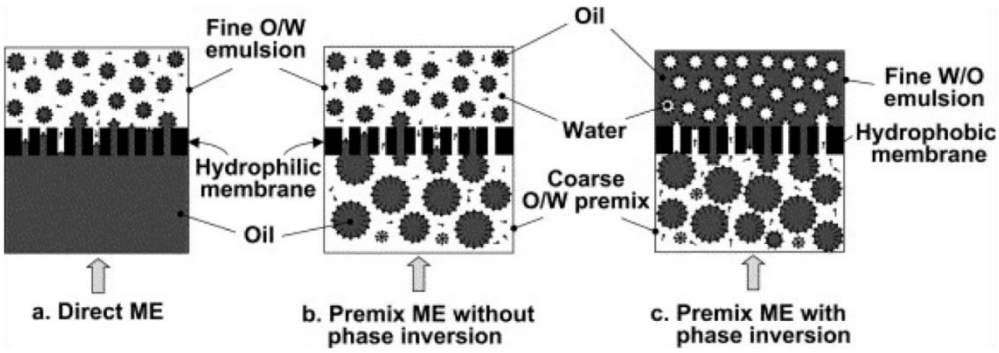

Figure 3.2. Illustrating emulsion production using direct and premix membrane emulsification methods. *Taken from Ref. [9]*.

In direct ME the dispersed phase is pressed through the membrane forming fine droplets at the membrane/continuous phase interface as illustrated by Figure 3.2a. Regular droplet detachment is facilitated by relatively low shear stresses acting at the membrane/continuous phase interface. In literature, this shear stress is generated by one of three processes: a) recirculation of continuous phase using a pump known as crossflow ME[4, 10, 11] (Figure 3.3a), b) agitation in a stirring vessel[12, 13] (Figure 3.3b) and c) rotation[14, 16] or vibration[17, 18] of the membrane in a stationary continuous phase (Figure 3.3c). In the absence of shear, droplets can be spontaneously detached from pore outlets at very low disperse phase fluxes[19] (Figure 3.3d).

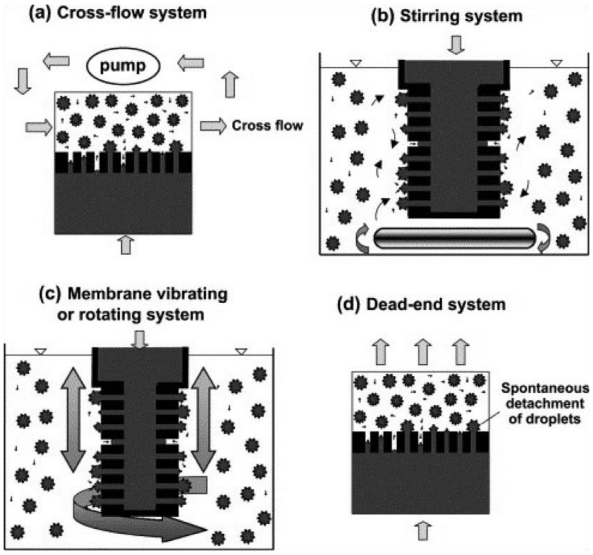

Figure 3.3. ME systems for controlling shear and hydrodynamic conditions near the membrane surface. *Taken from Ref [9]*.

3.2. Rotating Membrane Emulsification (RME)

The concept of inducing shear for droplet detachment due to the motion of the membrane itself, as opposed to the displacement of the continuous phase across the membrane surface has been investigated in recent years by three research groups.[19, 20, 21] The systems employed have many similarities and all three use tubular membranes that rotate within a vessel containing the continuous phase as depicted by Figure 3.4.

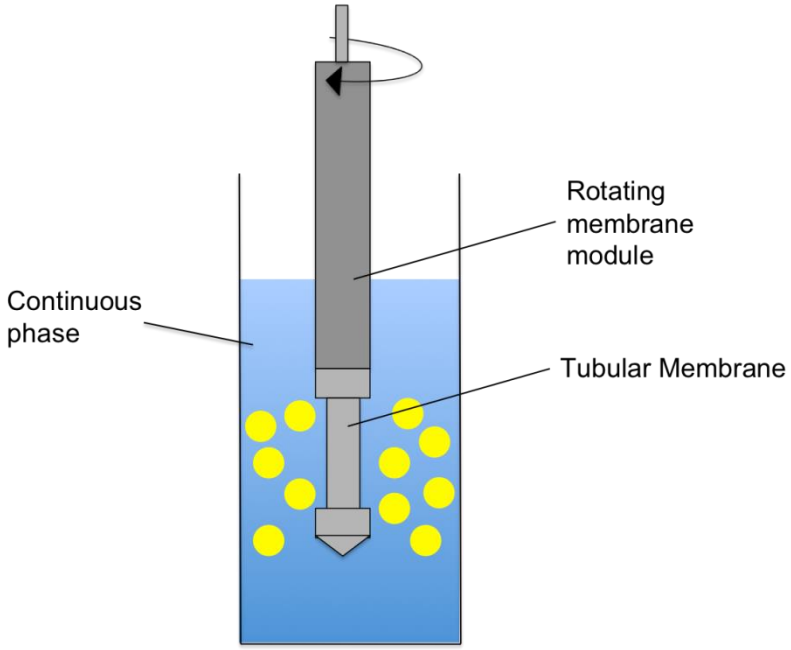

Figure 3.4. The basic principle and set-up of rotating membrane emulsification (RME). The rotating membrane module is connected to the tubular membrane allowing it to be rotated within a vessel containing the continuous phase. *Redrawn from Ref. [9]*.

In 2001, Williams patented a novel rotary membrane emulsification device developed at the University of Leeds for 'the production of controlled emulsions and particulate systems using membranes made from stainless steel, ceramic or a polymer film'.[14] The first published data using this rotary emulsification device was presented by Aryanti *et al.* at the "EUROMEMBRANE 2006" conference held in Italy.[20] A tubular membrane made of stainless steel with precise laser drilled holes was reported. The membrane was 10 mm in diameter and had a pore size of 100 µm in a regular square pore arrangement, so that the effective membrane area was 26.7

cm^2. The study investigated the production of paraffin wax droplets in water using two emulsifiers: Tween 20 (polyoxyethylene sorbitan monolaurate) and SDS (sodium dodecyl sulphate). Carbomer (a crosslinked polyacrylic acid polymer) was used in both cases as a stabiliser and a viscosity modifier. The rotating membrane was shown to be capable of producing monodisperse droplets with diameters ranging from 81 to 567 μm using both emulsifiers. Reported membrane rotational speeds varied from 0 to 1500 rpm and it was shown that the droplet diameter decreased with increasing membrane rotational speed, as expected.

This work was extended by Vladisavljević and Williams[16] in a later complementary study exploring the effects of rotational speed and apparent viscosity on the production of paraffin wax droplets in water. The emulsifier used in this case was Tween 20, whilst Carbomer was again used as a thickener. In this work, the droplet size was seen to decrease as the concentration of Carbomer increased, an effect attributed to the increase in the apparent viscosity of the continuous phase. They also reported that that an optimal membrane rotation speed of 350 rpm yielded droplet size uniformity when the concentration of the Carbomer was between 0.1 and 0.25 wt%. However when the rotation speed was increased to 1500 rpm, the droplets broke up producing satellite daughter droplets in the high shear conditions.

In rotational membrane emulsification, the centrifugal force due to the rotation of the membrane in the continuous phase acts alongside the shear induced at the membrane surface to drive droplet detachment.[19, 20] This causes droplets to detach faster from the membrane surface (i.e. at a smaller size) in comparison to simple dead-end or cross-flow emulsification systems at the same nominal shear rate across the membrane surface. In a shear rate range consistent with laminar flow, the shear applied at the membrane surface is constant and self-similar across the entire membrane surface. At higher shear rates, the flow is turbulent and the local shear rate varies across the membrane surface and over time. These constantly changing shear rates affect both the mean droplet size and the size distribution. Although there is no reported systematic investigation of these effects, it is postulated that droplet production in a turbulent regime will increase the polydispersity in the emulsion droplets created.[22]

In 2009, Yuan *et al.* investigated the performance of slotted pores in producing emulsion droplets using a stainless steel rotating membrane.[22] From previous studies

it has been shown that rectangular pores require less shear in comparison to round pores on flat membranes.[23, 24, 25, 26] In this publication, Yuan *et al.*[22] compared the production of paraffin wax oil droplets in water (Tween 20 as emulsifier and Carbomer as a thickening agent) to determine the performance of four slotted pores (laser drilled with different aspect ratios) in comparison with the round pore membrane that had been used in earlier studies from the same group.[20] The four slotted pores used in the study are described in Table 3.1.

Membrane	Pore size (µm)	Aspect ratio
A	80 × 80	1
B	56.5 × 113	2.3
C	48 × 136	3
D	136 × 48	3
Round pore	100	1

Table 3.1. Geometry data of the slotted pores used to compare performance versus round pores in rotating membrane emulsification. *Data taken from Ref. [22]*.

It was found that the droplets in emulsions produced using rectangular and square pores had lower size polydispersity than those from the equivalent round ones. However, the droplets were considerably larger due to the larger surface area.

In 2006, a new rotating membrane emulsification device for the production of droplets was presented at the 10th Aachen Membrane Colloquium.[19] The membrane was developed at Zurich, Switzerland, at the ETH Zentrum Laboratory of Food Process Engineering, by Professor Erich Windhab's group. A 100 mm diameter membrane tube with pore diameters of 1 to 5 µm was used.

The larger membrane studied within Windhab's group was manufactured by Stork Veco B.V. (Netherlands) with an aim of producing small monodisperse droplets using a larger membrane, by ensuring that the 'droplet history' of each droplet was as similar as possible. The membrane was made from an etched nickel foil sheet with equally spaced pores of around 5 µm in diameter. This diameter was further reduced to 1 µm using Plasma Enhanced Chemical Vapour Deposition (PECVD).[19] The membrane is inserted into a vessel that is marginally larger than the membrane

itself (Figure 3.5). The large membrane diameter is rotated at high speeds in a narrow annular gap specifically designed to create a high shear rate at the membrane surface whilst maintaining laminar flow with a consistent shear rate at each pore.

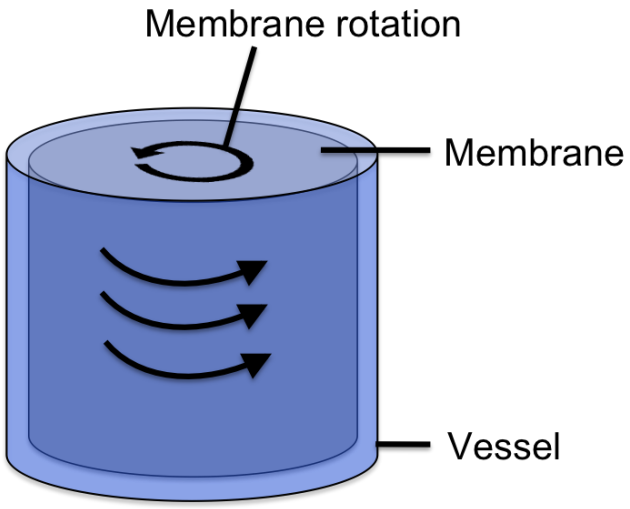

Figure 3.5. Illustration of rotating membrane emulsification with a narrow annular gap between the membrane and the vessel as employed by Windhab's group.

In their paper, Schadler and Windhab investigated the influence of the annular gap width, the membrane rotation speed and the dispersed phase volume fraction on the production of water droplets in sunflower oil stabilised using polyglycerol polyricinoleate (PGPR).[19] They report that the droplet diameter decreases with increasing rotation speed (1000 to 8000 rpm) for a fixed annular gap of 1 mm. In particular a drastic decrease in the droplet diameter is reported between 4000–5000 rpm due to the high angular velocities causing the formation of Taylor vortices, which in turn lead to smaller droplets. It was also found that changes in the annular gap dictated the formation of Taylor vortices. At 0.5 mm, no Taylor vortices were formed therefore the droplets produced were larger than those produced at 1 mm. The study also reports that the volume fraction of the dispersed phase has little or no influence on the droplet sizes produced.

In 2012, an SPG rotating membrane device developed at the Centre for Formulation Engineering, Department of Chemical Engineering, University of Birmingham was reported. Norton and co-workers used this device to investigate the production of W/O/W emulsions.[21] The primary emulsion of water droplets in sunflower oil

stabilised using PGPR was prepared using a conventional high-shear mixer, producing droplets with a mean diameter of around 200 nm. The primary emulsion was then expressed through the SPG membrane into a water phase containing glucose and Tween 20. The SPG membrane used was 5 cm long, 1 cm in diameter with a mean pore diameter of 2.8 μm. The W/O/W emulsion droplets produced decreased in droplet size as the rotational speed was increased. It was also found that if the trans-membrane pressure (Section 3.3) was increased the droplet size increased due to the formation of a larger interfacial area.

In 2013 the production of oil in water emulsions using this SPG membrane was also investigated.[27] The dispersed phase used was sunflower oil. The influence of rotational velocity, trans-membrane pressure and emulsifier was investigated. It was found that the droplet size decreased with increasing rotational velocity and decreasing trans-membrane pressures. When Tween 20 was used as an emulsifier, the droplet size was seen to increase with decreasing Tween 20 concentration due to a lower driving force of surfactant adsorption. However, at high surfactant concentrations, changes in the rotational velocity produced no changes in the mean droplet size. Whey Protein Isolate (WPI) and Xanthan Gum (XG) were also investigated to investigate the use of protein as an emulsifier and the gum as both a stabiliser and a thickener agent.

Although there have been many reports on the use of membrane emulsification to produce near monodisperse emulsion droplets, the majority of these studies are focused on emulsions stabilised using surfactants.[9, 28, 29] There are very few reports on the use of particulate stabilisers to produce low polydispersity emulsions.[5, 13, 30] Yuan *et al.* investigated the use of 80 nm silica as a particulate emulsifier using cross-flow membrane emulsification.[5] They reported that increasing the cross-flow velocity decreased the droplet size without significantly affecting the width of the size distribution. Thompson *et al.* investigated the effect shear rate and disperse flux on the droplet size using a stirred cell membrane emulsification device.[13] They found that the droplet size increased as the disperse flux increased and decreased with increasing shear rates. Xu *et al.* investigated the effect of flow rate in a microfluidic channel and found that at low flow rates the droplets coalesced as they were not immediately covered with particles, whilst increasing the flow rate decreased coalescence as the mutual contact between the droplets was decreased.[30]

The work presented in this thesis aims to advance the current knowledge of producing particle-stabilised emulsions using membrane emulsification, by investigating and optimising several chemical and mechanical parameters (in particular the effect of pH, electrolyte, shear, disperse flow rate and particle concentration) and how they influence the droplet size and size distribution. The data is related to the particle adsorption kinetics for each parameter.

3.3. Process of droplet formation

A key requirement in membrane emulsification is the permeation of the dispersed phase through the membrane into the continuous phase. The trans-membrane pressure (P_{tm}) affects the flux of the dispersed phase through the membrane. It is defined as the difference between the pressure of the dispersed phase, P_d, and the mean pressure of the continuous phase, P_c;[31]

$$\Delta P_{tm} = P_d - \frac{\left(P_{c,in} - P_{c,out}\right)}{2} \qquad \text{(Equation 3.1)}$$

where $P_{c,in}$ and $P_{c,out}$ are the pressures of the flowing continuous phase at the inlet and at the outlet of the membrane device, respectively.

The disperse phase flux is also affected by the critical permeation (capillary) pressure. The critical permeation pressure, P_c, is defined as the minimum pressure difference over a membrane pore needed to start the production of droplets from that pore (assuming all the pores are ideal cylinders).[4]

$$P_c = \frac{4\gamma\cos\theta}{d_p} \qquad \text{(Equation 3.2)}$$

where γ is the interfacial tension, $\cos\theta$ the contact angle of the dispersed phase to the membrane surface and d_p the membrane pore diameter.

The transmembrane pressure has to be greater than the critical pressure to produce an emulsion. If the transmembrane pressure becomes too small the dispersed phase cannot be forced through the membrane, whilst if too high it is forced out as a jet stream and produces large polydisperse droplets.[4]

The dispersed phase flux, J_d is related to the transmembrane pressure according to Darcy's expression;[31]

$$J_d = \frac{K\Delta P_{tm}}{\mu L}$$ (Equation 3.3)

where, K is membrane permeability, ΔP_{tm} is pressure drop from point b to a (transmembrane pressure), μ is the dynamic viscosity and L is the length over which the pressure drop occurs (or membrane thickness in the case of membrane emulsification).

The process of a droplet formation and detachment from an individual membrane pore is based on two mechanisms as proposed by Peng and Williams;[2]

- droplet growth (inflation of the dispersed droplet at the pore tip),
- droplet detachment (where the droplet detaches and moves away from the pore tip).

In membrane emulsification, distortion of the droplet shape occurs resulting from imperfections in membrane pore and from the local hydrodynamic forces acting on the droplet through shear, buoyancy forces, the gravitational force and from the wettability of the droplet on the membrane surface.

Controlling the formation of the droplet and its size can be achieved by balancing the forces acting on the droplet at the capillary pore, which controls the droplet growth period (residency time on the membrane). Once the droplet growth period ends, the droplet detaches from the pore and breaks away from the dispersed phase flow within the pore capillary.[2]

Assuming the formation of a rigid spherical droplet, the main forces acting on the droplet produced using rotating membrane emulsification are illustrated in Figure 3.6.

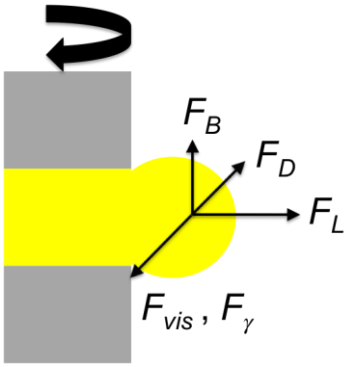

Figure 3.6. Illustrating the main forces acting on a forming droplet from a capillary pore on a rotating membrane emulsification reactor. *Taken from Ref. [32]*

where F_γ is the interfacial tension (dispersed phase adhesion at pore opening), F_{vis} is the dynamic viscosity of the dispersed phase, F_D is the drag force (created by the continuous phase flowing past the droplet parallel to the membrane surface), F_B is the buoyancy force (related to the density difference between the phases under gravity) and F_L is the dynamic lifting force (asymmetric velocity profile of the continuous phase near the droplet).

The drag, buoyant and lifting forces play an important role in overcoming the resistive forces of the interfacial tension and viscous forces to shear off the droplet. The relative motion between the membrane surface and the continuous phase applies a drag force on the droplet. The buoyancy force is a result of the differences in the specific densities of the continuous and dispersed phases, and the role this force plays in the detachment process is linked to the membrane displacement and operation condition. The lifting force is determined by the hydrodynamics of the dispersed phase permeating through the membrane pores. A higher throughput of flux leads to a larger lifting force for a particular pore size.

The resistive interfacial tension and viscous forces are influenced by the constituents present in the formulation, and the dynamic viscosity of the dispersed phase. These resistive forces are also related to the wetting of the dispersed phase at the pore opening and are consequently influenced by the pore geometry. If the wettability is low, a thin connection neck leads to a lower resistance force producing smaller droplets as the detachment process occurs faster.[23, 33, 34] For sub-micron sized droplets the buoyancy force can be neglected as it is about 6 - 9 orders of magnitude smaller than the drag and interfacial tension forces. When larger droplets are

produced (~200 μm and above), the buoyancy force becomes much more significant.[35]

The shear acting at the membrane surface due to the membrane rotation causes the deformation of the droplets. The resistive force of interfacial tension acts in two ways; a) resisting the shear force in the direction parallel to the membrane surface, b) resisting the shear force perpendicular to the membrane surface. Once the magnitude of interfacial tension force parallel to the membrane surface equals the shear force, the droplet will detach.[2]

References

1. G. T. Vladisavljević, I. Kobayashi and M. Nakajima, Production of uniform droplets using membrane, microchannel and microfluidic emulsification devices, *Microfluid Nanofluid*, 2012, **13**, 151-178.
2. S. J. Peng and R. A. Williams, Controlled production of emulsions using a crossflow membrane: Part I: Droplet formation from a single pore, *Chem. Eng. Res. Des.*, 1998, **76**, 894-901.
3. T. Nakashima and M. Shimizu, Porous glass from calcium alumino boro-silicate glass, *Ceramics*, 1986, **21**, 408-412.
4. R. A. Williams, S. J. Peng, D. A. Wheeler, N. C. Morley, D. Taylor, M. Whalley and D. W. Houldsworth, Controlled production of emulsions using a crossflow membrane: Part II: Industrial scale manufacture, *Chem. Eng. Res. Des.*, 1998, **76**, 902-910.
5. Q. Yuan, O. J. Cayre, M. Manga, R. A. Williams and S. Biggs, Preparation of particle-stabilized emulsions using membrane emulsification, *Soft Matter*, 2010, **6**, 1580-1588.
6. S. M. Joscelyne and G. Trägårdh, Membrane emulsification - a literature review, *J. Membrane Sci.*, 2000, **169**, 107-117.
7. C. Charcosset, I. Limayem and H. Fessi, The membrane emulsification process - a review, *J. Chem. Technol. Biot.*, 2004, **79**, 209-218.
8. A. J. Gijsbertsen-Abrahamse, A. van der Padt and R. M. Boom, Status of cross-flow membrane emulsification and outlook for industrial application, *J. Membrane Sci.*, 2004, **230**, 149-159.
9. G. T. Vladisavljević and R. A. Williams, Recent developments in manufacturing emulsions and particulate products using membranes, *Adv. Colloid Interface Sci.*, 2005, **113**, 1-20.
10. V. Schröder, O. Behrend and H. Schubert, Effect of dynamic interfacial tension on the emulsification process using microporous, ceramic membranes, *J. Colloid Interface Sci.*, 1998, **202**, 334-340.
11. Q. Yuan, R. Hou, N. Aryanti, R. A. Williams, S. Biggs, S. Lawson, H. Silgram, M. Sarkar and R. Birch, Manufacture of controlled emulsions and particulates using membrane emulsification, *Desalination*, 2008, **224**, 215-220.

12. M. M. Dragosavac, M. N. Sovilj, S. R. Kosvintsev, R. G. Holdich and G. T. Vladisavljević, Controlled production of oil-in-water emulsions containing unrefined pumpkin seed oil using stirred cell membrane emulsification, *J. Membrane Sci.*, 2008, **322**, 178-188.
13. K. L. Thompson, S. P. Armes and D. W. York, Preparation of Pickering emulsions and colloidosomes with relatively narrow size distributions by stirred cell membrane emulsification, *Langmuir*, 2011, **27**, 2357-2363.
14. R. A. Williams, *'Controlled dispersion using a spinning membrane reactor'*, UK Patent Application PCT/GBOO/04917, 2001.
15. S. R. Kosvintsev, G. Gasparini, R. G. Holdich, I. W. Cumming and M. T. Stillwell, Liquid-liquid membrane dispersion in a stirred cell with and without controlled shear, *Ind. Eng. Chem. Res.*, 2005, **44**, 9323-9330.
16. G. T. Vladisavljević and R. A. Williams, Manufacture of large uniform droplets using rotating membrane emulsification, *J. Colloid Interface Sci.*, 2006, **299**, 396-402.
17. Y. Hatate, H. Ohta, Y. Uemura, K. Ijichi and H. Yoshizawa, Preparation of monodispersed polymeric microspheres for toner particles by the Shirasu porous glass membrane emulsification technique, *J. Appl. Polym. Sci.*, 1997, **64**, 1107-1113.
18. J. Zhu and D. Barrow, Analysis of droplet size during crossflow membrane emulsification using stationary and vibrating micromachined silicon nitride membranes, *J. Membrane Sci.*, 2005, **261**, 136-144.
19. V. Schadler and E. J. Windhab, Continuous membrane emulsification by using a membrane system with controlled pore distance, *Desalination*, 2006, **189**, 130-135.
20. N. Aryanti, R. A. Williams, R. Hou and G. T. Vladisavljević, Performance of rotating membrane emulsification for O/W production, *Desalination*, 2006, **200**, 572-574.
21. A. K. Pawlik and I. T. Norton, Encapsulation stability of duplex emulsions prepared with SPG cross-flow membrane, SPG rotating membrane and rotor-stator techniques - A comparison, *J. Membrane Sci.*, 2012, **415-416**, 459-468.

22. Q. Yuan, N. Aryanti, R. Hou and R. A. Williams, Performance of slotted pores in particle manufacture using rotating membrane emulsification, *Particuology*, 2009, **7**, 114-120.

23. I. Kobayashi, M. Yasuno, S. Iwamoto, A. Shono, K. Satoh and M. Nakajima, Microscopic observation of emulsion droplet formation from a polycarbonate membrane, *Colloids Surf. A: Physicochem. Eng. Asp.*, 2002, **207**, 185-196.

24. I. Kobayashi, M. Nakajima, K. Chun, Y. Kikuchi and H. Fujita, Silicon array of elongated through-holes for monodisperse emulsion droplets, *AIChE Journal*, 2002, **48**, 1639-1644.

25. I. Kobayashi and M. Nakajima, Effect of emulsifiers on the preparation of food-grade oil-in-water emulsions using a straight-through extrusion filter, *Eur. J. Lipid Sci. Tech.*, 2002, **104**, 720-727.

26. I. Kobayashi, S. Mukataka and M. Nakajima, Effect of slot aspect ratio on droplet formation from silicon straight-through microchannels, *J. Colloid Interface Sci.*, 2004, **279**, 277-280.

27. A. K. Pawlik and I. T. Norton, SPG rotating membrane technique for production of food grade emulsions, *J. Food Eng.*, 2013, **114**, 530-537.

28. E. Egidi, G. Gasparini, R. G. Holdich, G. T. Vladisavljević and S. R. Kosvintsev, Membrane emulsification using membranes of regular pore spacing: Droplet size and uniformity in the presence of surface shear, *J. Membrane Sci.*, 2008, **323**, 414-420.

29. R. G. Holdich, M. M. Dragosavac, G. T. Vladisavljević and S. R. Kosvintsev, Membrane emulsification with oscillating and stationary membranes, *Ind. Eng. Chem. Res.*, 2010, **49**, 3810-3817.

30. Q. Y. Xu, M. Nakajima and B. P. Binks, Preparation of particle-stabilized oil-in-water emulsions with the microchannel emulsification method, *Colloids Surf. A: Physicochem. Eng. Asp.*, 2005, **262**, 94-100.

31. C. Charcosset, Preparation of emulsions and particles by membrane emulsification for the food processing industry, *J. Food Eng.*, 2009, **92**, 241-249.

32. R. A. Williams, Q. Yuan, S. Collins. Membrane Emulsification, In: *Encyclopedia of Surface and Colloid Science*: Second Edition, Taylor & Francis, New York, 2010, 1-27

33. T. Kawakatsu, G. Trägårdh, C. Trägårdh, M. Nakajima, N. Oda and T. Yonemoto, The effect of the hydrophobicity of microchannels and components in water and oil phases on droplet formation in microchannel water-in-oil emulsification, *Colloids Surf. A: Physicochem. Eng. Asp.*, 2001, **179**, 29-37.

34. I. Kobayashi, M. Nakajima and S. Mukataka, Preparation characteristics of oil-in-water emulsions using differently charged surfactants in straight-through microchannel emulsification, *Colloids Surf. A: Physicochem. Eng. Asp.*, 2003, **229**, 33-41.

35. M. Rayner and G. Tragardh, Membrane Emulsification modelling: How can we get from characterisation to design?, *Desalination*, 2002, **145**, 165-172.

CHAPTER 4: EXPERIMENTAL METHODOLOGY

NOMENCLATURE

α	Degree of protonation/association
B_o	Bond number
D_e	Equatorial diameter in pendant drop
D_H	Hydrodynamic diameter
D_s	Horizontal diameter in pendant drop
D_{sol}	Diffusion coefficient of solution
δ	Chemical shift
E	Electric field
ε_r	Dielectric constant of medium
ε_o	Permittivity of free space
g	Gravitational constant
γ	Interfacial tension
H	Droplet correction factor
k	Boltzmann constant
η	Viscosity
Δp	Pressure difference
R_d	Droplet radius
R_c	Radius of capillary
S	Pendant droplet factor
T	Absolute temperature
μ_e	Electrophoretic mobility
v	Velocity
ζ	Zeta potential

ABBREVIATIONS

CMC	Critical micelle concentration
DLS	Dynamic light scattering
GPC	Gel Permeation Chromatography

^{1}H NMR	Proton nuclear magnetic resonance
LDV	Laser Doppler velocimetry
MEB	Milli-equivalent of added base
NIBS	Non-invasive back-scatter
RME	Rotational membrane emulsification
SEM	Scanning electron microscopy
TEM	Transmission electron microscopy
UV-Vis	Ultraviolet-Visible

4.1. Introduction

Numerous experimental and characterisation-based techniques have been employed to acquire the data presented within the results chapters of this thesis. This chapter is divided into five sections. The first section details the materials used to fabricate bespoke pMMA-b-pDMAEMA di-block copolymers used within the experimental work and their subsequent characterisation. Also mentioned within this section is the synthetic route of fabricating these di-block copolymers, however this is not part of this study. The second section of this chapter describes in detail the synthesis of polystyrene latex particles sterically stabilised using the di-block copolymers. Also considered within this section is the use of ^{1}H NMR to characterize the grafting density of this polymer on the surface of the latex particles. The third section outlines the equipments and techniques to obtain the data along with any experimental parameters employed.

Since a large number of techniques and equipments have been used, the descriptions will be concise. However, where appropriate references have been provided for further reading. The production of controlled emulsion droplets using particulate stabilisers via a Rotational Membrane Emulsification (RME) reactor is described in section 4. This section gives detailed information about the membrane used, the reactor set-up and techniques used to characterise the resulting emulsions. The final section describes the use of pendant drop tensiometry and a new microtensiometry device to study the particle adsorption kinetics at liquid/liquid interfaces.

4.2. pMMA-b-pDMAEMA diblock copolymer

Bespoke di-block copolymers based on pMMA-b-pDMAEMA, with controlled molecular architectures, were synthesised using Reversible Addition-Fragmentation chain Transfer (RAFT) living free-radical polymerisation for this project by Chamelic Ltd (Leeds, U.K). A brief description of the synthesis is given in Section 4.2.2. More detailed information regarding the synthesis of these di-block copolymers can be found in the following references.[1, 2]

4.2.1. Materials

The following chemicals and reagents were used as received:

- Dimethylaminoethyl methacrylate (DMAEMA, ≥98%, Sigma-Aldrich)
- Methyl methacrylate (MMA, ≥98%, Sigma-Aldrich)
- Toluene (≥99%, Fisher Scientific)
- Azobisisobutyronitrile initiator (AIBN, Sigma-Aldrich)
- Dichloromethane (≥99%, Sigma-Aldrich)
- Hexane (anhydrous, ≥95%, Sigma-Aldrich)
- Chloroform ($CDCL_3$, ≥99%, Sigma-Aldrich)
- RAFT chain transfer agent, Cyanopropyldithiobenzoate (CPDB) (≥97%)

4.2.2. Synthesis

Controlled living free-radical polymerisation using the Reversible Addition-Fragmentation chain Transfer (RAFT) methodology was used to copolymerise MMA with DMAEMA. This was done in a solution of toluene at 80°C in a 1 L round bottom flask. In a typical run, the flask was filled with a solution containing: Freshly purified MMA (25 g, 0.25 mol), the chain transfer agent CPDB (3.82 g, 1.5×10^{-2} mol, 85% purity), the initiator AIBN (1.23 g, 7.5×10^{-3} mol) and the solvent toluene (7.51 g). The solution was degassed via nitrogen bubbling at 0°C for 20 minutes, before being immersed into an oil bath at 80°C ± 2°C for 3 hours. After the polymerisation was complete, the reaction was cooled and diluted with dichloromethane. The polymer was then recovered by precipitation into cold hexane and dried under vacuum. This process removes any residual un-reacted monomer

and produces polymers with purity greater than 99% confirmed by using ^{1}H NMR and Gel Permeation Chromatography (GPC).

The molecular weights and polydispersity were determined by ^{1}H NMR spectroscopy in $CDCl_3$. A range of these di-block copolymers were supplied that had a fixed pMMA block length with varying pDMAEMA block lengths. The structure of these bespoke di-block copolymers are illustrated by Figure 4.1. Detailed information regarding the block lengths can be found in Table 4.1 below.

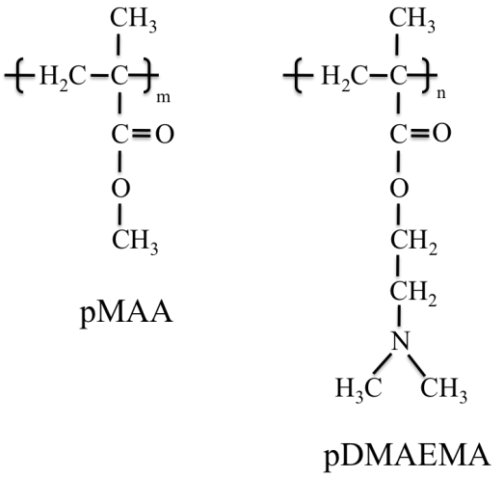

Figure 4.1. Chemical structure of pMMA-b-pDMAEMA di-block copolymer (m, n refer to the block units). *Redrawn from Ref. [1]*

Batch Entry	Block lengths	Average molecular number, M_n (g mol^{-1})	Polydispersity (PDI)
GB 167	$pMMA_{14}$-b-$pDMAEMA_{20}$	4770	1.14
GB 168	$pMMA_{14}$-b-$pDMAEMA_{54}$	10110	1.20
GB 169	$pMMA_{14}$-b-$pDMAEMA_{108}$	18600	1.20
WB 76	$pMMA_{16}$-b-$pDMAEMA_{245}$	40340	1.10

Table 4.1. Block length units, average molecular number (determined using ^{1}H NMR) and the polydispersity details of the pMMA-b-pDMAEMA di-block copolymers used in this study determined by Chamelic Ltd.

4.2.3. Potentiometric Titration

Potentiometric titrations of weakly basic or acidic polymers are useful to attain information on the degree of protonation of the polymer as a function of the background pH.

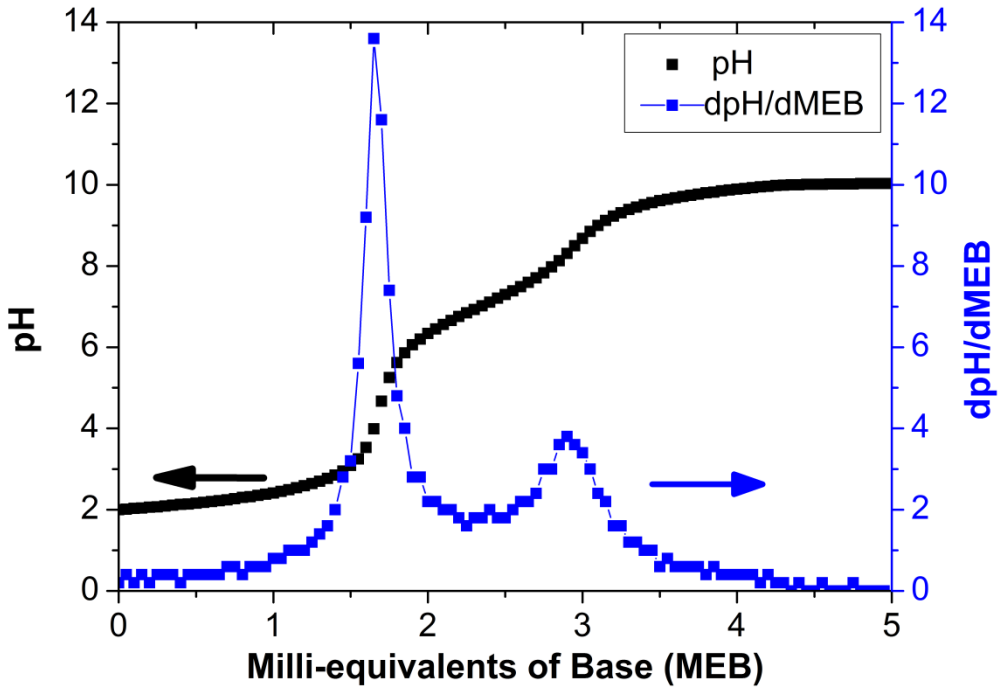

Figure 4.2. Illustrating the general form of a potentiometric titration curve for a pMMA-b-pDMAEMA diblock copolymer.

Data from a potentiometric titration curve of one of the copolymer samples used in this study is given in Figure 4.2. Here, the polymer solution has been initially adjusted to a low pH, the change in pH is monitored and recorded as a function of added base (in milli-equivalent volumes of added base, MEB). In general, for a weakly basic polymer such as pDMAEMA, the titration curve will exhibit two inflection points, relating to the onset of proton association with the polymer and to complete proton association, respectively. The positions of these inflection points are usually determined by plotting $\Delta pH/\Delta MEB$ as a function of added base. An example of this plot is also illustrated in Figure 4.2. It is clear from the figure that the two inflection points from the curve can be converted into distinguishable peaks.

The distance between these two peaks (ΔMEB^*), measured in MEB can then be related to the concentration of the proton associating species.

The data from the titration curve can provide information about the degree of proton association (α) of the polymer. In all the studies considered here, the potentiometric titrations were conducted by titrating a base solution against an acidic copolymer solution. For every addition of base, the addition of hydroxide ions may undergo two possible interactions; either a) associating with and neutralising a free proton in solution or b) neutralising and associating with a proton from the tertiary amine site of the di-block copolymer. Another alternative is that the hydroxide ion does not undergo any of these interactions and instead remains as a free hydroxide ion within the solution. These scenarios can be expressed as:

$$[\text{OH- added}] = \Delta[\text{free } OH^-] - \Delta[\text{free } H^+] - \Delta[BH^+] \qquad \text{(Equation 4.1)}$$

where BH^+ represents a proton association from the tertiary amine site of the di-block copolymer. The total amount of base added throughout the titration can then be written as:

$$[\text{total } OH^- \text{ added}]_j = \{[\text{free } OH^-]_j - [\text{free } OH^-]_0\} - \{[\text{free } H^+]_j - [\text{free } H^+]_0\} - \{[\text{free } BH^+]_j - [\text{free } BH^+]_0\} \qquad \text{(Equation 4.2)}$$

where 0 and j represent initial and *j*th addition of base.

The total concentration of OH^- can be determined from the total volume of base added, whilst the free hydroxide and proton concentrations can be determined from the pH measurements. Assuming that at low pH all the tertiary amine sites are fully protonated, it is possible to calculate the concentration of the protonated amine units on the di-block copolymer, at any stage of the titration. The degree of association (α) of the di-block copolymer can be expressed as:

$$\alpha = \frac{\left[BH^+\right]_j}{\left[BH^+\right]_0} \qquad \text{(Equation 4.3)}$$

This allows tracking of α throughout the course of the titration. It is conventional to present the degree of association as a function of pH of the polymer solution.

For the titration measurements, various polymer concentrations were studied. All the solutions were prepared using Milli-Q water and adjusted to pH 2 using small quantities of concentrated HNO_3. The solutions were then left overnight to equilibrate and the pH was adjusted prior to titration if necessary. The titration was performed using a solution of KOH and added to the polymer solution in 50 µL volume additions. Up to 5 minutes was given to allow the base to interact with the polymer solution before measuring the pH and subsequent base addition.

4.3. pMMA-b-pDMAEMA sterically stabilised latex particles

The di-block copolymers outlined in Table 4.1 (Section 4.2.2) were used to synthesise sterically stabilised polystyrene latex particles. In particular the influence of the polymer block length and reaction temperature on the particle size was studied.

4.3.1. Synthesis

The polystyrene latex particles were prepared via emulsion polymerisation, based on the method described by Amalvy *et al.*[3] using styrene monomer and ammonium persulfate as the initiator. Styrene monomer (≥99%, Sigma Aldrich, U.K) was firstly vacuum distilled at 45°C to remove any impurities. The ammonium persulfate (APS), initiator (Sigma Aldrich, U.K) and all other reagents were of analytical grade and were used without further purification. Milli-Q water (Millipore Corporation) with a resistivity of 18.2 MΩ cm^{-1} was used in all the preparations. A 100 mL three necked round bottom flask was used with a magnetic stirrer. The heating and stirring was controlled using a thermostated hotplate (IKA RCT basic).

In a typical 50 mL preparation, the di-block copolymer (0.5 g) was dissolved in Milli-Q water (40 mL) adjusted to pH 3-4 using HNO_3 and was left to stir overnight. Once the polymer had completely solubilised, the polymer solution was added to the round bottom flask. A water-cooled reflux condenser was connected to the flask was immersed into an oil bath at room temperature. Nitrogen was purged through the polymer solution in order to remove oxygen from the system via one of the necks. After 20 minutes, the initiator (5 mg) was dissolved in Milli-Q water (5 mL) and was added to the flask and left to stir for 20 minutes. The monomer styrene (5 mL) was added drop by drop into the flask using a syringe and was left for 30 minutes to saturate into the aqueous phase. The temperature was then ramped up to the required working temperature. Once the system had reached the reaction temperature the nitrogen was taken out and the reaction was left to proceed for 24 hours.

At the end of the reaction, the flask was removed from the oil bath and allowed to cool for 20 minutes. The latex was then passed through glass wool to remove any unreacted monomer and coagulum formed during the reaction process. The latex was then dialysed against Milli-Q water (replaced every few hours) to remove

residual traces of monomer and initiator still present in the particle dispersion. The dialysis tubing used had a molecular weight cut-off that matched the molecular weight of the polymer used in the synthesis. The dialysis tubing was left to soak in Milli-Q water overnight and washed prior to use. The dialysis treatment was considered to be complete when the surface tension of the water droplet was 72.8 ±0.2 mN m^{-1} (i.e. that of an air/water interface).

4.3.2. Determining stabiliser grafting density via 1H NMR spectroscopy

^{1}H NMR spectroscopy (done by Dr. Alexandre Richez) was performed on the latex particles to determine the grafting density of the steric stabiliser (pMMA-b-pDMAEMA) on the polystyrene latex particle surface.

A 500 MHz Bruker ^{1}H NMR spectrometer was used and tetramethyl silane was used as a reference sample. The sterically stabilised particles were initially dried in a vacuum oven and a small amount was dissolved in $CDCl_3$ and added to a 5 mm NMR tube. After performing the spectroscopy, the intensity signals from the polystyrene and the stabiliser were analysed by integration of the peaks. The two oxymethylene protons adjacent to the ester group in the DMA residue produced a signal at a chemical shift value, δ 4.0 (this peak was chosen as it is not obscured by overlapping polystyrene signals). This was compared to the five aromatic protons due to styrene residues at δ 6.0 - 8.0 as illustrated by Figure 4.3. This comparison of the peaks allows the stabiliser content to be calculated.[3]

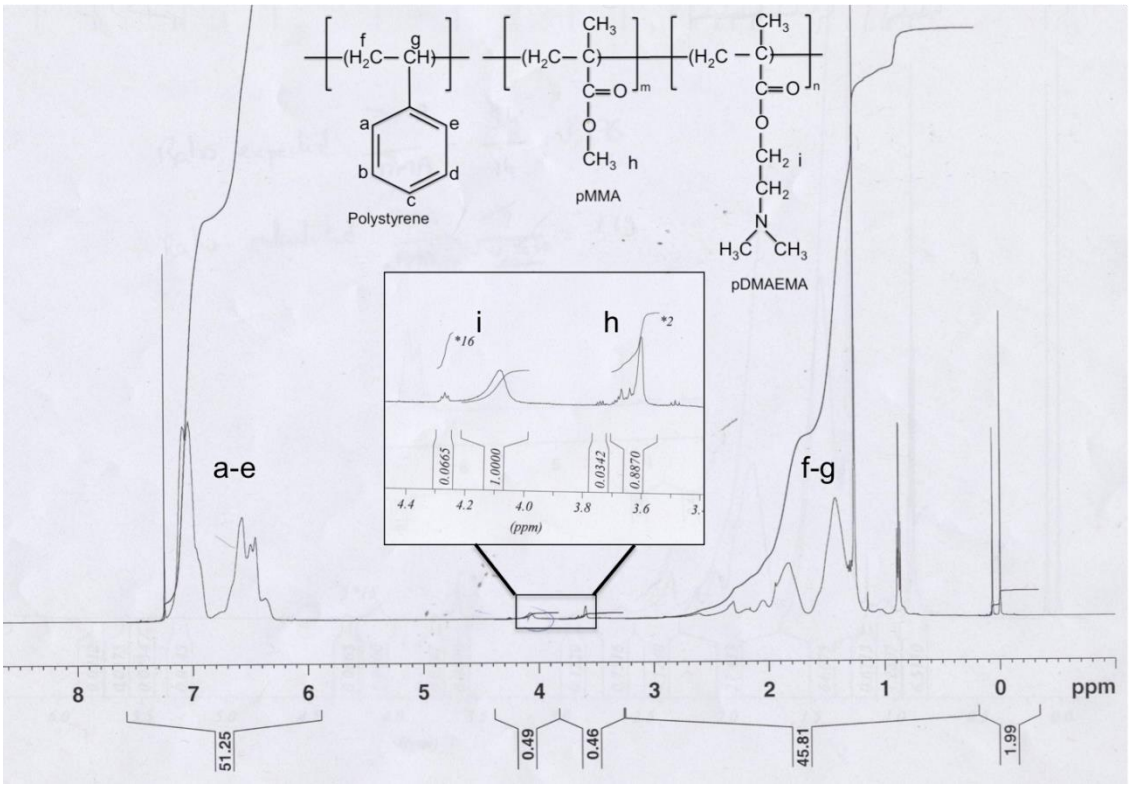

Figure 4.3. ^{1}H NMR spectra of polystyrene latex particles dissolved in $CDCl_3$ to allow calculation of stabiliser content. Integration of the oxymethylene proton peaks at δ 4.0 (inset) are compared to the aromatic proton peaks of the styrene at δ 6.0-8.0 to determine the grafting density of the stabiliser.

Assuming that all the stabiliser is located on the surface of the latex particles the grafting density, Γ, (in mg m^{-2}), is calculated by comparing the stabiliser content with the particle surface area (determined from intensity-averaged particle diameter using DLS). The typical errors associated with these Γ values are on the order of ±10%.

4.4. Experimental techniques

This section outlines general colloidal experimental and analytical techniques employed during this study. Where necessary the operating conditions and protocols are described.

4.4.1. Dynamic Light Scattering (DLS) - Polymer characterisation

DLS (also known as photon correlation spectroscopy and quasi-elastic light scattering) is a powerful optical technique to determine the diffusion coefficient of particles in suspension/polymers in solution on the basis that particles undergoing Brownian motion produce fluctuations in the scattered light. Deconvolution of the temporal correlation function obtained through these measurements eventually leads to gaining information of particle size distribution. A monochromatic light beam, such as a laser is shone onto the colloidal sample, which in turn scatters the light. If the particles or polymers are smaller than the wavelength of the light source, the light is scattered in all directions (also known as Rayleigh scattering), if they are larger, then the intensity of scattering will be angle dependent (Mie scattering).

Particles and polymers in suspension undergo random movement due to collisions with the solvent molecules, with each other, and with the vessel walls that they are contained within, due to fluctuations in the thermal energy of the solvent molecules. This motion is described as Brownian motion. A distinguishing feature of Brownian motion is that larger objects move relatively slowly giving rise to smaller scattered light intensity fluctuations, whilst smaller objects move faster, a relationship described by the Stokes-Einstein equation (equation 4.4). The light scattered by these moving objects produces constructive and destructive interference patterns, which results in fluctuating scattering intensities at the detector. In DLS, measuring the rate of these fluctuating intensities reveals information regarding the diffusion coefficient of the objects in a given solvent. There are a number of mathematical models that can be used to fit the scattering data in order to determine the diffusion coefficient, these are; number weighted cumulant model and CONTIN which is an inverse Laplace transformation analysis algorithm. The Stokes-Einstein equation[4] can then be used to extract the hydrodynamic diameter (D_H) of the object;

$$D_H = \frac{k \times T}{3\pi \times \eta \times D_{sol}}$$ (Equation 4.4)

where k is the Boltzmann constant, T the absolute temperature, η the viscosity of the solvent and D_{sol} the diffusion coefficient of the object in solution.

DLS also utilizes a digital correlator to measure the similarities between intensity signals over a period of time known as the correlation function. Comparing the intensity signals after very short time intervals (nano to micro seconds) the correlation of the signals will be strong (correlation function = 1), whilst larger time intervals will lead to an eventual decay of the correlation function to 0 (no correlation). Decay in the correlation function is used to obtain the particle diameter. Larger objects move slower so fluctuations in signal are much smaller meaning the signals have longer decay times as shown by Figure 4.4. In contrast, smaller particles move faster leading to larger intensity fluctuations causing faster signal decays.

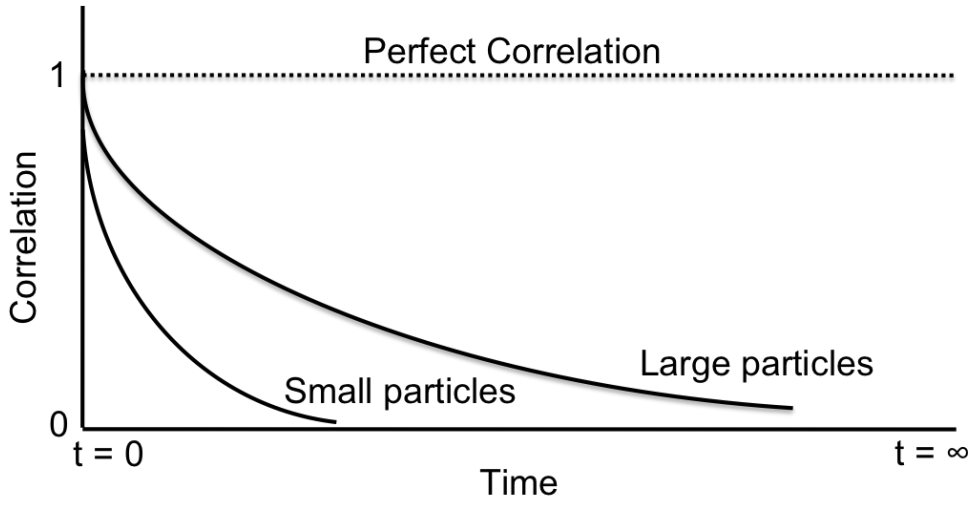

Figure 4.4. Illustrating the correlation function of signals attained from large and small particles.

The DLS measurements in this research were conducted using a Brookhaven BI-200SM instrument equipped with a 633 nm helium-neon (He-Ne) laser to estimate the critical micelle concentration (cmc) of the di-block copolymers by measuring the

size of the objects present in solution at different polymer concentrations. In a typical experiment, the quartz cells were washed with a detergent and subsequently rinsed with copious amount of Milli-Q water and underwent ultrasonic treatment prior to use. The di-block copolymers were solubilised in Milli-Q water (Millipore Corporation) at a concentration of 1000 ppm adjusted to pH 4 using 0.1M HNO_3 and left to stir overnight. This solution was then diluted with Milli-Q water at pH 4 to obtain different polymer solution at concentrations varying from 50 to 1000 ppm (in this case there is no further dilution).

For the measurements, 5 cm^3 of the polymer at a particular concentration and pH was filtered using a hydrophilic non-pyrogenic 0.4 µm membrane syringe filter (Sartorius Stedim Biotech GmbH) to remove any dust particulates in the solution. The angle studied for the light scattering measurements was chosen to be 90° in accordance to similar studies performed in literature.[2] The duration of one measurement was varied between 5 to 10 minutes depending on the ease of attaining a correlation. Typically 10 measurements were taken for one data point and averaged. All the measurements were carried out at constant temperature of 25°C, controlled by a water bath circulator.

4.4.2. Dynamic Light Scattering (DLS) - Particle characterisation

DLS was used to measure the changes in hydrodynamic diameter of sterically-stabilised latex particles as a function of pH and electrolyte concentrations. This was performed using the Zetasizer Nano ZS (Malvern). The zetasizer also uses a helium-neon laser with a wavelength of 633 nm and utilizes a non-invasive back-scatter (NIBS) technology.[5] Instead of using the conventional 90° angle used in most DLS measurements, the zetasizer uses a backscatter angle of 173°. The main components of the zetasizer are; a laser, detector and a focusing lens. The lens allows the positioning of the beam to maximise the scatter information depending on the size of the particles measured.[5] Shining of the laser onto a solution of spherical particles undergoing Brownian motion, causes a Doppler shift to slightly higher or lower frequencies depending on whether the particle is moving towards or away from the detector. Over the measurement timescale these shifts will produce a Doppler frequency broadening peak.[4] A pattern of beat frequencies is produced when the broadened scattered signal is mixed with the incident light, allowing the calculation

of the particle diffusion coefficient which is used to calculate the particle size using Equation 4.4.

Samples were prepared to a concentration of 1000 ppm at various electrolyte (KNO_3) concentrations (ranging from no added electrolyte to 1M). The samples were given 5-10 minutes to equilibrate to the working temperature of the instrument prior to conducting measurements. To measure a sample, two vials were prepared in order to titrate low pH (vial 1) and high pH values (vial 2). The pH was adjusted using HNO_3 and KOH. For any data point, 10 measurements were taken and then averaged. Measurements of the size of model monodisperse particles of known hydrodynamic diameter were carried out regularly to calibrate the instrumentation.

4.4.3. Electrophoretic mobility

The electrophoretic mobility of colloidal particles can be measured using electrophoresis. Electrophoresis is the application of an electric field across an electrolyte causing charged particles/molecules suspended in the electrolyte to become attracted towards the electrode having opposite charge. In electrophoresis, if the viscous and electrostatic forces are at equilibrium, the particles will move with constant velocity. The velocity v, will be dependent on the strength of the electric field E, dielectric constant of the medium ε_r, viscosity of the solvent η, and the zeta potential ζ (electrokinetic potential of the slipping plane in the electric double layer, associated with the particle). The exact location of the shear plane is unknown. In addition to bound ions in the Stern layer, a layer of solvent bound to the particle also forms part of the kinetic unit. The boundary of this bound solvent layer is described as the slipping plane is reasonably assumed to be located a small distance away from the Stern layer as illustrated in Figure 4.5.

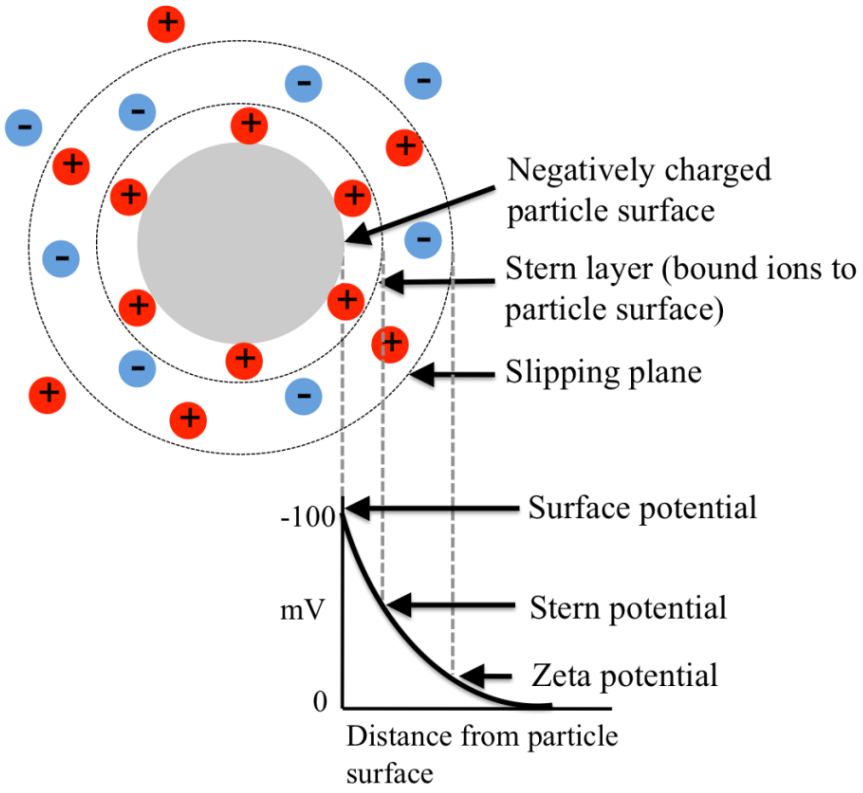

Figure 4.5. Schematic representation of zeta potential. *Redrawn from Ref. [5]*

The electrophoretic mobility (μ_e) can be expressed as:

$$\mu_e = \frac{v}{E} \qquad \text{(Equation 4.5)}$$

where v is the electrophoretic velocity and E is the electric field strength.

The most widely used theory for electrophoresis was developed by Smoluchowski in 1903.[6] The theory can be used for dispersed particles for any shape at any concentration, providing that the thickness of the electric double layer is small compared to the particle size (and for the polymer micelles in solution used in this study) and that the surface conductivity is assumed to be negligible.[7] The theory is expressed as:

$$\mu_e = \frac{\varepsilon_r \varepsilon_0 \zeta}{\eta}$$

(Equation 4.6)

where ε_r is the dielectric constant of medium, ε_0 is the permittivity of free space and η is the dynamic viscosity.

The electrophoretic mobility can be measured using Laser Doppler Velocimetry (LDV), which is an established technique for measuring fluid flows in engineering studies. An incident beam is shone at the cell and the light scattered is collected at an angle of 17° which is combined with a reference beam.[5] The detector measures the fluctuation in the intensity signals, which relates to the velocity of the particles moving in the media. A processor is used to convert the intensity signals into mobility values for the dispersed particles.

The Zetasizer Nano ZS (Malvern), was used to measure the electrophoretic mobility of the sterically stabilised latex particles. The samples were prepared at a concentration of 0.1 wt% in varying electrolyte (KNO_3) concentrations (no added electrolyte to 1M). For a particular sample two vials were prepared, one to titrate low pH's whilst the other for high pH values. The pH was adjusted using HNO_3 and KOH. Up to 10 measurements were taken and averaged to attain a single data point. The machine was regularly calibrated using model particulate systems.

4.4.4. Interfacial tension measurements

Surface and interfacial tension measurements were obtained using a droplet shape analysis (pendant drop method) surface tensiometer (DSA100, Easydrop FM40, KRÜSS, Germany). In the pendant drop method, liquid A is injected into a needle to form a droplet at the end of the needle tip into either air or into a liquid B to measure the surface and interfacial tension respectively. The droplet that is formed is observed optically using a CCD camera and the tension is measured by fitting a Young-Laplace model to the shape of the droplet.

Suspending a droplet of liquid A in air or liquid B at mechanical equilibrium is possible due to the balance of gravitational and surface forces.[8] The forces acting on a curved surface can be summarised by Young-Laplace equation (equation 4.7) which describes the pressure difference (Δp), both above (p_1) and below (p_2) the

curvature of the droplet at the apex (r_1) and a specific coordinate (r_2) in order to obtain the interfacial tension (γ):

$$\Delta p = \gamma\left(\frac{1}{r_1} + \frac{1}{r_2}\right) \qquad \text{(Equation 4.7)}$$

Bashforth and Adams related the Laplace equation to the drop profile by a non-linear differential equation.[9] They calculated tables of contours to fit the droplet geometry profile (Figure 4.6)[10], however this was very tedious as photographs of the droplet would have to be compared with tabulated values.

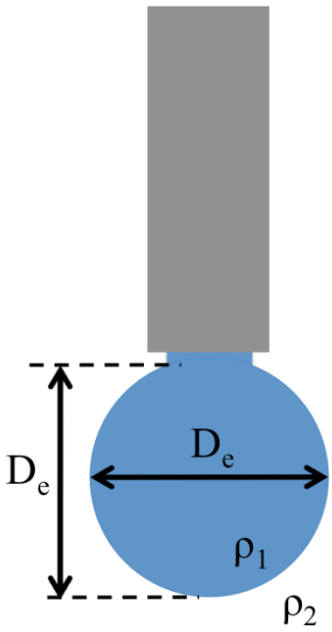

Figure 4.6. Schematic of pendant drop geometry. *Adapted from Ref. [10]*.

To simplify this, Andreas *et al.*[11] proposed the following empirical equation, where g is the gravitational constant, D_e the equatorial diameter of the droplet, $\Delta\rho$ is the density difference between the two liquids and H is a correction factor:

$$\gamma = \frac{gD_e^2\Delta\rho}{H} \qquad \text{(Equation 4.8)}$$

The correction factor, H is based on the droplet factor of the pendant drop, S, expressed by:

$$S = \frac{D_s}{D_e} \qquad \text{(Equation 4.9)}$$

where D_s is the diameter measured horizontally at a diameter D_e away from the apex of the droplet.

In the pendant drop device, Equations 4.8 and 4.9 are fitted to digitized images of the drop to obtain the surface/interfacial tension values. This method has an error of between 0.01 and 0.2 mN m^{-1} depending on the shape of the droplet formed, as this impacts on the droplet fitting analysis tool.

4.4.5. Scanning Electron Microscopy

Scanning Electron Microscopy (SEM) is a technique that utilizes a high-energy electron beam which scans across the surface of the sample. SEM measures secondary and backscattered electrons that interact with the atoms of the sample. The interactions are characteristic of the topography, composition and electrical conductance of the sample. For poor conducting samples, it is necessary to coat the sample with a thin layer (2 - 5 nm) of metal (e.g. platinum/palladium), which provides a highly conductive surface that strongly scatters the electron beam. The SEM technique allows magnification of the samples up to 25,000 times with a resolution of 5 nm. Therefore the micrographs obtained from SEM allow for a three dimensional representation of the surface of the sample.

To prepare the samples for SEM analysis, microscope slides were cut into small pieces and placed on an SEM stub using double sided tape. However, this surface is not conductive and thus conductive paint was applied on the bottom side of the glass slide to provide conduction between the SEM stub and the sample. A droplet containing a diluted suspension of the particles was pipetted onto the slide. A droplet of ethanol was then deposited on top to spread the particles evenly across the slide. Ethanol was used as it is a volatile solvent and therefore quickly evaporates. After evaporation, the sample was stored in a sample box at ambient temperature in order to prevent dust particles interfering with the sample. Once dried, the samples were

then sputter coated with a platinum/palladium film prior to analysis. The SEM used in this study was performed with a LEO 1530 Field Emission Gun (FEG) SEM instrument operated at 3 kV. The SEM experiments were carried out by myself at the Leeds Electron Microscopy and Spectroscopy Centre (LEMAS).

4.4.6. Transmission Electron Microscopy

Transmission electron microscopy (TEM) and optical microscopy techniques broadly work on the same principle. In the case of optical microscopy, light at different wavelengths is used whereas in TEM an electron beam is used as the source. Electrons have a smaller wavelength than light and hence higher resolution images can be obtained up to a few angstroms (10^{-10} m). An electron beam is emitted at the top of the microscope through a vacuum, which is focused into a narrow beam using electromagnetic lenses. The beam is transmitted through the specimen and depending on the density of the sample, the electrons are either scattered or lost from the beam. The unscattered electrons hit a fluorescent screen and the image of the sample is displayed as a shadow. The variation in darkness of the image is due to density differences within the sample. The image can be studied directly or photographed using a CCD camera.

To prepare samples for TEM analysis, a droplet of the particles at a concentration of 0.1 wt% was deposited onto a Holey Carbon film 400 Mesh copper (50)' grid. Once deposited the sample was allowed to dry at ambient temperature for 24 hours prior to analysis. The samples were analysed using a Phillips CM100 TEM operated at 100 kV with the help of Dr. Mike Ward at the LEMAS centre.

4.5. Pickering emulsions produced via a Rotational Membrane Emulsification (RME) reactor

This section outlines the use of two different particulate stabilisers in the production of Pickering emulsions using a new rotational membrane emulsification (RME) reactor. It outlines the materials used, set up of the RME reactor and emulsion characterisation.

4.5.1. Materials

The key properties of the materials used in this study for the two particulate systems for the production of O/W emulsions are listed in Table 4.2.

	System 1	System 2
Aqueous (Continuous) Phase	**800 nm** FUSO silica colloids dispersed in Milli-Q water (Size determined using DLS)	**91.2 ± 3.2 nm** sterically stabilised ($pmma_{16}$-$pdmaema_{245}$) polystyrene latex particles dispersed in pH 9.3 Milli-Q water. (Size determined using DLS)
Oil (Dispersed phase)	Glyceryl Trioctanoate (Tricaprylin)	Hexadecane oil
Viscosity of oil @20°C	26 mPa. s	3.34 mPa. s
Specific density of oil	0.95	0.773

Table 4.2. Composition and properties of O/W emulsions presented in this research study.

The 800 nm silica colloids were purchased from FUSO Chemical Co. Ltd. These colloids are essentially monodisperse and spherical in shape as illustrated by the SEM micrograph illustrated in Figure 4.7.

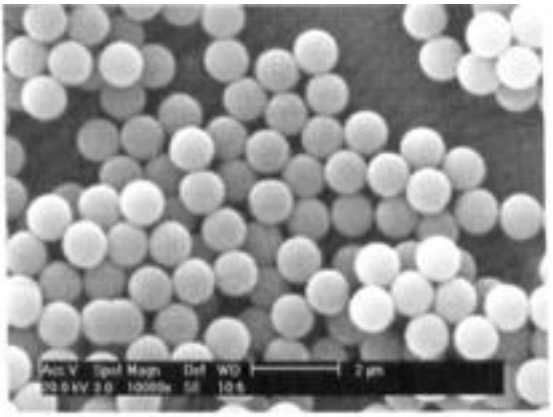

Figure 4.7. Scanning electron micrograph: 800 nm FUSO silica (Scale bar = 2 µm).

The polystyrene latex particles stabilised by $pMMA_{16}$-$pDMAEMA_{245}$ were synthesised using emulsion polymerisation (based on the recipe of Amalvy *et al.*[3]) as outlined in Section 4.3.1. Dried SEM micrographs of these latex particles indicated particle diameters ranging from 85 – 100 nm as shown by Figure 4.8.

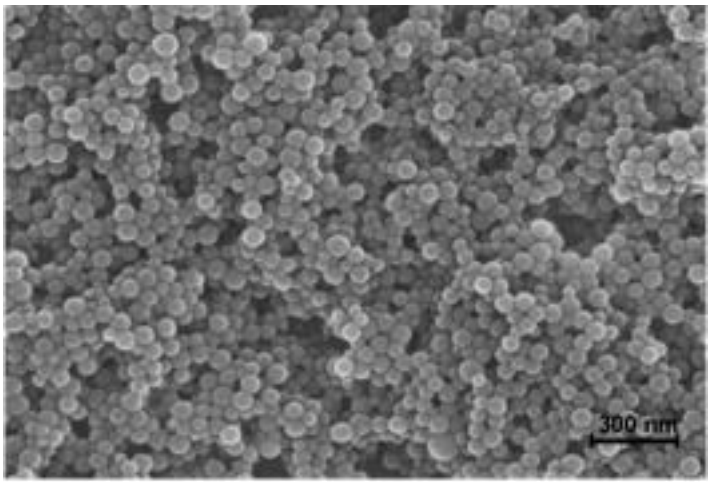

Figure 4.8. Scanning electron micrograph: $pMMA_{16}$-$pDMAEMA_{245}$ stabilised polystyrene latex particles (Scale bar = 300 nm).

4.5.2. RME setup and procedure

The emulsions were produced using a stainless steel membrane mounted on an overhead stirrer motor (IKA, Eurostar digital agitator). Prior to conducting the

experiments, the wettability of the continuous and dispersed phases were imaged to ensure the production of oil-in-water emulsions as illustrated by Figure 4.9.

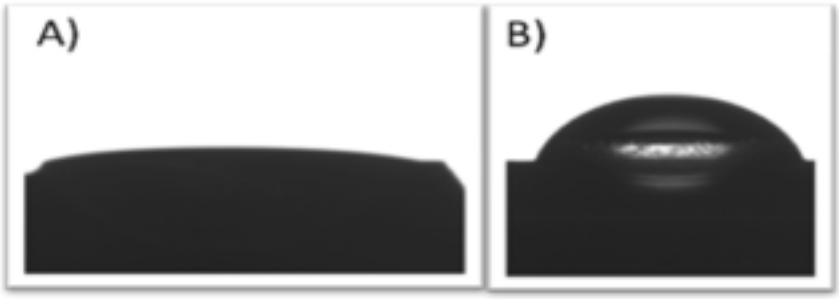

Figure 4.9. Illustrating the preferential wetting of water droplet (A) over oil droplet (B) on the membrane surface.

The membrane was carefully placed into a stationary cylindrical vial (Figure 4.10). The steel membrane is laser drilled with a pore size of 80 µm × 80 µm illustrated by Figure 4.11.[12] The membrane has a diameter of 8 mm, length of 25 mm and a membrane wall thickness of 0.5 mm. It contains 108 pores, which are drilled in a controlled array; further information on the properties and characteristics of this membrane can be found in an earlier publication.[12]

The volume of continuous phase used in the experiments was 25 mL, with varying pH, electrolyte and particle concentrations. Prior to emulsification the particle dispersion was sonicated for 20 minutes, dispersed using a vortex mixer and the particle size was subsequently checked using DLS before use. The membrane rotational speed was kept constant for a given experiment. The rotational speeds were systematically varied from 500 to 1500 rpm.

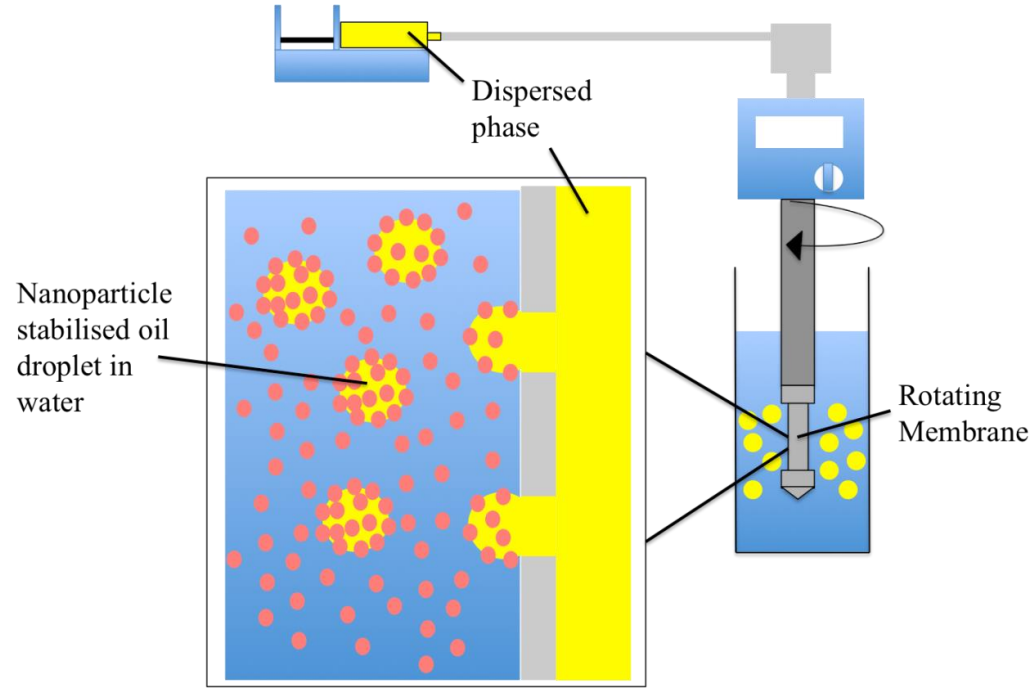

Figure 4.10. Schematic illustration of the RME reactor system. The illustration (left) shows a cross sectional view of oil droplets being stabilised by nanoparticles through particle adsorption from the continuous phase. *Redrawn from Ref. [12]*.

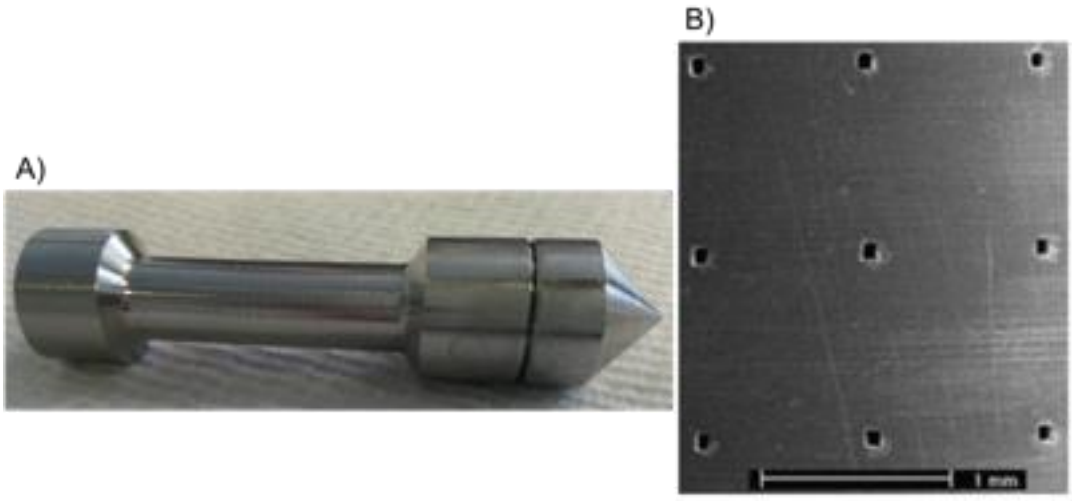

Figure 4.11. Laser drilled 80 µm × 80 µm stainless steel membrane used throughout the membrane emulsification experiments, A) Digital micrograph of the membrane and B) SEM micrograph of the membrane pores (Scale bar = 1 mm), *Taken from Ref. [13]*.

In a typical experiment, the dispersed phase is introduced from a syringe mounted on a syringe pump (Razel A99FMZ, Fisher Scientific, U.K) with a wide variety of pumping rates from 0.075×10^{-6} to 75×10^{-6} m^3 h^{-1}. The use of syringe pump allows the expression of the dispersed phase through the membrane to be accurately controlled. The flow rates examined in this study ranged from 1×10^{-3} to 1 mL min^{-1} to compare the droplet sizes obtained with previous surfactant stabilised emulsions using the same membrane pore size. All the emulsification experiments were conducted at room temperature.

4.5.3. Emulsion characterisation and analysis

The emulsion droplets were imaged using optical microscopy to subsequently calculate the number average droplet diameter and droplet size distribution. The distortion of the droplets was prevented by using pipettes with an opening at least 2 times wider than the maximum droplet size. The size measurements were carried out using the Java-based image processing software 'ImageJ' (developed at the National Institutes of Health). The images were taken immediately after the emulsification experiments were complete. Optical microscopy was consistently used to measure the droplet size instead of any of the light scattering measurement techniques described above to accurately take into account all droplet sizes.

4.6. Particle adsorption to liquid-liquid interfaces

This section outlines the use of a pendant drop tensiometer device (4.6.1) and a microtensiometer (4.6.2) to investigate kinetics of particle adsorption to liquid-liquid interfaces.

4.6.1. Dynamic studies via pendant drop measurements

The theory behind the use of pendant drop techniques for measurement of surface/interfacial tension is mentioned earlier in Section 4.4.4. This technique was used to measure the changes in interfacial tension over time for a variety of different particle and oil systems:

- 800 nm FUSO silica with tricaprylin oil
- 300 nm sulfate stabilised polystyrene latex particles (supplied by IDC, USA) with hexadecane oil
- pMMA-b-pDMAEMA sterically stabilised latex particles with hexadecane oil

The changes in interfacial tension with time was measured by recording a video of a droplet (containing a dispersion of particles at different concentrations) immersed into a cuvette containing one of the oils for a period of time (usually 5000 seconds). Once the recording was complete, the resulting movie was played back in the Drop Shape Analysis software accompanying the pendant drop device. For every video frame, the shape of the droplet was fitted to a Young-Laplace model which yielded an interfacial tension value, which was plotted as an isotherm.

4.6.2. Dynamic studies using a Microtensiometer

A custom-built microtensiometer device developed at Carnegie Mellon university[14] was used as an alternative method to investigate particle adsorption kinetics. In the pendant droplet technique, an important experimental parameter concerns the balance between gravitational and surface tension forces as described by the Bond number, B_0, in Equation 4.10, where ρ is the density, g the gravitational force, R_c the radius of the capillary and γ the interfacial tension;

$$B_0 = \frac{\Delta\rho g R_c^2}{\gamma}$$ (Equation 4.10)

In the pendant droplet technique the Bond number is around 0.3, while in the microtensiometer the Bond number is smaller than 0.01, which is achieved by either matching the densities of the two fluids or reducing the surface area of the interface. By reducing the Bond number the interface becomes spherical. This is an important parameter as with increasing Bond numbers, the curvature of the interface becomes non-uniform and the capillary pressure becomes significantly different at each point on the interface.[15] Under these conditions where the interface is deformed, accurate measurement of pressure change becomes impossible which affects the calculation of surface tension.

In the case where the droplet is spherical, direct measurement of both the pressure jump across the interface and the radius of the spherical interface can be used to calculate the surface tension by the Young-Laplace equation (Equation 4.7). The pressure jump across the interface is measured using a pressure transducer, whilst a syringe pump is used to control the size of the microscopic droplet formed at the end of the glass capillary. The main features of the device are illustrated in Figure 4.12 and Figure 4.13.[14]

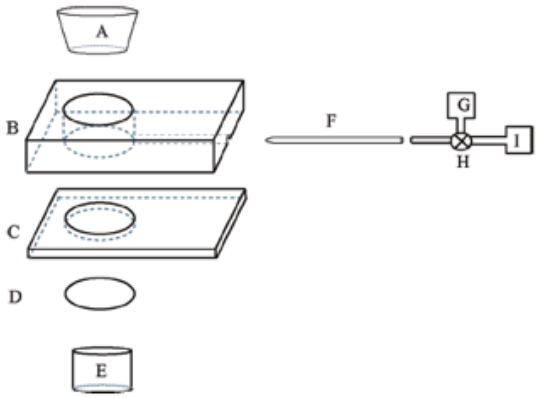

Figure 4.12. Schematic diagram illustrating the components of the microtensiometer device used in this study. The different parts of the microtensiometer include A: microscope condenser, B: PDMS well and holder, C: PDMS spacer, D: coverslip, E: objective and image analysis, F: glass capillary, G: pressure transducer, H: 3-way solenoid valve and I: constant pressure head. *Taken from Ref. [14]*.

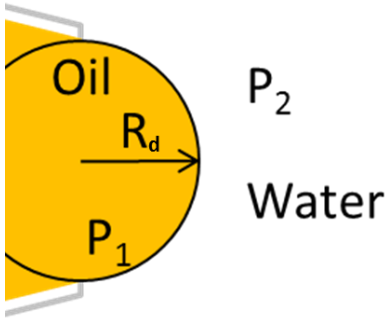

Figure 4.13. Magnified view of the capillary tip (F). An oil droplet endcap is formed at the capillary tip into a reservoir well of water. The droplet radius (R_d), internal (P_1) and outer (P_2) pressure are measured for calculation of the interfacial tension using Young-Laplace equation. *Redrawn from Ref.* [16].

Further details regarding the fabrication of the sample cell and capillaries can be found in a publication by Prof Lynn Walker's group that developed this instrument at Carnegie Mellon University.[14] In a typical experiment, the glass capillaries were cleaned using sulphuric acid and rinsed with acetone. The capillaries were washed

with acetone for a number of times and allowed to dry in an oven. Once dried the capillaries were tested for axis-symmetry using a microscope and to ensure that the tip of the capillary was not damaged by the cleaning procedure.

Before measuring the interfacial tension of liquid-liquid interfaces, a clean air-water interface was studied to ensure the value of an pure air/water surface tension could be obtained (72.8 mN m^{-1}), characteristic of the absence of any impurity in the system. The cell was cleaned and replaced with a particle dispersion to be studied. An oil droplet was formed using a constant pressure head (generated by a water column connected to the 3-way solenoid valve). The interface was recorded using a Diagnostic Instrument Spot RT Monochrome digital camera connected to the microscope. LabVIEW (Laboratory Virtual Instrument Engineering Workbench) developed at National Instruments, was used to process recordings of the interface to determine changes in the droplet radius and to monitor the pressure changes (subtraction of the hydrostatic pressure head at the capillary tip from the measured constant pressure head) to attain interfacial tension measurements.

References

1. F. L. Baines, N. C. Billingham and S. P. Armes, Synthesis and solution properties of water-soluble hydrophilic-hydrophobic block copolymers, *Macromolecules*, 1996, **29**, 3416-3420.
2. U. Chatterjee, S. K. Jewrajka and B. M. Mandal, The amphiphilic block copolymers of 2-(dimethylamino)ethyl methacrylate and methyl methacrylate: Synthesis by atom transfer radical polymerization and solution properties, *Polymer*, 2005, **46**, 10699-10708.
3. J. I. Amalvy, G. F. Unali, Y. Li, S. Granger-Bevan, S. P. Armes, B. P. Binks, J. A. Rodrigues and C. P. Whitby, Synthesis of sterically stabilized polystyrene latex particles using cationic block copolymers and macromonomers and their application as stimulus-responsive particulate emulsifiers for oil-in-water emulsions, *Langmuir*, 2004, **20**, 4345-4354.
4. D. J. Shaw, ed., *Introduction to Colloid and Surface Chemistry*, Butterworth-Heinemann, London, 1992.
5. Malvern, *Zetasizer, Nano ZS Manual*. Issue 2.1, July 2004.
6. M. v. Smoluchowski, *Bull. Int. Acad. Sci. Cracovie*, 1903, **184**, 756.
7. M. W. Kozak and E. J. Davis, Electrokinetics of concentrated suspensions and porous media: I. Thin electrical double layers, *J. Colloid Interface Sci.*, 1989, **127**, 497-510.
8. E. Y. Arashiro and N. R. Demarquette, Use of the pendant drop method to measure interfacial tension between molten polymers, *Mat. Res.*, 1999, **2**, 23-32.
9. F. Bashforth, ed., *An Attempt to Test the Theories of Capillary Action by Comparing the Theoretical and Measured Forms of Drops of Fluid*, Cambridge University Press, London 1883.
10. M. Korenko and F. Simko, Measurement of interfacial tension in liquid-liquid high-temperature systems, *J. Chem. Eng. Data.*, 2010, **55**, 4561-4573.
11. J. M. Andreas, E. A. Hauser and W. B. Tucker, Boundary tension by pendant drops, *J. Phys. Chem.*, 1938, **42**, 1001-1019.
12. M. S. Manga, O. J. Cayre, R. A. Williams, S. Biggs and D. W. York, Production of solid-stabilised emulsions through rotational membrane emulsification: influence of particle adsorption kinetics, *Soft Matter*, 2012, **8**, 1532-1538.

13. Q. Yuan, N. Aryanti, R. Hou and R. A. Williams, Performance of slotted pores in particle manufacture using rotating membrane emulsification, *Particuology*, 2009, **7**, 114-120.
14. N. J. Alvarez, L. M. Walker and S. L. Anna, A microtensiometer to probe the effect of radius of curvature on surfactant transport to a spherical interface, *Langmuir*, 2010, **26**, 13310-13319.
15. R. Miller and L. Liggieri, eds., *Bubble and drop interfaces*, Koninklijke Brill NV, Leiden, 2011.
16. M. D. Reichert and L. M. Walker, Interfacial Tension Dynamics, Interfacial mechanics, and response to rapid dilution of bulk surfactant of a model oil–water-dispersant system, *Langmuir*, 2013, **29**, 1857-1867

CHAPTER 5: SYNTHESIS AND CHARACTERISATION OF STERICALLY STABILISED LATEX PARTICLES

NOMENCLATURE

α	Degree of protonation
d_p	Particle diameter
I	Initial ionic concentration
M	Initial monomer concentration
P	Initiator concentration
T	Absolute temperature

ABBREVIATIONS

DLS	Dynamic Light Scattering
LCST	Lower critical solution temperature
MEB	Milli-equivalents of added Base

5.1. Particle synthesis

5.1.1. Introduction

Colloidal dispersions are typically made up of particles that are sufficiently small (usually less than 1 μm) distributed throughout another (continuous) phase. There is no sharp distinction between colloidal and non-colloidal dispersions. Many systems that exist in nature contain colloidal particles that are dispersed throughout a liquid phase (e.g. water) and hence have received much attention. The understanding of colloidal systems is very important especially for applications in areas such as precipitation, water treatment, flotation, food processing, lubrication and detergency etc.

Polymer latexes have been extensively studied as model systems to increase our fundamental understanding of key aspects of colloidal science. To understand and describe the behaviour of colloidal systems, many mathematical models often assume that the particles are both spherical and size monodisperse. The use of polymer latex systems is therefore attractive as they are usually spherical and can be synthesized with relatively narrow particle size distributions. One method of producing such polymer latexes is via emulsion polymerisation which is outlined in the subsequent section.

5.1.2. Emulsion polymerisation

The process of emulsion polymerisation has been extensively used within industry since the 1930's. In the early stages very little was known about the mechanism and kinetics associated with the polymerisation process due to the complexity of the heterogeneous system. One of the earliest theories on emulsion polymerisation was proposed by Harkins.[1] The model was based on the following components; water as the continuous phase, with monomers such as styrene as the dispersed phase, water soluble initiators such as persulfate ions and a stabiliser such as anionic surfactants. At the beginning of the polymerisation process, the reaction vessel contains the water phase which also includes the initiator, electrolytes, small quantities of dissolved monomer and other minor ingredients. The rest of the monomer is dispersed as stable emulsion droplets and partially solubilised within the surfactant

micelles. The reaction is heated and the initiator (persulfate ions) molecules decompose into sulfate radicals.

In the early theories it was proposed that the monomer droplet itself polymerised, however Harkins[1] dismissed the idea of particle nucleation occurring within the monomer droplet, based on the observation that the final latex particle was generally much smaller than that of the monomer droplet. In addition, the number of particles at the end of the reaction was typically a thousand times more than the number of monomer droplets, hence the monomer droplets was considered to act as a reservoir for the monomer. The polymerisation was instead thought to occur within the monomer swollen micelles and the polymerisation progressed by drawing additional monomer from droplets through the aqueous phase. As the polymerisation process progresses, the size of the monomer droplets decrease in order to replenish the aqueous phase with more monomer. Although the Harkins model is not consistent with all experimental systems, it does represent an ideal case. It should be noted that emulsion polymerisation can vary greatly depending on the components used and that no single mechanism will account for all emulsion polymerisations.

Harkins also reported that the polymerisation starts upon the migration of the free radicals into the swollen micelles. This causes a depletion of the monomer from the micelles and causes mass transfer from the monomer droplet to the site of newly formed and growing polymer particles. This process has now been revised and it more commonly accepted that the initiation step actually occurs in the aqueous phase, forming oligomeric radical chains.[2, 3] The propagation of the oligomeric chains may undergo in the aqueous phase until a sufficient size occurs making them insoluble in the aqueous phase. The insoluble oligomeric chains may either a) continue to polymerise by entering a swollen micelle, b) by aggregation with other oligomeric chains or c) by entering a monomer droplet. All three routes are possible and the route taken depends on the emulsion system used.

The process of emulsion polymerisation occurs in 3 steps, the first step is the initiation stage characterised by particle nucleation in which the particle number is determined. This stage is regarded as complete when the micelles disappear. The second stage is the particle growth. At this stage the polymerisation proceeds by drawing monomer from the aqueous phase and the particle number remains relatively constant. The monomer droplet shrinks in size in order to replenish the

aqueous phase. This second stage is considered complete when all the monomer droplets disappear. The last stage of the polymerisation process is the additional particle growth in the absence of monomer droplets. At this stage, almost all of the monomer is confined within the swollen latex particles. After a period of time a 100% monomer conversion is achieved. In order to produce latex particles with a relatively narrow particle size distribution, the nucleation period needs to be short followed by a long growth period without coagulation.

Styrene is commonly used as a monomer in academic emulsion polymerization experiments due to its convenience in laboratory handling. After polymerisation, amorphous polystyrene latex particles are produced that are spherical, insoluble is the dispersion medium and are relatively low in size polydispersity. Persulfate is commonly used as the initiator, however it can produce a surface of mixed functional groups such as sulfate, hydroxyl and under some processing conditions carboxyl. These mixed surface groups originate from the initiator fragments that are chemically bound to polymer chains during polymerization as well as from surface oxidation.

A systematic studied was carried out by Goodwin *et al.*[4] looking at the influence of electrolyte strength, monomer concentration, initiator concentration and temperature on the size of particles produced in an emulsifier-free system. A range of particle sizes between 0.1 to 1 μm was obtained by adjusting the reaction conditions. From their data they derived a formula from which the particle size could be predicted from the preparation conditions;

$$\log d_p = 0.238\left[\log\frac{[I][M]^{1.723}}{[P]} + \frac{4929}{T}\right] - 0.827 \qquad \text{(Equation 5.1)}$$

where d_p is the particle diameter, T the absolute temperature, I the initial ionic strength, M the initial monomer concentration and P the initiator concentration.

Similar results have also been published by other authors.[5] It is evident that the components, the method of addition and the reaction conditions all influence the final product characteristics.

In addition to surfactants, the use of chemically grafted or the physical adsorption of polymers to enhance the stability of the polymer latex particles is well established.[6] The polymeric stabilisers that are commonly used are usually non-ionic or anionic in character, common examples include poly(ethylene oxide),[7] poly(acrylic acid) and poly(acrylic acid) based di-block copolymers.[8, 9] Whilst only a few reports exist on the use of cationic di-block copolymers as latex stabilisers.[10, 11] These stabilisers are based on 2-dimethylaminoethyl methacrylate (DMAEMA). The advantage of using this steric stabiliser is that it is a tertiary amine methacrylate and hence has a pH-responsive property that than can be used to produce core-shell particles (where the core is e.g. polystyrene and the shell is made of the DMAEMA polymer). In this thesis the use of pMMA-b-pDMAEMA as a steric stabiliser for producing latex particles is investigated. The characterisation of the di-block copolymer and the sterically stabilised particles is detailed in the subsequent sections.

5.2. Solution properties of pMMA-b-pDMAEMA di-block copolymer

5.2.1. Dynamic light scattering

The di-block copolymers used in this work comprise of a hydrophobic component (pMMA) and a hydrophilic component (pDMAEMA). It should be noted that these di-block copolymers are readily soluble in weakly acidic aqueous environments (pH ≈ 4).[12] The pDMAEMA block contains a tertiary amine group, that protonates and selectively solubilises in a weakly acidic aqueous environment. Such hydrophobic-hydrophilic block copolymers have been reported to form micelle structures in solvents, which are selective for one of the blocks.[13-16]

Dynamic light scattering (DLS) measurements were performed to investigate the micellar hydrodynamic diameter of pMMA-b-pDMAEMA solutions as a function of polymer concentration, prepared at pH = 4 in the presence of 0.01M KNO_3. The data in Figure 5.1 highlight changes in the hydrodynamic diameter as a result of increasing pDMAEMA block length.

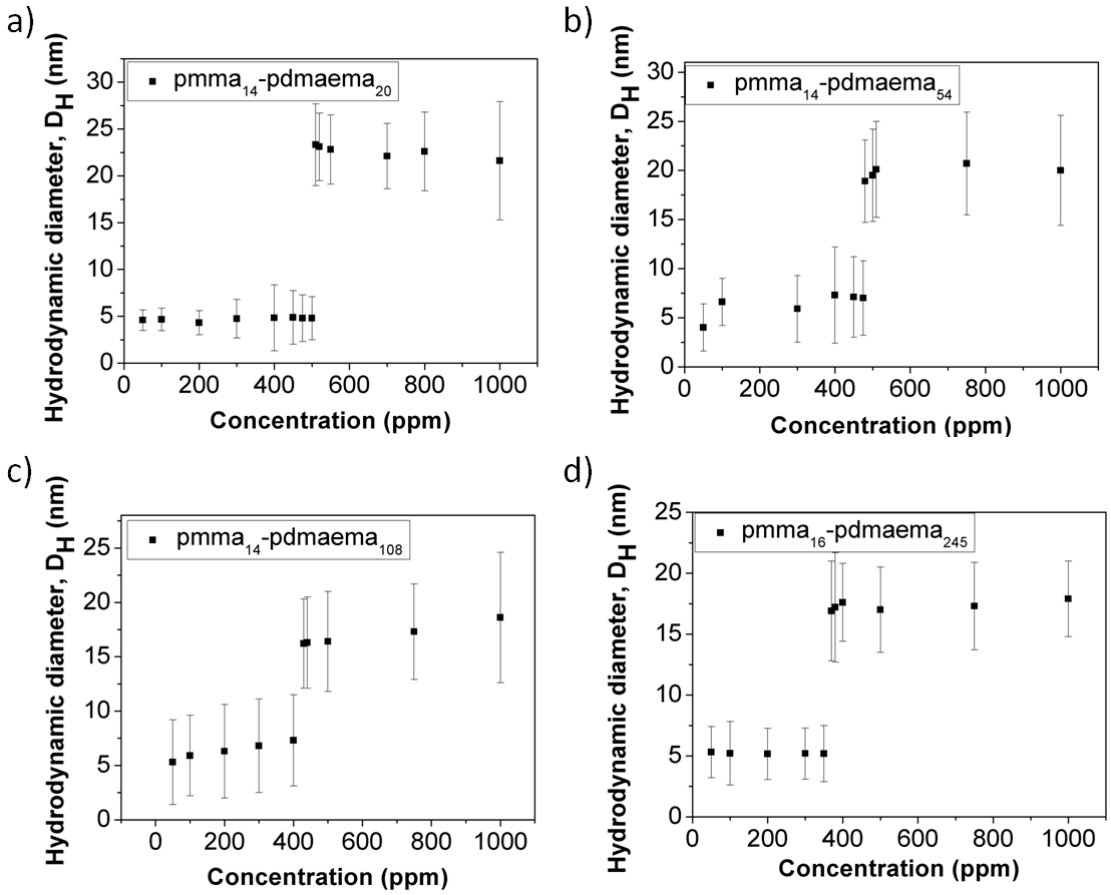

Figure 5.1. Variation in hydrodynamic diameter as a function of polymer concentration for four different pDMAEMA block lengths; a) 20, b) 54, c) 108 and d) 245. The polymer solutions are prepared at pH 4 in presence of 0.01M KNO_3 (T = 25°C).

The DLS technique is not able to gather information relating to the size of the micelle core and corona individually, however the hydrodynamic diameter does gives an indication of the diameter of the copolymer aggregate. At low polymer concentrations (less than 400 - 500 ppm) the copolymer exists as individual chains (unimers). At polymer concentrations the critical micelle concentration the copolymer chains aggregate forming micelles. The micelles consist of a hydrophobic micellar core (pMMA) and a hydrophilic corona (pDMAEMA).

The DLS data shows that the micelles of the copolymer with the greatest asymmetry ($pMMA_{14}$-b-$pDMAEMA_{108}$ and $pMMA_{16}$-b-$pDMAEMA_{245}$) are the smallest. The data clearly shows that as the pDMAEMA block length increases, the micelle diameter decreases. This phenomena can be described by the packing parameter

theory.[17] The longer pDMAEMA chains lead to a bigger hydrophilic head group and hence they form smaller aggregates in solution with a higher degree of curvature. The trend observed from these data presented in table 5.1 matches observations previously reported by Xiao *et al.*[18] In addition the transition from unimers to equilibrium micelles occurs at different critical micelle concentrations for each of the polymers studied (Table 5.1) and at values similar to that observed by Baines *et al.*[16] and Chatterjee *et al.*[19]

Batch Entry	Block lengths	CMC (ppm)
GB 167	$pMMA_{14}$-b-$pDMAEMA_{20}$	510
GB 168	$pMMA_{14}$-b-$pDMAEMA_{54}$	480
GB 169	$pMMA_{14}$-b-$pDMAEMA_{108}$	430
WB 76	$pMMA_{16}$-b-$pDMAEMA_{245}$	370

Table 5.1. The critical micelle concentration of pMMA-b-pDMAEMA diblock copolymers determined via DLS as a function of changing pDMAEMA block lengths in pH 4 aqueous solutions at 25°C.

The data also demonstrates that the surface activity of these diblock copolymers mainly depends on the influence of the hydrophobic block (pMMA) due to its packing density at the interface. As the pDMAEMA block length increases the packing density of the hydrophobic chains also increase which in turn leads to a reduction in the critical micelle concentration.[18]

The change in the hydrodynamic diameter as a function of solution pH at 25°C for a 1000 ppm $pMMA_{16}$-b-$pDMAEMA_{245}$ is presented in Figure 5.2. This is a typical plot also observed with the other copolymers that have been studied.

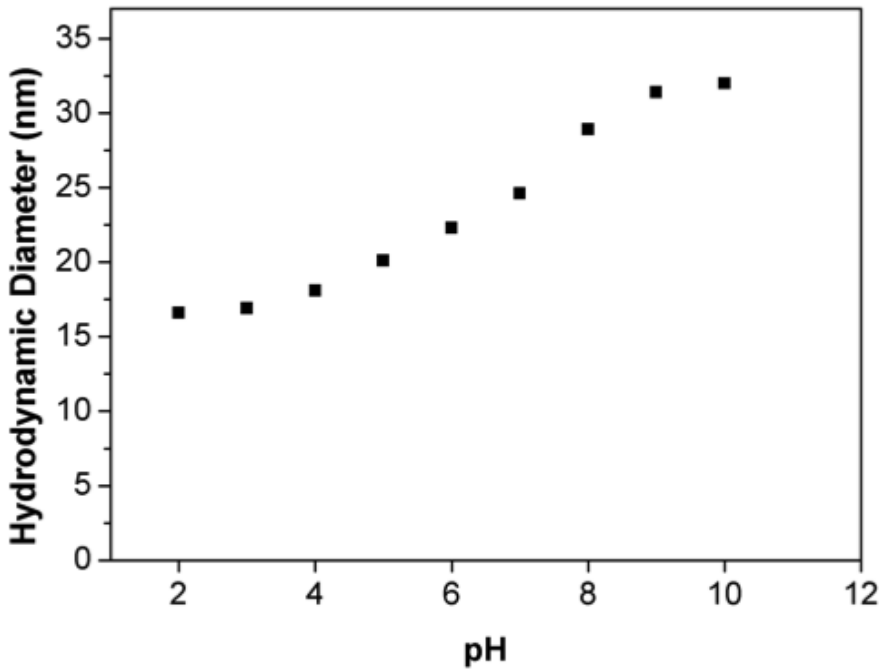

Figure 5.2. Change in hydrodynamic diameter as a function of solution pH for $pMMA_{16}$-b-$pDMAEMA_{245}$ (T = 25°C).

The hydrodynamic diameter of the micelles increases as a function of increasing pH. At high pH values the electrostatic repulsion of the hydrophilic head groups is reduced since the degree of protonation is very low (Section 4.2.3). At lower pH values, the pDMAEMA chains are more protonated, resulting in stronger electrostatic repulsion and effectively, therefore, larger head group dimensions producing correspondingly smaller aggregates.[18]

5.2.2. Potentiometric titrations

Potentiometric titrations were conducted on an aqueous solution of a di-block copolymer (pMMA-b-pDMAEMA) sample. The titration data, where the solution pH is measured as a function of milli-equivalents of added base (MEB), for a 1000 ppm solution of $pMMA_{14}$-b-$pDMAEMA_{20}$ is shown in Figure 5.3. Also shown on the same figure is the plot of $\Delta pH/\Delta MEB$ as a function of added base. The curves presented in Figure 5.3 are representative of multiple titrations for the different di-block copolymers studied at various concentrations ranging from 50 to 500 ppm.

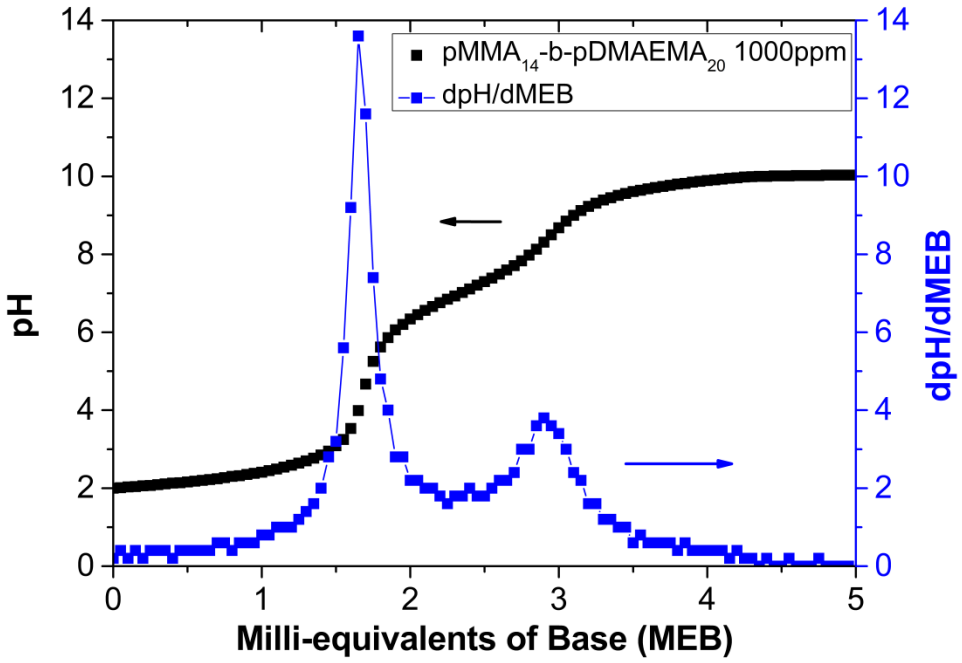

Figure 5.3. Changes in the solution pH as a function of added milli-equivalents of base for a 1000 ppm aqueous solution of $pMMA_{14}$-b-$pDMAEMA_{20}$ (black). Also shown is the ΔpH/ΔMEB as a function of added base (blue).

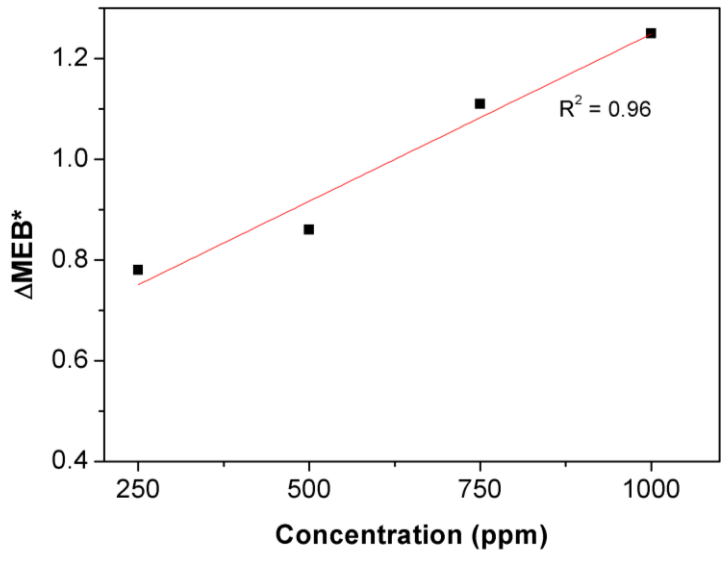

Figure 5.4. Change in ΔMEB* as a function of polymer concentration for aqueous solutions of $pMMA_{14}$-b-$pDMAEMA_{20}$.

The gap between the two peaks in the ΔpH/ΔMEB versus milli-equivalents of added base is defined as ΔMEB*. A plot showing the dependence of ΔMEB* on the

polymer concentration of $pMMA_{14}$-b-$pDMAEMA_{20}$ is presented in Figure 5.4. The data presented in Figure 5.4 shows a clear linear relationship between different polymer concentrations and ΔMEB*. Such data is important as it can allow the possibility of evaluating the concentration of $pMMA_{14}$-b-$pDMAEMA_{20}$ in a solution where the composition is unknown.

The titration data presented in Figure 5.3 for each polymer concentration can be converted into a plot illustrating the degree of association (α) of the DMAEMA chains (section 5.1.3). A plot of pH versus α for a 1000 ppm $pMMA_{14}$-b-$pDMAEMA_{20}$ aqueous solution is presented in Figure 5.5. The plot is representative of multiple titrations over a range of polymer concentration.

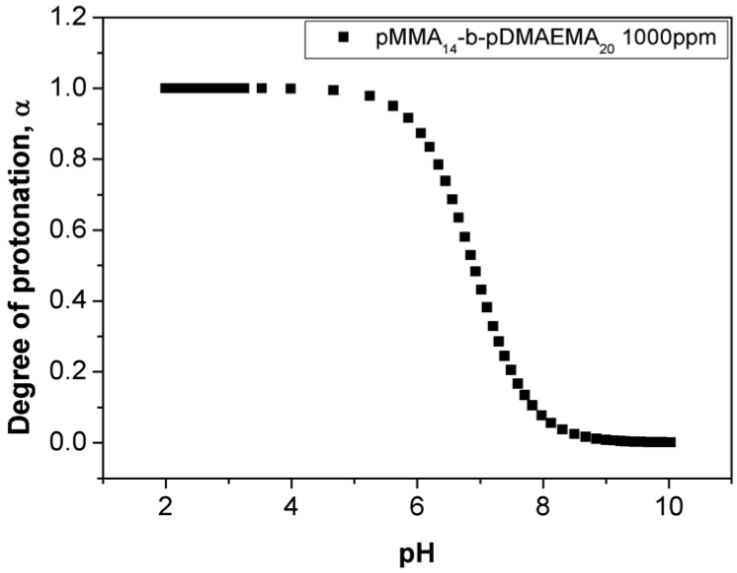

Figure 5.5. Degree of polymer association as a function of pH, for a 1000 ppm aqueous solution of $pMMA_{14}$-b-$pDMAEMA_{20}$.

The data presented in Figure 5.5 shows that the majority of the polymer association occurs over a narrow pH range. Assuming maximum proton association at the starting conditions (very low pH), the addition of base initially has no effect on the proton association until the solution pH becomes greater than 6. After pH 6, further addition of base causes a decrease in the proton association. It can be seen that at pH 8 the copolymer has less than 5% residual proton association. The addition of more base, causes further dissociation until α reaches a value of zero at a solution pH of 9-

10. The degree of protonation data confirms that the pDMAEMA block is weakly basic with a pK_a value of around 7.5.[11]

5.3. Factors affecting particle synthesis

5.3.1. Effect of polymer chain length and reaction temperature

The effect of the pDMAEMA polymer chain length and the reaction temperature on the emulsion polymerisation of styrene was investigated by comparing the particle size obtained at pH 9 where the dispersion remains stable and as individual particles. Table 5.2 and 5.3 summarise the particle size data obtained at pH 8, as a function of pDMAEMA block length and reaction temperature and the size polydispersity of these particles. Scanning electron micrographs of these particle samples are presented in Figure 5.6 and 5.7.

The particle size data presented in Table 5.2 illustrates that the particle size increases as the pDMAEMA block length increases for a fixed pMMA block length. This is because the molecular weight of the copolymer increases with increasing pDMAEMA block length. This reduces the concentration of stabiliser molecules present for a given weight % of polymer in the reaction and thus larger particles are created as confirmed by DLS and SEM. There is a small difference in the particle size when comparing data from DLS and SEM micrographs. This is because in SEM the particles are dry and hence only the latex particles are observed, whilst in DLS the particles are measured as a dispersion and hence both the latex core as well as the polymer shell is detected .

Sample No	pDMAEMA block length	DLS latex hydrodynamic diameter, D_z (nm) (polydispersity)	SEM latex diameter, D_n (nm)
SM01	54	57 (0.06)	53 (0.06)
SM02	108	68 (0.08)	64 (0.09)
SM03	254	87 (0.05)	84 (0.07)

Table 5.2. Effect of increasing pDMAEMA block length on the particle size of sterically stabilised polystyrene latex particles prepared at a reaction temperature of 70°C.

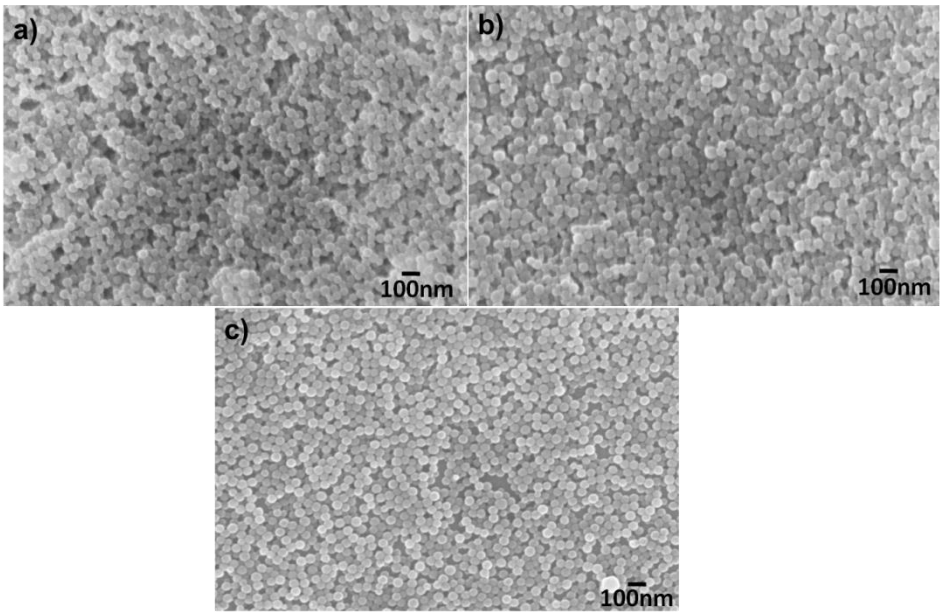

Figure 5.6. Scanning electron micrographs of polystyrene latex particles stabilised by varying pDMAEMA block lengths; a) 54, b) 108 and c) 245, produced via emulsion polymerisation at 70°C.

Sample No	Reaction temperature (°C)	DLS latex diameter, D_z (nm) (polydispersity)	SEM latex diameter, D_n (nm)
SM04	50	342 (0.11)	335 (0.13)
SM05	60	155 (0.07)	150 (0.09)
SM01	70	57 (0.06)	53 (0.06)

Table 5.3. Effect of reaction temperature on the particle size of $pMMA_{14}$-b-$pDMAEMA_{54}$ sterically stabilised polystyrene latex particles.

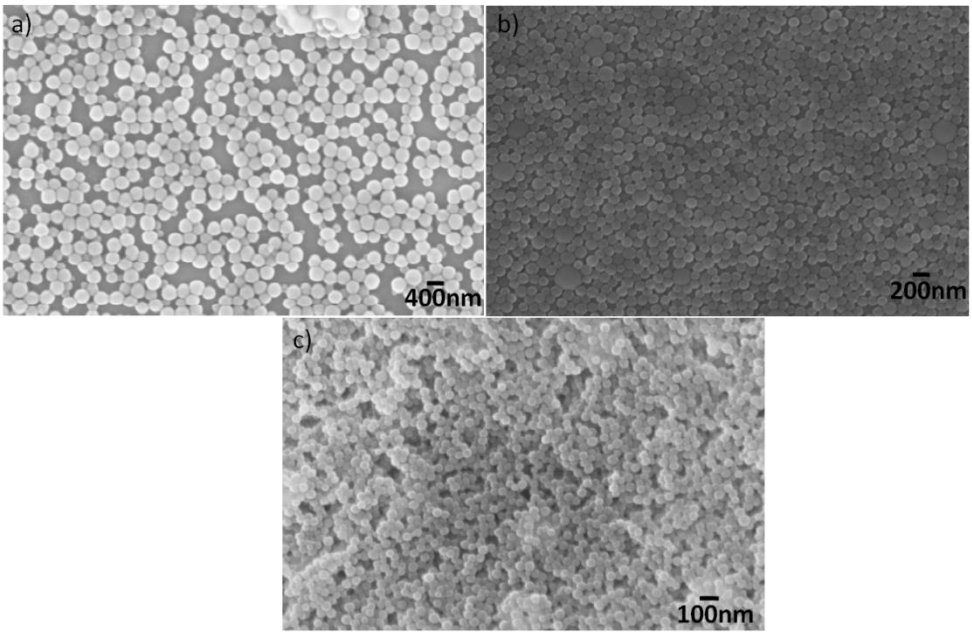

Figure 5.7. Scanning electron micrographs of polystyrene latex particles stabilised by $pMMA_{14}$-b-$pDMAEMA_{54}$, via emulsion polymerisation at different reaction temperatures; a) 50°C, b) 60°C and c) 70°C.

The data presented in Table 5.2 illustrates that by increasing the reaction temperature the particle size decreases. This inverse dependence between the reaction temperature and particle size is a result of the decomposition rate of the initiator. As the temperature increases, the decomposition rate of the initiator increases. In addition, raising the temperature also increases the monomer solubility in the aqueous phase, resulting in an increase in the concentration of the growing chains causing a reduction in the bead size.[9, 20]

5.3.2. Polymer grafting density measurements

The grafting density of the polymer chains provides important information about the number of polymer chains present on the particle surface and how this influences the properties of the core-shell particles. ^{1}H NMR was performed by dissolving the latex particles in $CDCl_3$ and measuring the associated spectra. The intensity signals from the polystyrene and stabiliser are analysed via integration of the relevant proton signals. Figure 5.8 illustrates a typical ^{1}H NMR spectra obtained for polystyrene latex particles sterically stabilised by pMMA-b-pDMAEMA.

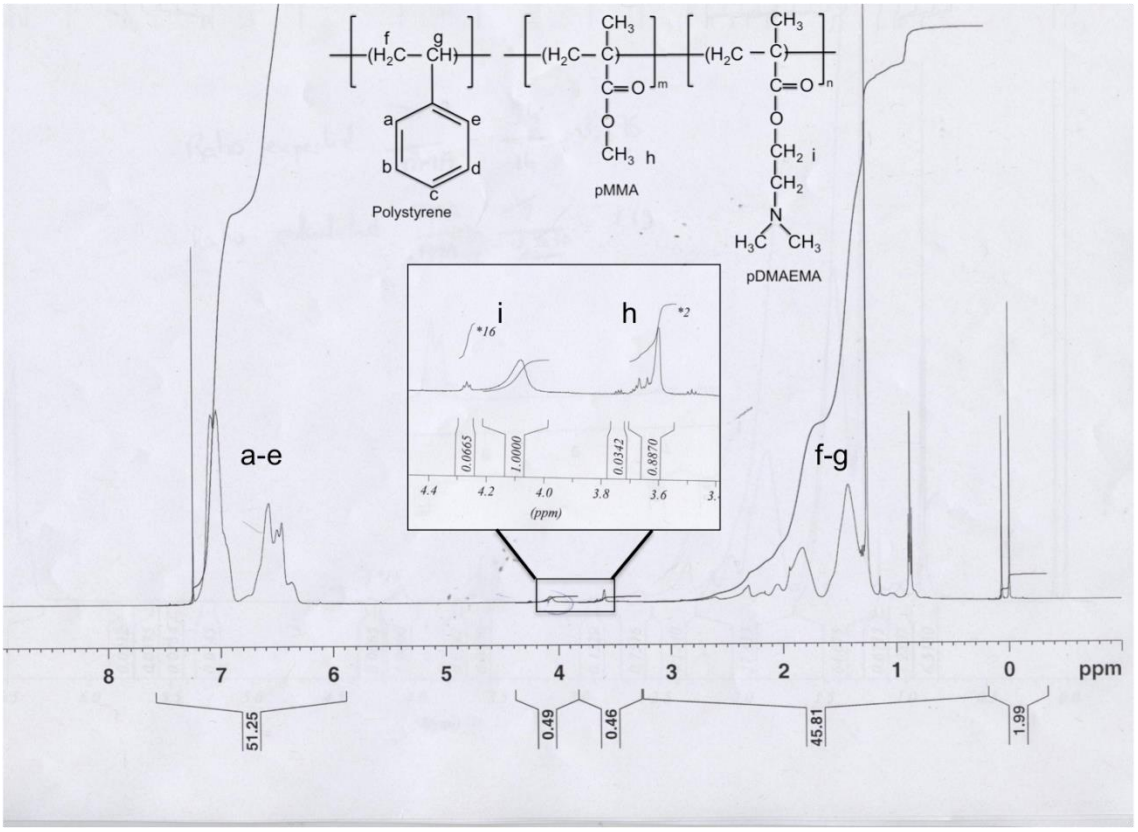

Figure 5.8. ^{1}H NMR spectra of polystyrene latex particles sterically stabilised using pMMA-b-pDMAEMA dissolved in $CDCl_3$ to allow calculation of stabiliser content and thus the grafting density.

It was assumed that the stabiliser was uniquely located on the surface of the particles. The oxymethylene proton peaks (around δ 4.0) were compared to the aromatic peaks of styrene (δ 6.0-8.0). The grafting density, Γ, was calculated by comparing the stabiliser content (which takes into account the integration peaks) with the available particle surface area (based on intensity-averaged particle diameter using DLS).[11] The information relating to the grafting density of samples SM01 and SM03 (Table 5.1) is presented in Table 5.4. The grafting density values obtained for the polystyrene latex particles match well with the values obtained by Amalvy *et al.*[11] for the same core-shell particle system. They also achieved a grafting density value of 0.3 mg m^{-2}.

The weakly cationic nature of the stabiliser means that the polymer chains occupy considerably more latex surface area per chain. This gives grafting density values that are considerably lower than those observed with other polymerisation techniques such as dispersion polymerisation.[11]

Sample No	DMA peak integration (^{1}H)	Polystyrene peak integral (^{1}H)	Particle Diameter (nm)	Particle surface area (m^2)	Polystyrene per particle (g)	Stabiliser (mg)	Stabiliser content (wt%)	Adsorbed amount, Γ (mg m^{-2})
SM01	0.48	26.97	54	1.39×10^{-14}	1.02×10^{-16}	3.22×10^{-14}	3.01	0.23
SM03	0.53	32.53	87	3.35×10^{-14}	4.01×10^{-16}	1.01×10^{-14}	2.53	0.30

Table 5.4. Polymer grafting density data using ^{1}H NMR for samples SM01 and SM03.

The data can be further examined to obtain information regarding the number of polymer chains and subsequently the number of tertiary amine groups present per particle. This is summarised in Table 5.5.

	SM01	SM03
Average molecular number, M_n (g mol^{-1})	10110	40340
Chains/nm^2	1.8×10^{-2}	4.5×10^{-3}
Chains/particle	53	29
Amine groups/particle	2862	7105

Table 5.5. Details regarding the area occupied, number of polymer chains and amine groups per particle derived from the grafting density data.

The data in Table 5.5 shows that the area and the number of polymer chains occupied on the surface of the particle decreases with increasing pDMAEMA block length which fits in with the polymer packing theory.[17] In addition, increase in the pDMAEMA block length directly results in an increase in the number of amine

groups present per particle. This information will be important when comparing the use of these particles for stabilising Pickering emulsions.

5.4. Particle characterisation

5.4.1. Hydrodynamic diameter and electrophoretic mobility measurements

5.4.1.1. Effect of pH

The hydrodynamic size and electrophoretic mobility was measured to ascertain the behaviour of pMMA-b-pDMAEMA sterically stabilised polystyrene latex in aqueous media. Changes in the particle hydrodynamic diameter and electrophoretic mobility as a function of solution pH for samples SM01 and SM03 are presented in Figure 5.9.

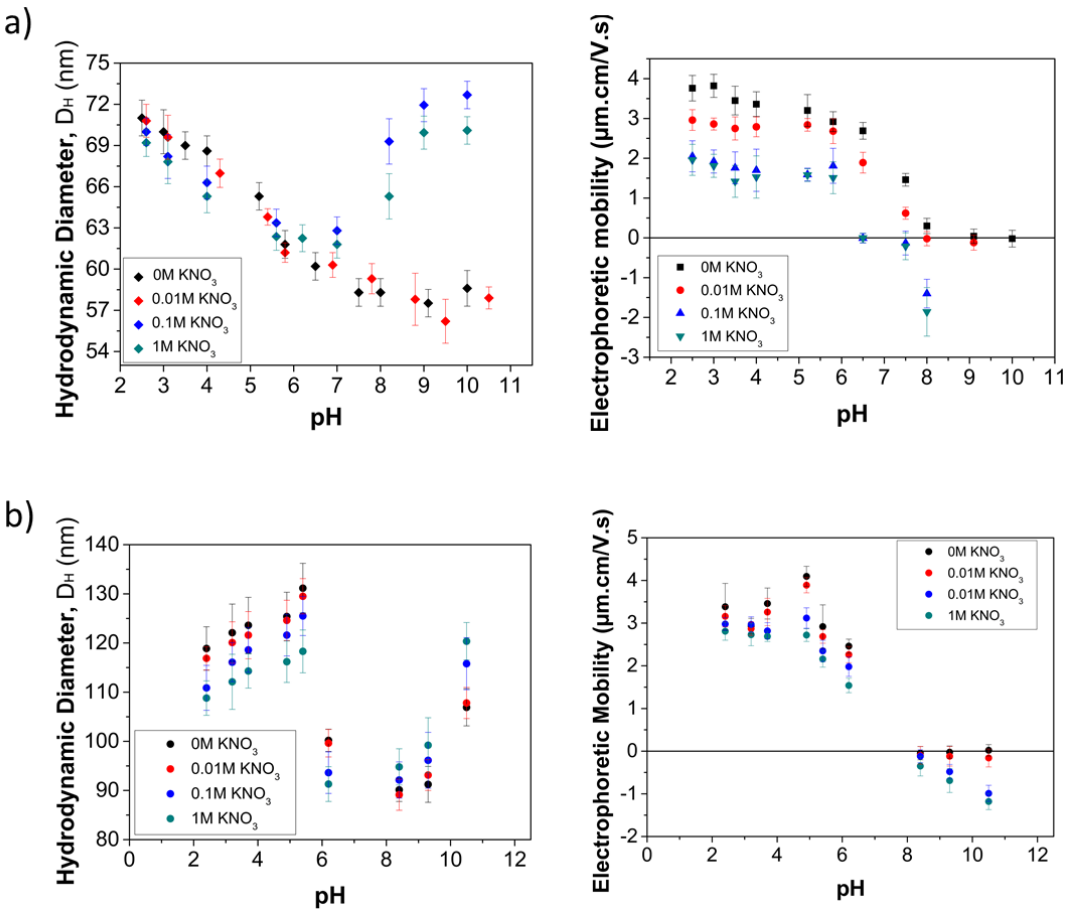

Figure 5.9. Changes in the particle hydrodynamic diameter and electrophoretic mobility as a function of pH for sample a) SM01 and b) SM03 in the presence of varying background KNO_3 electrolyte concentration; 0M (black), 0.01M (red), 0.1M (blue) and 1M (green).

In general, the latex samples exhibit changes in both the hydrodynamic size and electrophoretic mobility as a function of pH (Figure 5.9). In the case where the particles are dispersed with no background electrolyte, a number of key features can be highlighted; 1) as the pH is decreased from around pH 9 to pH 3, both the hydrodynamic diameter and electrophoretic mobility increase due to the protonation of the amine groups on the pDMAEMA block. Increasing the pH of the particle dispersion above 9, shows an increase in the measured particle size whilst the particle mobility remains close to zero; The polymer is essentially uncharged and collapsed at these pH's and the small increase in size is probably caused by the formation of aggregation of the latex particles driven by an intersegmental attraction between the uncharged pDMAEMA chains on the surface of adjacent particles.

5.4.1.2. Effect of background electrolyte

The effect of background electrolyte on both the hydrodynamic diameter and particle mobility is also shown in Figure 5.9. It can be seen that at any pH less than 9, an increase in background electrolyte causes a reduction in the particle mobility. The addition of electrolyte screens the surface charges present on the polymer and the strength of this charge screening increases with electrolyte concentration. A reduction in particle size is also observed as a result of the partial collapse of the charged polymer chains at increased electrolyte levels. At pH 9 and above, the insolubility of the polymer increases and therefore the strength of the intersegmental attraction increases leading to the formation of large aggregates. At pH 10, increase in the salt concentration gives arise to a higher negative electrophoretic mobility value.

5.4.2. Temperature responsiveness

The pMMA-b-pDMAEMA di-block copolymers are not only responsive to pH stimuli, they have also been shown to be temperature responsive.[21, 22] The pDMAEMA polymer chains have a lower critical solution temperature (LCST) that occurs between 40 - 50°C. The LCST dictates the solvency of the polymer in solution; i.e. the polymer is miscible below this critical temperature and becomes unstable and precipitates in solution above this value. The latex particles grafted

with di-block copolymers were investigated for changes in the hydrodynamic diameter as the dispersion temperature changes as a function of solution pH. The effect of electrolyte concentration on the particle size was also investigated. The latex particles used in this study were sterically stabilised using $pMMA_{16}$-b-$pDMAEMA_{245}$ at 65°C (Sample SM04). Therefore the particle size is different to sample SM03 i.e. larger, so the changes in the hydrodynamic diameter and mobility of these particles to pH are first presented in Figure 5.10.

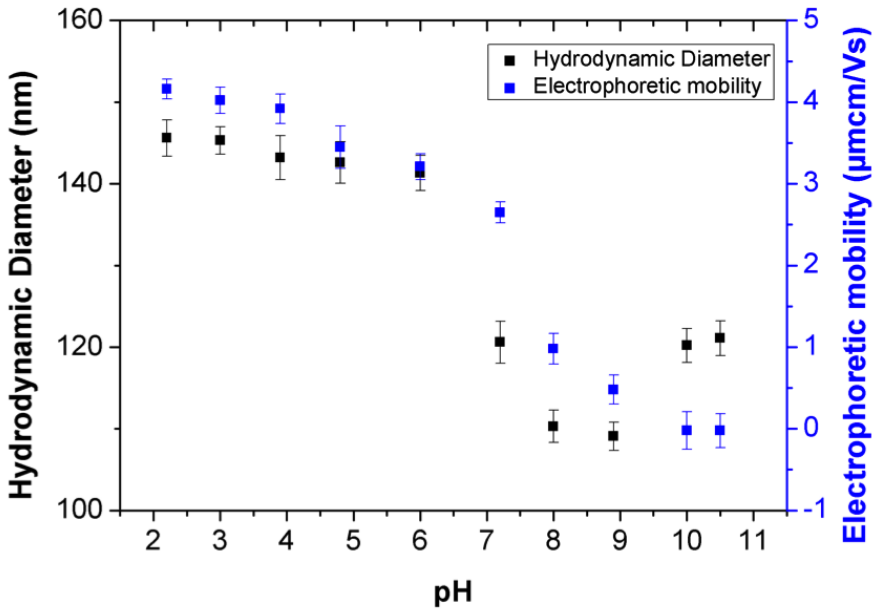

Figure 5.10. Changes in the hydrodynamic diameter and electrophoretic mobility as a function of pH for sample SM04.

The changes in the particle size and mobility follow the same trends as discussed in Section 5.4.1.

5.4.2.1. Effect of temperature

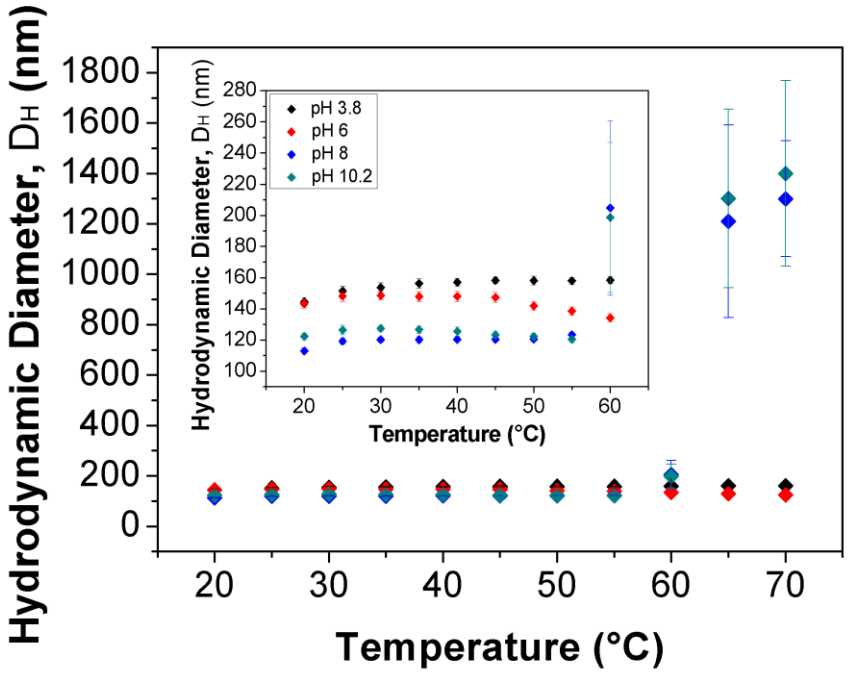

Figure 5.11. Changes in the particle hydrodynamic diameter of sample SM04 with temperature as a function of solution pH with no added background electrolyte.

In acidic pH (pH 3.8), the hydrodynamic diameter remains relatively unchanged as a function of increasing temperature. At this pH, the pDMAEMA chains are strongly protonated; the polymer is highly soluble under these conditions and adopts an extended configuration in solution. At pH 6, we find that the hydrodynamic diameter decreases as the temperature is increased. At pH 6, the polymer is less strongly protonated and will be partially collapsed, even at room temperature; clearly, this decreased baseline polymer solvency is sufficient to result in a further decrease in solvency as the temperature increases resulting in a reduction in the observed hydrodynamic diameter. At pH 8 and 10.2, the polymer is more fully collapsed onto the particle surface and no change is observed as the temperature is increased until reaching an LCST value above 50°C. At this point the pDMAEMA chains entirely lose solvency and particle aggregation is observed above this point.

5.4.2.2. Effect of added electrolyte concentration

The addition of electrolyte causes a general decrease in particle sizes observed at pH's below 6 due to a screening of the surface charges on the polymer (Figure 5.12.). In the case of 10mM KNO_3 background electrolyte, no change in particle size is observed for particles dispersed at pH 8 and 10.2 until they reach the LCST and particle aggregation is observed above 50°C. In the case where 100mM KNO_3 is used, the hydrodynamic diameter at all pH's remain unchanged with increasing temperature until the LCST is achieved. It should be noted at temperatures below 50°C, the hydrodynamic diameters at pH 8.1 and 10.2 are larger than pH's 2.8 and 6.2 due to particle aggregation induced by electrolyte addition. Above the LCST the insolvency of the polymer causes an increase in the particle aggregate size observed for pH's 8.1 and 10.2 (Figure 5.13), whilst the particle size remains unaffected at the lower pH's (2.8 and 6.2).

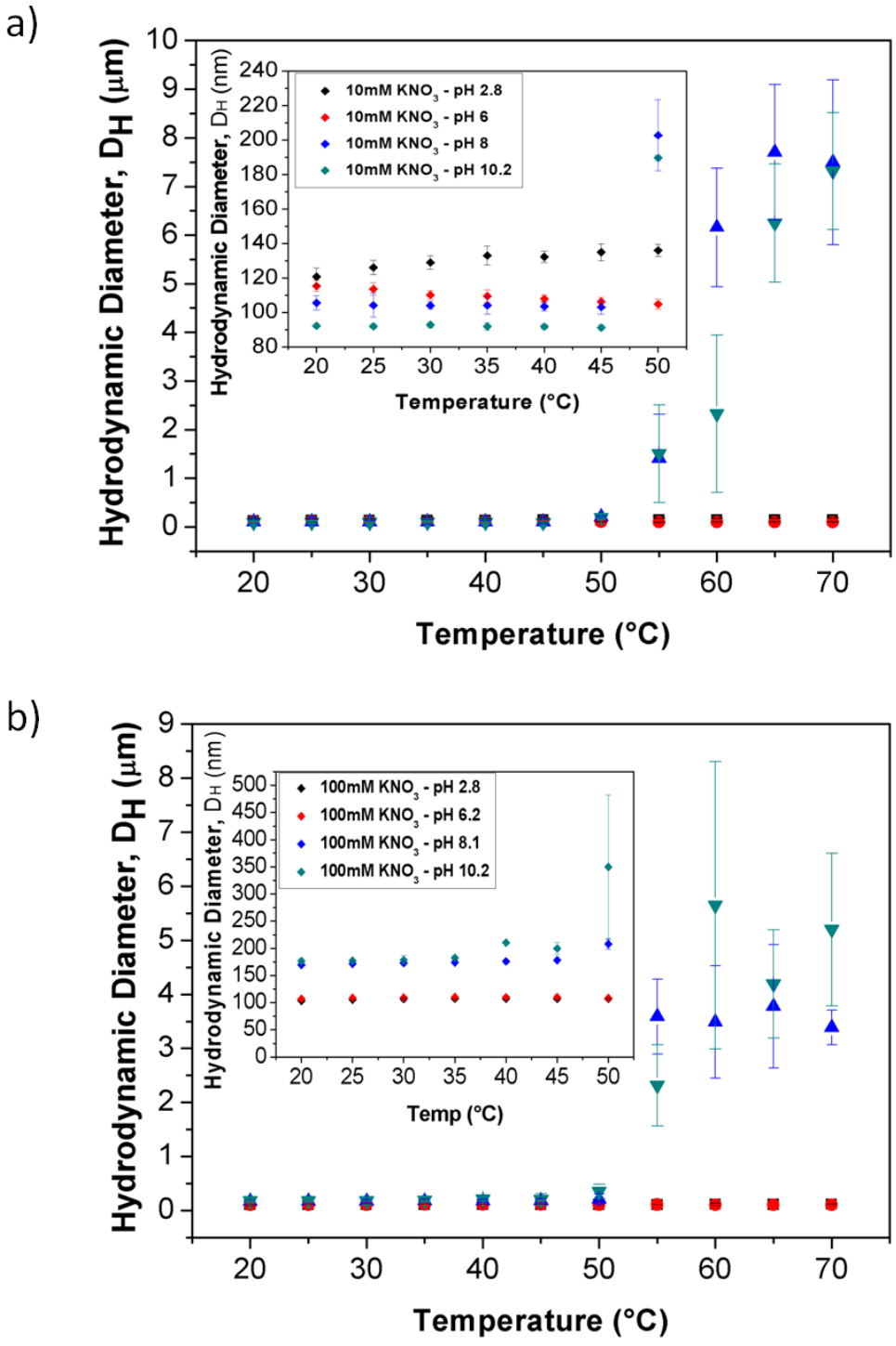

Figure 5.12. Changes in the particle hydrodynamic diameter of sample SM04 with temperature as a function of solution pH in the presence of a) 10mM KNO_3 and b) 100mM KNO_3 background electrolyte.

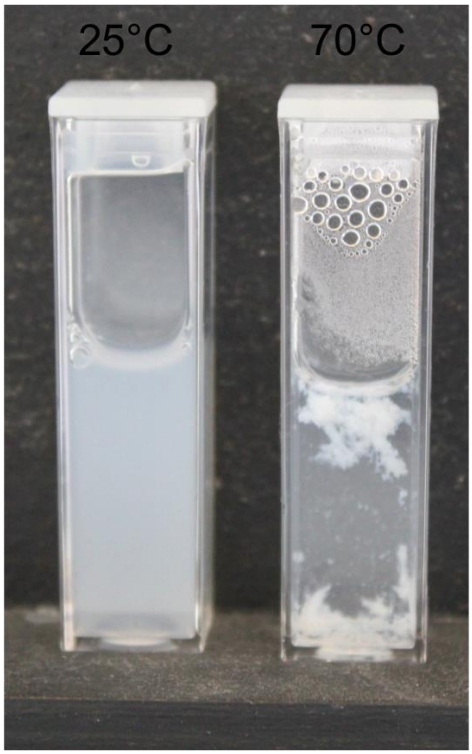

Figure 5.13. Digital micrograph showing a stable particle dispersion of sample SM04 at 25°C and particle aggregation at 70°C for particles dispersed at pH 8.1 and 100mM KNO_3 background electrolyte concentration.

5.5. Conclusions

Polystyrene latex particles sterically stabilised using pMMA-b-pDMAEMA were prepared using an emulsion polymerization technique. The particle size obtained can be controlled by changing the polymer block length or/and the synthesis temperature. The pDMAEMA chains are weakly cationic exhibiting a pK_a value around pH 7.5. Below this pH the polymer on the particle surface becomes protonated and the chains extend out into solution (exhibiting an increase in size), whilst above this pH the polymer loses its charge and becomes insolvent, thus collapses back onto the particle surface (reduction in particle size). In addition the pDMAEMA chains exhibit an LCST value around 50°C at pH values above 8, below which the polymer is solvated (stable particle dispersion), whilst above this value, the polymer becomes insoluble, which causes inter-segmental attraction between the polymer chains leading to particle aggregation. The aggregation observed increases with increasing electrolyte concentration.

References

1. W. D. Harkins, A general theory of the mechanism of emulsion polymerisation, *J. Am. Chem. Soc.*, 1947, **69**, 1428-1444.
2. R. G. Gilbert, ed., *Emulsion Polymerization: A Mechanistic Approach*, Academic Press, London, 1995.
3. P. A. Lovell and M. S. El-Aasser, eds., *Emulsion Polymerization and Emulsion Polymers*, Wiley, New York, 1997.
4. J. W. Goodwin, J. Hearn, C. C. Ho and R. H. Ottewill, Studies on the preparation and characterisation of monodisperse polystyrene lattice, *Colloid Polym. Sci.*, 1974, **252**, 464-471.
5. P. Kasargod and R. M. Fitch, Emulsifier-free all-sulfonate polystyrene colloids from a new peroxide initiator, *Polym. Colloids II*, 1980, 457-475.
6. D. H. Napper, ed., *Polymeric Stabilization of Colloidal Dispersions*, Academic Press, London, 1983.
7. V. S. Stenkamp and J. C. Berg, The role of long tails in steric stabilization and hydrodynamic layer thickness, *Langmuir*, 1997, **13**, 3827-3832.
8. K. R. Rogan, A. C. Bentham, I. A. George and D. R. Skuse, Colloidal stability of calcite dispersion treated with sodium polyacrylate, *Colloid Polym. Sci.*, 1994, **272**, 1175-1189.
9. C. Burguiere, S. Pascual, C. Bui, J.-P. Vairon, B. Charleux, K. A. Davis, K. Matyjaszewski and I. Betremieux, Block copolymers of poly(styrene) and poly(acrylic acid) of various molar masses, topologies, and compositions prepared via controlled/living radical polymerization. Application as stabilizers in emulsion polymerization, *Macromolecules*, 2001, **34**, 4439-4450.
10. F. L. Baines, S. Dionisio, N. C. Billingham and S. P. Armes, Use of block copolymer stabilizers for the dispersion polymerization of styrene in alcoholic media, *Macromolecules*, 1996, **29**, 3096-3102.
11. J. I. Amalvy, G. F. Unali, Y. Li, S. Granger-Bevan, S. P. Armes, B. P. Binks, J. A. Rodrigues and C. P. Whitby, Synthesis of sterically stabilized polystyrene latex particles using cationic block copolymers and macromonomers and their application as stimulus-responsive particulate emulsifiers for oil-in-water emulsions, *Langmuir*, 2004, **20**, 4345-4354.

12. F. L. Baines, N. C. Billingham and S. P. Armes, Synthesis and solution properties of water-soluble hydrophilic-hydrophobic block copolymers, *Macromolecules*, 1996, **29**, 3416-3420.
13. Z. Tuzar and P. Kratochvil, Block and graft copolymer micelles in solution, *Adv. Colloid Interface Sci.*, 1976, **6**, 201-232.
14. C. Price, Colloidal properties of block copolymers, In: *Developments in Block Copolymers-1*, *ed*. I. Goodman, Applied Science Publishers, London, 1982.
15. P. Munk, C. Ramireddy, M. Tian, S. E. Webber, K. Procházka and Z. Tuzar, Block copolymer micelles in aqueous media, *Makromol. Chem., Macromol. Symp.*, 1992, **58**, 195-199.
16. F. L. Baines, S. P. Armes, N. C. Billingham and Z. Tuzar, Micellization of Poly(2-(dimethylamino)ethyl methacrylate-block-methyl methacrylate) copolymers in aqueous solution, *Macromolecules*, 1996, **29**, 8151-8159.
17. J. Eastoe, ed., *Surfactant Chemistry*, Wuhan University Press, Wuhan, 2003.
18. G. Xiao, Z. Hu, G. Zeng, Y. Wang, Y. Huang, X. Hong, B. Xia and G. Zhang, Effect of hydrophilic chain length on the aqueous solution behavior of block amphiphilic copolymers PMMA-b-PDMAEMA, *J. Appl. Polym. Sci.*, 2012, **124**, 202-208.
19. U. Chatterjee, S. K. Jewrajka and B. M. Mandal, The amphiphilic block copolymers of 2-(dimethylamino)ethyl methacrylate and methyl methacrylate: Synthesis by atom transfer radical polymerization and solution properties, *Polymer*, 2005, **46**, 10699-10708.
20. Z. Song and G. W. Poehlein, Kinetics of emulsifier-free emulsion polymerization of styrene, *J. Polym. Sci., Part A: Polym. Chem.*, 1990, **28**, 2359-2392.
21. F. A. Plamper, M. Ruppel, A. Schmalz, O. Borisov, M. Ballauff and A. H. E. Müller, Tuning the thermoresponsive properties of weak polyelectrolytes: Aqueous solutions of star-shaped and linear Poly(N,N-dimethylaminoethyl Methacrylate), *Macromolecules*, 2007, **40**, 8361-8366.
22. B. M. Reis, S. P. Armes, S. Fujii and S. Biggs, Characterisation of the dispersion stability of a stimulus responsive core-shell colloidal latex, *Colloids Surf. A: Physicochem. Eng. Asp.*, 2010, **353**, 210-215.

CHAPTER 6: USING STERICALLY STABILISED LATEX PARTICLES TO PRODUCE PICKERING EMULSIONS

6.1. Introduction

This chapter describes and outlines the use of polystyrene latex particles sterically stabilised with a pH-responsive polymer to stabilise Pickering emulsions (section 2). Such emulsions can further be used as templates for the fabrication of pH-responsive colloidosome microcapsules (section 3). In addition it is demonstrated that these capsules can be used as size-exclusion membranes to retain and control the release of water soluble species as a function of pH.

6.2. Production of Pickering emulsions stabilised by sterically-stabilised PS latex particles using homogenisation

6.2.1. Introduction

Pickering emulsions are emulsions stabilised by solid particles that adsorb onto the liquid–liquid interface, a phenomena described after its discovery by S. U. Pickering in 1907.[1] The potential of using Pickering emulsions for technological applications has driven renewed interest in this area over the past decade or so. The two dimensional assembly of colloidal material at oil/water interfaces can be used as a template for creating new materials such as organic/inorganic composite particles,[2] microfibers and films[3, 4] and hollow particulate microcapsules often referred to as colloidosomes.[5, 6]

In addition to the three phase contact line and energy of particle desorption (Chapter 2), there are numerous other factors that need to be considered in the preparation of particle stabilised emulsions. Other factors that influence emulsion stability include particle concentration, particle shape, oil type and the presence of other additives such as electrolytes.[7]

In light of recent studies showing that emulsion droplets can be stable to coalescence at low surface coverage of the droplet by particles,[8, 9] for most particle stabilised emulsions, the particle concentration is an important factor. Increases in the particle concentration can lead to an increase in stable emulsion volume fraction and/or cause a reduction in the droplet size.[7] The limit of this is dictated by the particle size. In most cases a complete coverage with particles is considered to be necessary for emulsion stability. The presence of excess particles form an additional 3-D network that surrounds the droplet and improves stability.[10]

The location of the particle prior to emulsification is another important factor. Yan and Masliyah reported the production of o/w emulsions stabilised with hydrophobic particles.[11] In their investigation they used kaolinite clay particles were coated with asphaltenes to obtain hydrophobic particles. They were dispersed in the aqueous phase prior to emulsification and thus they were able to stabilise o/w emulsions. The effect of particle location adds an additional factor. The maximum stability of an emulsion can be obtained by having the particles with the appropriate wettability in the appropriate continuous phase (i.e. to obtain the most stable o/w emulsions the

particles should be dispersed in the water continuous phase). Binks and Lumsdon also showed how changes in pH affect the partitioning of partially hydrophobic silica nanoparticles between toluene and water.[12] They found that at low pH's the oil preferred to be distributed in oil, whilst at high pH's they preferred water. At the intermediate pH's they were present in both phases. Hence, these findings verified the Bancroft rule[13] in solid stabilised emulsions prepared using equilibrium multiphase systems.

The oil type affects the interfacial tension, the contact angle and the interactions between the particles surface and the liquids as well as the energy of particle attachment to an interface.[14] Silica particles that had the same surface treatment were found to produce o/w emulsions when non-polar oils were used whilst w/o emulsions were produced using polar oils.[15] Both the location of the particle and the oil type can be related back to the contact angle of the particle in an emulsion system.

Particle size is also an important parameter as it dictates whether it remains suspended in solution and hence at the oil/water interface. It has been reported experimentally that by decreasing the particle size, the emulsion stability increases with the formation of smaller droplets until a critical particle size is achieved.[16] Tambe and Sharma used 4 and 37 μm alumina particles to stabilise decane in water emulsions. They found that using a particle mixture of two different particle sizes produced a less stable emulsion. This is because when the large particles are present there is no ordering in the arrangement of the particles at the interface in contrast to when only small particles are used.[17] This leads to the conclusion that polydispersity of fine particles reduce the stability of the emulsions and disrupt their ability to form a mechanical protective barrier against coalescence.

Well defined spherical particles are often used for theoretical studies to help simplify analysis and calculations. However, in reality particles are not always spherical and the particle shape does have an impact on the emulsion stability. In addition, particle roughness also plays an important role. It has been reported that rough particles produce less stable emulsions in comparison to smoother particles.[9] This is because the particle roughness causes changes in the particle contact angle at the interface and hence dictates the emulsion stability. From all the factors

mentioned above, the influence of particle shape is the least understood in determining emulsion stability.[14]

There is a copious amount of literature investigating the use of relatively inert particles like silica and carbon to stabilise emulsions. More recently, particles that are responsive to numerous stimuli such as pH, temperature and/or light have been synthesised to act as emulsifiers. Their ability to influence the behaviour of the emulsions through the effect of stimuli is of technological interest. One example of such particles are sterically stabilised particles, which are particles grafted with a co-polymer. The sterically-stabilised particles are capable of becoming charged to influence the wettability of the particles to stabilise emulsions. One such steric stabiliser used is [2-(dimethylamino)ethyl methacrylate - block - methyl methacrylate) (pDMAEMA-b-pMMA) di-block copolymers. The pMMA anchors onto the particle surface, whilst the pDMAEMA acts as the stabiliser.[18] The pDMAEMA chain contain a tertiary amine group which can become charged and uncharged and this influences its wettability to stabilise emulsions. The latex particles are also temperature responsive since the pDMAEMA chains have a LCST (low critical solution temperature) around 50°C, above which it becomes insoluble and becomes less hydrophilic.[19] Another similar system is silica nanoparticles modified with an anionic polyelectrolyte poly(styrenesulphonate).[20] In this system the polymer charge is independent of pH and ionic strength. More recently latex particles stabilised using poly(glycerol monomethacrylate) has been shown to stabilise emulsions. By varying the degree of polymerisation of the pGMA chains, the wettability of the particles change and influence the emulsion behaviour.[21, 22]

Adsorbing surface-active polymers onto the surface of nanoparticles or grafting them from their surface drives in most cases the production of extremely efficient particle emulsifiers.[6] The enhanced emulsification effectiveness of polymer grafted particles in comparison to bare particles is attributed to the surface activity of the polymer. The grafted surface-active polymer chains such as pDMAEMA can penetrate the oil/water interface and decrease the interfacial tension,[20] whilst bare particles have no effect on the interfacial tension.[9, 23] In addition the polymer may impede droplet flocculation of two approaching droplets via steric or electrosteric repulsion forces preventing thin film drainage.[24]

In this work, I examine the effect of both pH as well as ionic strength on stability of the produced emulsions using two pMMA-b-pDMAEMA sterically stabilised latex particle samples (SM01 and SM03) (Chapter 5). In particular, the aim is to expand on previous work[18, 25] to investigate the influence of latex particles of similar size but varying pDMAEMA block length on emulsion stability.

6.2.2. Materials and Methodology

6.2.2.1. Preparation

Once the particles were synthesised via emulsion polymerisation (Chapter 4 and 5) and cleaned via dialysis, the particle concentration was assessed by gravimetric studies. The particles were then diluted accordingly to obtain a suspension at a concentration of 2 wt% in 5 mL of Milli-Q water at different pH (ranging from pH 2 to 11, adjusted using HNO_3 and KOH). In this case, the background electrolyte concentrations were also varied from a case where no electrolyte was added to a case where the electrolyte concentration was 1M KNO_3. Once the particle dispersions were prepared, an equal volume of hexadecane oil (≥99%, Sigma-Aldrich) was added to the vial (compensating for the addition of acid/alkali), to subsequently produce emulsions containing equal volumes of both the continuous and dispersed phases via homogenisation. The latter step was performed using a rotor-stator, which was previously cleaned with a solution of Decon 90 surfactant followed by washes in Milli-Q water, ethanol (≥99%, Fisher Scientific) and acetone (≥99%, Sigma-Aldrich) and was left to dry before use. The samples were homogenised using an Ultra Turrax T25 (IKA) homogeniser for 2 minutes at a rotation speed of 15,000 rpm. The stability of the emulsions was assessed as a function of time by recording the apparent changes in the level/volume of coalesced oil at the top of the sample. The rotor was cleaned with water, ethanol and acetone after preparing each sample and left to dry before use.

6.2.2.2. Characterisation

Digital images of the emulsions contained within the vials were taken with a Canon EOS 550D camera immediately after the emulsions were made and after 24 hours. This was used to measure the stability of the emulsions with respect to time. In

particular, the amount of oil coalesced after 24 hours was assessed at the different pH's and electrolyte concentrations.

The emulsions were also characterised using light scattering by using a Mastersizer 2000 (Malvern) to obtain information regarding the droplet size and their size distribution for the different emulsification conditions. During a measurement the sample is passed through a focussed laser beam.[26] The sample scatters the light at an angle that is inversely proportional to their size. The angular intensity is measured using multiple photosensitive detectors. This angular intensity is the primary source of information used to calculate the sample size based on either Mie scattering (angle dependent) or by using the Fraunhofer approximation. The Fraunhofer approximation does not require any of the optical properties of the sample to be known (whereas the properties are needed for Mie scattering) and thus it leads to significant errors. The Mastersizer also contains a short wavelength blue light for increased sub-micron resolution, which is used in conjunction with the forward and backward scatter.

To prepare samples for measurement, the cell of the Mastersizer was filled with Milli-Q water prepared at the desired pH and electrolyte concentrations. A few drops of the emulsions were added until light signal was obscured to generate a size measurement. Typically 10 measurements were taken for each sample, which were averaged and plotted as size distributions based on volume %.

In addition optical micrographs of the droplets were taken using an Olympus BX51 microscope. The droplets were analysed using Cell^D (Olympus) imaging software to obtain information regarding both the size and size distribution of the emulsion droplets.

6.2.3. Results and Discussion

6.2.3.1. Stability of emulsions - effect of pH

The two latex samples (SM01 and SM03) were dispersed in Milli-Q water at varying pH and electrolyte concentrations to investigate their ability to stabilise emulsions under these different initial conditions. The emulsions were left to stand for 24 hours and the stability of the emulsions was assessed by digital micrographs and droplet size after 1 hour and 24 hours. It should be noted that in this emulsion

stability study, both the base particle size and the pMMA block lengths are relatively similar (14 and 16) therefore this study investigates the influence of the pDMAEMA block length and the polymer density. Emulsions prepared using both latex samples at varying pH values for no added electrolyte to the continuous phase are illustrated in Figure 6.4.

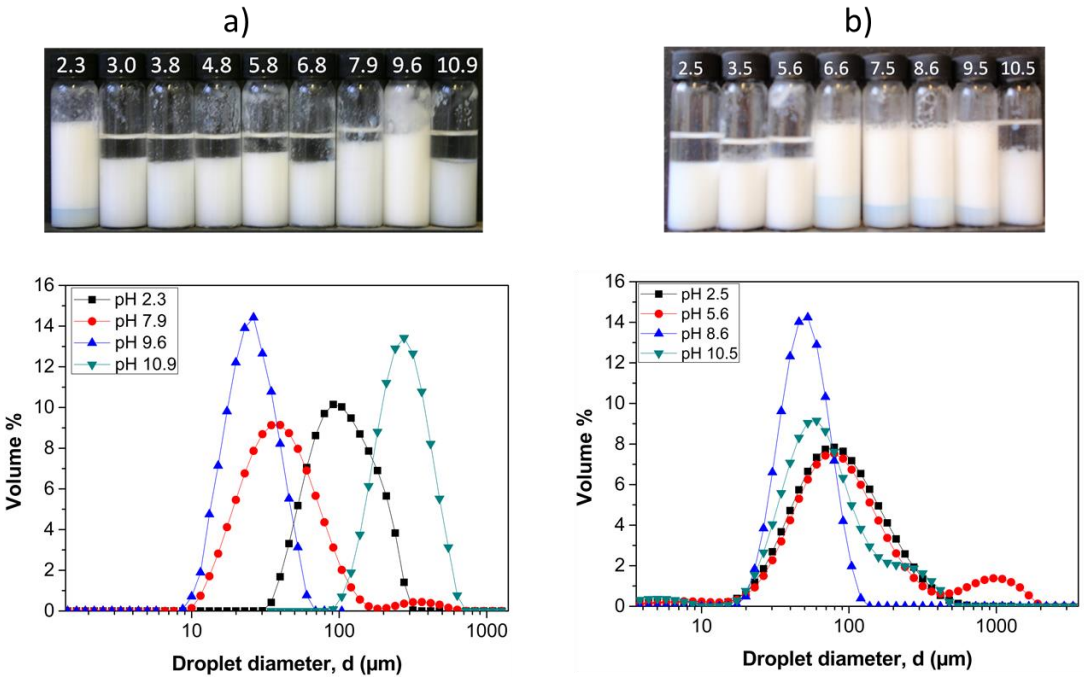

Figure 6.1. Emulsions stabilised with polystyrene latex particles sterically stabilised using a) SM01 and b) SM03. The figure shows digital micrographs of the emulsions, 24 hours after they were produced (top) and the droplet diameter distribution based on volume % as a function of pH for no added electrolyte to the continuous phase.

Digital micrographs and droplet size data of emulsions stabilized using latex particles stabilized with SM01 (Figure 6.1a) show varying degrees of stability as a function of pH. At pH 9.6 the emulsion is observed as being very stable and yields the smallest droplet size (mean size of 25 µm) with the narrowest droplet size distribution. At this pH the pDMAEMA chains are deprotonated and collapse on the surface of the particle, allowing the latex to act as an efficient particulate emulsifier and strongly adsorb on the oil-water interface. One deduces from these data that the low affinity of the polymer for the continuous phase drives adsorption of the particles for the interface. Increasing the pH to 10.9, a layer of oil phase is clearly

visible above the emulsion phase, indicating that the emulsion is unstable and that it is undergoing coalescence followed by macroscopic phase separation. This is confirmed by the droplet size distribution data showing a broad distribution with a mean diameter of around 200 µm. At pH 10.9 the polymer is collapsed on the surface of the particle and the insolubility of the polymer into the continuous phase causes particle aggregation as demonstrated with an increase in particle size (Figure 6.1 left). This means that the particles are likely to adsorb on the surface of the droplets as aggregates, which leads to an increase in droplet size. When pH is lowered in the range from 7.9 to 3, the emulsions become unstable and a layer of oil is observed above the emulsion phase. This is due to the pDMAEMA chains becoming protonated and cationic and becoming very soluble in the water phase.[27] This reduces the affinity of the particles for the oil/water interface and this in turn destabilizes the emulsion. These observations of emulsion stability/instability as a function of pH matches previous reports.[18, 25]

When reducing the pH further to pH 2.3, the emulsion created appears stable and produces droplets of around 100 µm. This observation does not match the findings reported by Amalvy *et al.*[26] who found 100% coalescence at pH 2.2 with no added electrolyte to the continuous phase. The observation of a stable emulsion at pH 2.3 in the system studied here can be potentially explained with regards to charge screening of the pDMAEMA chains. Upon adjusting the pH to 2.3, the background electrolyte concentration increases significantly and this screens the cationic charge of the polymer. This causes the polymer to collapse on the particle surface and increase the affinity of the latex to the oil/water interface producing stable emulsions. In addition the sterically stabilised particles used in this study have different chain lengths and polymer densities compared to the particles investigated by Amalvy *et al.*[25]

The trend in emulsion stability as a function of pH (under no added electrolyte conditions) is slightly different when using SM03 (Figure 6.1b). At pH 9.5 and 10.6 the digital micrographs show that the emulsions are similar to the emulsions stabilized using the previous latex sample. However, as the pH is lowered below 9.5, stable emulsions are observed from pH 9.5 to pH 6.6. As a typical example from this range of pH, droplet size data show a monomodal peak with an average droplet size of 40 µm at pH 8.6. The observation of stable emulsions at pH values as low as 6.6 can be explained if we consider the grafting density of the di-block copolymer on

the surface of the particles (obtained from ^{1}H NMR Chapter 4 and 5) as illustrated by Table 6.1.

	SM01	SM03
Average molecular number, M_n (g mol^{-1})	10110	40340
Chains/nm^2	1.8×10^{-2}	4.5×10^{-3}
Chains/particle	53	29
Amine groups/particle	2862	7105

Table 6.1. Grafting density data of the diblock co-polymer on the surface of latex particles (Re-inserted from Chapter 5).

The grafting density data presented in Table 6.1 show that for latex particles stabilized with SM03 the number of pDMAEMA chains per particle is around 29 which is a relatively low. This low grafting density means that the affinity of the particle for the interface is less dictated by the behaviour of the polymer compared to particles stabilised by SM01. The particles have good affinity for the interface which is not compensated for fully by the protonation of the polymer until below pH 6.6. Further decreasing the pH below 6.6 up to pH 2.5, the polymer becomes fully protonated and induces a much lower affinity for the interface for the particles. This results in turn in macroscopic phase separation as seen by the presence of an oil layer above the emulsion phase at these low pH's as well as the broad bi-modal size distribution data shown in Figure 6.4. It is interesting to note that in the case of SM03 the emulsion at pH 2.5 is unstable, compared to the stable emulsion seen with SM01. This is because $pDMAEMA_{254}$ has more tertiary amine groups (up to 4.5 times more) in comparison to $pDMAEMA_{54}$, so the number of amine groups per particle is much larger. This means that at pH 2.5, even though electrolyte is added via pH adjustment, this process is less efficient at screening the charge on the polymer and thus an unstable emulsion is obtained.

6.2.3.3. Stability of emulsions - effect of added electrolyte concentration

The effect of added electrolyte concentration on the stability of emulsions was investigated across the pH range. Emulsions stabilised by both of the latex particle

samples synthesized were investigated here and the appearance of the emulsions and the size distribution of the droplets produced were recorded. Figure 6.2 shows some of the data recorded for such emulsions produced at a range of pH's and with a background electrolyte concentration of 10mM.

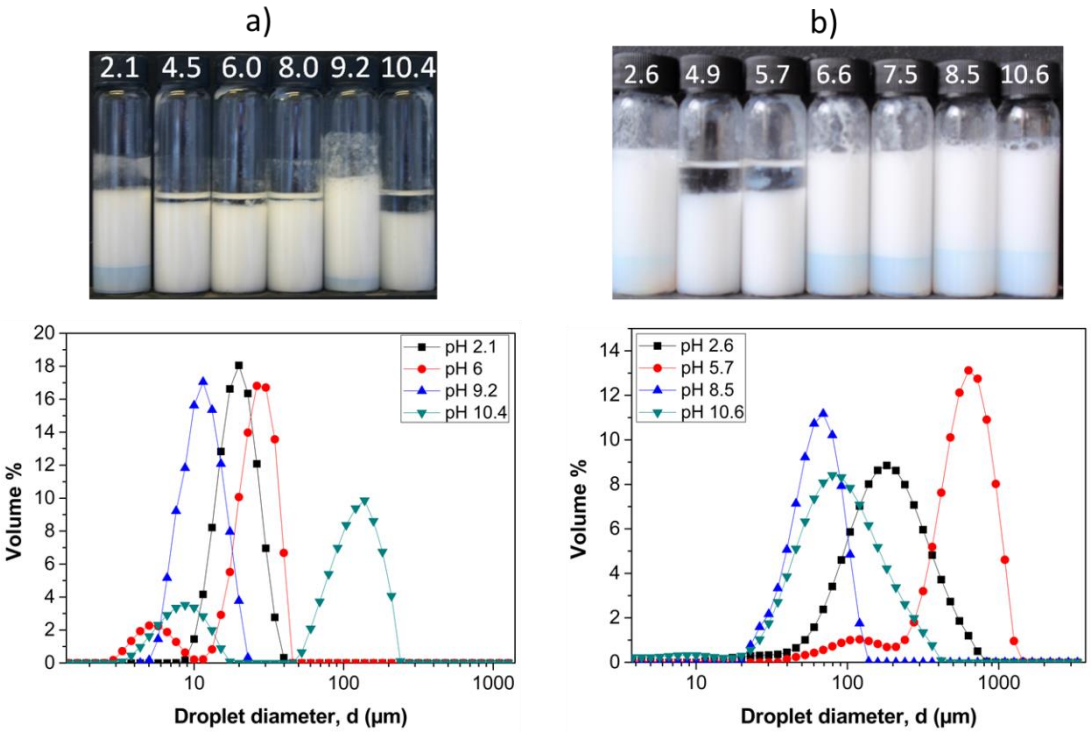

Figure 6.2. Emulsions stabilised with polystyrene latex particles sterically stabilised using a) SM01 and b) SM03. The figure shows digital micrographs of the emulsions, 24 hours after they were produced (top) and the droplet diameter distribution based on volume % as a function of pH in the presence of 10mM KNO_3 background electrolyte (after 24 hours).

The addition of 10mM KNO_3 background electrolyte to the aqueous phase generally improves the stability of the emulsions stabilised with latex particles stabilised $pDMAEMA_{54}$. Comparing the digital micrographs in Figure 6.2a with those presented in Figure 6.1a, one can see a drastic reduction of the volume of coalesced oil phase present on top of the emulsion phase at the lower pH values for an increased background electrolyte. This improved stability is attributed to screening of the charges present on the polymer below its pK_a. In this case, the polymer becomes less soluble in the continuous phase and adopts a less extended configuration (as seen in Figure 5.9) which potentially improves the wettability of

the particles at the oil/water interface. This is further confirmed by the droplet size data showing a shift towards smaller recorded emulsion droplet diameter at 10mM as compared to the case where no additional salt is present.

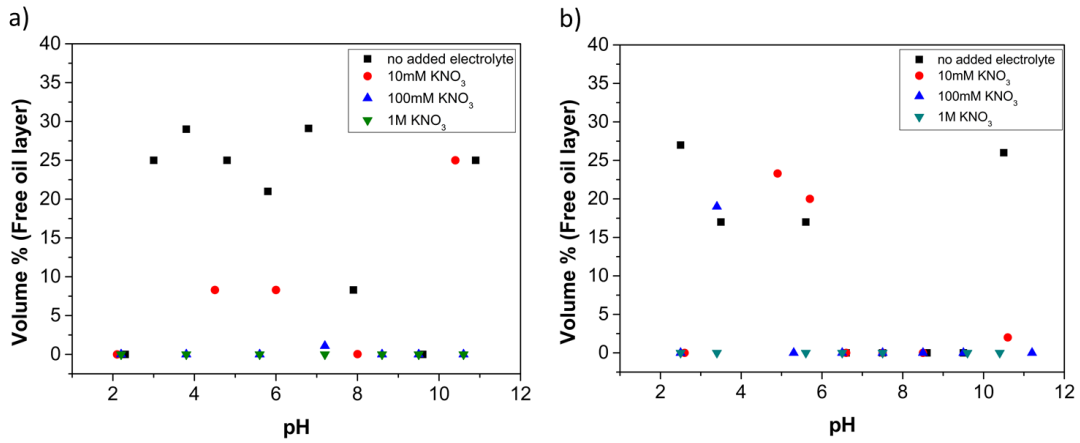

Figure 6.3. Plot of volume % of free oil layer as a function of pH and electrolyte concentration stabilised by a) SM01 and b) SM03 after 24 hours.

In the case of emulsions stabilised by the SM03, the addition of electrolyte seems to increase the stability of the emulsions created at pH 2.6 and 10.6 (Figure 6.3) that showed a relatively large volume of coalesced oil on their surface after 24Hrs in the absence of added electrolyte. The appearance of a stable emulsion at pH 2.6 (Figure 6.2b) is indicative of the influence of the protonation of the polymer on the successful adsorption of the particles to the oil-water interface. Indeed, by adding electrolyte to the particle system prior to emulsification, the charged groups on the particle polymer sheath are (to an extent) screened from each other and from those of neighbouring particles. This phenomenon appears to facilitate a more efficient adsorption of the particles to the interface since the corresponding emulsions do not show any coalescence after 24 hours, oppositely to their counterparts prepared without added electrolyte. However, a noticeable amount of oil coalescence is present for emulsions prepared at pH 4.9 and 5.7. In this case, the combination of the added electrolyte and the electrolyte provided by the added acid counter ion to reach these moderately acidic pH's does not appear sufficient to screen the polymer charges sufficiently to efficiently drive the particles to the interface. This is also indicated by the fact that these two systems produces droplets with a bi-modal distribution at relatively large sizes. At pH 10.6, the addition of electrolyte yields a stable emulsion by potentially driving the particles to the oil/water interface where

they subsequently adsorb and stabilise the droplets. The grafting density is also much lower than SM01 which may potentially explain the improvements in stability.

The digital micrographs and droplet size distribution of emulsions created using both latex particulate systems with the addition of 100mM KNO_3 background electrolyte is presented in Figure 6.4. Emulsions produced with $pDMAEMA_{54}$ do not appear to present coalesced oil layers at any pH. The average droplet sizes are similar at all pH's and have shifted to larger sizes in comparison to the droplet sizes obtained with 10mM added electrolyte concentration. The size distribution in Figure 6.4 also appear much broader, potentially indicating particle flocculation (polymer insolvency) at the high pH values and aggregation at the lower pH values leading to larger droplet sizes.[28]

Emulsions produced at all pH's except pH 3.4 showed no coalesced oil after 24 hours when using latex particles stabilised using $pDMAEMA_{245}$ (although a longer time period such as 1 week or 1 month needs to be examined in the future for a stricter test). A small volume of oil phase appears above the emulsion phase indicating that at this pH the amine groups are protonated and have a reduced affinity for the interface. The addition of electrolyte to these particles also cause flocculation (due to polymer insolvency) (high pH) and aggregation (low pH) as a broad/bi-modal size distributions are observed for emulsions created at pH's 2.5, 5.3 and 11.2.

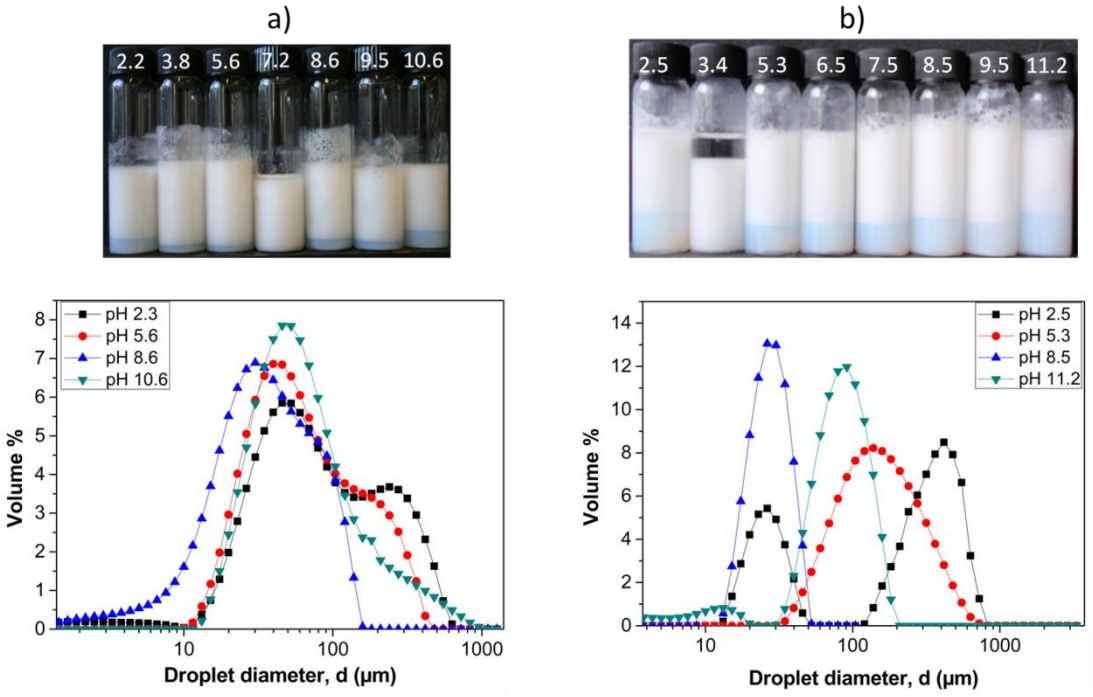

Figure 6.4. Emulsions created with polystyrene latex particles sterically stabilised using a) SM01 and b) SM03. The figure shows digital micrographs of the emulsions, 24 hours after they were produced (top) and the droplet diameter distribution based on volume % as a function of pH in the presence of 100mM KNO_3 background electrolyte.

The addition of 1M KNO_3 (Figure 6.5) produces stable emulsions across the whole pH range for both latex systems. However, due to the high electrolyte concentration, the particles are aggregated and this leads to droplets having either broad or a bi-modal size distribution. The observation of improved stability as a function of electrolyte concentration matches the findings presented by Amalvy *et al.*,[25] who reported a reduction in coalescence of emulsions created at pH 2.2 with increasing electrolyte concentration.

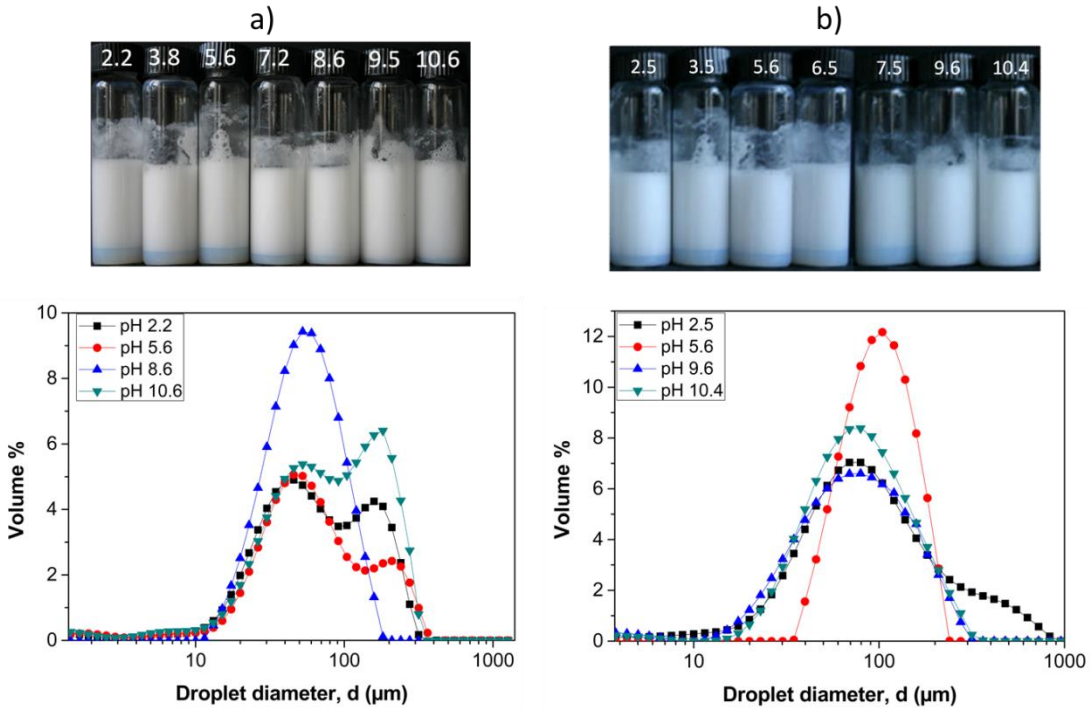

Figure 6.5. Emulsions created with polystyrene latex particles sterically stabilised using a) $pMMA_{14}$-b-$pDMAEMA_{54}$ and b) $pMMA_{16}$-b-$pDMAEMA_{245}$. The figure shows digital micrographs of the emulsions, 24 hours after they were produced (top) and the droplet diameter distribution based on volume % as a function of pH in the presence of 1M KNO_3 background electrolyte.

In conclusion it has been shown that both the pH and electrolyte concentration have an influence on the emulsion stability to droplet coalescence. Furthermore comparing particles with two different pDMAEMA chain lengths and grafting densities also have an influence on the emulsion behaviour.

6.3. pH-responsive 'Colloidosome' microcapsules from emulsion templates[1]

6.3.1. Introduction

Designing novel encapsulation systems for efficient delivery of actives has been of great focus in recent times both in the academic and industrial domain.[30] The potential for delivering actives accurately, site-specifically and controlling dosage have been the key drivers for the surge in interest. Although many different systems have been developed,[30-32] very few reach manufacturing stage due to the associated complexities in producing such highly functional capsules.

One particular class of microcapsule systems holding great promise are those fabricated based on particle-stabilised emulsion templates often referred to as 'colloidosomes'. The first structures of these type were reported by Velev *et al.*[5, 33, 34] who introduced oil emulsion droplets into a dispersion of micron-sized latex particles. The particles coated the droplet and provided stability to the system. The inter-particle interactions were tailored by the adsorption of surfactants onto the particle surface prior mixing the droplets into the particle suspension. This process was referred to by the authors as 'interaction tailored colloid assembly'. In the third paper of the series they introduced the concept of manufacturing water-core structures that were developed further by Dinsmore *et al.*[6] who coined the term 'colloidosomes'.

Yi *et al.*[35] and Ashby *et al.*[36] improved the size distribution of the fabricated colloidosomes using a technique based on the self-assembly method. In this technique the particle suspension is introduced into a co-flowing, surfactant rich continuous phase using a tapered capillary. Cayre *et al.*,[37] Noble *et al.*[89] and Duan *et al.*[39] developed other types of colloidsome microcapsules using a gel trapping technique. In this process, instead of a liquid core, the aqueous dispersed phase and the particle monolayer on the interface is trapped resulting in colloidosomes with a solid-like core. This technique allows for a better support of the shell giving added

[1] The research presented in this section also contains some data collected by Mr. James Hitchcock, an M.Sc. student working in our labs, and are included in his MSc thesis (August 2011). The data which were obtained by James that are presented in this section will be explicitly acknowledged.

stiffness and ability to the droplets produced with the aim of improving the strength of the structures.

The production of these microcapsules is done by permanently locking the particle monolayer adsorbed onto the particle surface via chemical and physical processing (annealing, chemical cross-linking or physical bridging through adsorption of high molecular weight polymers).[40] The encapsulation of actives in these microcapsules is likely to be achieved on the basis of size-exclusion, as the interstices between the particles control the pore size in these microcapsule membrane. The porosity can be potentially controlled by various means e.g. annealing processes or changing the particle size forming the monolayer. One of the important advantages in the fabrication of such capsule systems is that they can be easily prepared using common industrial emulsification techniques and are therefore adapted for being scaled-up to an industrially relevant scale.

Over the last decade several examples of colloidosome microcapsules have been developed reporting a range of membrane properties and functionalities.[6, 37-39, 41] Initial studies on the release properties of colloidosome microcapsules have focused on the extent of annealing to control the release rate of different chemical species.[42] To date, there have been only few systems that have demonstrated and reported the use of responsive materials within the microcapsule membrane, to control the rate of release of encapsulated species. For example, the use of microgel particles that swell in response to an external stimuli e.g. temperature.[43] Recently, it has been demonstrated that it is possible to use a sterically-stabilised latex particles to create a permanent shell around the emulsion droplet.[21, 40, 44, 45]

It has been shown in principle that polystyrene latex particles coated with a responsive polymer shell made of pMMA-b-pDMAEMA can be used to fabricate colloidosome microcapsules.[40] As mentioned previously in Chapter 6, the polymer forming the particle shell provides responsive properties as it expands away from the particle surface at low pH's and collapses back onto the surface at high pH's. The permanent locking of the particle monolayer is achieved by annealing the polymer shell on the particle surface or by cross-linking the polymer on adjacent particles within the monolayer.[40, 45] The cross-linking method allows one to work at high concentrations as the cross-linker is located within the dispersed oil phase, thus the reaction is limited to the polymer in contact with the oil phase. This process avoids

potential risks for cross-linking adjacent particle monolayers (on separate emulsion droplets). This prevents the potential issue of multiple capsules inter-locking and fusing together which can limit and restrict the concentrations that one can work at.[46]

The work described in the subsequent sections details the fabrication of such colloidosome microcapsules and demonstrate that they can be used as a pH-responsive system to control the loading and the eventual release of water soluble species.

6.3.2. Materials and Methods

6.3.2.1. Preparation of capsules

Previous studies within the research group have investigated the use of 1, 2-bis(2-isodoethyloxy)ethane (BIEE) to cross-link the amine groups, however this cross-linking mechanism appeared to occur over several days. Walsh *et al*. used a poly(propylene glycol)diglycidyl ether (PPG-DGE), an oil soluble cross-linker that showed improvements in the reaction times.[47] In their work, they cross-linked primary and/or secondary amines whilst in this study, PPG-DGE was shown to cross-link the tertiary amines from the hexadecane oil phase.

The hexadecane phase was firstly prepared; 0.3 g of PPG-DGE was dissolved in 25 mL of hexadecane oil from which 3 mL was taken and added to a 3 mL, 2 wt% particle dispersion of the polystyrene latex particles sterically stabilised using $pMMA_{16}$-b-$pDMAEMA_{254}$ in Milli-Q water at pH 8.5. The two phases were homogenised for 2 minutes at a rotating speed of 20,000 rpm. The emulsion was left to stand at room temperature for 30 minutes for the cross-linking to occur. A study was also conducted on the effect of cross-linking time and concentration of the cross-linker on the formation of the capsules.

In order to remove the internal oil phase of the microcapsule, a 2:1 ratio of isopropanol (IPA) to water was prepared. 0.1 mL of the emulsion was added to 0.9mL of the isopropanol/water mixture in a 1 mL eppendorf centrifuge tube and was redispersed using a Vortex Genie mixer (Scientific Industries) for 30 seconds and a carousel mixer for 30 minutes. Once dispersed the sample was centrifuged for 2 minutes at 7,000 rpm to sediment the capsules and remove the supernatant. These

centrifugation and re-dispersion cycles were repeated 3 times and a further three times using 0.9 mL pure IPA to ensure full removal of the oil in the samples. The microcapsules were then washed twice using centrifugation and redispersion cycles with firstly 0.9 mL 2:1 IPA/water mixtures and then with 0.9 mL pure Milli-Q water. This resulted in the string-bag capsules being dispersed in water with a water filled core. Further details regarding the process of how the oil core is removed is outlined in Section 6.3.3.

6.3.2.2. Loading of dextran within the microcapsule core

After the removal of the oil core the microcapsules dispersed in water had a collapsed appearance. Subsequently, the pH of the aqueous suspension was changed to 3 using a 0.1M HNO_3 solution to allow protonation of the unreacted amine groups on the di-block copolymers within the particle membrane, to maximise the membrane porosity of the microcapsules. Thereafter, a mother solution of FITC (Fluoresceinisothiocyanato) dextran (<1/10 of total volume) was added to the microcapsule system to reach a concentration of 1wt% and allowed to mix on the carousel for 30 minutes. The sample was then further diluted (10x) with Mill-Q water and the pH was adjusted to 10 using a 0.1M NaOH solution. The pH was increased to 10 minimize the membrane porosity. The excess dextran was removed by centrifugation of the microcapsules, removal of the supernatant and then redispersion into pH 10 water. The obtained loaded microcapsules were used to investigate the controlled release of the FITC dextran at different pH's.

6.3.2.3. Confocal microscopy studies

Once, the microcapsules were loaded with FITC dextran (Molecular weight = 70,000) and the excess dextran removed from bulk via centrifugation, the sample was divided into two equal volumes. One was washed three times using pH 10 water and the other washed three times using pH 3 water, this was to ensure that the final pH's of both dextran-loaded samples were close to 10 and 3, respectively. The capsules were stored for 5 hours before confocal micrographs on both samples were recorded.

Release studies were conducted using a confocal laser scanning microscope (Zeiss LSM 510 META Axiovert 200M). Using a step size of 1µm several Z-scan images were recorded for each sample. These images were overlapped to produce a 3D reconstruction of the samples. Additionally one 1µm slices through the microcapsule samples at pH's 3 and 10 were taken to distinguish whether the dextran was located on the capsule shell or present within with the capsule core. To quantify whether dextran was encapsulated or released as a function of pH, fluorescent intensity measurements were done on at least 50 capsules at both pH's. Care was taken not to include any intensity measurements associated with the capsule shell when calculating the intensity for the microcapsule core.

6.3.3. Results and Discussion

As reported in section 6.2 the ability for the sterically stabilised latex particles to stabilise oil/water emulsions was demonstrated to be most efficient at basic pH's. This is highlighted again in Figure 6.6 showing a digital photograph of the emulsions prepared at different pH conditions and an optical micrograph of the droplets prepared at pH 8.5. All emulsions prepared at pH's between 8.5 and 9 were subsequently used as templates for the preparation of the colloidosome microcapsules as these produced the most stable emulsions.

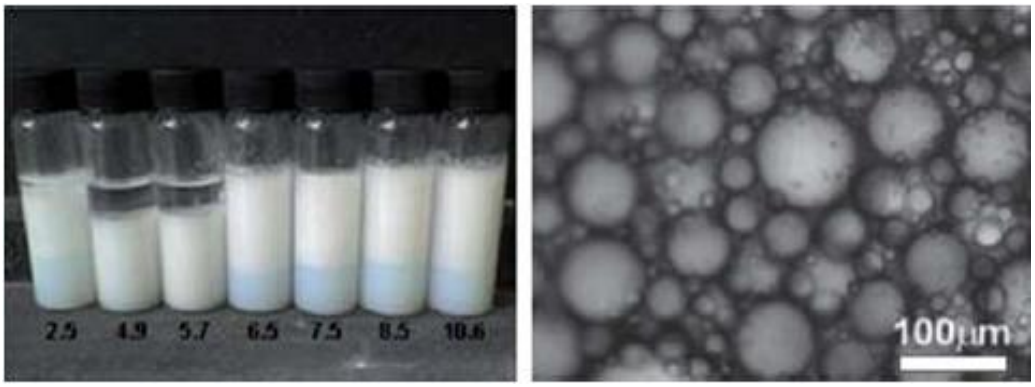

Figure 6.6. Emulsions prepared with 2wt% sterically stabilised polystyrene latex particles dispersed in the aqueous phase and an equal volume of oil phase. The images show emulsions created as a function of pH (left) and an optical micrograph of the emulsion sample prepared at pH 8.5.

The microcapsules were obtained by the cross-linking the particles adsorbed at the oil-water interface using an oil-soluble cross-linker with very low solubility in the aqueous phase. This allows the possibility of working with high emulsion droplet volume fractions which is advantageous for creating such systems on a large scale.[20, 40, 44] The cross-linker quarternizes the amine groups (has been confirmed when using the BIEE cross-linker and is likely for PPG but remains to be confirmed/explored) present on the di-block copolymer which potentially reduces the pH responsive properties of the polymer. However, as the data will demonstrate below this potential issue does not appear to be significant enough to affect the responsive properties of the microcapsules produced via this method. The cross-linker was added to the oil phase and an equal volume of aqueous phase containing the particle dispersion at pH 8.5 - 9 was added and emulsified using the Ultra-Turrax emulsifier. When using the BIEE cross-linker, 24 hours was sufficient to ensure that the microcapsules could sustain the removal of the oil phase using the co-solvent treatment described in section 6.2.2.1. In the case of the PPG-DGE cross-linker, the cross-linking time needed to ensure a fully cross-linked structure was considerably reduced to 30 minutes.

In order to encapsulate water soluble species with the microcapsule core, it is necessary to remove the oil core using a co-solvent that is miscible with both the oil and aqueous phases. The images in Figure 6.7 clearly show that the capsules swell upon the addition of IPA to the system. It is postulated that the IPA diffuses into the capsule core initially (there is a large driving force this and the IPA and oil and miscible), causing an increase in the internal pressure of the capsule (which causes the emulsion droplets with a particulate membrane lightly cross-linked using 0.1 wt% BIEE to rupture). At the boundaries of the capsule (crosslinked using a 2 wt% cross linking concentration), mixing of the oil, IPA and water can occur and some of the oil is solubilised into the IPA-water mixture giving a 1-phase solution. As this process continues the IPA-oil core is gradually solubilised to a 1-phase mixture, which will have a constant composition throughout the whole system and so there is no longer an elevated pressure inside the capsules and they relax. This whole process is governed by the chemical potentials, diffusion rates and mixing. The IPA is miscible with both the oil and water, but the oil and water can only mix in the presence of IPA. Clearly, the diffusion of the IPA throughout the whole system (inside and outside the capsules) is quicker than the mixing/solubilisation of the 3-

components into a 1-phase system. So we have a swelling and then relaxation. Figure 6.8 shows the reduction/removal of the oil phase in the microcapsule core with subsequent washes with IPA:water washes.

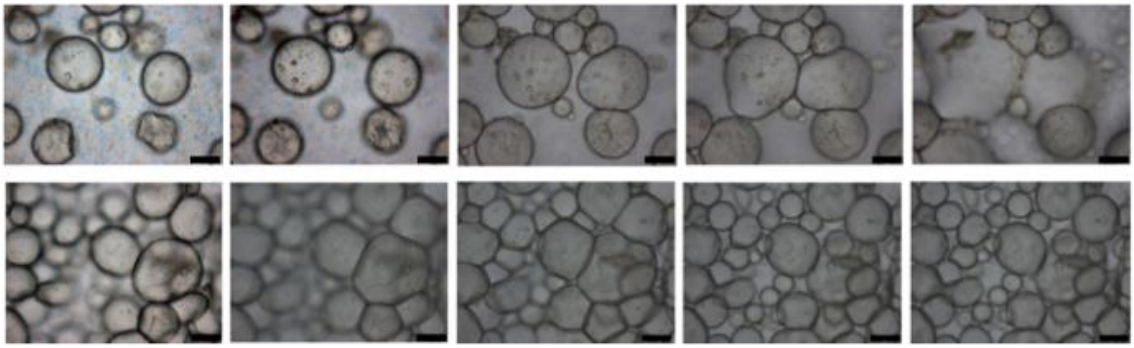

Figure 6.7. Optical micrographs of two emulsion samples using two different cross-linker concentrations, 0.1 wt% (top) and 2 wt% (bottom) that are cross-linked for 24 hours. The first image in both sets is taken shortly after the addition of isopropanol and subsequent images are taken every 15s. (Scale bar = 100µm).

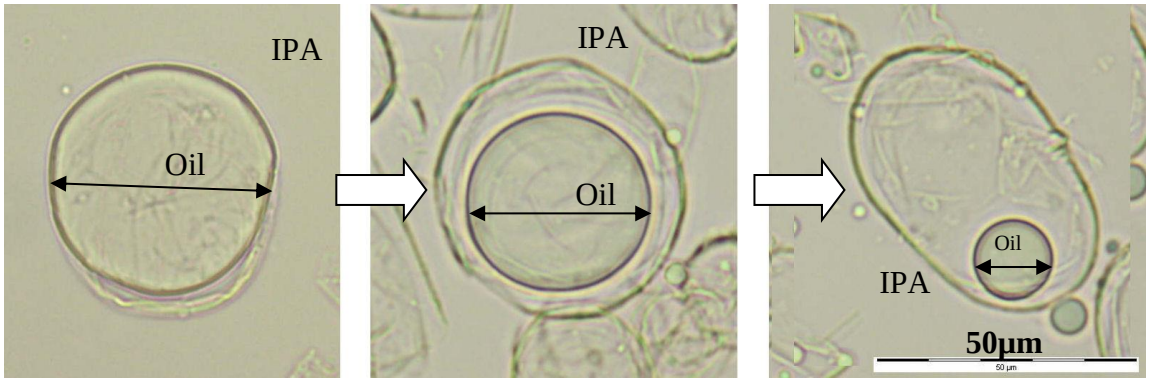

Figure 6.8. Optical micrographs showing the reduction/removal of oil phase over time inside a colloidosome microcapsule in the IPA:water wash cycle. *[Data acquired by Mr. James Hitchcock and used with his permission]*.[48]

Increases in the core volume causes the particle films to push against each other. Where the film is unmodified or lightly cross-linked, it is expected that the film will rupture during core volume expansion as illustrated by Figure 6.7. In the case, where 2 wt% cross-linker concentration is used the particle films are cross-linked to a suitable degree and are able to sustain induced pressure from the volume expansion. It should also be noted that in the case of the higher cross-linker concentration the

particle membrane of the microcapsules was found to be very strong and not as elastic as the lightly cross-linked system. The swelling due to the addition of isopropanol was hardly noticeable.

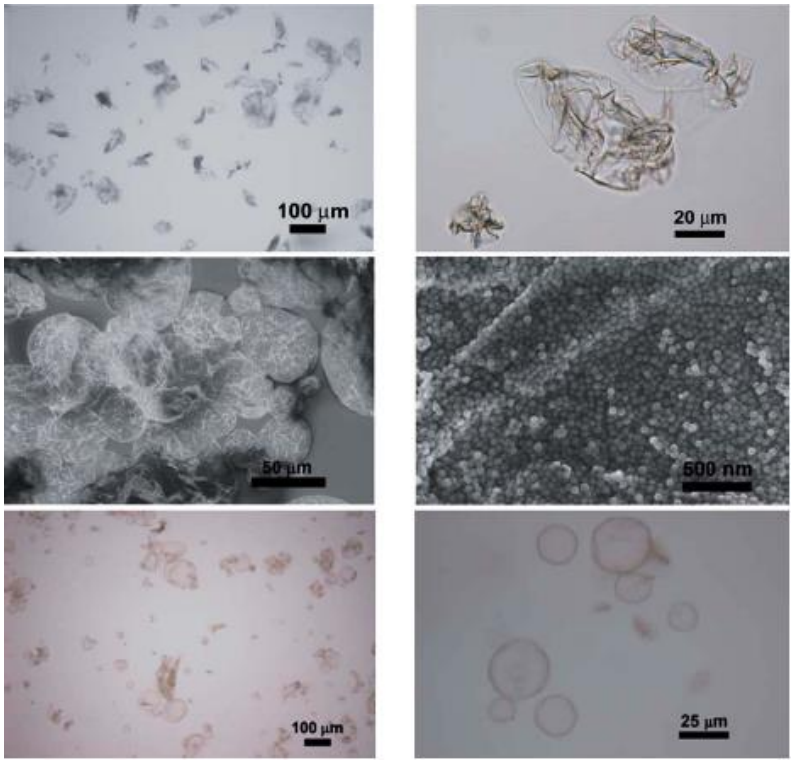

Figure 6.9. Micrographs of microcapsules prepared using a 1wt% BIEE cross-linker concentration at different stages. The optical micrographs (top) show the microcapsules suspended in water after the removal of the oil core, the scanning electron micrographs (middle) showing the dried microcapsules, and optical micrographs (bottom) illustrating the microcapsules in suspension after the addition of dextran to the aqueous phase to reach a 1 wt% concentration.

Upon the gradual removal of the oil core using isopropanol, the microcapsules were observed to collapse on themselves as illustrated by Figure 6.9 (top image). This is most likely due to a small amount of the oil phase located around the microcapsule membrane during the washing process (where most of the oil has been removed), causing the microcapsules to deflate and collapse onto themselves.

The microcapsules were observed using scanning electron microscopy, that further demonstrated successful cross-linking of the particle membrane. The middle images in Figure 6.9 show a number of ‘folded’ microcapsules from a sample prepared using a cross-linker concentration of 1wt%. The bottom images demonstrate that

these microcapsules are able to re-swell after removing the oil phase from the core. This re-swelling is achieved by firstly switching the aqueous pH to acidic values, causing the (non-crosslinked) amine groups within the polymer on the surface of the particles to protonate. This causes an increase in the inter-particle distance within the particle membrane maximising the membrane pore size, thus increasing the membrane porosity. Although at these acidic pH values the polymer expands, this is insufficient for the complete and homogeneous re-swelling of the microcapsules (in these condition only 20% of the microcapsules were seen to re-swell). In contrast, when a 70 kDa dextran molecule was added to the aqueous continuous phase, this was observed to force the re-swelling of (almost all, ~90%) the microcapsules.

The mechanism of this re-swelling still needs to be investigated in greater detail. However, it can be postulated that this is due to the presence of a large difference in chemical potential between the aqueous continuous phase and the inner core of the microcapsule. This results in driving the labeled dextran into the core of the capsule along with water, equalising the concentration on both sides of the microcapsules. It is likely that it is this process that causes the microcapsules to swell up back to their original size. This process and procedure corresponds to step 2 in Figure 6.10.

The procedure regarding the loading and retention of the dextran molecules within the microcapsules and its subsequent release in response to pH stimuli is described by Figure 6.9.

Once the dextran penetrates into the core of the microcapsule and the system equilibrates (step 2), the pH of the aqueous continuous phase is switched to pH 10 to ‘close’/reduce the membrane pores by deprotonating the amine groups within the polymer causing it to collapse onto the particle surface. The excess dextran is washed off using multiple centrifugation and re-dispersion cycles (step 3). The last step (step 4) describes how these microcapsules can selectively release their contents by switching the pH back to acidic values causing the polymer to protonate and thus increase the inter-particle distance making the membrane more porous.

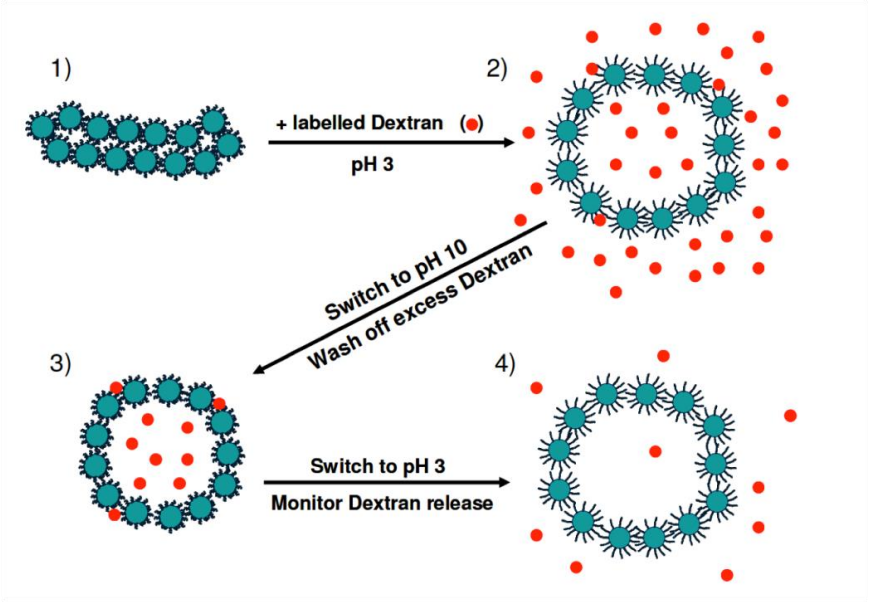

Figure 6.10. Schematically illustrating the procedures for loading the dextran molecules within the responsive colloidosome microcapsules and subsequently releasing it into the continuous in response to pH stimuli.

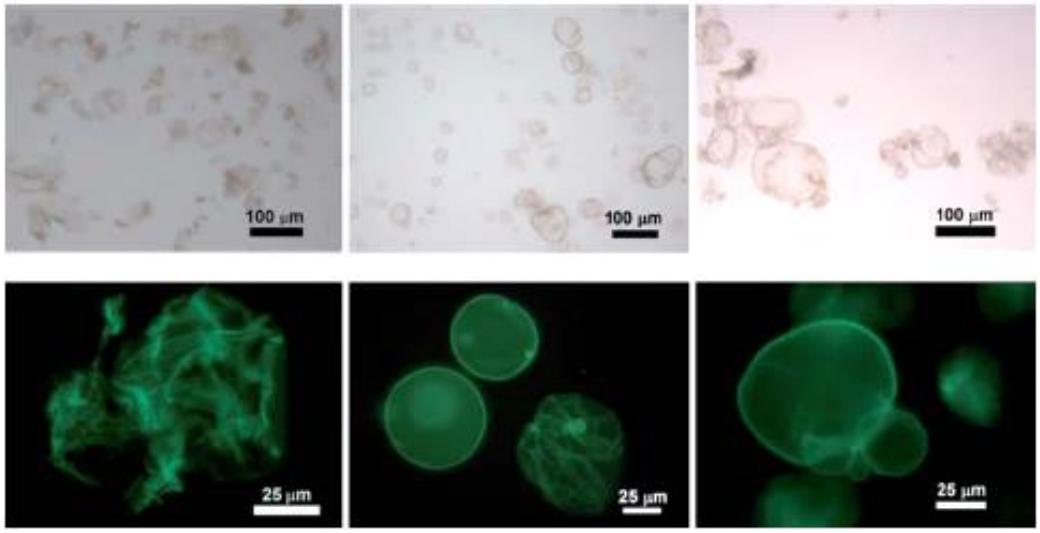

Figure 6.11. Transmitted (top) and fluorescence (bottom) optical micrographs of the colloidosome microcapsules corresponding to step 3 of Fig. 6.12, where the dextran is encapsulated at pH 10 using different BIEE cross-linking concentrations of 0.1 wt% (left), 0.5 wt% (middle) and 1 wt% (right). The dextran is loaded at pH 3 and the excess is removed using multiple washing steps after changing the pH to 10.

The process of encapsulating the dextran species within the microcapsule cores as a function of cross-linking concentration is presented in Figure 6.10. When a low cross-linking concentration (0.1 wt%) is used, it is clear from the micrographs that most of the microcapsules remain collapsed and are unlikely to be loaded with the fluorescently-labelled dextran molecules. This matches the observations presented in Figure 6.11, since the microcapsule membrane is not robust at this BIEE cross-linker concentration. Thus the process of removing the oil core could cause the rupture of the particle film in this case. However, the micrograph does show that the dextran appears to adsorb onto the surface of the resulting structures. In the case of the other two samples (0.5 wt% and 1 wt%), the optical micrographs show that upon loading with dextran the microcapsules swell back to a shape similar to that of their initial spherical structure. This fact that the microcapsules have swollen back to their initial shape suggests that at these cross-linker concentrations the dextran is not only adsorbed on the surface of the microcapsules, but is also present with the core. However, further evidence is needed to confirm the presence of dextran within the microcapsule membranes as the optical microscope used in these observations does not provide 3-dimensional information. This is provided later in this section. It should be noted in the case where 0.5 wt% and 1 wt% BIEE cross-linking concentration was used, no significant loss of dextran was recorded during the washing process. This suggests that colloidosome microcapsules cross-linked with either 0.5 wt% or 1 wt% of BIEE cross-linker may be candidate systems for the successful encapsulation and retention of 70 kDa dextran molecules.

In addition to the BIEE cross-linker we also investigated an alternative crosslinker; poly(propylene glycol) diglycidyl ether (PPG-DGE) to cross-link the polymer stabiliser on adjacent particles at the oil-water interfaces. This epoxy based compound reacts efficiently with primary and secondary amine groups. Its efficacy in reacting with tertiary amines has not been demonstrated, however, we show in the subsequent section that it was successful in permanently locking the particles used in our system for the preparation of the corresponding colloidosome microcapsules.[32] The pDMAEMA block of the stabiliser used in this study contains a tertiary amine. The cross-linker reacted sufficiently to create a permanently particle shell as evident by scanning electron microscopy as illustrated in Figure 6.12.

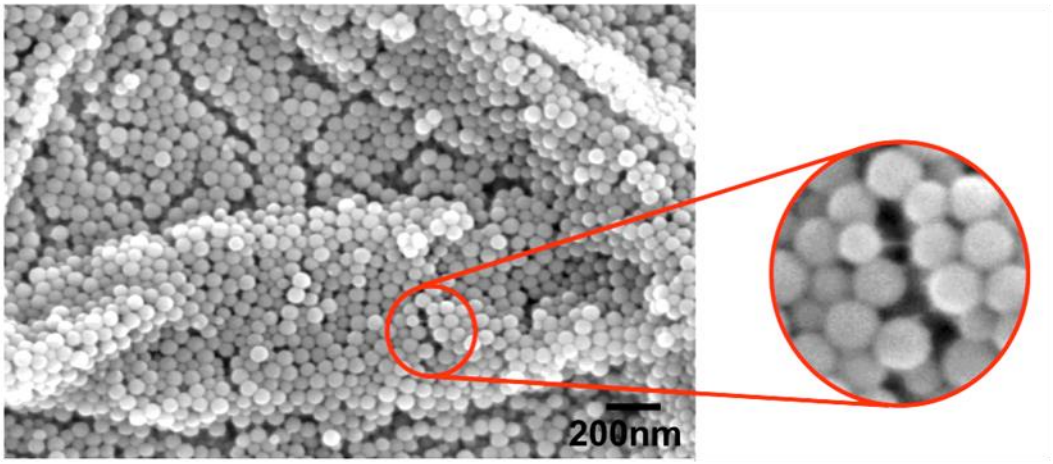

Figure 6.12. Successful cross-linking of the polymer stabiliser between the adjacent particles using the PPG-DPG cross-linker. *[Data acquired by Mr. James Hitchcock and used with his permission]*.[48]

The responsive properties of these microcapsules produced using the PPG-DPG cross-linker were tested after removal of the oil core as described by the procedure in Figure 6.10. The microcapsules were loaded with the fluorescently-labelled dextran by adding an excess to a suspension of capsules dispersed at pH 3. At this pH the size of the membrane pores are maximised due to the protonation of the amine groups. Once the capsules are loaded with dextran the pH is switched to pH 10, deprotonating the amine groups and causing the pore size to decrease with the aim of retaining the loaded dextran. Multiple washes with pH 10 water are subsequently carried out to remove any excess dextran in the continuous phase.

Optical fluorescent micrographs of the dextran-loaded microcapsules are illustrated in Figure 6.13. It is clear from the micrograph shown that there is little/no dextran present in the continuous phase in comparison to the fluorescent intensity observed within (on the surface of) the capsules. This observation was further verified by performing intensity measurements. These data demonstrate that although there is strong adsorption of the dextran on the outer membrane shell, the desorption from the shell and leakage from the interior of the capsule is relatively low at pH 10 (shown later in Figure 6.14b).

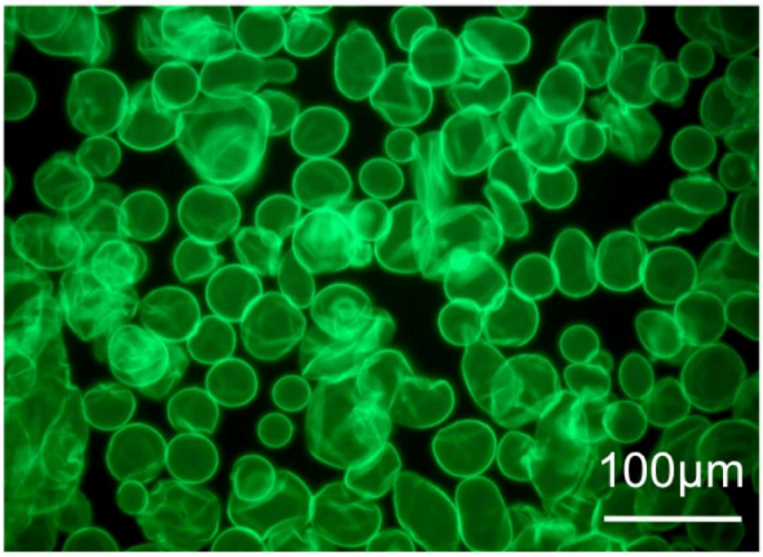

Figure 6.13. Fluorescent optical micrographs of the colloidosome microcapsules loaded with labelled dextran at pH 10. At this pH the pores are minimised in their size allowing the detran to be encapsulated with minimal leakage. These capsules were cross-linked using the PPG-DPG cross-linker. *[Data acquired by Mr. James Hitchcock and used with his permission]*.[48]

To confirm the location of the dextran and to investigate the potential for pH induced release of the dextran, fluorescence confocal microscopy was performed on these microcapsules. The ability of confocal microscopy to allow 3-D visualisation of the location of the fluorescent species allows for differentiation between the dextran molecules adsorbed onto the microcapsule surfaces and those present in their cores. The microcapsules were initially loaded with dextran at acidic pH values and then switched to pH 10 to close the pores of the capsules as mentioned above. The sample was then divided into two equal volumes where one was kept at pH 10 for 5 hours, whilst the other was kept at pH 3 for 5 hours.

The fluorescence confocal micrographs presented in Figure 6.14a shows these microcapsules at the two different pH's representing a 1µm slice through the microcapsule. It is clear from this image that a significant amount of the dextran is adsorbed onto the shell of the microcapsule. From the images it is clearly evident that at pH 10 the dextran is retained within the interior of the microcapsules. At pH 3, the micrograph clearly shows that the dextran is released from the microcapsule

core into the continuous phase as the polymer on the surface of the particle film protonates increasing the pore size, but it is also clear that the desorption of the dextran from the microcapsule surface is limited.

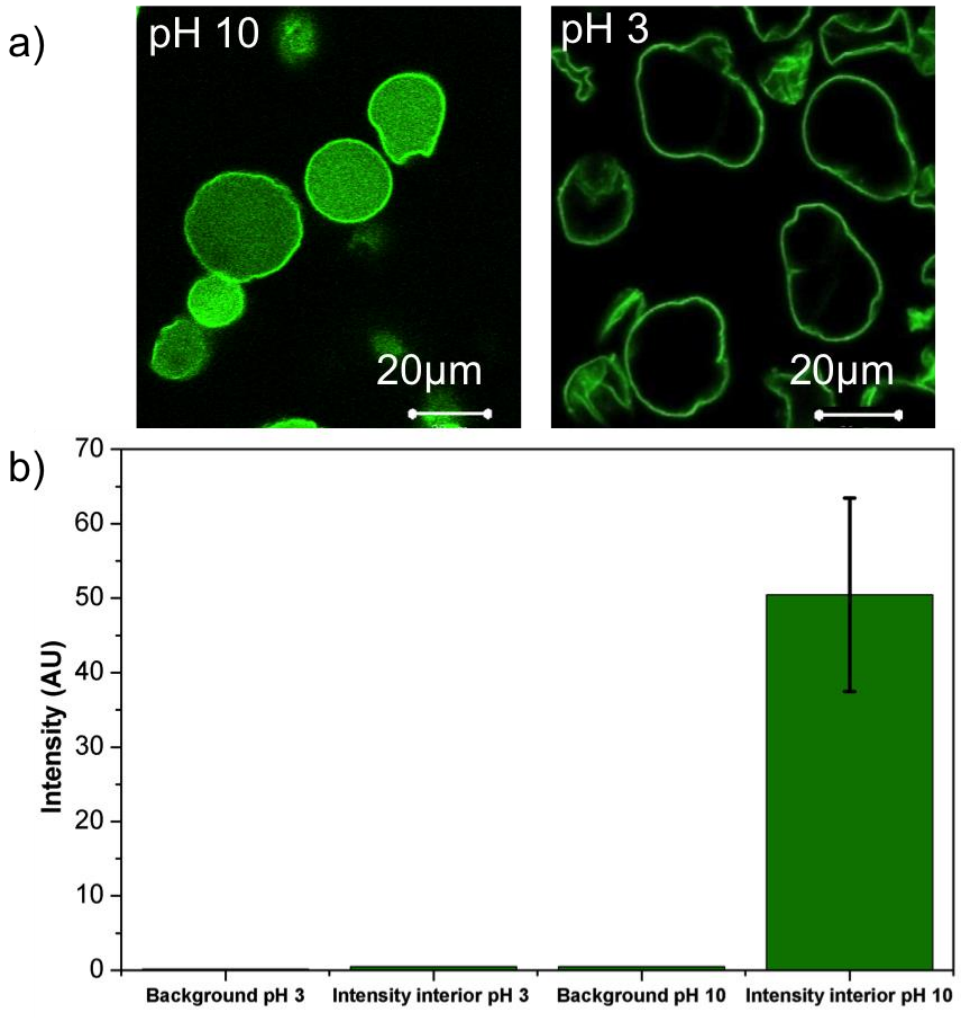

Figure 6.14. (a) Fluorescent confocal micrographs (1 μm slice) of two colloidosome microcapsules loaded with labelled-dextran kept at pH 10 and pH 3 for 5 hours after loading. (b) Fluorescent intensity measurements carried out on the microcapsules present in a), detailing both the average intensity of the continuous phase and the capsule core. *[Data acquired jointly by myself and Mr. J. Hitchcock]*.[48]

Fluorescent intensity measurements of the microcapsule interior and the continuous phase were performed for both samples and is presented in Figure 6.14b. These observations were made under the same conditions using the same exposure time of

the camera so that the images could be directly compared to each other. It can be concluded from these data that the dextran concentration is in equilibrium between the interior of the capsule and the continuous phase (background) at pH 3. At pH 10 the intensity observed is much higher within the capsule core in comparison to the background, which demonstrates successful retention of the 70 kDa dextran within the sample of microcapsules over a period of 5 hours.

Conclusions

It has been demonstrated that polystyrene latex particles grafted with sterically stabilised polymer (pMMA-b-pDMAEMA), behave as a pH-responsive particulate emulsifier for the preparation of oil in water Pickering emulsions. Emulsions are readily formed at pH values around 8 - 9 in the presence of 2 wt% latex by mass. Unstable emulsions (over the course of 24 hours) with macroscopic phase separation occurs at acidic pH values due to the protonation of the amine groups on the pDMAEMA block, which presumably reduces the affinity of the particles to the oil/water interface. The addition of electrolyte to the system increases emulsion stability as the electrolyte screens the charges present on the polymer, thus increasing the affinity of the particles to adsorb at the interface and stabilise the oil droplets.

These solid-stabilised emulsions can then be used as templates for the fabrication of pH-responsive colloidosome microcapsules. Using the pH-responsive properties of the particulate membrane shell, the microcapsules can successfully encapsulate and control the release of labelled dextran molecules as a function of changes in the environmental pH. The pH-responsive membrane is produced by chemically cross-linking the polymer chains on adjacent particles at the interface. Confocal microscopy studies conducted at different pH’s showed that at acidic pH’s the membrane porosity is maximised and a rapid equilibrium of the dextran molecules occurs between the continuous phase and the capsule core. On the other hand the dextran molecules are retained at basic pH over 5 hours. The data clearly demonstrates that the colloidosome microcapsule membrane can be used to control the release rate of large molecules and acts as a size exclusion membrane.

References

1. S. U. Pickering, Emulsions, *J. Chem. Soc., Trans.*, 1907, **91**, 2001-2021.
2. T. Chen, P. J. Colver and S. A. F. Bon, Organic-inorganic hybrid hollow spheres prepared from TiO-stabilized Pickering emulsion polymerization, *Adv. Mater.*, 2007, **19**, 2286-2289.
3. Y. He, Preparation and modification of ZnO microspheres using a Pickering emulsion as template, *Mater. Lett.*, 2005, **59**, 114-117.
4. C. Zeng, H. Bissig and A. D. Dinsmore, Particles on droplets: From fundamental physics to novel materials, *Solid State Commun.*, 2006, **139**, 547-556.
5. O. D. Velev, K. Furusawa and K. Nagayama, Assembly of latex particles by using emulsion droplets as templates. 1. Microstructured hollow spheres, *Langmuir*, 1996, **12**, 2374-2384.
6. A. D. Dinsmore, M. F. Hsu, M. G. Nikolaides, M. Marquez, A. R. Bausch and D. A. Weitz, Colloidosomes: Selectively permeable capsules composed of colloidal particles, *Science*, 2002, **298**, 1006-1009.
7. B. P. Binks and T. S. Horozov, eds., *Colloidal Particles at Liquid Interfaces*, Cambridge University Press, Cambridge, 2006
8. B. R. Midmore, Preparation of a novel silica-stabilized oil/water emulsion, *Colloids Surf. A: Physicochem. Eng. Asp.*, 1998, **132**, 257-265.
9. E. Vignati, R. Piazza and T. P. Lockhart, Pickering emulsions: Interfacial tension, colloidal layer morphology, and trapped-particle motion, *Langmuir*, 2003, **19**, 6650-6656.
10. S. Abend and G. Lagaly, Bentonite and double hydroxides as emulsifying agents, *Clay Miner.*, 2001, **36**, 557-570.
11. Y. Yan and J. H. Masliyah, Solids-stabilized oil-in-water emulsions: Scavenging of emulsion droplets by fresh oil addition, *Colloids Surf. A: Physicochem. Eng. Asp.*, 1993, **75**, 123-132.
12. B. P. Binks and S. O. Lumsdon, Stability of oil-in-water emulsions stabilised by silica particles, *Phys. Chem. Chem. Phys.*, 1999, **1**, 3007-3016.
13. W. D. Bancroft, Theory of emulsification, *J. Phys. Chem.*, 1913, **17**, 501-519.
14. B. P. Binks, Particles as surfactants-similarities and differences, *Curr. Opin. Colloid Interface Sci.*, 2002, **7**, 21-41.

15. B. Binks and S. Lumsdon, Effects of oil type and aqueous phase composition on oil-water mixtures containing particles of intermediate hydrophobicity, *Phys. Chem. Chem. Phys.*, 2000, **2**, 2959-2967.

16. D. E. Tambe and M. M. Sharma, The effect of colloidal particles on fluid-fluid interfacial properties and emulsion stability, *Adv. Colloid Interface Sci.*, 1994, **52**, 1-63.

17. S. Tarimala and L. L. Dai, Structure of microparticles in solid-stabilized emulsions, *Langmuir*, 2004, **20**, 3492-3494.

18. J. I. Amalvy, S. P. Armes, B. P. Binks, J. A. Rodrigues and G. F. Unali, Use of sterically-stabilised polystyrene latex particles as a pH-responsive particulate emulsifier to prepare surfactant-free oil-in-water emulsions, *Chem. Commun.*, 2003, 1826-1827.

19. R. Murakami, B. P. Binks, S. P. Armes, S. Fujii,, Temperature-induced inversion of nanoparticle-stabilized emulsions, *Angew. Chem., Int. Ed.*, 2005, **44**, 4795-4798.

20. N. Saleh, T. Sarbu, K. Sirk, G. V. Lowry, K. Matyjaszewski and R. D. Tilton, Oil-in-Water emulsions stabilized by highly charged polyelectrolyte-grafted silica nanoparticles, *Langmuir*, 2005, **21**, 9873-9878.

21. K. L. Thompson and S. P. Armes, From well-defined macromonomers to sterically-stabilised latexes to covalently cross-linkable colloidosomes: exerting control over multiple length scales, *Chem. Commun.*, 2010, **46**, 5274-5276.

22. K. L. Thompson, S. P. Armes and D. W. York, Preparation of Pickering emulsions and colloidosomes with relatively narrow size distributions by stirred cell membrane emulsification, *Langmuir*, 2011, **27**, 2357-2363.

23. J. Drelich, C. L. White and C. Fang, Measurement of interfacial tension in fluid-fluid systems, In: *Encyclopedia of Surface and Colloid Science, Second Edition*, Taylor & Francis, 2007, 2966-2980.

24. C. D. Anderson and E. S. Daniels, eds., *Emulsion polymerisation and latex applications*, Vol. 14, iSmithers Rapra Publishing, 2003

25. J. I. Amalvy, G. F. Unali, Y. Li, S. Granger-Bevan, S. P. Armes, B. P. Binks, J. A. Rodrigues and C. P. Whitby, Synthesis of sterically stabilized polystyrene latex particles using cationic block copolymers and

macromonomers and their application as stimulus-responsive particulate emulsifiers for oil-in-water emulsions, *Langmuir*, 2004, **20**, 4345-4354.

26. Malvern Mastersizer 2000 Operators Guide, Issue 2, 1999.
27. V. Bütün, S. P. Armes and N. C. Billingham, Synthesis and aqueous solution properties of near-monodisperse tertiary amine methacrylate homopolymers and diblock copolymers, *Polymer*, 2001, **42**, 5993-6008.
28. J. W. J. de Folter, M. W. M. van Ruijven and K. P. Velikov, Oil-in-water Pickering emulsions stabilized by colloidal particles from the water-insoluble protein zein, *Soft Matter*, 2012, **8**, 6807-6815.
29. H. N. Yow and A. F. Routh, Formation of liquid core-polymer shell microcapsules, *Soft Matter*, 2006, **2**, 940-949.
30. B. G. De Geest, N. N. Sanders, G. B. Sukhorukov, J. Demeester and S. C. De Smedt, Release mechanisms for polyelectrolyte capsules, *Chem. Soc. Rev.*, 2007, **36**, 636-649.
31. P. J. Dowding, R. Atkin, B. Vincent and P. Bouillot, Oil core-polymer shell microcapsules prepared by internal phase separation from emulsion droplets. I. Characterization and release rates for microcapsules with polystyrene shells, *Langmuir*, 2004, **20**, 11374-11379.
32. L.-Y. Chu, S.-H. Park, T. Yamaguchi and S.-i. Nakao, Preparation of thermo-responsive core-shell microcapsules with a porous membrane and poly(N-isopropylacrylamide) gates, *J. Membr. Sci.*, 2001, **192**, 27-39.
33. O. D. Velev, K. Furusawa and K. Nagayama, Assembly of latex particles by using emulsion droplets as templates. 2. Ball-like and composite aggregates, *Langmuir*, 1996, **12**, 2385-2391.
34. O. D. Velev and K. Nagayama, Assembly of latex particles by using emulsion droplets. 3. Reverse (Water in Oil) system, *Langmuir*, 1997, **13**, 1856-1859.
35. G. R. Yi, V. N. Manoharan, S. Klein, K. R. Brzezinska, D. J. Pine, F. F. Lange and S. M. Yang, Monodisperse micrometer-scale spherical assemblies of polymer particles, *Adv. Mater.*, 2002, **14**, 1137-1140.
36. N. P. Ashby, B. P. Binks and V. N. Paunov, Formation of giant colloidosomes by transfer of pendant water drops coated with latex particles through an oil-water interface, *Phys. Chem. Chem. Phys.*, 2004, **6**, 4223-4225.

37. O. J. Cayre, P. F. Noble and V. N. Paunov, Fabrication of novel colloidosome microcapsules with gelled aqueous cores, *J. Mater. Chem.*, 2004, **14**, 3351-3355.

38. P. F. Noble, O. J. Cayre, R. G. Alargova, O. D. Velev and V. N. Paunov, Fabrication of hairy colloidosomes with shells of polymeric microrods, *J. Am. Chem. Soc.*, 2004, **126**, 8092-8093.

39. H. Duan, D. Wang, N. S. Sobal, M. Giersig, D. G. Kurth and H. Möhwald, Magnetic colloidosomes derived from nanoparticle interfacial self-assembly, *Nano Lett.*, 2005, **5**, 949-952.

40. Q. Yuan, O. J. Cayre, S. Fujii, S. P. Armes, R. A. Williams and S. Biggs, Responsive core-shell latex particles as colloidosome microcapsule membranes, *Langmuir*, 2010, **26**, 18408-18414.

41. S. Laïb and A. F. Routh, Fabrication of colloidosomes at low temperature for the encapsulation of thermally sensitive compounds, *J. Colloid Interface Sci.*, 2008, **317**, 121-129.

42. H. N. Yow and A. F. Routh, Release profiles of encapsulated actives from colloidosomes sintered for various durations, *Langmuir*, 2009, **25**, 159-166.

43. D. B. Lawrence, T. Cai, Z. Hu, M. Marquez and A. D. Dinsmore, Temperature-responsive semipermeable capsules composed of colloidal microgel spheres, *Langmuir*, 2006, **23**, 395-398.

44. K. L. Thompson, S. P. Armes, J. R. Howse, S. Ebbens, I. Ahmad, J. H. Zaidi, D. W. York and J. A. Burdis, Covalently cross-linked colloidosomes, *Macromolecules*, 2010, **43**, 10466-10474.

45. S. Biggs, R. A. Williams, O. J. Cayre and Q. Yuan, '*Microcapsules and methods'*, WIPO Patent application number: WO/2009/037482, 2010.

46. H. Skaff, Y. Lin, R. Tangirala, K. Breitenkamp, A. Böker, T. P. Russell and T. Emrick, Crosslinked capsules of quantum dots by interfacial assembly and ligand crosslinking, *Adv. Mater.*, 2005, **17**, 2082-2086.

47. A. Walsh, K. L. Thompson, S. P. Armes and D. W. York, Polyamine-functional sterically stabilized latexes for covalently cross-linkable colloidosomes, *Langmuir*, 2010, **26**, 18039-18048.

48. J. Hitchcock, '*Investigating the Efficiency of Smart Microcapsules Prepared from Cross-Linked Solid-Stabilised Emulsions.*' (M.Sc. Thesis, University of Leeds, August 2011).

CHAPTER 7: Production of solid-stabilised emulsions using Rotary Membrane Emulsification (RME)

NOMENCLATURE

k_{ad}	Adsorption rate constant
A_d	Surface area of droplet covered with particles
$A_{d,\,cr}$	Critical surface coverage value
$A_{d,\,0}$	Total surface area of droplet
τ_{ad}	Adsorption time
$\tau_{ad,cr}$	Critical adsorption time
τ_{drop}	Droplet lifetime on membrane

7.1. Introduction

This chapter describes and outlines an optimization study carried out on the use of rotational membrane emulsification (RME) to produce controlled Pickering emulsions. In this study two particulate emulsifiers (model silica colloids and sterically stabilised latex particles) are used to investigate and optimize various chemical and mechanical parameters related to RME for controlled droplet production.

7.2. Surfactant-free emulsions stabilised by silica particles

7.2.1. Surface chemistry of silica

Silica (SiO_2) consists of four oxygen atoms surrounding a single silicon atom in a tetrahedral arrangement as shown in Figure 7.1.

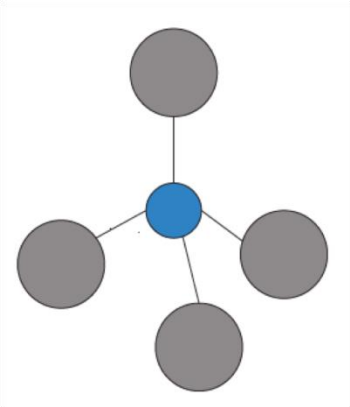

Figure 7.1. Schematic of tetrahedral arrangement of four oxygen atoms surrounding a silicon atom.

The silicon atoms are joined together by oxygen via siloxane bonds (Si-O-Si). Depending on the method used to produce the silica particles, the surface may contain hydroxyl (silanol) groups, which can hydrogen bond with water adsorbed onto its surface, giving rise to a negative surface charge density.[1] This negative surface charge can be assumed to be uniformly distributed over the particle surface.

Silica particles were used as a 'model' system to investigate and optimise the production of solid-stabilised emulsion droplets using a rotary membrane emulsification technique. Although there have been many reports on the use of membrane emulsification to produce near monodisperse emulsion droplets, the majority of these studies are focused on surfactant-stabilized emulsions.[2-4] There are very few reports on the use of particulate stabilisers to produce low polydispersity emulsions.[5-7] Therefore in this emulsification study ultra-high purity (>99.5% SiO_2), near monodisperse 800 nm silica particles with a density of 2.26 g cm^{-3} were used which were obtained from Fuso Chemical Co. Ltd (Japan). 800 nm silica particles were chosen due to the potential of very high attachment energies at the interface (Chapter 2). Furthermore, for membrane emulsification experiments a large quantity of particles are usually required and therefore 800 nm silica was chosen as it was relatively inexpensive and available in a large quantity. To remove trace impurities, the silica particles were washed three times using ethanol (typically 1 g of silica was dispersed in 25 mL of ethanol and left on the carousel for 30 minutes, centrifuged for 3 mins at 5000 rpm and the supernatant was replaced with fresh ethanol). After 3 washes with ethanol, three wash cycles with Milli-Q water (25 mL) were performed before finally dispersing into water at the desired pH and electrolyte concentration.

Zeta potential measurements (see Chapter 4) were carried out to measure the zeta potential as a function of environmental pH and background electrolyte concentration as illustrated in Figure 7.2, to assess the stability of the silica dispersion.

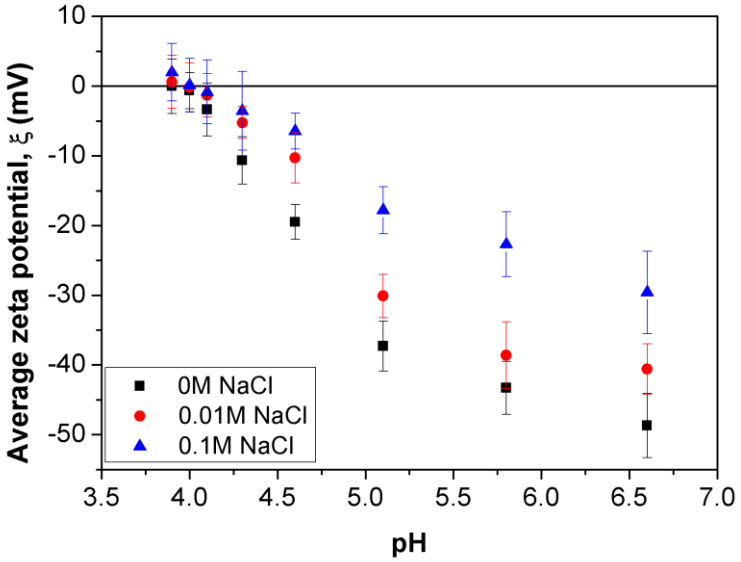

Figure 7.2. Illustrating the changes in zeta potential of 800 nm FUSO silica colloids as a function of pH at varying NaCl electrolyte concentrations.

The zeta potential titration illustrates that under no added electrolyte conditions the silica is highly negatively charged around pH 6.5, with zeta potential values close to -50 mV. As the pH is decreased the silanol groups on the surface become uncharged, resulting in a decrease in the measured zeta potential. As the pH is decreased to 4, all the silanol groups are protonated, hence the zeta potential measured reduces to 0mV. This is known as the point of zero charge or the isoelectric point (i.e.p). This value has been previously reported in literature for FUSO silica particles[8] and also matches the specification reported by FUSO Chemical Company Ltd.[9]

The addition of background electrolyte also influences the zeta potential measured. Comparing the values around pH 6.5, it is evident that by increasing the ionic strength of the background electrolyte there is a reduction in the zeta potential measured. This can be explained by changes in the electric double layer thickness (see Chapter 4) and the screening of surface charges which potentially improve their adsorption to the liquid-liquid interface. This is due to the attraction of a layer of counter-ions towards the negatively charged surface of silica in order to achieve overall electroneutrality.[10] As the ionic strength of the electrolyte is increased the concentration of counter ions surrounding the silica surface increases, reducing the Debye length (length over which significant charge separation occurs). This

screening of the surface charge therefore reduces the zeta potential observed at the slip plane.

To examine the stability of the silica dispersion in terms of size, dynamic light scattering measurements were undertaken for two different pH's as illustrated in Figure 7.3.

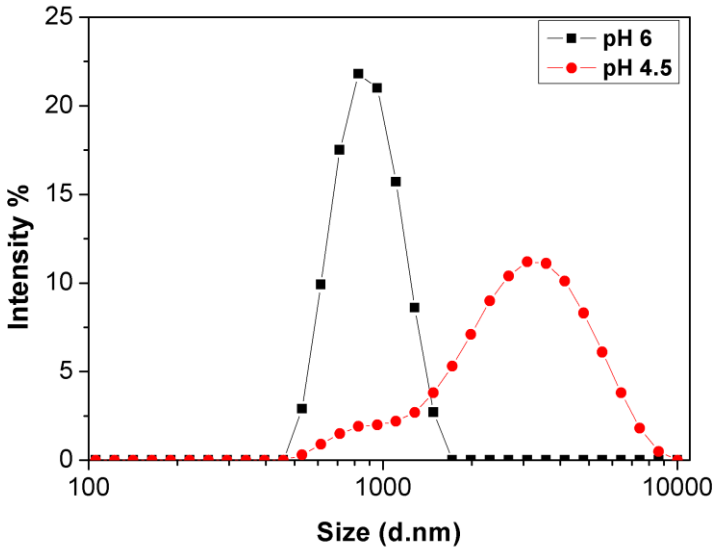

Figure 7.3. Illustrating the size distribution of 800 nm FUSO silica colloidal dispersions at two different pH values in an electrolyte concentration of 0.01M NaCl.

The size distribution data shows that at pH 6 that the silica dispersion is highly stable. A monomodal peak is observed with a particle size of around 800nm in diameter. This stability is due to the highly negative charge density on the silica surface. Therefore the repulsive forces dominate over the attractive van der Waals force leading to a stable particle dispersion. Decreasing the pH of the dispersion to 4.5 (close to the i.e.p), there is little/no charge stabilization on the silica surface which causes instability in the particle dispersion. The screening of the surface charge decreases the repulsive forces between the particles, allowing the attractive van der Waals forces to dominate, causing them to form aggregates. Performing sizing measurements at pH 4.5, a bi-modal size distribution is obtained with particle aggregate sizes of approximately 3 – 4 µm.

Performing zeta potential and particle size measurements show that the silica dispersion is stable at ~pH 6. The stability of the silica particles in terms of their size over a typical membrane emulsification period of 60 minutes was also measured at pH 6 at various electrolyte concentrations (Figure 7.4).

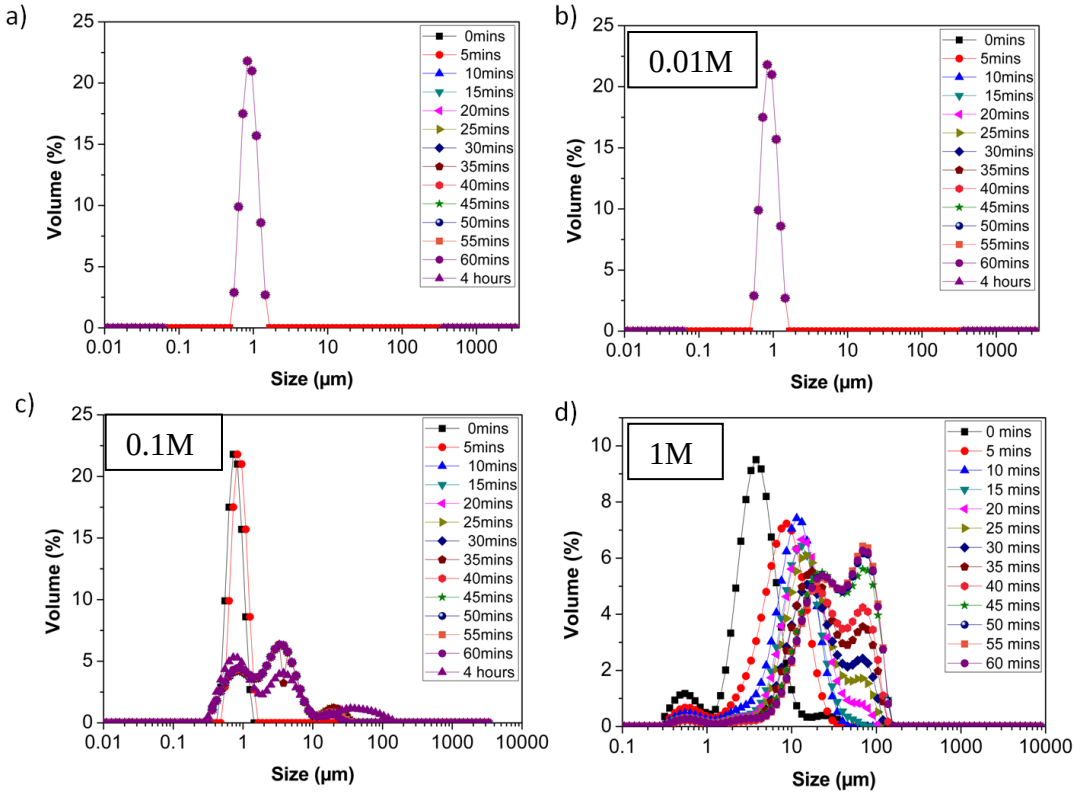

Figure 7.4. Variation in size of 800 nm FUSO silica colloids dispersion at pH 6 over a typical emulsification time period at 4 different electrolyte concentrations; a) no added electrolyte, b) 0.01M, c) 0.1M and d) 1M NaCl.

The data in Figure 7.4 shows that when the silica particles are dispersed with either no added electrolyte or 0.01M NaCl, they remain stable over the 60 minute measuring period. As the electrolyte concentration increases to 0.1M and 1M NaCl, the particles aggregate over the typical emulsification period. Particle aggregation occurs as the Debye length decreases with increasing electrolyte concentration, thus van der Waals attractive forces between the particles dominate, leading to particle aggregation.

Before conducting membrane emulsification experiments it was important to ensure that at pH 6 the particles were able to adsorb to the tricaprylin/water interface.

Tricaprylin oil was selected as the disperse phase in this study, as it has been previously demonstrated that silica particles are able to stabilise tricaprylin droplets in water using both homogenisation and microchannel emulsification techniques.[7] Therefore a preliminary emulsion study (using an Ultra-Turrax homogeniser) was conducted to determine the effect of electrolyte concentration on emulsion stability at pH = 6, by comparing digital micrographs and light diffraction data as illustrated in Figure 7.5. The purpose of this study was to determine the starting pH and electrolyte conditions in order to optimise emulsion droplet production using rotational membrane emulsification.

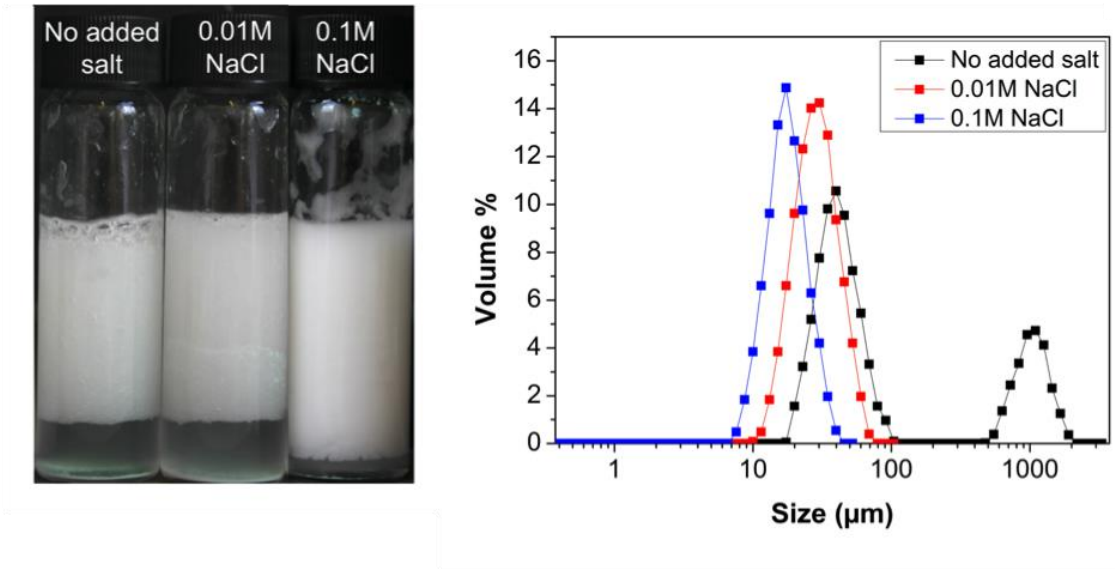

Figure 7.5. Silica stabilised emulsions produced at pH 6 under different electrolyte concentration via homogenisation. Emulsion stability determined using digital micrographs (left) and droplet size distribution (right), 24 hours after preparation.

Emulsions created in the absence of added background electrolyte produced droplets having a bi-modal size distribution, 24 hours after the initial emulsion had been created. The size distribution data shows a peak at around 40 µm, with a secondary peak at around 1000 µm. This larger peak is attributed to instability in the emulsion leading to coalescence and creaming. This instability is also visualised in the digital micrographs where coalesced droplets can be seen. The clear phase visible below the emulsion phase is a result of water drainage which sediments to the bottom due

to the density difference. The addition of background NaCl electrolyte shows an apparent increase in emulsion stability as a function of added electrolyte concentration. Size distribution data performed after 24 hours yielded monomodal peaks of around 30 μm (for 0.01M NaCl) and 15 μm (0.1M NaCl). Furthermore, the water phase is much smaller than that observed at no added and 0.1M NaCl electrolyte conditions. Therefore silica dispersions prepared at pH 6 in the presence of 0.1M NaCl electrolyte was taken as the starting conditions for the membrane emulsification experiments.

7.2.2. Influence of pH and background electrolyte

Initial studies were focused on investigating the role of pH and electrolyte concentration of the continuous phase on droplet production using rotary membrane emulsification. These conditions would then be used to explore the impact of membrane rotational speed, injection rate of the disperse phase and particle concentration on the droplet size and size distribution (to be discussed later in the chapter). As mentioned in section 7.2.1, the starting pH and electrolyte conditions were based on preliminary experiments examining particle dispersion and emulsion stability.

The average droplet size and polydispersity as a function of varying pH conditions at a fixed electrolyte concentration of 0.1M NaCl are given in Figure 7.6. The initial membrane rotation speed and disperse injection rate of 1000 rpm and 0.1 mL min^{-1}, were based on emulsion droplet data produced using surfactant stabilisers (see Figures 5a and 5b).[11] These membrane rotational speed and oil injection rate values were used as they produced the smallest droplet size with the lowest coefficient of variation in the surfactant system studied. The initial particle concentration used is 4.0 wt%. The data illustrated in Figure 7.6 and subsequent studies was obtained by taking optical micrographs of 100 droplets and measuring them using ImageJ software.

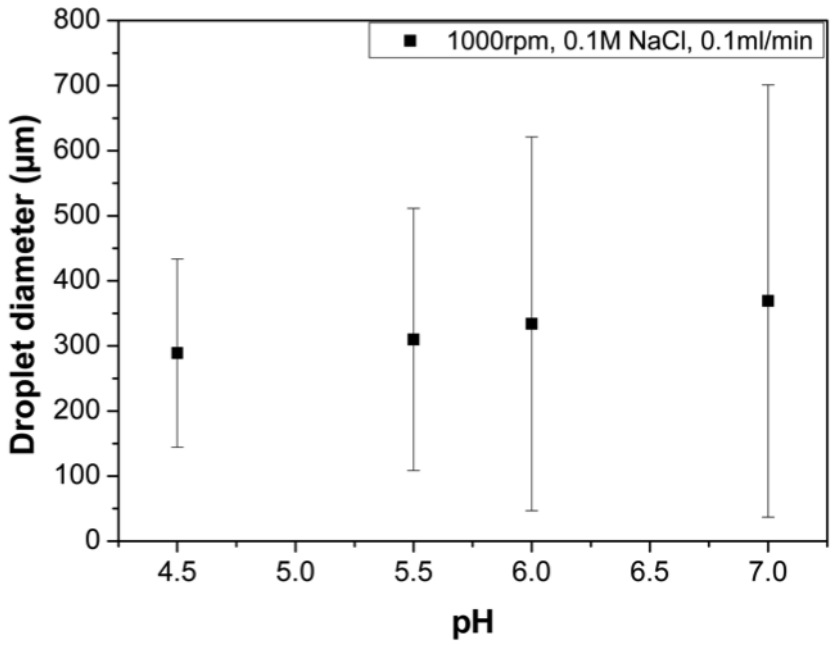

Figure 7.6. Effect of pH on the diameter of tricaprylin droplets produced using RME. The continuous phase consisted of 4.0 wt% of 800 nm silica colloids in 0.1M NaCl background electrolyte. The membrane rotational speed and oil injection rate were kept constant at 1000 rpm and 0.1 mL min^{-1}, respectively.

The effect of pH on the droplet diameter is inconclusive from the data presented in Figure 7.6 due to the large scatter in the data which represents the polydispersity of the emulsion sample. However, the data does show an apparent decrease in the polydispersity of emulsion droplets as the pH decreases from pH 7.0 to 4.5. This decrease in polydispersity can be attributed to an improvement in the stability of the droplets produced. Binks and Lumsdon have previously investigated the stability of 12 nm silica stabilised Pickering emulsions examining the effects of pH and electrolyte concentration.[12] They reported on the stability of oil in water emulsions created at varying pH's at two extreme NaCl electrolyte concentrations. They found that pH 4 also yielded the most stable emulsions irrespective of the NaCl electrolyte concentration used.

The apparent decrease in polydispersity as a function of decreasing pH can be attributed to changes in the particle adsorption rate. Improvements in the particle adsorption rate will help facilitate the production of droplets which are low in polydispersity as evident from the droplet size data illustrated in Figure 7.6. It should be noted that in general oil-water interfaces are negatively charged, most

probably due to the adsorption of hydroxyl ions at the interface.[13] This may potentially explain why the pH of the silica dispersion and its resultant charge will influence the particle adsorption rate. At pH 7, the silica surface is highly negatively charged (as confirmed by zeta potential measurements in Figure 7.2), therefore an electrostatic repulsion force exists between the particles and the oil-water interface, potentially leading to low particle adsorption rates. As the pH is decreased, so does the surface charge on the silica which reduces the electrostatic repulsion between the particles and the interface and hence changes the contact angle leading to improvements in the particle adsorption rate. As a result the droplet polydispersity decreases.

Although the data in Figure 7.6 suggests that the lowest polydispersity in the emulsion sample is achieved at pH 4.5 (i.e. close to the i.e.p), it is found from particle size data that at this pH the silica dispersion is unstable (see Figure 7.3). This instability causes the colloidal dispersion to undergo flocculation and sedimentation during the membrane emulsification process, making data interpretation difficult from one experiment to another. In order to maintain stable silica dispersions throughout the emulsification process, pH 6 was chosen as the optimal pH to work at. This is because the droplet size and polydispersity can ultimately be controlled and improved when investigating other parameters which will be discussed later.

Figure 7.7 illustrates the droplet size data as a function of added electrolyte concentration at a fixed pH value of 6. The membrane rotation speed and disperse injection rate of 1000 rpm and 0.1 mL min^{-1} respectively. The particle concentration used was fixed at 4.0 wt%.

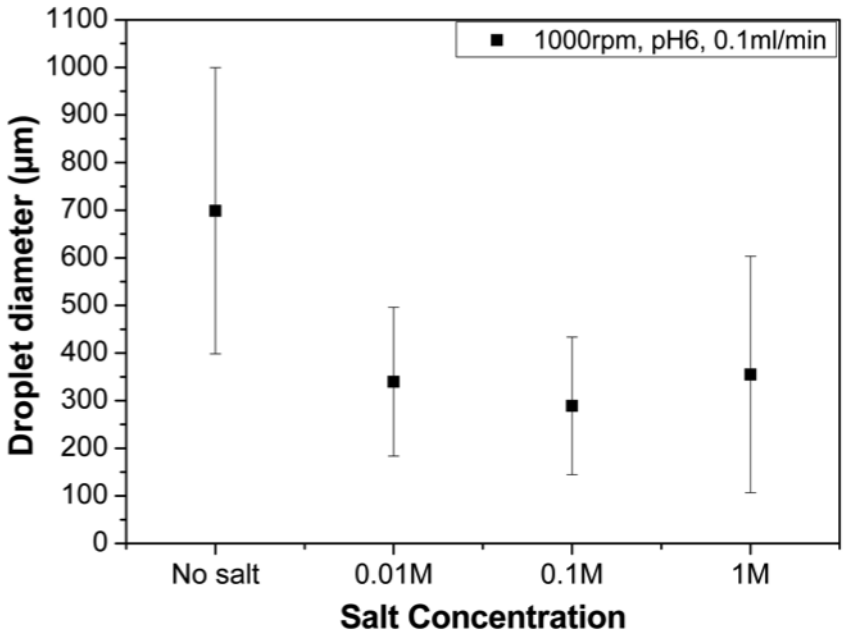

Figure 7.7. Effect of added NaCl electrolyte concentration on the diameter of tricaprylin droplets produced using the RME. The continuous phase consisted of 4.0 wt% of 800 nm silica colloids dispersed at a pH = 6. The membrane rotational speed and oil injection rate were kept constant at 1000 rpm and 0.1 mL min^{-1}, respectively.

The trend observed from Figure 7.7 shows that the addition of background electrolyte prior to emulsification results in a reduction in the mean droplet size and size distribution. The addition of electrolyte to the colloidal dispersion screens the negative surface charge on the silica particles. This favours the approach of the particles to the oil-water interface and their subsequent adsorption as there is a reduction in the electrostatic repulsion between the particles and the interface. The trend in Figure 7.7 shows an apparent decrease in the droplet diameter between electrolyte concentrations of 0 and 0.1M NaCl. Further addition of electrolyte results in an increase in both the average droplet size polydispersity.

As the electrolyte concentration is increased between 0 and 0.1M NaCl, a reduction in the average droplet size suggests the addition of electrolyte improves the particle adsorption kinetics of the silica particles to the liquid-liquid interface. When the silica dispersion contains no added electrolyte the Debye length around the particles and droplet exceeds 960 nm (in pure water).[14] The rate of diffusion of the particles

over this length scale may impact the kinetics of adsorption towards the forming droplet. As a result both the diffusion and adsorption of the silica particles are likely to be relatively slow when no electrolyte is added to the colloidal dispersion. If we assume that the adsorption process is diffusion (due to Brownian motion) limited the time taken for the 800 nm silica particles to adsorb to the oil-water is around 0.76 s in pure water (i.e. no added electrolyte). In comparison, the droplet residency time at the membrane is around 1.06×10^{-3} s (assuming that the droplet grows to a size of 150 µm which is twice the size of the membrane pore at a rate of 0.1 mL min^{-1}). It is clear from these calculations that the adsorption rate at low electrolyte concentrations is very slow leading to production of droplets with low particle coverage. This can be visualised in Figure 7.8 showing optical micrographs of droplets that shows an incomplete particle coverage for no added electrolyte as well at an electrolyte concentration of 0.01M NaCl.

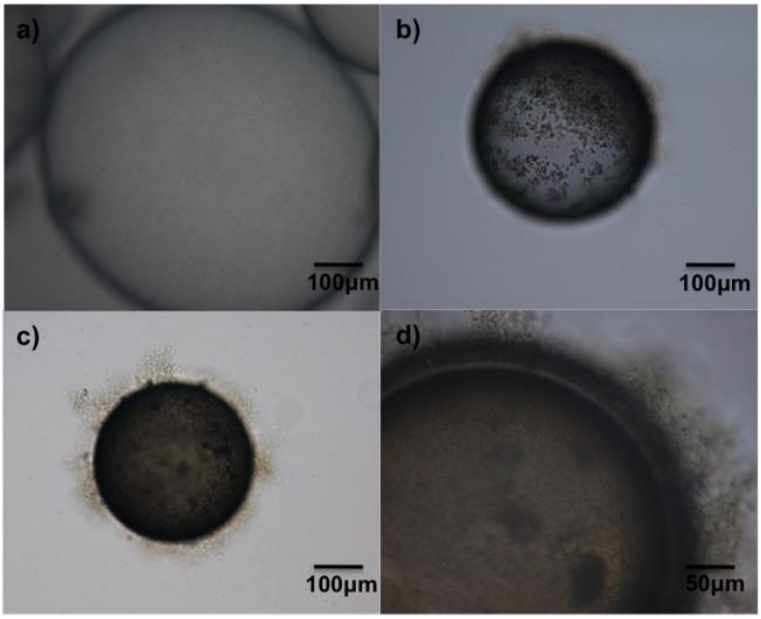

Figure 7.8. Optical micrographs of tricaprylin droplets prepared in a) no added electrolyte, b) 0.01M NaCl, c) 0.1M NaCl and d) 1M NaCl electrolyte concentrations. The micrographs show differences in the particle coverage and adsorption of flocs at high electrolyte concentrations. The continuous phase consisted of 4.0 wt% of 800 nm silica colloids in 0.1M NaCl background electrolyte. The membrane rotational speed and oil injection rate were kept constant at 1000 rpm and 0.1 mL min^{-1}, respectively.

The incomplete particle coverage observed at no added and low NaCl electrolyte concentrations are in agreement to data published by Midmore *et al*.[15] They found that it was possible to produce stable paraffin oil droplets having a particle coverage as low as 29% using Ludox silica particles at low electrolyte concentrations. Kinetically stable emulsions with very low particle surface coverage values have also been reported by numerous authors.[16-19] Gautier *et al.*[19] obtained stable emulsions with particle coverage values as low as 10% without the addition of background electrolyte. The addition of 0.1M NaCl electrolyte increased the overall surface coverage to around 78%. In their discussion they outline two potential mechanisms that could be used to explain why droplets with low particle surface coverage can be obtained. They proposed that these two mechanisms were due to 1) particle bridging and 2) attractive interactions between particles at neighbouring interfaces, respectively. These differences in critical surface coverage values will also be a result of varying particle adsorption rates leading to stable droplets of varying degrees of particle coverage on the droplet surface.

At low electrolyte concentrations the particle collision events at the interface are high (typically in the order of 10^{10} particles cm^{-1} s), (in the lifetime of a 150 µm droplet growing at the membrane wall, it will come into contact with 10^6 particles whilst only 10^5 particles are needed for a complete monolayer coverage on the droplet surface based on a hexagonal close packing arrangement) therefore the adsorption process is not diffusion limited. The assumption made here is that the particles in the continuous phase remains stagnant and that the contact is due to the droplets moving (due to the rotation of the membrane) as it grows on the membrane surface. The main mechanism is therefore due to changes in charge screening at the interface as well as at the particle surface, leading to faster particle adsorption. This can be confirmed upon comparing the particle surface coverage of the tricaprylin droplets in Figure 7.8. At 0.01M the droplets appear patchy, whilst at 0.1M the droplet surface appears completely covered. Furthermore, it is evident from the micrograph that small aggregates are present on the droplet surface at 0.1M. This enhances the stability of the droplets by forming a large steric barrier, that prevents droplets from coming into close contact and coalescing.

At 1M NaCl concentration, the average droplet size and polydispersity increases. At this ionic strength the Debye length is very small (0.3 nm) and thus causes instability in the silica dispersion forming large aggregates (Figure 7.8). The data in

Figure 7.4 clearly show that the silica dispersion in the presence of 1M NaCl becomes highly unstable and can aggregate to a mean size of 60 µm. Performing simple calculations on these aggregates, show that their diffusion times (~ 4000 s) to the interface are much slower in comparison to the residency time of the droplet at the membrane (1.06×10^{-3} s) in order to achieve sufficient droplet coverage. The formation of large aggregates also results in a decrease in the total number of particles in the continuous phase to adsorb and stabilise newly formed droplets. Combination of these two processes (colloidal instability and decrease in the total number of particles in the continuous phase) result in an increase in droplet size and the polydispersity at this specific electrolyte concentration.

7.2.3. Membrane rotational speed

In section 7.1.2, the data suggested that the pH and electrolyte concentration of the continuous phase impacted the adsorption rate of the particles onto the surface of the oil droplet. To gain further insight into the effect of the adsorption kinetics in the emulsification process two complementary parameters were investigated. Namely, the membrane rotational speed, which affects 1) the droplet residency time at the surface of the membrane and the shearing of the silica particles to the interface due to the turbulence caused by membrane rotation and 2) the particle concentration in the continuous phase. These variables affect the rate of particle collision with the droplet growing on the membrane surface.

The average droplet size and polydispersity as a function of membrane rotational speed is presented in Figure 7.9. The experiments were conducted at the optimised pH and electrolyte concentrations highlighted in section 7.1.2, and at a fixed volumetric flow rate of 0.1 mL min^{-1}.

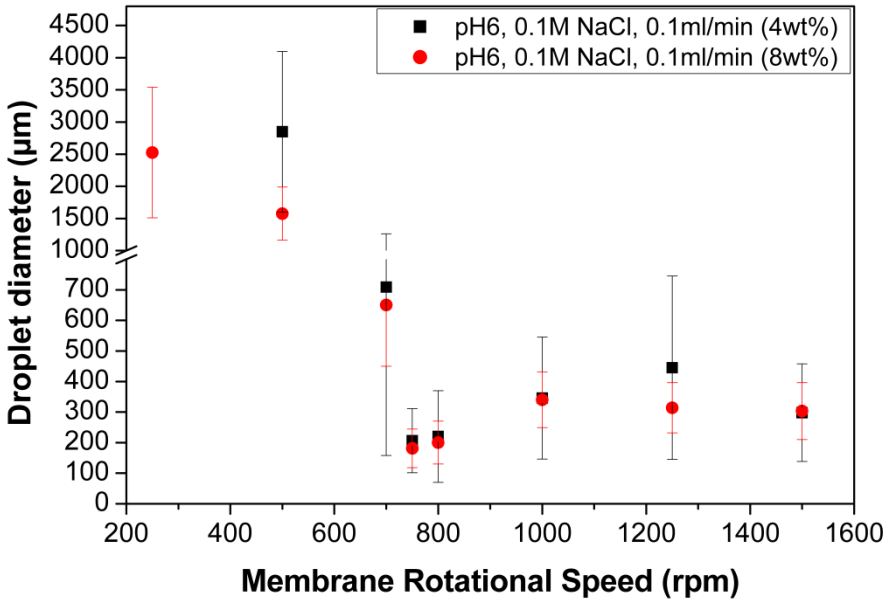

Figure 7.9. Variation in the droplet diameter of tricaprylin droplets using a) 4 wt% and b) 8 wt% 800 nm FUSO silica colloids as a function of membrane rotational speed using RME. The continuous phase has a background electrolyte concentration of 0.1M NaCl and at pH = 6. The oil injection rate is kept constant at 0.1 mL min^{-1}.

The data illustrated in Figure 7.9 are collected at two particle concentrations, viz. 4 and 8 wt%. At both these particle concentrations the droplet size as a function of membrane rotational speed essentially remains invariant at high rotational speeds. At low rotational speeds (200 - 500 rpm), the shear generated from the rotation of the membrane is very low leading to a low droplet detachment efficiency. It is assumed that under these conditions, the droplets continue to grow on the membrane surface reaching final droplet sizes that are up to 10 times greater in magnitude in comparison to the actual membrane pore size. It is difficult to pinpoint whether these large droplet sizes are a result of a large single droplet growing at the membrane or by coalescence of multiple small droplets from adjacent pores, due to the opaqueness of the silica dispersion. The data show that an optimum value in droplet size and size variation occurs at a rotational speed of 700 to 800 rpm. At higher rotational speeds (1000 to 1500 rpm) a small increase in droplet size and polydispersity is observed.

The droplet size data can be directly compared to the surfactant system studied by Vladisavljević and Williams, who also studied the effect of rotation speed on the mean droplet size and size variation illustrated in Figure 7.10.[20] They showed that as the membrane speed increased, the average droplet size reduced monotonically. This is because in a surfactant system there are sufficient amount of stabiliser molecules to rapidly coat the growing interface. In addition, there is a constant equilibrium surface tension, as the kinetics of adsorption of surfactant systems is fast in comparison to the rate of creation of new interface. As a result, the main governing factor controlling the droplet size is the shear field generated by the rotation of the membrane. In contrast to the surfactant system, it is interesting to note that in the case of the silica stabilised system, the data seems to show a minimum in average droplet size at 700 - 800 rpm.

This critical area of the graph is believed to be a result of competition between particle adsorption and the shear induced droplet detachment process. The generation of shear from the rotation of the membrane acts to detach the droplet from the membrane surface. For the droplets to remain stable against coalescence, they need to be coated with sufficient particulate emulsifiers adsorbed at the interface at the time of droplet detachment.

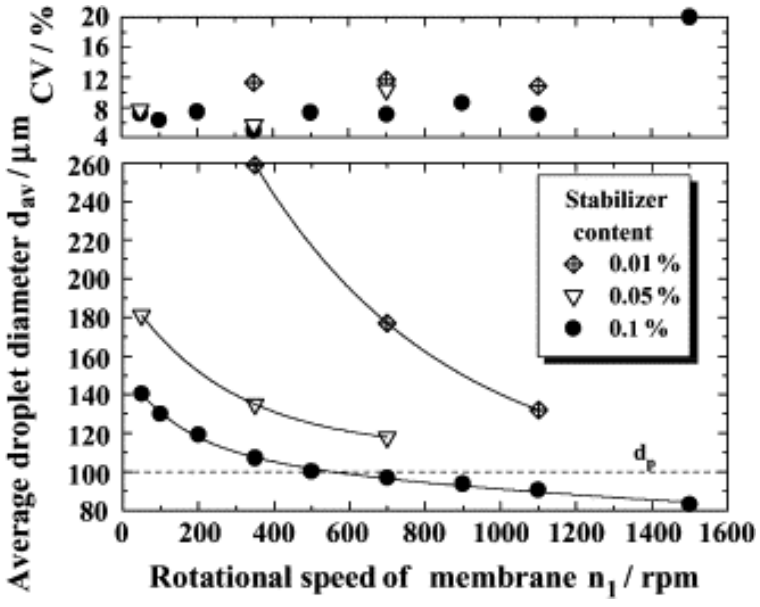

Figure 7.10. Effect of membrane rotational speed on paraffin wax droplet sizes emulsified with 2wt% Tween 20 in presence of different Carbomer concentrations. *Taken from Ref. [20]*.

If the adsorption and attachment process is sufficiently rapid, a monotonically decreasing droplet size can be expected (towards a limiting value) as a function of increasing membrane rotation as seen for a standard surfactant system.[20] In the case of the silica stabilised system examined here, the rate of particle adsorption is insufficient to fully stabilise the droplets prior to detachment at high rotation speeds. At these high rotation values the shear produces small oil droplets that are initially unstable. They coalesce to a larger droplet size until a sufficient particle coverage is reached, thereafter remaining stable. Whitesides *et al.*[21] and Arditty *et al.*[22] described this process as limited coalescence. When the emulsion is prepared, the oil drops coalesce to form droplets of a larger size as after a coalescence event, the droplets undergo a relaxation process that causes the two droplets to fuse into one. This causes the average droplet size to increase at short time intervals and will reach an asymptotic value at after a long time interval. This is because initially the particles are unable to fully cover the oil-water interface and thus the droplets coalesce to a limited extent. Due to this process of coalescence, the total interfacial area is now reduced allowing for a greater degree of particle coverage and particle re-arrangement at the interface and this limits further droplet coalescence.

The particle numbers in the continuous phase at both 4.0 and 8.0 wt% are sufficient to ensure complete coverage of the droplet assuming a diffusion limited collision process. Simple calculations of particle loading show that at a particle concentration of 4.0 wt% there is a sufficient amount of particles to adsorb onto the interface. Assuming an ideal case in which the continuous phase comprises of silica colloids (at a concentration of 4.0 wt%) at their primary particle size of 800 nm, the phase contains 1×10^{12} particles, whilst only 1×10^{5} particles are needed to form a complete monolayer on a 150 µm droplet. At a background electrolyte of 0.1M NaCl the Debye length around the particle and droplet is approximately 1nm, therefore the diffusion time of the 800 nm silica colloids over this length is 0.9 µs. The lifetime of the droplet at the membrane surface is 10 ms, therefore assuming a diffusion limited process the particles have sufficient time to diffuse to the interface and consequently adsorb.

In reality, over the course of the emulsification (typical emulsification period of 60 minutes) of the full volume of oil, the silica dispersion at 0.1M NaCl aggregates (Figure 7.4). The data shows that the dispersion aggregates over time to a mean size

of 3.2 μm. Performing particle loading and diffusion calculations on this aggregated particle size, shows that there is still a sufficient amount of particles in the system and that their diffusion across the Debye length is still much faster than the lifetime of the droplet. Therefore it can be concluded that the system under these specific conditions is able to stabilise the droplets at the point of detachment from the membrane.

The observation of a minimum in droplet size and size variation at 750 rpm suggests that the adsorption of the silica colloids to the interface is not diffusion-limited. Instead the rate of particle adsorption is the main governing factor. Considering the process of particle attachment, a number of mechanisms can be highlighted; i) the particles must collide with the free interface, ii) the particles then have to adhere to the interface, iii) the particles adsorb into the interface as the oil displaces the water on the particle surface. At the particle concentrations used in this emulsification experiments, stage 1 of the attachment process is easily satisfied. Simple calculations show that there are enough particles in the system and therefore enough contacts, at a rate which allows for sufficient amount of particles adhering to the interface for efficient stabilisation. The second stage is affected by the charge on the particle and droplet, however under conditions where the electric double layer is sufficiently weak, deposition and initial adhesion will occur at a rate which allows for sufficient amount of particles to adhere to the interface for efficient stabilisation. Stage 3 is complex and not easily modelled, the process of displacement wetting requires the oil to displace water on the particle surface. Assuming that the contact angle of the particles at the interface is 90°, we have a condition where there is no net gain for the oil over the water phase and so the rate of displacement may not be large. If the contact angle is smaller than 90° (likely in this system), the displacement rate will be even lower. Therefore this displacement wetting stage is critical. Although the collision frequency is increased with the addition of more particles (4 to 8 wt%), the particles need to remain long enough at the interface to; a) preferentially wet the interface and b) remain irreversibly adsorbed. If the particles are at the interface less than the critical adsorption time they will diffuse away from the interface into the bulk. This will cause the droplets to undergo limited coalescence until a critical particle coverage is obtained preventing further coalescence.

This optimal membrane rotational speed (750 rpm) was then used to investigate the influence of the oil injection rate on droplet size and size variation.

7.2.4. Oil injection rate

The data obtained for the effect of oil injection rate on the droplet size is presented in Figure 7.11. The injection rates investigated were chosen based on previous emulsification data stabilised by surfactants using the RME.[11]

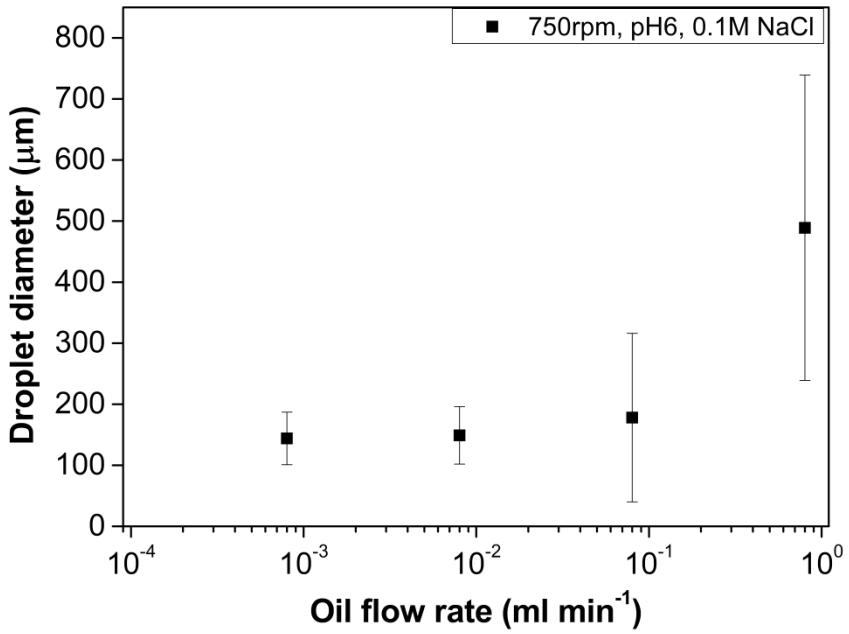

Figure 7.11. Effect of oil injection rate on the droplet size of tricaprylin droplets as produced using RME. The continuous phase is comprised of 4 wt% 800 nm FUSO silica colloids dispersed at pH 6 in 0.1M NaCl. The membrane rotational speed is kept constant at 750 rpm.

In this experiment the membrane rotational speed i.e. the shear force that drives droplet detachment is constant. Therefore, changes in the oil injection rate equates directly to a change in the production rate of new interfacial area. It is clear from the data presented in Figure 7.11 that there is a critical injection rate determining the stability of the emulsion droplets produced. Below 0.1 mL min^{-1}, the droplets appear very stable whilst at and above this critical value coalescence is observed. This

suggests again that there must be some barrier to particle adsorption onto the interface.

Assuming a constant droplet size detachment (say 80 µm which is the same as the membrane pore size), the lifetime of the droplet on the membrane will range from seconds to milliseconds across the injection rates examined. However, in all cases the particle diffusion time across the Debye length (1 nm in 0.1M NaCl electrolyte) around the particle and droplet is much quicker as illustrated by Table 7.1, therefore the adsorption process is not diffusion limited.

Oil injection rate (mL min^{-1})	Droplet lifetime on membrane (s)	Time for particle diffusion in 0.1M NaCl electrolyte (s)	
		Primary particle size = 800 nm	Aggregated particle size = 3.2 µm
1.0	1.6×10^{-5}	9.33×10^{-7}	3.18×10^{-6}
0.1	1.6×10^{-4}	9.33×10^{-7}	3.18×10^{-6}
0.01	1.6×10^{-3}	9.33×10^{-7}	3.18×10^{-6}
0.001	1.6×10^{-2}	9.33×10^{-7}	3.18×10^{-6}

Table 7.1. Comparison of droplet lifetimes on the membrane and particle diffusion times across the Debye length around the particle and droplet. At all oil injection rates the size of the droplets detaching is assumed constant at 80 µm.

The observation of limited coalescence under certain conditions when using the RME suggests that there must be a barrier to particle adsorption, as the timescales of droplet growth is sufficiently long to ensure that the adsorption is not diffusion limited. In the case of a non-diffusion controlled process, the adsorption kinetics will govern the critical stabilisation time according to;[6]

$$A_d = A_{d,0}\left(1 - e^{-k_{ad}\tau_{ad}}\right) \qquad \text{(Equation 7.1)}$$

where A_d is the surface area of the droplet covered with particles, $A_{d,o}$ is the total surface area of a droplet, k_{ad} is the adsorption rate constant and τ_{ad} is the adsorption time.

Assuming a critical particle coverage ($A_{d,cr}/A_{d,0}$)[22] is required to stabilise the droplets, when the coverage reaches a critical surface value $A_{d,cr}$, we can give a corresponding critical adsorption time $\tau_{ad,cr}$ through:

$$\tau_{ad,cr} = \frac{1}{k_{ad}} \ln\left(1 - \frac{A_{d,cr}}{A_{d,0}}\right) \qquad \text{(Equation 7.2)}$$

The term, $\ln(1-A_{d,cr}/A_{d,0})$ will be a constant value at the critical degree of coverage, therefore the critical adsorption time will be determined and dependent on the adsorption rate constant, k_{ad}.

For the experiments reported here a droplet formation time, τ_{drop}, can be defined. Comparison of the droplet formation time and the critical adsorption time of the particle will dictate the suitability of the emulsifier and whether the emulsions will undergo limited coalescence.[22] In general, the following conditions can be defined in particle stabilised emulsions produced using rotary membrane emulsification:

$\tau_{ad,cr} < \tau_{drop}$ the emulsion droplets produced will have narrow polydispersity with droplet size control;

$\tau_{ad,cr} \approx \tau_{drop}$ resulting emulsions will have a wider size distribution; and

$\tau_{ad,cr} > \tau_{drop}$ unsuitable for producing size controlled droplets.

The data in Figure 7.11 demonstrates that there is a critical oil injection rate for a fixed membrane rotational speed. The optimal oil injection rate based on the was determined to be 0.01 mL min^{-1}, this injection rate was then used to investigate the effect of particle concentration.

7.2.5. Particle concentration

Studying the effect of particle concentration on the stability and size control of the droplets produced, provides an alternative means of considering particle adsorption kinetics. Figure 7.12 illustrates the changes in the mean droplet size and their variation as a function of changing particle concentration in the continuous phase.

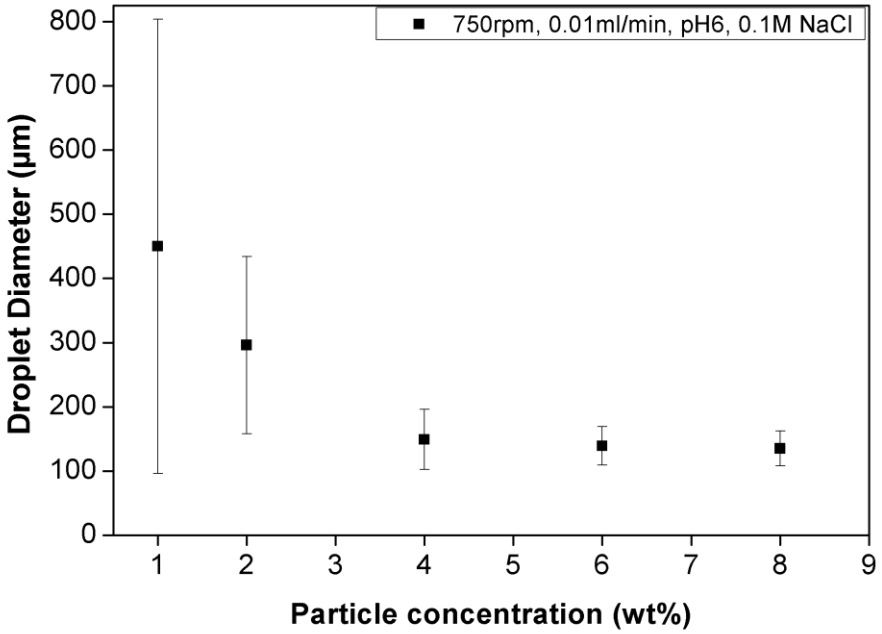

Figure 7.12. Changes in average droplet size and polydispersity as a function of particle concentration. The continuous phase contains a background electrolyte concentration of 0.1M NaCl and set at pH = 6. The oil injection and membrane rotational speed is kept constant at 0.01 mL min^{-1} and 750 rpm respectively.

It should be noted here that even at the lowest particle concentration (1 wt%), the system contains a large excess of particles to cover all of the oil/water interface created. Based on the volume of emulsion droplets produced, typically for a concentration of 1 wt% only 5% of the total amount of particles is required (based on the assumption that the droplets are all monodisperse with close hexagonal packing of the particles on the surface of the droplets). The differences in the average droplet size and polydispersity in Figure 7.12, demonstrates that the particle coverage is dictated by adsorption kinetics related to wetting of the interface and subsequent adsorption.

This study was conducted at optimal pH, electrolyte concentration, membrane rotational speed and oil injection rate. In addition, experiments were also conducted at particle concentrations of 0.1 and 0.5 wt%, but the emulsions produced at these conditions coalesced, forming a thin film of oil on top of the aqueous phase. It is

clear from the data that there is a critical particle concentration (4 wt%), above which stable near monodisperse oil droplets are produced.

The variation in droplet size as a function of particle concentration can be explained in terms of collision frequency and adsorption kinetics with the interface. At low particle concentrations (1 – 2 wt%), the collision frequency is relatively low however there are still a sufficient amount of particles to cover the interface if assuming every particle colliding with the interface is successfully adsorbed. Therefore the governing factor is the adsorption kinetics and not the collision frequency. This relates to insufficient particle coverage at the time of droplet detachment, at which point the droplets are not stable. Limited droplet coalescence occurs in this case until a sufficient coverage is reached, producing polydisperse droplets with large droplet size variation values. In section 7.1.4, equations governing the critical adsorption time were presented regarding critical particle coverage and control over droplet size. When the critical adsorption time is greater that the lifetime of the droplet on the membrane prior to detachment, the droplets coalesce to a limited extent with no control over their size and polydispersity. This could explain why large droplet sizes with a large polydispersity are observed for particle concentrations of 1 and 2 wt%.

In the case of higher particle concentrations (4 - 8 wt%), the collision frequency is high, however the kinetics of adsorption is the dominant factor. When the critical adsorption time is less than the droplet formation time, stable droplets with control over monodispersity can be produced (Figure 7.13).

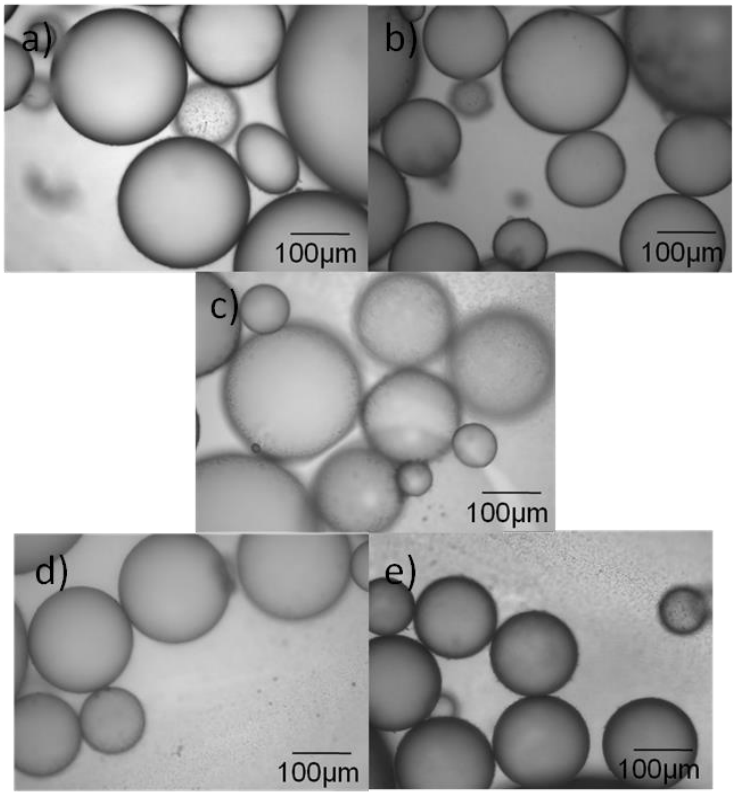

Figure 7.13 Optical micrographs of tricaprylin droplets produced at varying particle concentrations using 800 nm silica colloids; a) 1 wt% (D_{ave} = 450 µm), b) 2 wt% (D_{ave} = 296 µm), c) 4 wt% (D_{ave} = 149 µm), d) 6 wt% (D_{ave} = 139 µm) and e) 8 wt% (D_{ave} = 135 µm). The continuous phase is prepared with a background electrolyte concentration of 0.1M NaCl at a pH = 6. The membrane rotational speed and oil injection rates were kept constant at 750 rpm and 0.01 mL min^{-1}.

The images in Figure 7.13 show that with the optimisation of both chemical and mechanical parameters, it is possible to exert a high degree of control over the production of emulsion droplets stabilised with silica colloids using rotary membrane emulsification. This is particularly evident from Figures 7.13d to 7.13e which show droplet sizes of about two times the membrane pore size (80 µm) used in these experiments. In contrast, conventional emulsification techniques (homogenization) continuously produce interface therefore the kinetics of adsorption are less important. In this case the system is more dependent on the uptake of all the particles by the disperse phase over the duration of homogenization until an equilibrium size is achieved.[23] In such a turbulent environment, control over droplet

size distribution is difficult and the use of RME offers significant improvements in this domain. Although the droplet sizes presented here are very large (> 100 µm due to the large pore sizes), the study does provide an insight into the role of adsorption kinetics of particles at liquid-liquid interfaces.

7.3. Surfactant-free emulsions stabilised by sterically-stabilised latex particles

7.3.1 Introduction

The optimisation study conducted using the 800 nm silica colloids provides a platform to understand the role of particulate emulsifiers on the controlled production of emulsion droplets using rotary membrane emulsification. In this section we also present complimentary work on the use of polystyrene latex particles sterically stabilised with a pMMA-b-pDMAEMA di-block copolymer as Pickering emulsifiers for emulsions produced in the RME. The added advantage of using such particulate emulsifiers is that the steric stabilisers on the surface of the particle can potentially be cross-linked in situ to obtain colloidosome microcapsule structures as described in Chapter 5.[24, 25] There is little work to date on the use of sterically stabilised particles to stabilize emulsion droplets using membrane emulsification.[6] Thompson *et al.* used polystyrene latex particles stabilised by poly(glycerol monomethacrylate) to stabilise emulsions using a stirred cell membrane emulsification device. They investigated the effect of shear rate and disperse flux on the droplet size produced.[7] In this study, the role of the particles as well as the influence of membrane rotation (shear), volumetric flow rate and particle concentration will be investigated.

The RME is a sensible membrane emulsification rig to conduct a preliminary study on this system as it allows for small scale experiments to be conducted easily without the need for substantial quantities of the latex emulsifier.

For this study, polystyrene latex particles stabilized with $pMMA_{16}$-b-$pDMAEMA_{245}$ were used (SM03). The characterization of these particles is reported in Chapter 6. The oil used was hexadecane oil which has been reported previously in literature to be compatible with such particulate emulsifiers,[26, 27] and has also been tested in the lab as a suitable oil to make stable emulsions (Chapter 6). A standard rotor-stator homogenizer (Ultra-Turrax) was initially used to find the optimal pH and background electrolyte conditions to produce stable emulsions (Chapter 6). From these emulsion studies it was decided to perform the RME experiments at pH 9 and at a background electrolyte of 10mM KNO_3 to ensure that the particles were able to efficiently adsorb onto the growing droplets.

7.3.2. Effect of membrane rotation speed

In comparison to the silica particles, the polystyrene particles are much smaller (~90 nm). The mean droplet size as a function of membrane rotational speed and associated variation is presented in Figure 7.14. The flow rate was kept constant at 0.01 mL min^{-1} (optimised value from silica system) and the particle concentration was set at 2 wt%.

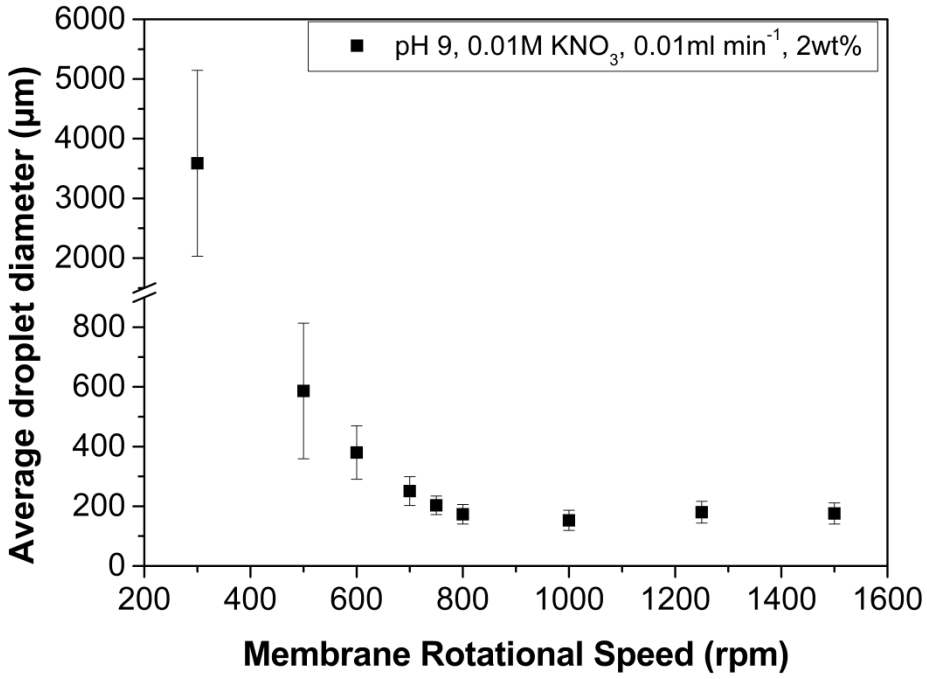

Figure 7.14. Variation in the average droplet size of hexadecane droplets as a function of membrane rotational speed. The continuous phase contains a background electrolyte concentration of 0.01M KNO_3 and set at pH = 9. The oil injection and particle concentration is kept constant at 0.01 mL min^{-1} and 2 wt%, respectively.

The data presented in Figure 7.14 is similar in its profile to that presented in Figure 7.9. As in the case of the silica system at low rotational speeds (250 and 500 rpm) the shear generated is small and therefore corresponds to a low droplet detachment efficiency. In surfactant systems it is possible to measure the droplet size before it detaches however when working with particles, due to the opaqueness of the polystyrene dispersion in the continuous phase it is difficult to detect whether the

large size is a result of a single droplet grown at the pore or the coalescence of multiple droplets. However under these rotational speeds, the droplet residency time would be long enough for sufficient particle coverage against coalescence, so it is assumed that the droplet grows to these larger sizes on the membrane surface.

As the membrane rotational speed is increased (500 - 800 rpm) the droplet size and size variation rapidly decreases from droplet sizes of ~600 µm (500 rpm) to ~150 µm (1000 rpm) as shown in Figure 7.15. This can be attributed to the increase in shear-induced detachment that induces an earlier detachment of the droplets from the membrane, resulting in smaller droplet sizes with narrow droplet size distributions. Further increase in the rotation speed (1000 - 1500 rpm) causes a small increase in both the droplet size and polydisperisty due to limited coalescence.

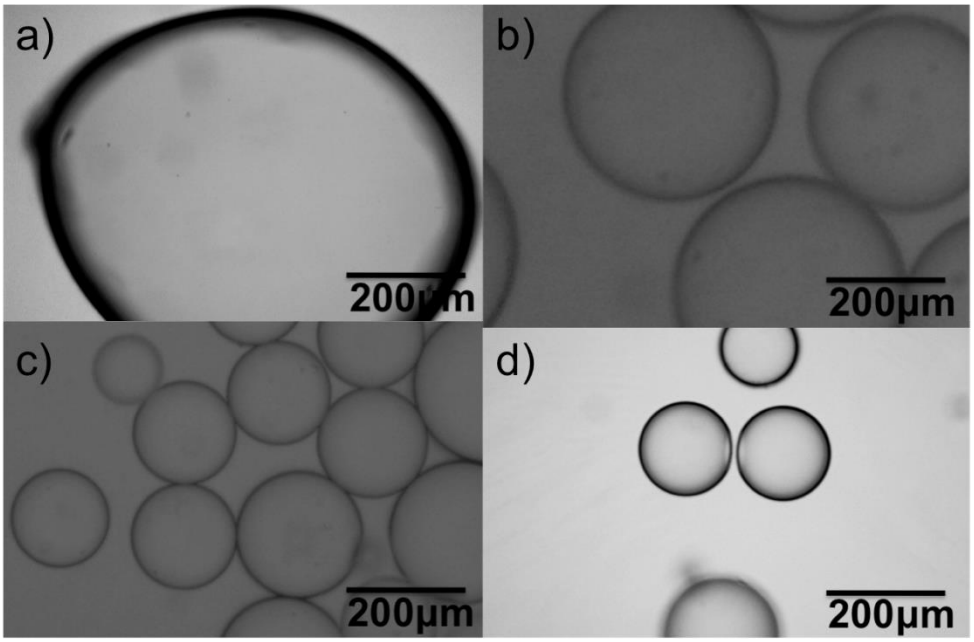

Figure 7.15. Optical micrographs of hexadecane droplets produced at varying membrane rotational speeds using sterically stabilised polystyrene latex particles; a) 500 rpm (D_{ave} = 586 µm), b) 600 rpm (D_{ave} = 380 µm), c) 700 rpm (D_{ave} = 211 µm) and d) 1000 rpm (D_{ave} = 153 µm). The continuous phase is prepared with a background electrolyte concentration of 0.01M KNO_3 at a pH = 9. The particle concentration and oil injection rates were kept constant at 2 wt% and 0.01 mL min^{-1}, respectively.

When silica particle stabilizers were used, the smallest droplet size with the narrowest size distribution was attained at a rotational speed of 750 rpm, whereas in the polystyrene system this appears to occur at 1000 rpm. If we consider the attachment process, it is found that as with the silica system the number of polystyrene latex particles in the continuous phase is largely sufficient to enable an excess number of contacts with the interface than what is needed for full coverage of the droplets before detachment from the membrane, even at the highest rotation speeds. The second stage is the adhering of the particles to the interface. In this case the sterically stabilised latex particles contain pDMAEMA chains that are pH responsive due to the presence of tertiary groups. At pH 9 the pDMAEMA chains become unprotonated and collapse onto the surface of the latex particle as water becomes a poor solvent for the polymer under these conditions. This is likely to improve the wettability of the particle and the non-soluble polymer shell provides an additional drive to the interface making it more favourable to stabilise the oil/water

interface (in comparison to the silica particles). The third stage of displacement wetting requires the oil to displace the water on the particle which is the critical step in the kinetics of particle adsorption. From Figure 7.9, the recorded changes in the droplet diameter as a function of membrane rotation suggests that stage 3 occurs faster for the latex system than for the silica, which potentially explains why stable droplets with narrow size distributions can be found at a higher rotation speed.

The optimal membrane rotational speed of 1000 rpm was then selected to investigate the influence of the oil injection rate.

7.3.3. Effect of oil injection rate

The data for the mean droplet size and size variation droplet polydispersity as a function of oil injection rate is presented in Figure 7.16.

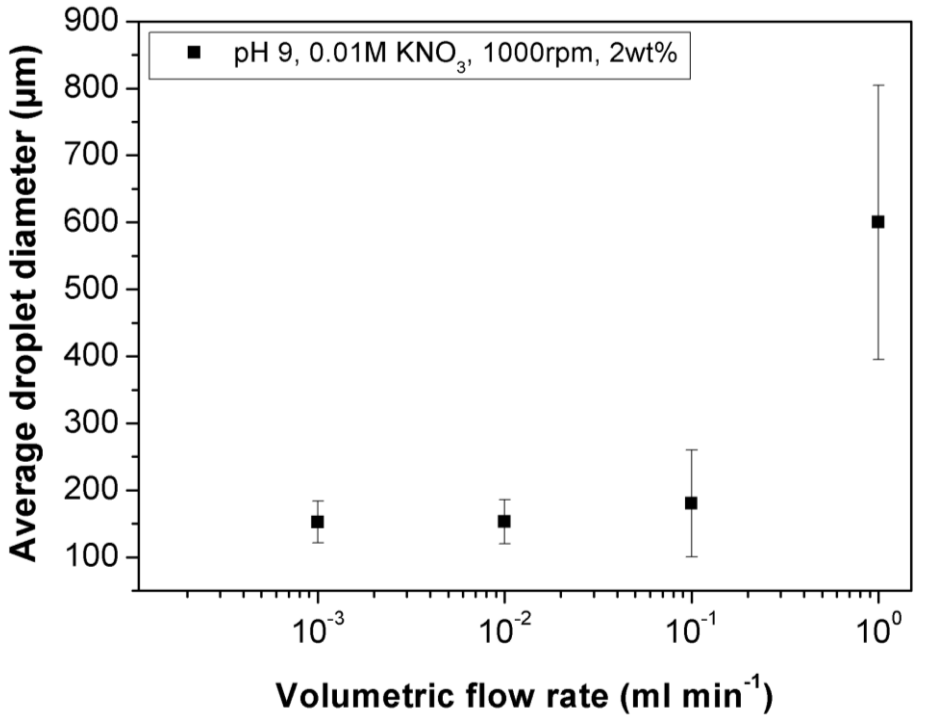

Figure 7.16. Variation in the average droplet size of hexadecane droplets as a function of oil injection rate. The continuous phase contains a background electrolyte concentration of 0.01M KNO_3 and set at pH = 9. The membrane rotational speed and particle concentration is kept constant at 1000 rpm and 2 wt%, respectively.

The data in Figure 7.16 illustrate that there is a critical injection rate which determines the stability of the droplets detaching from the rotating membrane. Previous membrane emulsification experiments have also reported an upper limit on the dispersed phase flow rate leading to an increase in drop size for constant shear rates.[28-30] This is due to a fixed characteristic time required for droplet detachment at a constant shear rate (membrane rotation). A higher injection rate will lead to droplets growing to large sizes prior to detachment. The trend observed in Figure 7.16 again matches the trend observed in the dataset obtained with the silica particles (Figure 7.12). Below 0.1 mL m^{-1} the droplets appear very stable whilst coalescence of the droplets after membrane detachment is observed above this critical value. This further suggests that in this particular membrane configuration, there is a barrier to adsorption onto the interface since particle loading is sufficient to ensure complete coverage. Clearly the presence of a critical injection rate emphasizes that the barrier is related to the kinetics of particle adsorption and is not diffusion limited.

The optimal injection rate was determined to be 0.01mL m^{-1} and this injection rate was used to investigate the effect of particle concentration when all the other parameters are kept constant.

7.3.4. Effect of particle concentration

The average droplet size and polydispersity as a function of particle concentration is illustrated in Figure 7.17.

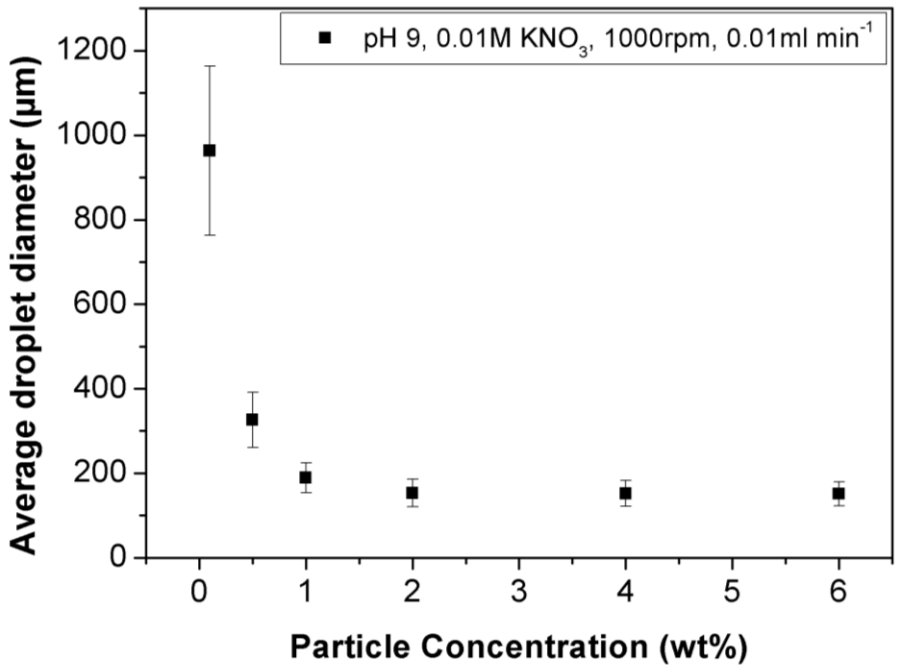

Figure 7.17. Changes in average hexadecane droplet size and associated variation as a function of particle concentration. The continuous phase contains a background electrolyte concentration of 0.01M KNO_3 and set at pH = 9. The oil injection and membrane rotational speed is kept constant at 0.01 mL min^{-1} and 1000 rpm respectively.

The data illustrated in Figure 7.17 shows that the droplet size decreases as a function of increasing particle concentration to a limit (2 wt%), above which further increase yields no improvements in droplet size. The continuous phase contains a large excess of particles even at the lowest particle concentration of 0.1 wt%. Performing simple calculations illustrates that at 0.1wt%, the system contains 6.2×10^{13} particles whilst only 3×10^{11} particles are needed to cover the total interface created in these experiments. Therefore there are more than enough particles in the system for a sufficient number of contacts with the interface and subsequent adsorption.

The data above demonstrate the production of relatively monodisperse emulsion droplets with core-shell latex stabilisers in a membrane emulsification rig and that the influence of particle adsorption kinetics helps to give some understanding for the success of this to optimize the conditions. The emulsions produced here are all at optimal pH, background electrolyte concentrations, membrane rotational speed and oil injection rate. It is clear from the data in Figure 7.17 that when all these parameters are constant there is a critical particle concentration between 1 to 2 wt%.

Above this concentration stable droplets with narrow size distributions can be produced whilst the same control is not exerted below this critical concentration and the droplets undergo limited coalescence to larger droplet sizes. This trend is similar to the one observed with the silica system.

Conclusions

Rotational membrane emulsification has been successfully employed for the controlled production of surfactant-free emulsion droplets stabilised using two particulate emulsifiers (silica and core-shell latex particles). The optimization of chemical and mechanical parameters, allowed the production of droplets that showed to have long term stability with a controlled droplet diameter and droplet size distribution. The advantage of this process over its counterparts is the ability to scale up production to produce large quantities of controlled sized emulsion droplets. In comparison to literature, the optimization study presented here has shed light on the influence of particle adsorption kinetics on the production of emulsion droplets via this process. The change in both the rotational speed and particle concentration gives variation in sizes which can be related back to the critical adsorption time needed for particles to wet the interface and subsequently adsorb. As long as the critical adsorption time is less than the droplet formation time and residency time at the membrane surface it is possible to produce well controlled droplet sizes with narrow droplet distributions.

References

1. S. H. Behrens and D. G. Grier, The charge of glass and silica surfaces, *J. Chem. Phys.*, 2001, **115**, 6716-6721.
2. G. T. Vladisavljević and R. A. Williams, Recent developments in manufacturing emulsions and particulate products using membranes, *Adv. Colloid Interface Sci.*, 2005, **113**, 1-20.
3. E. Egidi, G. Gasparini, R. G. Holdich, G. T. Vladisavljević and S. R. Kosvintsev, Membrane emulsification using membranes of regular pore spacing: Droplet size and uniformity in the presence of surface shear, *J. Membr. Sci.*, 2008, **323**, 414-420.
4. R. G. Holdich, M. M. Dragosavac, G. T. Vladisavljević and S. R. Kosvintsev, Membrane emulsification with oscillating and stationary membranes, *Ind. Eng. Chem. Res.*, 2010, **49**, 3810-3817.
5. Q. Yuan, O. J. Cayre, M. Manga, R. A. Williams and S. Biggs, Preparation of particle-stabilized emulsions using membrane emulsification, *Soft Matter*, 2010, **6**, 1580-1588.
6. K. L. Thompson, S. P. Armes and D. W. York, Preparation of Pickering emulsions and colloidosomes with relatively narrow size distributions by stirred cell membrane emulsification, *Langmuir*, 2011, **27**, 2357-2363.
7. Q. Y. Xu, M. Nakajima and B. P. Binks, Preparation of particle-stabilized oil-in-water emulsions with the microchannel emulsification method, *Colloids Surf. A: Physicochem. Eng. Asp.*, 2005, **262**, 94-100.
8. K. Sato, H. Yilmaz, Y. Hotta, A. Ijuin and K. Watari, Dispersion of ceramic particles in aqueous media with surface-grafted dispersant, *J. Am. Ceram. Soc.*, 2009, **92**, 256-259.
9. *FUSO Chemical Co. Ltd, Japan. www.fusokk.co.jp/eng/electronicmaterials/elec/01.pdf*.
10. D. J. Shaw, ed., *Introduction to Colloid and Surface Chemistry*, Butterworth-Heinemann, London, 1992.
11. Q. Yuan, N. Aryanti, R. Hou and R. A. Williams, Performance of slotted pores in particle manufacture using rotating membrane emulsification, *Particuology*, 2009, **7**, 114-120.
12. B. P. Binks and S. O. Lumsdon, Stability of oil-in-water emulsions stabilised by silica particles, *Phys. Chem. Chem. Phys.*, 1999, **1**, 3007-3016.

13. K. G. Marinova, R. G. Alargova, N. D. Denkov, O. D. Velev, D. N. Petsev, I. B. Ivanov and R. P. Borwankar, Charging of oil-water interfaces due to spontaneous adsorption of hydroxyl ions, *Langmuir*, 1996, **12**, 2045-2051.
14. J. N. Israelachvili ed., *Intermolecular and Surface Forces*, Academic Press, New York, 1992.
15. B. R. Midmore, Preparation of a novel silica-stabilized oil/water emulsion, *Colloids Surf. A: Physicochem. Eng. Asp.*, 1998, **132**, 257-265.
16. E. Vignati, R. Piazza and T. P. Lockhart, Pickering emulsions: Interfacial tension, colloidal layer morphology, and trapped-particle motion, *Langmuir*, 2003, **19**, 6650-6656.
17. B. P. Binks, J. H. Clint, G. Mackenzie, C. Simcock and C. P. Whitby, Naturally occurring spore particles at planar fluid interfaces and in emulsions, *Langmuir*, 2005, **21**, 8161-8167.
18. T. S. Horozov and B. P. Binks, Particle-stabilized emulsions: A Bilayer or a Bridging Monolayer?, *Angew. Chem., Int. Ed.*, 2006, **45**, 773-776.
19. F. Gautier, M. Destribats, R. Perrier-Cornet, J.-F. Dechezelles, J. Giermanska, V. Heroguez, S. Ravaine, F. Leal-Calderon and V. Schmitt, Pickering emulsions with stimulable particles: from highly- to weakly-covered interfaces, *Phys. Chem. Chem. Phys.*, 2007, **9**, 6455-6462.
20. G. T. Vladisavljević and R. A. Williams, Manufacture of large uniform droplets using rotating membrane emulsification, *J. Colloid Interface Sci.*, 2006, **299**, 396-402.
21. T. H. Whitesides, D. S. Ross, Experimental and theoretical analysis of the limited coalescence process: Stepwise limited coalescence, *J. Colloid Interface Sci.*, 1995, **169**, 48-59.
22. S. Arditty, C. P. Whitby, B. P. Binks, V. Schmitt and F. Leal-Calderon, Some general features of limited coalescence in solid-stabilized emulsions. *Eur. Phys. J. E: Soft Matter Biol. Phys.*, 2003, **11**, 273-281.
23. B. P. Binks and C. P. Whitby, Silica particle-stabilized emulsions of silicone oil and water: Aspects of emulsification, *Langmuir*, 2004, **20**, 1130-1137.
24. Q. Yuan, O. J. Cayre, S. Fujii, S. P. Armes, R. A. Williams and S. Biggs, Responsive core-shell latex particles as colloidosome microcapsule membranes, *Langmuir*, 2010, **26**, 18408-18414.

25. O. J. Cayre, J. Hitchcock, M. S. Manga, S. Fincham, A. Simoes, R. A. Williams and S. Biggs, pH-responsive colloidosomes and their use for controlling release, *Soft Matter*, 2012, **8**, 4717-4724.

26. J. I. Amalvy, S. P. Armes, B. P. Binks, J. A. Rodrigues and G. F. Unali, Use of sterically-stabilised polystyrene latex particles as a pH-responsive particulate emulsifier to prepare surfactant-free oil-in-water emulsions, *Chem. Comm.*, 2003, 1826-1827.

27. R. Murakami. B. P. Binks, S. P. Armes, S. Fujii,, Temperature-induced inversion of nanoparticle-stabilized emulsions, *Angew. Chem., Int. Ed.*, 2005, **44**, 4795-4798.

28. I. Kobayashi, M. Nakajima and S. Mukataka, Preparation characteristics of oil-in-water emulsions using differently charged surfactants in straight-through microchannel emulsification, *Colloids Surf. A: Physicochem. Eng. Asp.*, 2003, **229**, 33-41.

29. N. C. Christov, D. N. Ganchev, N. D. Vassileva, N. D. Denkov, K. D. Danov and P. A. Kralchevsky, Capillary mechanisms in membrane emulsification: oil-in-water emulsions stabilized by Tween 20 and milk proteins, *Colloids Surf. A: Physicochem. Eng. Asp.*, 2002, **209**, 83-104.

30. M. T. Stillwell, R. G. Holdich, S. R. Kosvintsev, G. Gasparini and I. W. Cumming, Stirred cell membrane emulsification and factors influencing dispersion drop size and uniformity, *Ind. Eng. Chem. Res.*, 2007, **46**, 965-972.

CHAPTER 8: PROBING PARTICLE ADSORPTION KINETICS AT OIL-WATER INTERFACES

Nomenclature

A	Area
A_0	Initial or mean area of the sinusoidal oscillation
A_A	Amplitude of the measured response of the area change
E_0	Elasticity
Hz	Hertz
R_d	Droplet radius
γ	Interfacial tension
γ_A	Amplitude of the measured response in interfacial tension

8.1. Introduction

The role of nanoparticles at liquid-liquid interfaces has recently attracted significant attention, driven by the development of novel functional materials from the self-assembly of particles at interfaces.[1] The adsorption of particles at liquid-liquid interfaces reduces the free energy leading to stable emulsions.[2] The energy change related to the adsorption of a single particle at the liquid-liquid interface depends on the particle radius and the surface free energies i.e. the interfacial tensions at the particle-oil, γ_{po}, particle-water, γ_{pw}, and oil-water, γ_{ow}, interface described by equation 8.1;

$$\Delta E = -\frac{\pi r^2}{\gamma_{ow}}\left[\gamma_{ow}\left(\gamma_{pw} - \gamma_{po}\right)\right]^2 \qquad \text{(Equation 8.1)}$$

This was later extended further to incorporate the influence of line tension.[3, 4] The thermodynamic processes involved in nanoparticle attachment at liquid-liquid interfaces are further described in numerous publications.[1, 5]

There is a copious amount of literature in the area of self-assembly of particles at liquid-liquid interfaces for production of a variety supra-colloidal structures. However, the kinetics of particle adsorption at liquid-liquid interfaces is less well understood. The use of pendant drop tensiometry as a method to investigate dynamic interfacial tension has been extensively used for surfactant systems at liquid interfaces; however, there are very few reports on the use of this technique to study particle adsorption.

The effect of particulates on the interfacial tension is not well understood and published results seem to be contradictory. Vignati *et al.*[6] investigated the effect of silica particle concentration and hydrophobocity on iso-octane/water and octanol/water systems. They show that the adsorption of hydrophilic particles does not modify the interfacial tension at any particle concentration. Increasing the hydrophobicity also had little influence on the interfacial tension measured. Drelich *et al.*[7] confirmed this observation and showed experimentally that the presence of hydrophobic silica particles had little effect on the interfacial tension at the paraffin oil/water interface.

The experimental data from Vignatti *et al.*[6] and Drelich *et al.*[8] contradict the conclusions made by Levine *et al.*[9] who developed a theoretical model to calculate the oil/water interfacial tension where particles were closely packed at a planar interface. They reported that, in the model, the interfacial tension did indeed depend on the particle hydrophobicity (decreasing interfacial tension as contact angle increases from 0° to 90°). This was supported by experiments made by Kim *et al.*[10] who found that graphene oxide lowered the interfacial tension. In 2006, Glaser *et al.*[11] demonstrated the interfacial activity of Janus nanoparticles at the hexane/water interface. They found that the interfacial activity could be increased by increasing the amphiphilic character of the particles. In 2007, Kutuzov *et al.*[12] investigated the adsorption of 5 nm CdSe nanoparticle to a toluene/water interface, to study changes in the dynamic interfacial tension as a function of particle concentration to infer details about the adsorption process. Stocco *et al.*[13] used a tracker pendant drop/rising bubble tensiometer device to measure the dynamic surface tension of silica particles at the air/water interface. They found that the surface activity was concentration dependent. Du *et al.*[14] studied the adsorption energy of citrate-stabilised gold nanoparticles on OFPA/water interface and found it scaled with the particle radius by measuring the dynamic interfacial tension. Recently Isa *et al.*[15] studied qualitatively the self-assembly of iron oxide core-shell particles (where the shell is comprised of poly(ethylene glycol) at the n-decane/water interface. Even more recently, Ferdous *et al.*[16] investigated the adsorption kinetics of alkanethiol-stabilised gold nanoparticles at the hexane-water interface. They reported that the time evolution of the interfacial tension at the early and latter stages infer a switch from diffusion-controlled kinetics to an interaction-controlled kinetics. It is also evident from all these publications that there is a barrier to particle adsorption at the interface (an observation also found in my rotational membrane emulsification work (Chapter 7), leading to relatively slow adsorption kinetics, typically around 10^3 - 10^4 s before equilibrium tension values are observed.

All these publications use nanoparticles whose behaviour is similar to that of surfactant molecules at liquid-liquid interfaces i.e. relatively low attachment energies. The adsorption kinetics of larger particles is less well understood and the aim of this study is to use dynamic tensiometry data using larger particles to investigate their effect on interfacial tension.

8.2. Pendant drop analysis

8.2.1. Silica

The droplet size data of tricaprylin oil droplets stabilised using 800 nm FUSO silica colloids, produced using membrane emulsification illustrated that the adsorption kinetics played a pivotal role in droplet stability and size. Therefore, pendant drop tensiometry was conducted to investigate the kinetics of adsorption for silica particles at a tricaprylin oil/water interface (Figure 8.1).

Initially the pure air/water interface was measured by expressing a 50 µL drop of water to obtain 72.8±0.2 mN m^{-1} to calibrate the pendant drop device. Afterwards the pure tricaprylin oil/water interface was measured (where the water was prepares at pH 6, containing 0.1M NaCl electrolyte). It should be noted that for the tricaprylin/water system a 50 µL drop of water was rapidly extruded into a cuvette containing 10 mL of tricaprylin oil at 20°C. The droplet was videoed and fitted to the Young-Laplace equation to obtain equilibrium interfacial tension values. These measurements were repeated three times and an average was taken. For the pure tricaprylin oil/water the droplet was videoed for ~3500 s (Figure 8.1, black squares). The isotherm remained essentially flat across this timescale with an equilibrium interfacial tension of 24.8±0.2 mN m^{-1} and matched the interfacial tension values reported in literature (24.91 mN m^{-1}) for a tricaprylin droplet expressed in 0.1M NaCl solution.[17] It should be noted that measurement of the tricaprylin/water interfacial tension was started as soon as the droplets were expressed from the syringe in the device (t_0 = 0). Thereafter, changes in the interfacial tension, as a function of particle concentration (dispersed at pH 6, 0.1M NaCl), were measured as a function of time.

To remove trace impurities the silica particles were washed three times using ethanol (typically 1 g of silica was dispersed in 25 mL of ethanol and left on the carousel for 30 minutes, centrifuged for 3 minutes at 5000 rpm and the supernatant was replaced with fresh ethanol). After 3 washes with ethanol, three wash cycles with Milli-Q water (25 mL). After the third wash, the interfacial tension of the supernatant was measured in air to confirm the removal of impurities. If the interfacial tension matched that of a pure air/water interface the particles dispersed into pH 6, 0.1M NaCl water for measurement. If the pure air/water interfacial tension was not obtained then further wash cycles were performed until the value

was reached. It should be noted that the measurements were started as soon as the droplets were expressed from the syringe in the device ($t_0 = 0$).

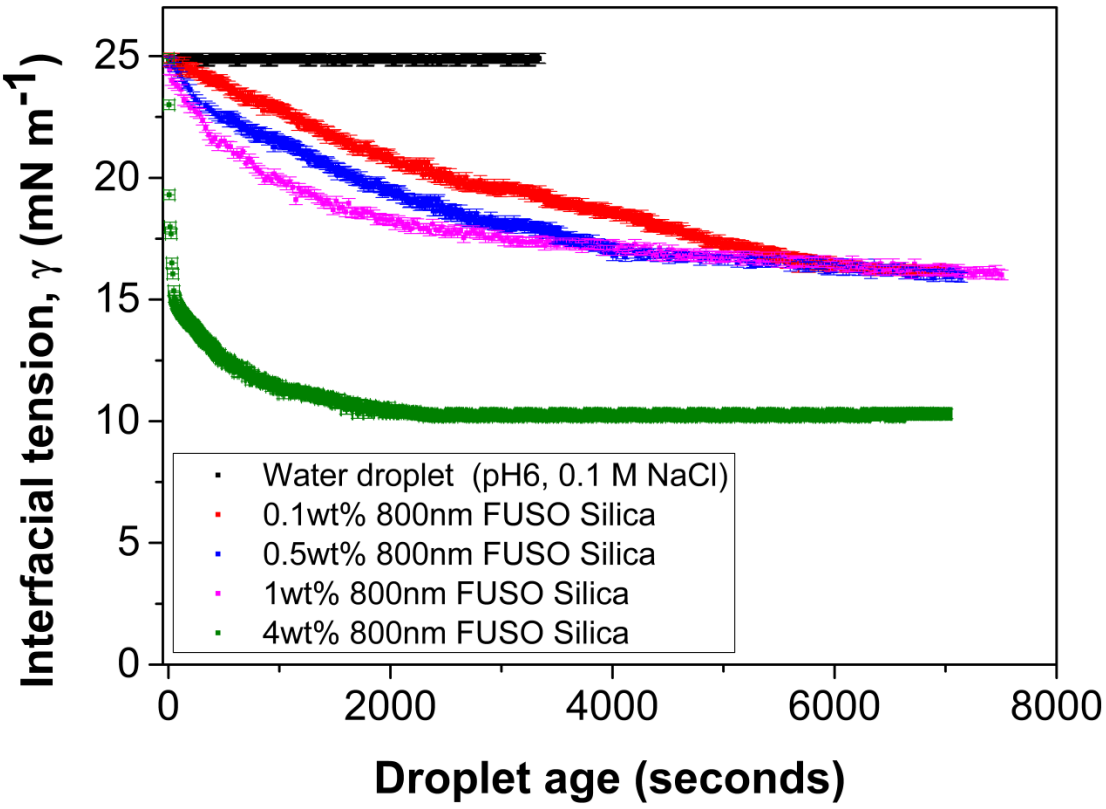

Figure 8.1. Dynamic interfacial tension of a water droplet in tricaprylin oil with 800 nm silica colloids at various particle concentrations.

Particle Concentration, (wt%)	Equilibrium interfacial tension value, γ_{eq}, (mN m^{-1})
0	24.8±0.2
0.1	16.1±0.2
0.5	16.1±0.2
1	16.1±0.1
4	10.3±0.5

Table 8.1. Equilibrium interfacial tension values for a tricaprylin/water interface laden with 800 nm FUSO silica particles at various particle concentrations.

The data in Figure 8.1 shows that there is a clear change in the interfacial tension that is particle concentration dependent. At particle concentrations of 0.1 to 1 wt%,

the isotherms reach an equilibrium interfacial tension value of 16.1 mN m^{-1} (Table 8.1), however the time taken to reach the equilibrium value decreases with increasing particle concentration. As the concentration is increased to 4wt% the isotherm shows an initial rapid drop in interfacial tension from 24.9 mN m^{-1} to ~16 mN m^{-1} within the first 40 seconds of the experiment, after which it slows and reaches an equilibrium tension value of 10.3 mN m^{-1} at around 2000 seconds (much faster in comparison to the other particle concentrations).

The analysis of the adsorption process in the pendant drop when using relatively large silica particles is complicated by gravitational settling.[13] The density difference will cause the silica particles to sediment (as illustrated by comparing the transparency increase in the right hand side of the droplet in Figure 8.2) and this may potentially help adsorption. In addition, sedimentation will also cause the droplet shape to change due to the weight of particles settling towards the bottom of the drop (illustrated by the dashed line in Figure 8.2); this will be interpreted in the drop shape as a change in the interfacial tension (Figure 8.2). The Figure also shows a good Young-Laplace fit to the droplet shape (red line around the droplet) at the three time intervals presented and therefore the change in the interfacial tension value is directly resultant from a change in droplet shape due to particle sedimentation. Therefore, these initial tests were considered inconclusive in terms of measuring the interfacial tension. However it should be noted that these silica particles do adsorb to oil/water interface as they stabilise tricaprylin/water emulsions as presented in Chapter 7.

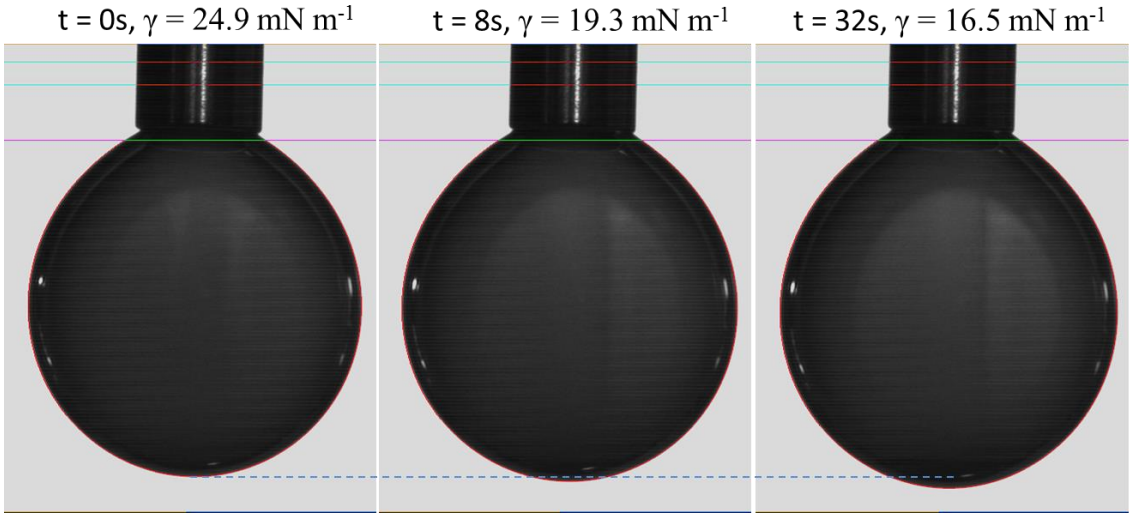

Figure 8.2. *Young-Laplace fits to 50µL water droplet (containing 4 wt% 800 nm FUSO silica particles dispersed at pH 6, 0.1M NaCl) in tricaprylin oil at time a) 0 s, b) 8 s and c) 32 s. Blue dashed line illustrates changes in the droplet height with time.*

8.2.2. Sulfate stabilised polystyrene latex

In order to eliminate sedimentation effects, the adsorption of 300 nm sulfate stabilised polystyrene latex 'model' particles at the hexadecane/water interface was investigated, since the density of polystyrene (1.05 g cm^{-3}) is much closer to that of water. The sulfate-stabilised latex particle dispersions were cleaned via a centrifugation and re-dispersion cycle and the supernatant was checked to see whether it matched the air/water surface tension value. The initial surface tension of the supernatant was 53.6 mN m^{-1} i.e. much lower than that of pure air/water interface (72.8 mN m^{-1}) suggesting that some sulfate molecules were adsorbing at the interface. Further centrifugation and redispersion cycles were performed until the surface tension of the supernatant matched that of an air/water interface. The particles were re-tested at the hexadecane/water interface to measure the dynamic interfacial tension at 20°C. Three measurements were taken and then averaged (typical error of ±0.2 mN m^{-1}).The isotherms obtained are presented in Figure 8.3.

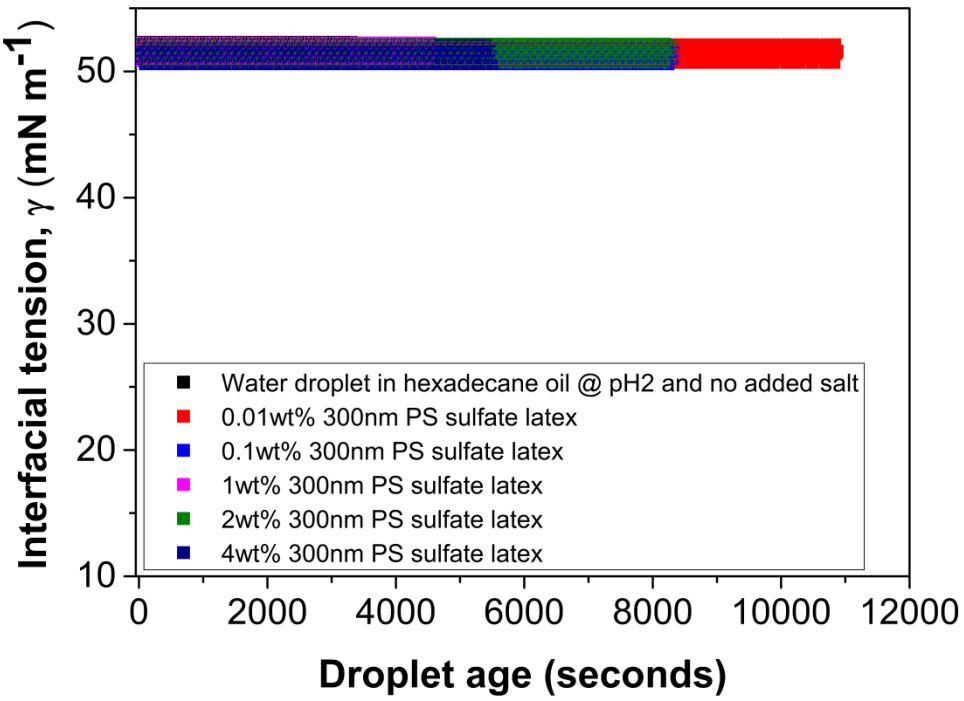

Figure 8.3. Dynamic interfacial tension of a water droplet in hexadecane oil with 300 nm sulfate-stabilised colloids (cleaned via centrifugation) at various particle concentrations.

The bare interfacial tension of the hexadecane/water interface was measured and it remained constant around 52.1±0.2 mN m^{-1}. This measured value matches the value reported in literature of 52 mN m^{-1}.[18] Upon the addition of the particles there was no measured effect on the dynamic interfacial tension. Based on this interpretation of the data, the changes in the interfacial tension observed with the silica, must be due to changes in the droplet shape caused by particle sedimentation and gravitational effects. This is because both the silica particles and these latex particles have shown to adsorb to the oil/water interface and stabilise emulsions however their adsorption does not change the interfacial tension.

8.2.2. Sterically stabilised polystyrene latex

The dynamic interfacial tension of a hexadecane oil/water interface was studied using 70 nm polystyrene latex particles sterically stabilised by $pMMA_{14}$-b-$pDMAEMA_{45}$ (SM01). These particles were cleaned via dialysis, periodically changing the outer phase until the outer phase produced a surface tension value of a

pure air/water interface i.e. 72.8 mN m^{-1}. These particles were then dispersed into pH 10 and 2 water to investigate the effect of pH and particle concentration on the interfacial tension of an hexadecane/water interface at 20°C. A 50 µL droplet of water was used and the measurements were repeated three times and an average was taken. The typical error was 0.2 mN m^{-1}. Figure 8.4 illustrates the dynamic interfacial tension when the particles are dispersed at pH 10 and 2, respectively, at a particle concentration of 0.01 wt%.

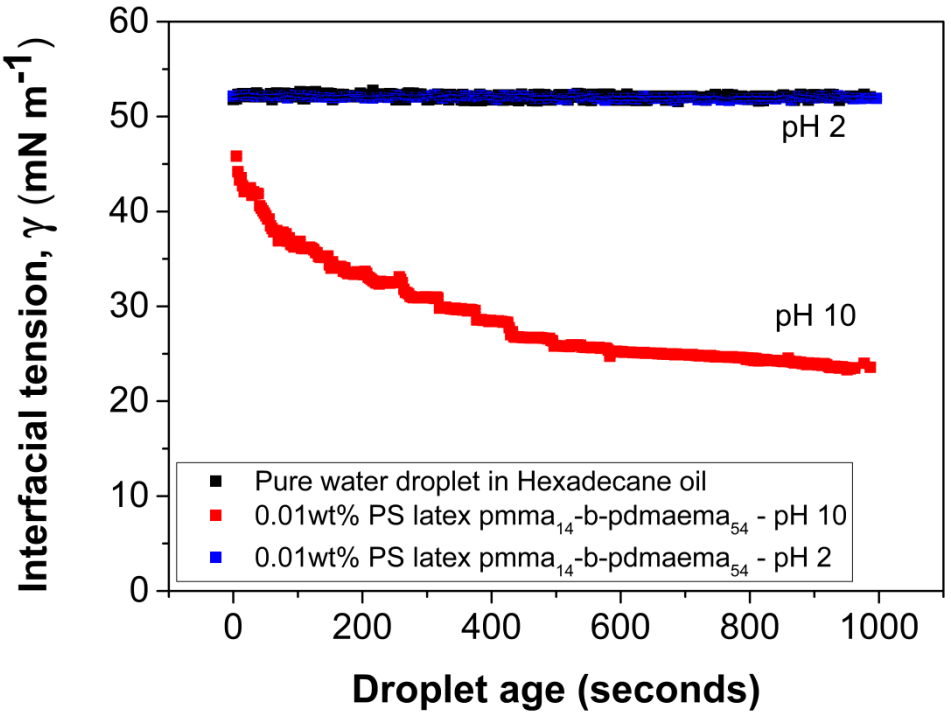

Figure 8.4. Dynamic interfacial tension of a water droplet in hexadecane oil with 90 nm $pMMA_{14}$-b-$pDMAEMA_{54}$ (SM01) sterically stabilised polystyrene latex colloids dispersed at pH 10 (red) and pH 2 (blue) at a particle concentration of 0.01 wt% at 20°C.

The interfacial tension for the bare hexadecane oil/water interface was measured to be constant at 52 mN m^{-1}. When the interfacial tension is measured with a particle concentration of 0.01 wt% dispersed at pH 2, the dynamic interfacial tension remains unaltered matching observations seen by Amalvy *et al.*[19] at an air/water interface. This suggests that either a) the particles do not adsorb at the oil/water interface or b) they do not affect the interfacial tension as the polymer when protonated has little affinity for the oil phase, but particle adsorption does occur. The

second mechanism is most likely here, since it has been demonstrated that emulsions can be stabilised by these particles dispersed at pH 2 even though some macroscopic phase separation does occur (Chapter 6).

At pH 10, the dynamic interfacial tension at t_0 is lower than that observed for a bare hexadecane/water interface and for particles at pH 2. This suggests that as the droplet is produced, some particles are already adsorbed onto the liquid-liquid interface. At pH 10 the polymer is collapsed onto the surface of the latex particle increasing its affinity for the interface and thus its adsorption. In addition, the polymer, even in its collapsed state it is able to penetrate the oil/water interface and, due to its surface active nature influences the interfacial tension (i.e. the behaviour is different to a bare solid particle at the interface). This observation again matches experimental surface tension measurements at an air/water interface.[19] The reduction in the interfacial tension is very rapid initially before it decreases more slowly over the next 600 seconds. The equilibrium interfacial tension occurs at ~23.5 mN m^{-1}. The eventual plateau in the data suggests a full coverage of the core-shell particles on the interface. The formation of a plateau also suggests that no further particle adsorption occurs and that an equilibrium interfacial is obtained. The influence of particle concentration was also investigated. Interfacial tension data for particles dispersed at pH 2 and 10, respectively, at a concentration of 0.1 wt% are presented in Figure 8.5.

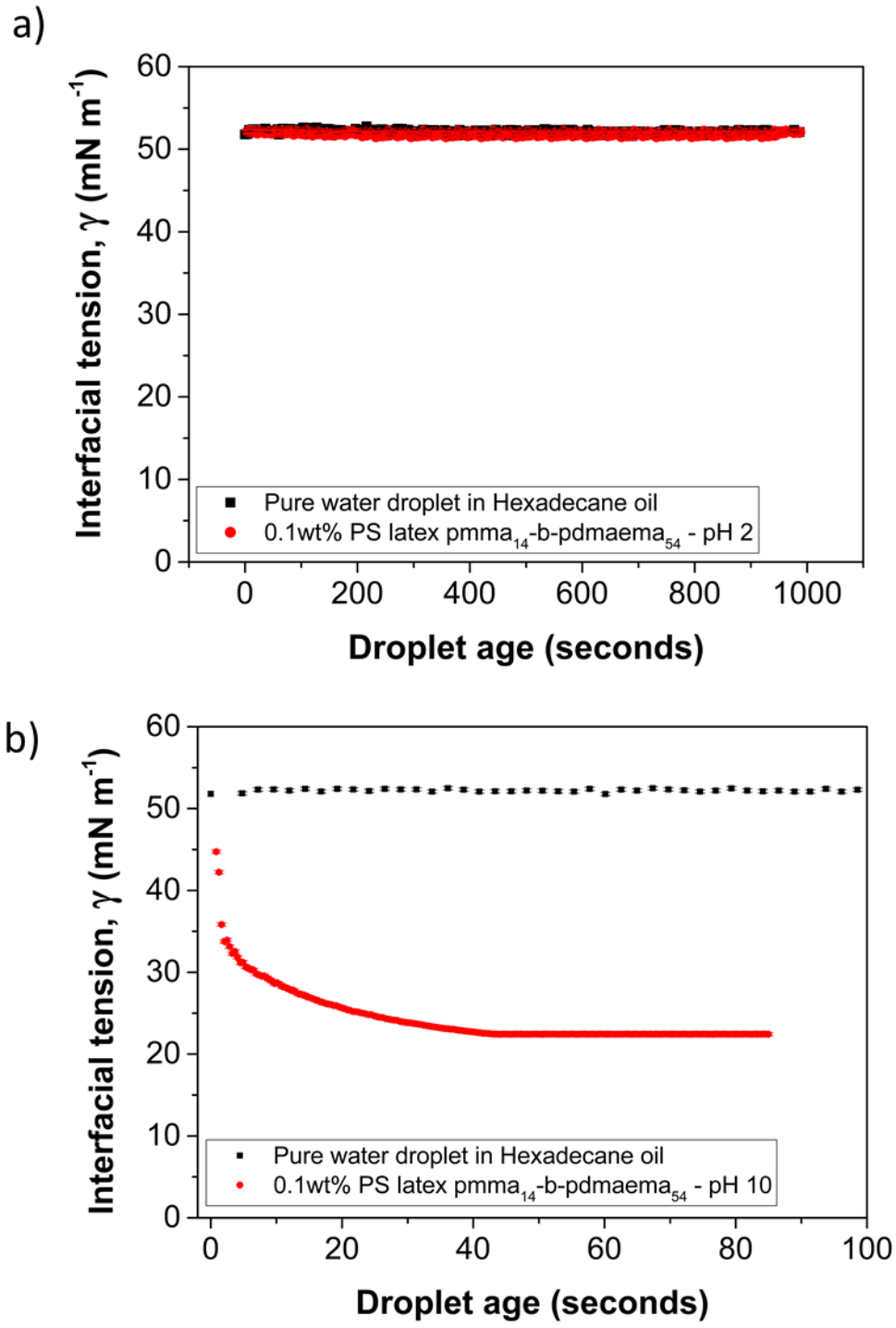

Figure 8.5. Dynamic interfacial tension of a water droplet in hexadecane oil with SM01 dispersed at a) pH 2 and b) pH 10 at a particle concentration of 0.1 wt%.

For the particles dispersed at pH 2 (Figure 8.5a), increasing the particle concentration to 0.1 wt% has no or very little effect on the dynamic interfacial tension. At pH 10 (Figure 8.5b), the interfacial tension again initially drops very rapidly before reaching an equilibrium value after approximately 40 s. The

equilibrium value of the interfacial tension is 22.4 mN m^{-1} and is similar to that seen above for the 0.01 wt% example suggesting that, in both cases, equilibrium coverage of the interface has been achieved. The increased rate of adsorption at the higher concentration is, of course, expected.

It can be concluded from the pendant drop tensiometry data that the adsorption of bare particles has little influence on the dynamic interfacial tension. In contrast, particles grafted with an amphiphilic polymer cause a decrease in the observed interfacial tension. In order to confirm these pendant drop tensiometry data, a complimentary study was conducted with the particle samples mentioned above using a microtensiometry device built at the Carnegie Mellon University, U.S.A. The results obtained from this study are given below.

8.3. Microtensiometry data

8.3.1. Silica

Before conducting dynamic interfacial tension measurements at the relevant liquid-liquid interface, the microtensiometry device was initially calibrated by measuring the air/water surface tension to ensure that the device internals were clean. It should be noted that in the microtensiometer, the interfacial tension of an oil droplet in water is measured rather than a water droplet in oil, as was used for the pendant drop experiments. The bare interfacial tension of a tricaprylin oil/water (pH 6, 0.1M NaCl) interface (droplet radius, R_d = 40 µm) was then measured at 20°C. The interfacial tension measured (24.9 mN m^{-1}) matched the value reported in literature.[17] The measurements were performed three times and averaged. The data had a typical error of ±0.5 mN m^{-1}. Afterwards the interfacial tension of a tricaprylin droplet (droplet radius, R_d = 40 µm) in water containing 0.01 wt% particles, at pH 6 and 0.1M NaCl was measured at 20°C. It should be noted that the particle concentration used in the microtensiometer is much lower than that used in the pendant drop device. This is because at higher particle concentrations it is difficult to image the interface due to the opaqueness of the particle dispersion. Dynamic interfacial tension data for the silica colloid is presented in Figure 8.5.

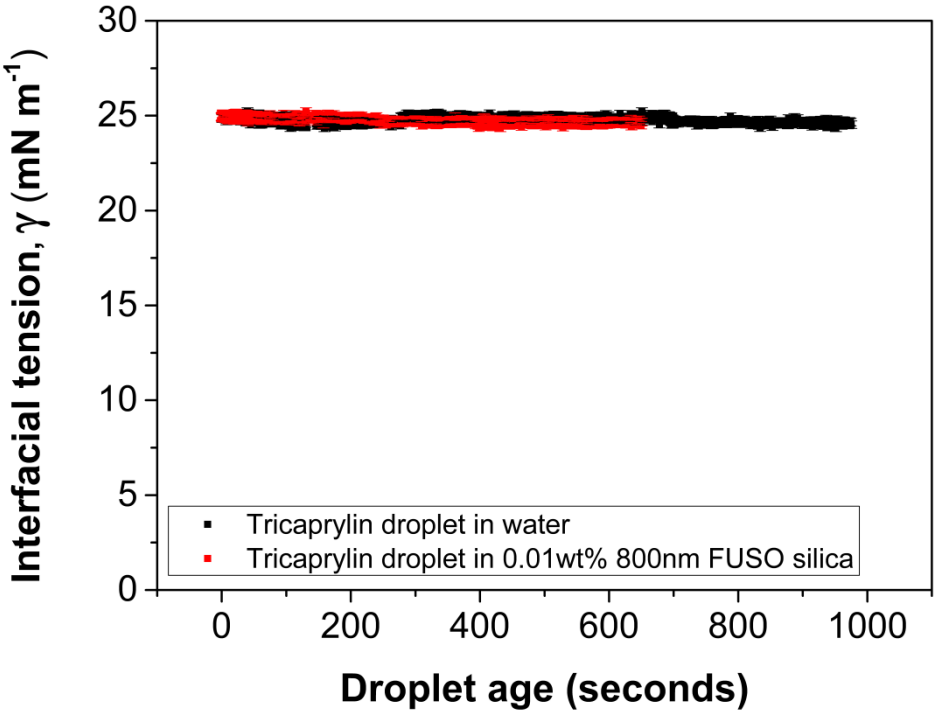

Figure 8.6. Dynamic interfacial tension of a tricaprylin droplet (Rd = 40 µm) in pH 6, 0.1M NaCl water containing a dispersion of 800nm silica colloids at a particle concentration of 0.01 wt% (T= 20°C).

The addition of 0.01wt% 800 nm FUSO silica dispersed at pH 6 has little effect on the dynamic interfacial tension and the data is effectively the same that of a bare tricaprylin/water interface. This observation matches data presented by Vignati *et al.*[6] and Drelich *et al.,*[7] showing that even if the bare particles are strongly attached to the interface, no reduction of interfacial tension reduction is detected.

In the microtensiometer device the Bond number (Chapter 4) is lower than that seen in the pendant drop device, meaning the droplet shape is less perturbed i.e. the effect of gravitational forces is less. The other advantage is that the actual pressure and droplet radius values are measured to give a measured interfacial tension, whereas in the pendant drop the interfacial tension is calculated using a nonlinear Young-Laplace model fit. Calculation by using a fit introduces error especially when the droplet experiences a change in shape due to gravitational effects.

8.3.2. Sulfate-stabilised polystyrene latex

The dynamic interfacial tension of a hexadecane/water interface laden with sulfate-stabilised latex particles at 20°C is presented in Figure 8.7.

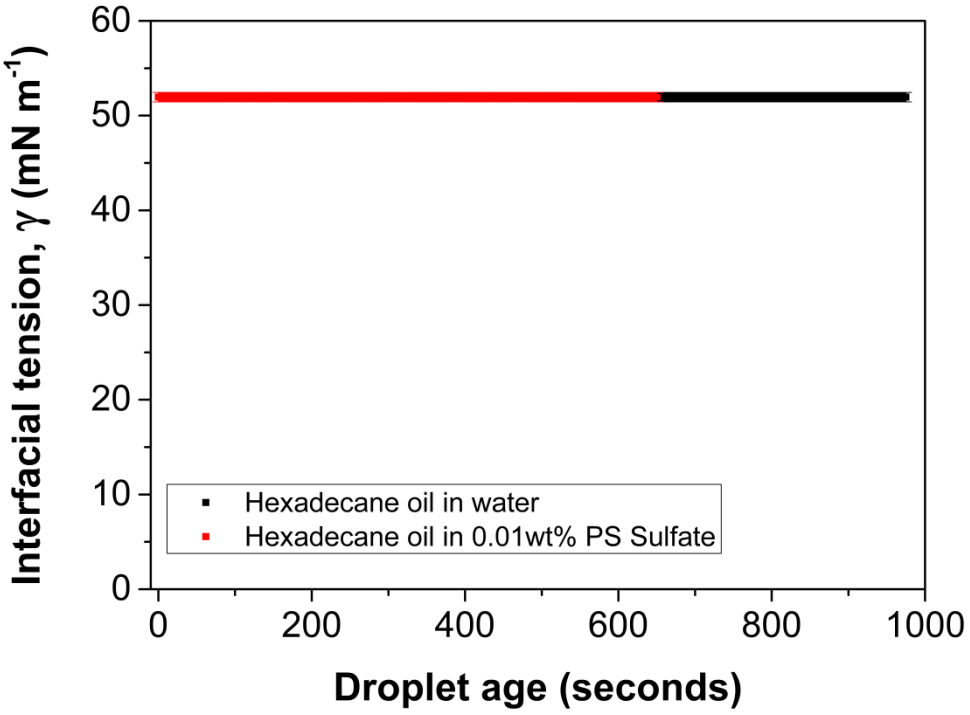

Figure 8.7. Dynamic interfacial tension of a hexadecane droplet (R_d = 40 µm) in water containing a dispersion of 300 nm sulfate-stabilised silica polystyrene latex particle at a particle concentration of 0.01 wt% (T=20°C).

Initially the pure hexadecane/water interfacial tension was measured (52 mN m^{-1}) matching values reported in literature.[18] The interfacial tension data matches the data obtained using pendant drop tensiometry. Since both isotherms are the same, the data again suggests that adsorption of unmodified (bare) latex particles do not change the interfacial tension.

8.3.3. pDMAEMA sterically stabilised polystyrene latex

The dynamic interfacial tension of a hexadecane droplet in water was also measured in the presence of 70 nm $pMMA_{14}$-b-$pDMAEMA_{54}$ (SM01) sterically stabilised

latex particles. The isotherm of the dynamic interfacial tension when the particle is dispersed at pH 2 is illustrated in Figure 8.8.

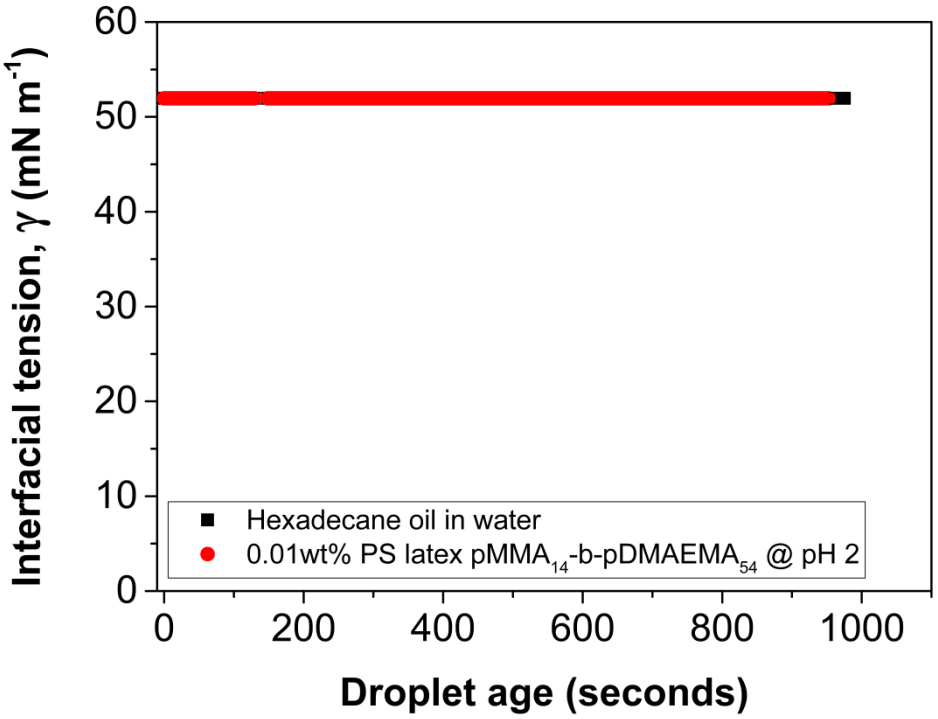

Figure 8.8. Dynamic interfacial tension of a hexadecane droplet (R_d = 40 µm) in water containing a dispersion of SM01 sterically stabilised polystyrene latex colloids dispersed at pH 2 at a particle concentration of 0.01 wt% (T = 20°C).

The data in Figure 8.7 shows that the dynamic interfacial tension both with and without the latex particles dispersed at pH 2 are the same. At pH 2, the amine groups on the polymer are fully protonated and the resultant cationic polyelectrolyte is oil insoluble. Under these conditions, the polymer is not surface active and hence, even with particle adsorption little or no change is observed on the dynamic interfacial tension.

The dynamic interfacial tension when the particles are dispersed at pH 10 is presented in Figure 8.9. The addition of 0.01 wt% of the sterically stabilised latex particles dispersed at pH 10 causes a significant decrease in the observed interfacial tension. Over the first 600 seconds as the particles adsorb the interaction of the surface-active polymer at the interface causes a rapid decrease in the interfacial tension from around 52 mN m^{-1} to 37 mN m^{-1}. At around 600 seconds the measured interfacial tension value decreases suddenly from 37 mN m^{-1} to 25 mN m^{-1};

interestingly, at this point the droplet size had increased sufficiently (>40 µm) on the verge of detachment from the capillary tip. To continue the measurement, the droplet was compressed and this sudden compression of the droplet pushed the particles at the interface closer together causing the observed large drop in interfacial tension. The interfacial tension stabilises for about 150 seconds before the droplet again increases in size nearing detachment; once again the droplet is compressed and the tension value relaxes to an equilibrium value of around 19±0.5 mN m^{-1}. Although the kinetics of adsorption cannot be simply deduced, due to the necessity of droplet compression, it is evident from the data that the drop in interfacial tension interfacial is caused by the interfacial activity of the surface attached polymer at pH 10 and not by the core particles. To test this hypothesis further, dilational elasticity measurements were performed at both pH 2 and 10.

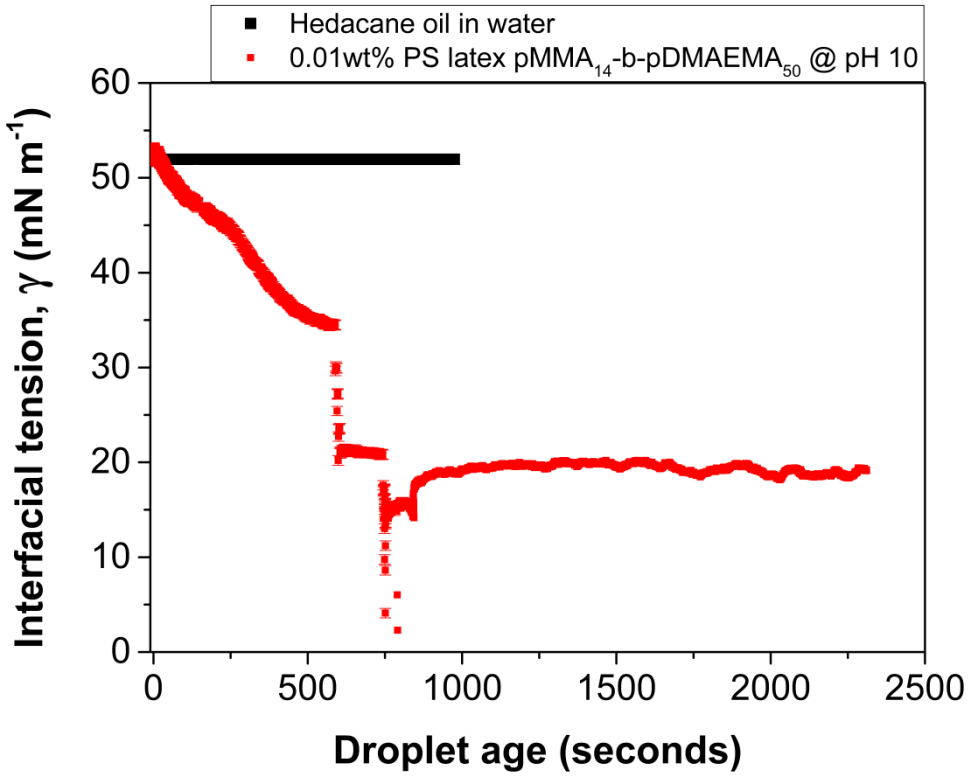

Figure 8.9. Dynamic interfacial tension of a hexadecane droplet (R_d = 40 µm) in water containing a dispersion of SM01 sterically stabilised polystyrene latex colloids dispersed at pH 10 at a particle concentration of 0.01 wt% (T = 20°C).

8.3.4. Dilational elasticity measurements

Dilational elasticity measurements were performed by oscillating the 40 μm droplet, once the equilibrium interfacial tension had been obtained for the sterically stabilised latex particles. This was done by changing the constant pressure head to the oscillatory pressure head, which can be varied over a frequency range of 0.15 – 2 Hz at an amplitude of about 50 - 100 Pa. The corresponding changes in the interfacial tension with this drive signal were measured. The dilational elasticity modulus is calculated by measuring the change in stress due to change in interfacial area of an interface. For a drop, the dilational elasticity modulus, E_0,[20] is given by;

$$E_0 = \frac{\partial \gamma}{\partial \ln A} \qquad \text{(Equation 8.1)}$$

where γ is the interfacial tension and *A* is the interfacial area.

The modulus is usually measured by imposing a sinusoidal oscillation to the surface area of the drop and the response in the interfacial tension is measured. If the strain applied is small ($\Delta A/A_0$) << 0.10 then equation 8.1 reduces to;

$$E_0 = \frac{\partial \gamma}{\partial \ln A} \approx \frac{\Delta \gamma}{\Delta A / A_0} \qquad \text{(Equation 8.2)}$$

which becomes

$$E_0 = A_0 \frac{\Delta \gamma}{\Delta A} = A_0 \frac{\gamma_A}{A_A} \qquad \text{(Equation 8.3)}$$

where A_0 is the initial or mean area of the sinusoidal oscillation, , where A_A is the amplitude of the measured response of the area change, γ_A is the amplitude of the measured response in interfacial tension.

After oscillating the interface, the interface is allowed to relax for ~500 s before oscillating at a new frequency.

The change in interfacial tension with changing interfacial area for the hexadecane/water interface in the presence of 0.01 wt% sterically stabilised latex particles (SM01) dispersed at pH 2 is presented in Figure 8.10.

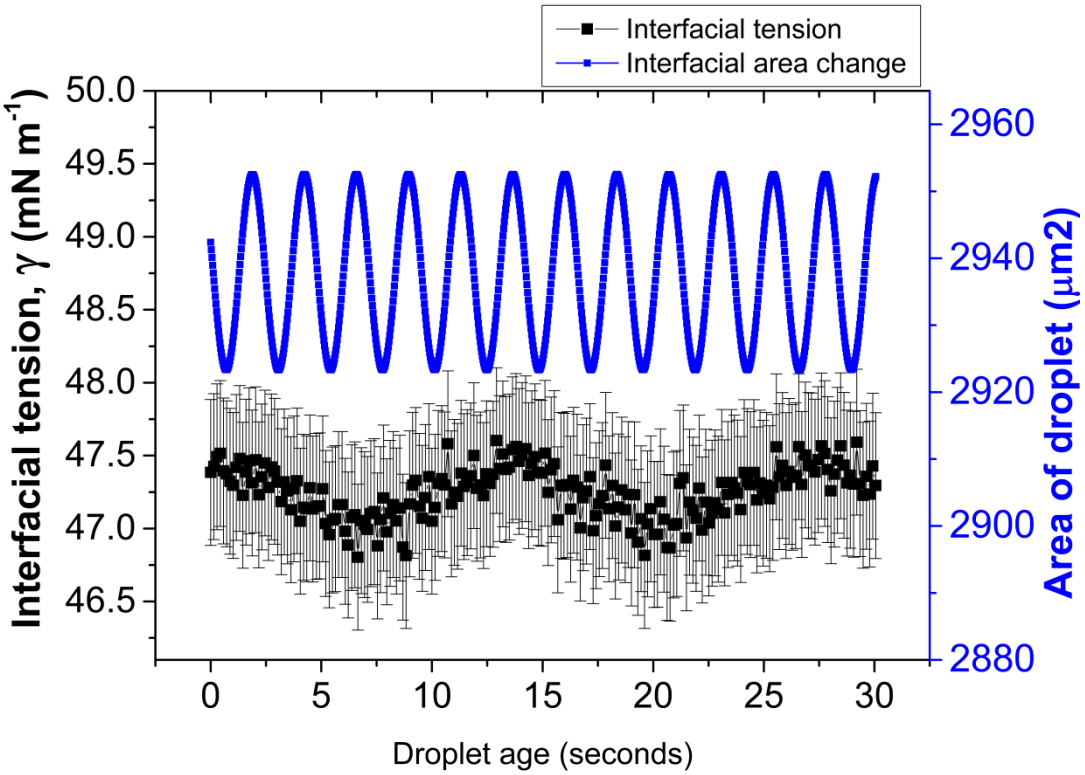

Figure 8.10. A typical plot of change in interfacial tension with changing interfacial area of a hexadecane droplet in water interface laden with 0.01 wt% of sterically stabilised polystyrene latex particles dispersed at pH 2 (T = 20°C).

By oscillating the interfacial area after equilibrium interfacial tension is obtained, the interface expands and contracts. During the expansion of the droplet, the interfacial area increases allowing additional particles to adsorb on the free interfacial area, whilst as the droplet contracts the particles on the interface rearrange and come into close contact. This oscillatory movement gives an insight into the elasticity of the interface i.e. the dilational elasticity modulus. The data in Figure 8.10 shows no change in the interfacial tension (as the data is noisy and all the data points are within error) as the droplet area expands and contracts. This behaviour was also seen at all frequencies tested and therefore the dilational elasticity modulus could not be calculated.

The change in interfacial tension with changing interfacial area for the hexadecane/water interface in the presence of 0.01 wt% sterically stabilised latex particles (SM01) dispersed at pH 10 is presented in Figure 8.11.

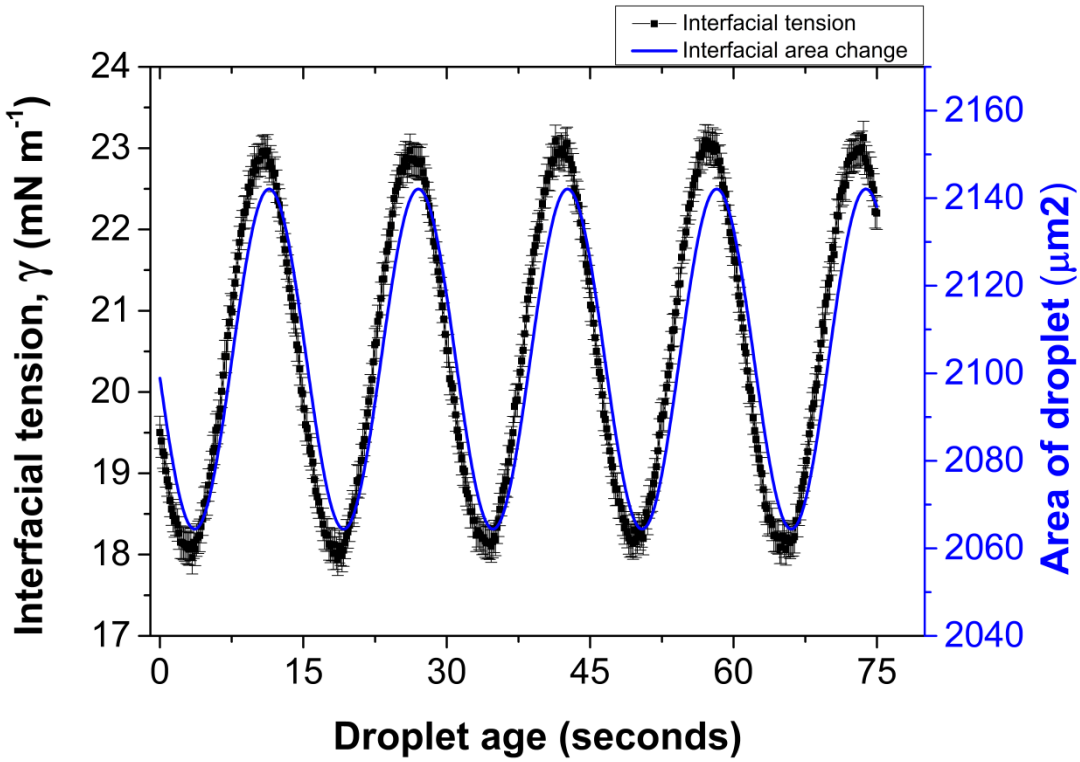

Figure 8.11. A typical plot of change in interfacial tension with changing interfacial area of a hexadecane droplet in water interface laden with 0.01 wt% SM01 dispersed at pH 10 (T = 20°C).

The data presented in Figure 8.11 shows that the change in interfacial tension due to changing interfacial area is much larger in comparison to the particles dispersed at pH 2. As the droplet compresses the particles come into closer contact that cause the polymer chains that are deprotonated to entangle with each other. As the droplet expands the entangled polymer chains on the particle surface stretch giving the interface an enhanced elastic behaviour. At pH 2, the polymer chains are highly protonated and are not expected to become entangled and hence, the change in interfacial tension as the droplet oscillated is much negligible. By performing a frequency sweep, the dilational elasticity modulus at all frequencies can be calculated using equation 8.3 and is presented in Figure 8.12.

The data shows that the dilational elasticity modulus increases as a function of increasing oscillation frequency until it reaches its high frequency limit, ε_o. Initially, with increasing frequency the dilational elasticity modulus increases. As the system reaches its high frequency limit the elasticity plateaus. This plateau occurs as further increase in the frequency of oscillation does not give enough time for additional

particles from the bulk to adsorb onto the interface, and therefore maximum change in the interfacial tension is achieved, hence little effect is seen on the elasticity. This high frequency limit is therefore concentration dependent.

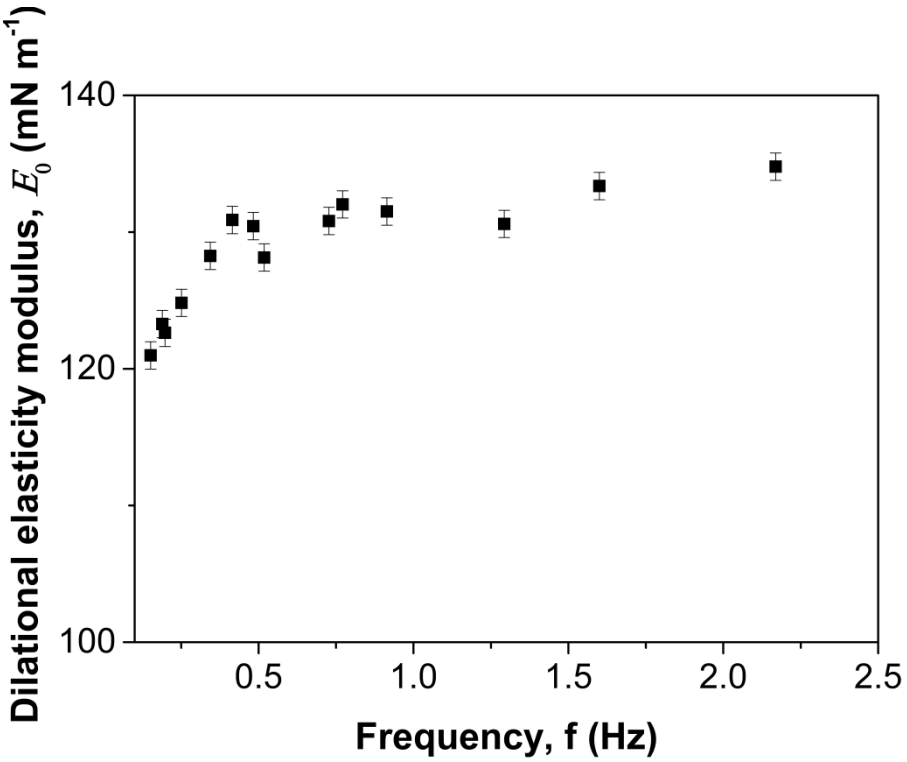

Figure 8.12. Dilational elasticity modulus of the hexadecane/water interface laden with 0.01 wt% SM01 dispersed at pH 10, as a function of oscillation frequency.

The dilational elasticity modulus observed with SM01 at pH 10 is much higher than that seen with surfactants and proteins at fluid-fluid interfaces. The elasticity modulus of various surfactants at an octane-water interface was measured by Giorgieva *et al.*[21] using a pendant drop device. They found that at an oscillating frequency of 0.1 Hz the elastic modulus for DTAB, TTAB, and CTAB were 2, 4 and 6 mN m^{-1} respectively. They concluded that the low elasticity moduli that they obtained was due in part to the bulk-surface exchanges of the surfactant molecules. In surfactant systems the exchange is very fast hence perturbation of the interfacial equilibrium becomes negligible and hence little or no effect on the surface tension value is observed away from its equilibrium value especially at low oscillation frequencies. This therefore leads to a low dilational elasticity modulus. In the case of

proteins (e.g. whey protein) the molecular transport to the interface is much slower and the interfacial equilibrium is perturbed to a larger extent. This means that even the smallest change in the interfacial area causes a large change in the interfacial tension resulting in a higher surface elasticity (~60 mN m^{-1} at 1 Hz).[22] In the case of SM01 the diffusion of the particles is much slower compared to surfactants and proteins. Furthermore the polymer may potentially entangle and thus can easily stretch and relax as the interfacial area changes. This therefore leads to a more elastic interface resulting in a higher dilational elasticity modulus (~135 mN m^{-1}) compared to typical surfactants and proteins.

Conclusions

Dynamic interfacial tension measurements show different behaviour depending on the particle system used. In the case of 800nm FUSO silica, a reduction in interfacial tension is observed with increasing particle concentration. However, gravitational settling makes it difficult to make definitive conclusions. Sulfate stabilized latex particles (similar density to water) were used to investigate the dynamic interfacial tension of the interface. It was found that when the particles were cleaned via centrifugation cycles, no visible changes in the interfacial tension is obtained. These data are also confirmed from data obtained from using a microtensiometer device for the same systems.

Using the sterically stablised latex particles the interfacial tension remains unaffected at pH 2, where the polymer is hydrated. At pH 10, the change in interfacial tension measured is large as the polymer becomes uncharged and penetrates the interface. Additionally elasticity measurements show that at pH 10 the interface is more elastic than at pH 2, as the polymer chains interlink that can be compressed and extended at the interface is oscillated.

References

1. B. P. Binks and T. S. Horozov, eds. *Colloidal Particles at Liquid Interfaces*, Cambridge University Press, Cambridge, 2006.
2. P. Pieranski, Two-dimensional interfacial colloidal crystals, *Phys. Rev. Lett.*, 1980, **45**, 569-572.
3. A. Neumann and J. Spelt, eds., *Applied Surface Thermodynamics*, Marcel Dekker, New York, 1996.
4. R. Aveyard and J. H. Clint, Particle wettability and line tension, *J. Chem. Soc., Faraday Trans.*, 1996, **92**, 85-89.
5. F. Bresme and M. Oettel, Nanoparticles at fluid interfaces, *J. Phys.: Condens. Matter*, 2007, **19**, 413101.
6. E. Vignati, R. Piazza and T. P. Lockhart, Pickering emulsions: Interfacial tension, colloidal layer morphology, and trapped-particle motion, *Langmuir*, 2003, **19**, 6650-6656.
7. A. Drelich, F. Gomez, D. Clausse and I. Pezron, Evolution of water-in-oil emulsions stabilized with solid particles: Influence of added emulsifier, *Colloids Surf. A: Physicochem. Eng. Asp.*, 2010, **365**, 171-177.
8. J. Drelich, C. L. White and C. Fang, Measurement of interfacial tension in fluid-fluid systems, In: *Encyclopedia of Surface and Colloid Science, Second Edition*, Taylor & Francis, 2007, 2966-2980.
9. S. Levine, B. D. Bowen and S. J. Partridge, Stabilization of emulsions by fine particles II. capillary and van der Waals forces between particles, *Colloids Surf. A: Physicochem. Eng. Asp.*, 1989, **38**, 345-364.
10. J. Kim, L. J. Cote, F. Kim, W. Yuan, K. R. Shull and J. Huang, Graphene oxide sheets at interfaces, *J. Am. Chem. Soc.*, 2010, **132**, 8180-8186.
11. N. Glaser, D. J. Adams, A. Böker and G. Krausch, Janus particles at liquid-liquid Interfaces, *Langmuir*, 2006, **22**, 5227-5229.
12. S. Kutuzov, J. He, R. Tangirala, T. Emrick, T. P. Russell and A. Böker, On the kinetics of nanoparticle self-assembly at liquid/liquid interfaces, *Phys. Chem. Chem. Phys.*, 2007, **9**, 6351-6358.
13. A. Stocco, W. Drenckhan, E. Rio, D. Langevin and B. P. Binks, Particle-stabilised foams: an interfacial study, *Soft Matter*, 2009, **5**, 2215-2222.

14. K. Du, E. Glogowski, T. Emrick, T. P. Russell and A. D. Dinsmore, Adsorption energy of nano- and microparticles at liquid-liquid interfaces, *Langmuir*, 2010, **26**, 12518-12522.
15. L. Isa, E. Amstad, K. Schwenke, E. Del Gado, P. Ilg, M. Kroger and E. Reimhult, Adsorption of core-shell nanoparticles at liquid-liquid interfaces, *Soft Matter*, 2011, **7**, 7663-7675.
16. S. Ferdous, M. Ioannidis and D. Henneke, Adsorption kinetics of alkanethiol-capped gold nanoparticles at the hexane–water interface, *J. Nanopart. Res.*, 2011, **13**, 6579-6589.
17. E. N. Jaynes and M. A. Flood, Protein films at oil-water interfaces: Interfacial tension measurement by the static drop method, *J. Dispersion Sci. Technol.*, 1985, **6**, 55-68
18. G. Li, S. Prasad and A. Dhinojwala, Dynamic interfacial tension at the oil/surfactant-water interface, *Langmuir*, 2007, **23**, 9929-9932.
19. J. I. Amalvy, G. F. Unali, Y. Li, S. Granger-Bevan, S. P. Armes, B. P. Binks, J. A. Rodrigues and C. P. Whitby, Synthesis of sterically stabilized polystyrene latex particles using cationic block copolymers and macromonomers and their application as stimulus-responsive particulate emulsifiers for oil-in-water emulsions, *Langmuir*, 2004, **20**, 4345-4354.
20. F. K. Hansen, Surface dilational elasticity of poly(oxy ethylene)-based surfactants by oscillation and relaxation measurements of sessile bubble, *Langmuir*, 2008, **24**, 189-197.
21. D. Georgieva, V. Schmitt, F. Leal-Calderon and D. Langevin, On the possible role of surface elasticity in emulsion stability, *Langmuir*, 2009, **25**, 5565-5573.
22. L. K. Shrestha, Y. Matsumoto, K. Ihara and K. Aramaki, Dynamic surface tension and surface dilational elasticity of mixed surfactant/protein systems, *J. Oleo Sci.*, 2008, **57**, 485-494.

CHAPTER 9: CONCLUSIONS AND FUTURE WORK

Conclusion

The chapters presented in this thesis have an associated summary. This brief section will therefore only contain an overall assessment of the work present as a whole in the broader context of scientific research and development.

It has been successfully demonstrated that emulsion polymerisation can be used to prepare polystyrene latex particles that are sterically stabilised using pMMA-b-pDMAEMA. These particulate systems exhibit responsive behaviour to both pH and temperature, which can be characterised by measuring changes in the hydrodynamic diameter in response to changes in these stimuli. In addition it has been shown that these sterically stabilised latex particles can be used as stabilisers to stabilise oil-in-water emulsions. Emulsion studies showed that the stability of hexadecane in water emulsions to coalescence was influenced by both pH and electrolyte concentration. Changes in the pH dictated the solvency of the pDMAEMA chains in water and thus controlled their affinity to the oil/water interface. The addition of electrolyte screened the charges on the polymer surface, thus driving particle adsorption to the interface.

The ability to influence the behaviour of the emulsion through the effect of these stimuli on these particles is of technological interest. These solid-stabilised emulsions can be used as templates for the fabrication of ‘colloidosome’ microcapsules for the encapsulation and release of actives. We demonstrate that the pDMAEMA chains on the surface of the particles can be chemically crosslinked on the droplet surface to form a membrane shell. Upon removal of the oil core, we show that the porosity of this membrane shell can be controlled by changes in the environmental pH. These microcapsules act as size-exclusion membranes and we demonstrate the retention and release of model dextran molecules as a function of pH. These microcapsules can also be potentially used in numerous other applications.

We also demonstrate that rotational membrane emulsification can be used to prepare particle stabilised emulsion droplets. The data in Chapter 7 illustrates that both

formulation chemistry as well as the membrane mechanical parameters can be used to exert control on the droplet size and droplet size distribution. The advantage of this production method is that is can be easily scaled up to industrially relevant scales. These data also infer details about the influence of particle adsorption kinetics on the droplet size. Variations in the droplet size with changes in the membrane rotational speed, volumetric flow rate and particle concentration can all be related back to the critical time needed for particles to wet the interface and then adsorb.

Finally we probe the adsorption kinetics of particle adsorption to liquid/liquid interfaces. We know that all the particle systems that are tested are able to stabilise emulsions, however particles that are clean, i.e., have no surface modifications do not change the interfacial tension with time. In contrast, when sterically stabilised latex particles the interfacial tension does change dramatically at pH 10 in comparison to pH 2 as the affinity for the interface is much greater at the high pH's. In addition dilational elasticity measurements show that the interfacial elasticity is also pH dependent.

Future work

This work has investigated the use of sterically-stabilised latex particles as emulsifiers, fabrication of colloidosome microcapsules based on emulsion templates and their adsorption to fluid-fluid interfaces using tensiometry. In Chapter 6 the preparation of colloidosome microcapsules from emulsion droplet precursors was presented. It was demonstrated that such microcapsule systems were able to encapsulate and release model actives (labelled dextran) at pH 10 and 2, respectively. In order to examine the permeability of colloidosome shells towards such relatively large actives in more depth, further encapsulation studies should be conducted. A range of latex particles (varying particle size and polymer chain length) should be prepared to probe the permeability of the colloidosome shell to determine the smallest molecular weight of active that can be successfully encapsulated. Performing release studies at more pH's would give a better insight regarding the porosity of these microcapsule structures. This could also be coupled with probing the effect of temperature on the encapsulation/release of model actives.

It would also be interesting to modify the steric stabiliser used in these studies. Since the pDMAEMA block is crosslinked the pH responsiveness of the amine groups may be potentially affected. To avoid this, a third block could be added which would be used to crosslink adjacent polymers.

In Chapter 7, the production of particle stabilised emulsions using rotary membrane emulsification was presented. This study could be further examined by investigating the effect of a) particles of same size with different pDMAEMA chain lengths and b) particles of different size with same pDMAEMA chain length on the droplet size and size distribution. The production of colloidosome microcapsules using the RME should also be exploited for the potential to develop a 'one pot synthesis' route. It would be interesting to examine whether particles with different aspect ratios have any effect on droplet shape, size and polydispersity. Investigating the production of water in oil emulsions using the RME would also be of academic/industrial interest.

The data investigating the adsorption of these sterically-stabilised latex particles was preliminary. Further work is needed to examine the effect of different pH's and polymer chain lengths on the interfacial tension. A series of experiments should be done to compare the dilational elasticity modulus as a function of pH, particle concentration and compare this to data obtained with polymer only. In addition the effect of temperature should also be examined.